EVALUATING DESIGN METHODS FOR ROCKFILL DAMS

BY

NEIL CLINTON PRIVAT

A Thesis Submitted to
The Faculty of Graduate Studies
In Partial Fulfillment of the Requirements for the Degree of

MASTER OF SCIENCE

Department of Civil Engineering
University of Manitoba
Winnipeg, Manitoba

THE UNIVERSITY OF MANITOBA

FACULTY OF GRADUATE STUDIES

*****

COPYRIGHT PERMISSION

EVALUATING DESIGN METHODS FOR ROCKFILL DAMS

BY

NEIL CLINTON PRIVAT

A Thesis/Practicum submitted to the Faculty of Graduate Studies of The University of Manitoba in partial fulfillment of the requirement of the degree

MASTER OF SCIENCE

ABSTRACT

This thesis examines the methods for designing flow through rockfill dams. Whether intentionally constructed as a flow-through structure or as a consequence of events, rockfill dams should be designed with consideration to flow through. A laboratory testing program and a scale-dam testing program have been conducted to assess the flow-through characteristics of rockfill and the initiation of particle movement on the downstream face on rockfill dams.

The laboratory-testing program consists of rockfill particle characterization including drag tank tests and particle surface area characterization. Large-scale permeameter tests were conducted with samples 1.5 meters long and 0.7 cubic meters in volume, to characterize the hydraulic properties of the rockfill. As well, miniature dams were constructed 0.5 meters tall to evaluate the flow characteristics of rockfill and the effects of void ratio, particle size, particle gradation, and dam geometry on the initiation of particle movement.

The scale dam testing program utilized the prediction of flow characteristics through the rockfill and prediction of the flow conditions that would induce particle movement to design the geometry of the scale dams. Construction and testing of the scale dams were successfully completed in the University of Manitoba Hydraulic Research and Testing Facility. The predictions were compared to the observed data and recommendations for use of the predictive tools were made.

ACKNOWLEDGEMENTS

I would like to take this opportunity to express my gratitude to my advisor, Dr. James Blatz for his infectious enthusiasm for research and professional development. His approach of treating graduate students as colleagues and providing me a sense of ownership of the research made my time at the university great.

Thank you to my colleagues in the Geotechnical grad lab: Greg Siemens, Deni Priyanto, Tim Krahn, Lukas Novy, German Ciro, Wisam Abdul-Razaq, Yadav Pathak, Mike van Helden, Jared Baldwin and the grad students in the Hydraulics lab. They have made a wonderful impact in both my research and my personal life (Poker anyone?).

Thanks to summer students Karl Rink, Elise Dyck, Kathryn Hearson, David Kurz and Carly Delavau, who wasn't assigned to the project but helped anyway. They made the heavy lifting easier, testing smoother, and the days fly by.

A warm thank you to Kerry Lynch and Narong Piamsalee the keepers of the geotech lab, for their insight and assistance; to Roy Hartle in the HRTF for many thousands of kilograms of assistance; Scott Sparrow, transportation; Dale Bourns and Gerry Woods in the metal workshop; Moray McVey and Grant Whiteside in the Structures Lab.

I would also like to recognize the financial support from Manitoba Hydro – Civil Engineering Department and from the Natural Sciences and Engineering Research Council of Canada (Collaborative Research and Development Grant).

Finally I would like to thank Vivian and Keith, my Mother and Father, for their support throughout my schooling. The free meals, advice and encouragement (positive and negative...Steven) went a long way in helping achieve this goal. Thank you Ken, for giving advice and hours of manual labour, and Ainsley for putting up with Ken and I.

I owe a debt of gratitude to all and will appreciate this experience always.

TABLE OF CONTENTS

LIST OF SYMBOLS AND ABBREVIATIONS

SYMBOLS

a - coefficient for non-Darcy fluid flow

A - gross cross-sectional area of flow

- also projected surface area

A_{ms} - surface area per mass of rock

A_R - aspect ratio of a dam

A_{vs} - volume-specific surface area (surface area per unit volume)

B_d - width of the downstream slope of a dam

B_c - width of the crest of a dam

B_u - width of the upstream slope

C_d - drag coefficient

cm - centimeters

cms - cubic meters per second

d - average, or second diameter of the rock

d_t - characteristic dimension of material in turbulent flow calculation

d_{50} - 50^{th} percentile diameter

e - void ratio

F_{hyd} - the hydraulic force on a particle

F_d - the force of drag on a particle

h - upstream water level

H - height of a dam

i - hydraulic gradient

k - hydraulic conductivity

kg - kilogram

k_t - turbulent hydraulic conductivity

l - litre

L - the characteristic length of the body along direction of flow

- also the length of a dam

m - meters

m - hydraulic mean radius

mm - millimeters

n - porosity

N - coefficient for non-Darcy fluid flow

Q - discharge

q - discharge per unit length of dam

R - Reynolds number

Re - pore Reynolds number

r_e - coefficient of oblateness and roughness

s - coefficient for non-Darcy fluid flow

S_{voids} - total surface area of a volume of voids

t - coefficient for non-Darcy fluid flow

V - velocity

V_{voids} - volume of voids within a control volume of porous media

V_V - velocity of flow in the voids of porous media

W - Wilkins' coefficient

y_{exit} - seepage face exit height

β_o - particle shape coefficient

γ_p - unit weight of particle

γ_w - unit weight of water

ρ - density of a fluid

η - dynamic viscosity of a fluid

θ - angle of the toe of a dam

θ_{ff} - angle of the emergent flow field

ξ - angle of the seepage force

U - uniform velocity flow field

- also void velocity

ν - kinematic viscosity

$\forall_p$ - particle volume

ABBREVIATIONS

ASTM - American Society for Testing and Materials
CDA - Canadian Dam Association
CS - Campbell Scientific
DA - Data Acquisition System
EU - European Union
FS - Factor of Safety
H - Horizontal
HRTF - Hydraulic Research and Testing Facility
IDF - Inflow design flood
IMPACT - Investigation of Extreme Flood Processes and Uncertainty
MD - Mini Dam, naming of the mini dams (ex. MD1 through MD15)
PVC - Poly vinyl chloride
V - Vertical
VW - Vibrating wire

LIST OF FIGURES

LIST OF TABLES

1 INTRODUCTION

1.1 GENERAL OVERVIEW

Rockfill is used throughout the world in the construction of hydraulic control structures. Typically the structures take the form of rockfill weirs and rockfill dams. Rockfill dams can be used to control runoff from storm events, manage river flows and provide water retention for energy generation, irrigation and recreation. Many rockfill dams are designed as flow-through structures due to the porous nature of the rockfill. Flow-through rockfill structures can either be intentionally designed, as in the case of flow attenuation, or can be a consequence of failure of a lower permeability material barrier to flow. In some cases, traditional zoned dams may function as flow-through rockfill dams after an internal lower permeability zone becomes compromised. Waste rock generated from mining operations can be deposited in a manner that creates a structure similar to a flow-through rockfill dam, though much greater in longitudinal extent (Hansen *et al.* 2000).

The Canadian Dam Association Dam Safety Guidelines (CDA 1999) outline requirements for rockfill dams in Section 8.8 'Flow Through Rockfill Dams'. This section states, "For the design flood, flow-through rockfill dams shall be designed to withstand the combined effects of the action of seepage emerging from the downstream face, along with any overflow without local or massive movement of rock particles."

Two primary criteria are considered in the design and operation of rockfill dams: the exit gradient and flow exiting the downstream seepage face. The downstream seepage face is where initiation of particle motion is most likely to occur due to high exit gradients and flow velocities. In most applications concerning flow through porous media, the dynamic velocity term can be eliminated from the formulation in the case of small flow velocities when assuming laminar flow conditions (Hansen 2003). In the case of flow through coarse rockfill, flow velocities tend to be high and this assumption is no longer valid. This is realized as flow through rockfill departs from Darcy's law at low Reynolds numbers (*Re*).

The physical properties that affect hydraulic conditions of rockfill include porosity, particle shape, particle size, particle roughness, and tortuosity of the voids. These tend to allow fully turbulent flow at low Reynolds Numbers relative to pipe flow. As such, when analyzing the hydraulic performance of coarse rockfill, the level of turbulence must be considered to establish the hydraulic gradient fields. The discussion in this thesis is limited to measurement of the fundamental non-Darcy flow parameters of rockfill required to characterize turbulent flow for use in rockfill dam assessment and design.

Numerous studies have been undertaken to examine the hydraulic properties of coarse rockfill and flow conditions in rockfill dams (Lawson 1987). Many methods have focused on developing scaling relationships (Venkataraman *et al.*

1998) and numerical models (Scheidegger 1974) for assessing hydraulic properties and flow conditions. Although these studies (and many not explicitly noted here) have provided significant insights into the hydraulic performance of rockfill dams, there is still need for quantitative physical measurements of the hydraulic properties and flow conditions.

1.2 Hypothesis and Objectives

The hypotheses for this research are defined as:

1. Flow in rockfill dams is not laminar and turbulent flow must be considered using a hydraulic gradient - bulk velocity relationship.
2. The initiation of particle movement on the exit face of a rockfill flow-through structure is a function of the flow through the structure and therefore particle movement can be predicted using the method developed by Hansen *et al.* (2005).

A research project was developed by The University of Manitoba and Manitoba Hydro to investigate The Canadian Dam Association Dam Safety Guidelines (CDA 1999) requirements for rockfill dams in Section 8.8 'Flow Through Rockfill Dams'. The objectives of this research were to characterize flow through a specific coarse porous media, as designated by Manitoba Hydro, and provide confidence in a method for predicting the initiation of particle movement.

1.3 ORGANIZATION OF THESIS

The literature review in Chapter Two provides descriptions, comparisons, and concepts published in the literature pertaining to this thesis. This chapter also provides a review of methods used in the evaluation of flow through porous media and prediction of particle movement.

Chapter Three contains the mechanical characterization of individual particles of coarse porous media used in the experimental program. Included in the characterization was the laboratory measurement of drag on the coarse porous material used. The description and development of non-basic properties used by others for application in coarse porous media problems is also presented.

Chapter Four describes the design and construction of a large-scale permeameter built at The University of Manitoba Hydraulic Research and Testing Facility. An experimental program using the large-scale permeameter has been conducted to measure the non-linear hydraulic characteristics of local coarse materials.

In Chapter Five, the design, construction and testing of small dams, referred to in this thesis as mini dams, is outlined. Test results and observations made during the experiments are included.

Chapter Six details the design, construction and testing of two larger prototype dams. Analysis for prediction of flow and initiation of particle movement is also provided. The key parameters and corresponding measurements recorded during the testing are included in detail.

Chapter Seven provides a detailed interpretation of the data from the mini dam and scale dam experiments, as well as review of the prediction of flow through dams and the prediction of the initiation of particle movement.

Chapter Eight draws conclusions from the research and details recommendations for consideration in the design of a flow-through dam structures. A summary of the thesis including limitations and recommendations for further research is included.

1.4 General Assumptions

In all further discussions in this document the following assumptions are implied unless otherwise indicated:

- The fluid being utilized is water, which varies in properties of viscosity and density by temperature alone.
- The change in viscosity of water with temperature can be neglected in comparison with other uncertainties present.
- The medium (granitic rockfill) is insoluble and chemically inert with respect to the fluid passing through it.

- The medium is homogeneous and isotropic with respect to porosity and permeability over the scale examined.

2 LITERATURE REVIEW

2.1 GENERAL

The literature review contained in this chapter is intended to identify current understanding regarding dam safety assessments for rockfill structures. The science and engineering principles currently used along with data from existing studies will be highlighted.

2.2 AGGREGATE CRUSHING TECHNIQUE

Jaw crushers are the local standard aggregate crushing apparatus for granite stones greater than 160 mm in diameter. Usually located near the beginning of an aggregate crushing plant, the jaw crushers reduce the stone by compression and shear, producing a minimal amount of fines. In their investigation on jaw crushers, Unland and Szczelina (2004) found that jaw crusher fragments are typically misshapen. The material produced is dependant on its initial shape and size and on the crusher parameters, but is generally flat and according to the Zingg diagram (Garga *et al.* 1991) is blade like (Figure 2.1). This is common for crushers that use single particle crushing by compression within the processing zone. In general, those machines cannot be used as crushers that produce well-shaped particles.

2.3 PARTICLE CHARACTERIZATION

When trying to assess flow through coarse porous media, hydraulic characterization of the particles is required. The hydraulic mean radius (Wilkins

1955, Garga *et al.* 1991) is a representative measure of the average diameter of a pore space within a porous media and is often used to represent the characteristic length parameter in a Reynolds equation (e.g. McCorquodale *et al.* 1978).

$$\mathrm{Re} = \frac{Vm}{nv} \qquad \textbf{Equation 2.1}$$

where,

Re	is the pore Reynolds number	
V	is the velocity	[m/s]
m	is the hydraulic mean radius	[m]
n	is the porosity	[-]
v	is the kinematic viscosity	[m^2/s]

As will be discussed later, Re varies depending on flow conductor (i.e. pipe flow *vs.* rockfill), and currently there is no standard convention for calculating the Reynolds number for flow through rockfill. Hydraulic mean radius will be affected by gradation (changes in void ratio) and angularity of particles (volume-specific surface area). The definition of hydraulic mean radius, m, is

$$m = \frac{V_{voids}}{S_{voids}} \quad \text{or} \quad m = \frac{e}{A_{vs}} \qquad \textbf{Equation 2.2}$$

where
- V_{voids} volume of voids within a control volume of porous media,
- S_{voids} total surface area of V_{voids},
- e void ratio,
- A_{vs} volume-specific surface area (surface area per unit volume), equals density of rock mass-specific surface area.

Garga *et al.* (1991) discuss the Zingg diagram for use in categorizing particle shape and estimating volume. By measuring three orthogonal axes of a rock particle and normalizing the measurements with respect to each other, a classification can be highlighted by the Zingg diagram. The three orthogonal axes (Figure 2.2) are described as: 'a' is the major axis, 'b' is the intermediate axis, and 'c' is the minor axis. Figure 2.1 shows the areas for each of the four basic shape classifications in the Zingg Diagram. The Zingg Diagram can be utilized for comparisons between rockfill masses. As well, Garga *et al.* (1991) use the Zingg Diagram to define spheroids and nonspheriods; and use this criterion to differentiate particle surface area versus volume equations.

In the calculation of volume for the particle surface area Garga *et al.* (1991) used the ellipsoidal volume (V_e) as an approximation of the true volume of a particle using the equation:

$$V_e = \frac{\pi}{6} a \cdot b \cdot c \qquad \textbf{Equation 2.3}$$

where,

a,b,c are the lengths of the three axis of the rock as shown in Figure 2.2

Garga *et al.* (1991) emphasize that V_e should not be employed to obtain the surface area of a single rock, but rather a mass of rock. This requires multiple rocks to be measured and some form of average be found.

To calculate hydraulic mean radius, Wilkins (1955) found it necessary to measure the surface area of crushed dolerite stone (specific gravity 2.87) for use in permeameter experimentation. A number of stones were carefully measured by tracing the surfaces on paper and the area calculated. Wilkins (1955) developed a plot of surface area per pound versus sieve size. Shown in Figure 2.3 are Wilkins' crushed dolerite measurements as scaled from his 1955 paper, idealized particles (perfectly spherical stones), and specific gravity corrected crushed granite rock (specific gravity 2.68) used in this study.

Garga *et al.* (1991) describe a method where nickel coating is used on rock samples to establish surface area. Garga *et al.* (1991) completed surface area evaluations for 225 limestone rocks of the same nominal size. Using three different methods, a relationship between the nickel coating rate (cm^2 per gram of nickel) and the mass of nickel produced a measure of surface area. Using statistical regression methods they produced equations relating surface area to rock equivalent ellipsoidal volume.

It is extremely difficult to accurately measure the total surface area of the volume of voids; Sabin and Hansen (1994) therefore developed a simplified method for determination of hydraulic mean radius. They reduced the problem by introducing void ratio as a measurable value, solving the equation for a sphere, and introducing a coefficient (r_e) for non-spherical shapes. This produces the following:

$$m = \frac{ed}{6r_e}$$ **Equation 2.4**

where,

e void ratio [-]
d the average, or second diameter of the rock [m]
r_e coefficient of oblateness and roughness [-]
- is 1.3 for coarse angular rock

A practical determination of m is fairly reliable for clean, mono-sized rock but is uncertain for a well-graded or non-homogeneous rockfill (Leps 1973).

2.4 Drag Coefficient of a Particle

The drag coefficient (C_d) is a number that describes a characteristic amount of aerodynamic drag caused by fluid flow, given by Equation 2.5.

$$C_d = \frac{2 \cdot F_d}{\rho V^2 A}$$ **Equation 2.5**

where F_d is the force of drag [N],
ρ is the density of the fluid [kg/m^3],
V is the velocity of the object relative to the fluid [m/s],
A is the reference area [m^2],
C_d is the drag coefficient [dimensionless constant].

Many techniques have been used to measure the drag coefficient of a sphere, including freely falling spheres in a liquid, wind tunnel testing, towed spheres, and 'sting mounted' spheres. A generally accepted standard drag curve was developed for a sphere by Hoerner and was reviewed by Bailey (1974).

The Reynolds number can be a useful dimensionless number to characterize the drag coefficient's dependence on velocity. The Reynolds number is the ratio of

the inertial forces of the medium to the viscous forces. For lower Reynolds numbers, the boundary layer, a thin layer of fluid near the surface in which the velocity changes from zero at the surface to the free stream value away from the surface, is laminar. For higher Reynolds numbers, the boundary layer is turbulent and the velocity is characterized by unsteady (changing with time) swirling flows inside the boundary layer.

At very low velocity, a stable pair of vortices are formed on the downstream side of a sphere. As velocity increases, the vortices become unstable and are alternately shed downstream. As velocity is increased even more, the boundary layer transitions to chaotic turbulent flow with vortices of many different scales being shed in a turbulent wake from the body. Each of these flow regimes produces a different amount of drag on the sphere (NASA 2006).

2.5 Fluid Flow

The motion of fluid flow through geotechnical materials can be described as taking place through an intricately branched network of open spaces interpenetrating a skeletal solid framework. Therefore, the two distinct elements to flow problems are: the properties of the fluid and the properties of the solid framework or medium (Hubbert 1940). The flow properties of the fluid can be defined by viscosity and density. Two of the more important hydraulic properties of the porous medium can be identified as porosity and hydraulic conductivity. The porosity may be defined as the ratio of voids in the medium to the total

volume of the medium. The hydraulic conductivity is a measure of the ability of a material to transmit fluids through the pore space.

2.5.1 Darcy's Law

The accepted definition for fluid flow in porous media, such as typical geotechnical materials, dates back to experiments on the flow of water through filter sands, published by Darcy (1856). In its present general form Darcy's Law states that:

$$Q = k\,A\,\frac{\Delta h}{\Delta l} \quad \text{or} \quad Q = k\,A\,i \qquad \textbf{Equation 2.6}$$

where
- Q is the discharge [m^3/sec]
- k is the hydraulic conductivity [-]
- A is the gross cross-sectional area of flow [m^2]
- Δh is the head loss over a distance [m]
- Δl is the length in the direction of flow [m]
- i is called the hydraulic gradient and equals $\Delta h/\Delta l$ [-]

As highlighted in Dudgeon (1964) much of the research since Darcy's results in 1856 has fallen into three main categories:

i. Correlating hydraulic conductivity with physical characteristics of porous media.

ii. Theoretical justification of Darcy's law.

iii. Studying the upper limit of validity of Darcy's law and determining relationships applicable to high flow rates.

The points of particular interest in this thesis are points i. and iii. which will be dealt with later in this chapter.

2.5.2 Flow Through Coarse Porous Media

Few experiments conducted to measure hydraulic properties of large coarse porous media have been reported, due to the large apparatus required and the physical difficulty of handling the material. Almost all reports indicate that the flow through coarse porous material is not laminar and therefore does not obey Darcy's Law (Hansen *et al.* 1995). Many experimental investigations have been carried out to determine the upper limit of validity of Darcy's law. It has been customary to express the upper limit of validity in terms of a Reynolds number, but the difficulty of determining a suitable characteristic length for the pores in porous medium, together with other factors such as particle shape, grading, and porosity, has led to a wide range of equations and limiting Reynolds numbers being reported. Reynolds numbers that have been reported range between authors from 1 to 100 (Scheidegger 1974), >300 (Martins 1990) and >500 (McCorquodale *et al.* 1978) based on an inconsistent definition of Reynolds number (particularly the characteristic length).

Flow through rockfill (a coarse porous media) is generally considered, with the exception of low flow rates, to be transitional (between laminar and turbulent), and fully turbulent. The transition from laminar to turbulent flow within the voids is gradual, and can be identified by experimentation. The flow through rockfill

can be described as a nonlinear relationship between hydraulic gradient and bulk velocity. A general power-law relationship can be stated as:

$$i = aV^N \qquad \textbf{Equation 2.7a}$$

alternatively the quadratic form is:

$$i = sV + tV^2 \qquad \textbf{Equation 2.7b}$$

where i is the hydraulic gradient (dimensionless)
V is the bulk velocity (m/s)
a & N are experimental coefficients
s & t are experimental coefficients.

(Hansen *et al.* 1995)

Although the two equations have different forms, George and Hansen (1992) have argued interchangeability of the two. Within this document Equation 2.7a was selected for use in interpreting data, as the coefficient N indicates the level of turbulence in the flow conditions. Where $N = 1$ is associated with laminar flow (obeying Darcy's Law), $N = 2$ is associated with fully turbulent flow and N between 1 and 2 is transitional flow in the voids (Garga *et al.* 1995).

Equation 2.7a was described by Engelund (1953) with a turbulent hydraulic conductivity (k_t) for the relationship for fully turbulent flow, $N = 2$:

$$i = \frac{V^2}{k_t} \qquad \textbf{Equation 2.8a}$$

with

$$k_t = \frac{1}{\beta_o} \cdot \frac{n^3}{1-n} \cdot g \cdot d_t \qquad \textbf{Equation 2.8b}$$

where k_t turbulent hydraulic conductivity (m^2/s^2)
β_o particle shape coefficient (= 3.6 for blasted/crushed rock)
n porosity
d_t characteristic dimension of material.

Current Norwegian practice states $d_t = 1.7 \times d_{10}$, although research currently being conducted in Norway (Hoeg *et al.* 2004) suggests that the standard practice should be updated to $d_t = 1.22 \times d_{20}$.

Table 2.1 estimates the minimum velocities necessary to achieve fully developed turbulent flow for various values of hydraulic mean radius from Hansen (1992). This calculation is based on McCorquodale *et al.* (1978) and uses Equation 2.1, assuming porosity, n = 0.45.

Table 2.1 – Velocities Required for Fully Turbulent Flow in Rockfill

Hydraulic Mean Radius	Minimum Velocity (m/s)
1 mm	0.2260
10 mm	0.0226
100 mm	0.0023
1000 mm	0.0002

2.6 SCALE

All models were constructed and the experiments conducted in accordance with Froude's model law (Jensen and Klinting 1983). The length scale of the model is λ, the time scale is $\lambda^{1/2}$, and the force scale is λ^3. As described by Jensen and Klinting (1983) when water flows through the porous material, some energy is

dissipated by heat. This dissipation is a function of hydraulic gradient. To obtain similitude between a hydraulic model and the prototype, it is necessary that the hydraulic gradients are identical in both cases (Jensen and Klinting, 1983).

2.7 PERMEAMETER EXPERIMENTATION

ASTM D2434, Standard Test Method for Permeability of Granular Soils (Constant Head) outlines the test method for determination of the coefficient of permeability by the constant head method for laminar flow through granular soils. Although flow through coarse porous media is transitional or turbulent, many of the fundamental considerations regarding a constant head permeameter were used in the design of the large-scale permeameter that was used in this research.

The ASTM standard requires that the minimum diameter of a permeameter be between 8 to 12 times that of the maximum particle size. During his literature review, Dudgeon (1964) located a paper that compared 'wall effects' to diameter and Reynolds number, using a correlation procedure and no direct measurement. Therefore, Dudgeon (1964) conducted explicit experiments for analysis of wall effects, and concluded that permeameter wall effects on coarse materials produced an average velocity increase of 5 to 10 percent. He also noted that this increase did not vary significantly with permeameter to particle diameter ratio ranging from 10:1 to approximately 5:1.

2.8 FLOW THROUGH DAMS

Wilkins (1955, 1956) performed experiments on crushed dolerite in packed columns and in a model dam. He was able to develop a method for sketching a turbulent flow net. In recent years, Garga *et al.* (1991) and Hansen *et al.* (1995) have developed relationships for flow through rockfill to allow the prediction of the stage-discharge rating curve and the location of the phreatic surface. As well, other authors have developed concepts to expand understanding of flow through conditions in these structures.

Hansen *et al.* (2005) identify three important design criteria for flow-through rockfill structures: the gross volumetric flow rate through the structure, the height of the seepage face associated with the flow, and which particle within the seepage face is the most unstable. The first two will be discussed below and the third in Section 2.9.

2.8.1 Stage – Discharge Rating Curve

The stage-discharge rating curve presented by Hansen *et al.* (1995) is an empirical equation obtained from experimental data. In developing the stage-discharge equation (Equation 2.9), the aspect ratio of each dam and the relative upstream water level were of key importance.

$$i_{eff} = 0.8 A_R^{-3/2} \left(\frac{h}{H} \right)^{1.4} \qquad \textbf{Equation 2.9}$$

where (see Figure 2.4),

$$A_R = \frac{1}{H}\left(B_u + B_c + \frac{1}{2}B_d\right)$$

i_{eff} is the effective hydraulic gradient [-]
h is the upstream water level [m]
H is the height of dam [m]
A_R is the aspect ratio of the embankment [-]
B_u is the width of the upstream slope [m]
B_c is the width of the crest portion [m]
B_d is the width of the downstream slope [m]

Hansen *et al.* (1995) discuss six non-Darcy flow equations and present Wilkins' (1955) equation (Equation 2.10) as being favoured by the mining industry.

$$V_V = W\, m^{0.5}\, i^{0.54} \qquad \textbf{Equation 2.10}$$

where V_V is the velocity in the voids ($V=V_V \cdot n$) [m/sec]
n is the porosity of the media [-]
W material-dependant coefficient [$m^{0.5}$·sec]
m is the mean hydraulic radius [m]
i is the hydraulic gradient [-]

W is 5.243 $m^{0.5}$·sec for crushed rock. Equation 2.10 requires determination of the hydraulic mean radius, which for well-graded material is difficult to determine. If Equation 2.10 is solved for hydraulic gradient, similar to that of the Equation 2.7a, the exponent (N) on V is approximately 1.86. As discussed previously, N depends on the level of turbulence and therefore Wilkins' equation would only apply to one level of turbulence. If the data is available, a hydraulic gradient versus bulk velocity relationship can be determined using Equation 2.7a, and therefore Wilkins' (1955) equation would not be required.

Equation 2.7a, Equation 2.10 or equivalent can be applied to Equation 2.9, thus developing a relationship between discharge (a function of velocity) and upstream water level.

2.8.2 Pore Pressure Modeling

Wilkins (1955) used a simplified version of Equation 2.10 to construct turbulent flow nets. Pore pressures at any location can be estimated from the flow net. As well, if the parameters are known, the discharge through the structure can be estimated.

A finite element modeling computer program, such as GeoStudio developed by Geo-Slope International Ltd., can be used to model the flow and piezometric head through a rockfill structure. The finite element program can also be used to model the phreatic surface and exit height within a structure. The above-mentioned software was designed and intended to use Darcy's Law, and hence is valid only in a laminar flow regime.

Townsend *et al.* (1991) applied finite difference expressions associated with Darcy's Law for edge nodes, and found that the method provided a workable model for piezometric head, even though flow was actually nonlinear. However, Townsend *et al.* (1991) concluded that the mean absolute deviation in pore pressures between non-Darcy and laminar flow was less than 10%.

2.8.3 Seepage Face Exit Height

The area that water exits the downstream slope of a dam is referred to as the seepage face and the upper most height of the seepage face is called the exit height. The height of the seepage face may be above the downstream water level as it is generally independent of downstream levels (Hansen 1995). Water will flow down the face of the dam until it reaches the height of the downstream water level. As well, flow through the dam will be exiting along the length of the overflow, producing a wedge of water.

Hansen *et al.* (2005) calculated exit height by applying Equation 2.10 and assuming the angle of the exit gradient beneath the seepage face may be approximated by the angle θ of the dam toe. Assuming a rectangular channel cross-section and $Q = VA = nV_V \; y_{exit} L$:

$$y_{exit} = \frac{Q}{nLWm^{0.5}(\tan\theta)^{0.54}} = \frac{q(\cot\theta)^{0.54}}{nWm^{0.5}} \qquad \textbf{Equation 2.11}$$

where,

y_{exit}	is the seepage face exit height	[m]	
Q	is the total discharge	[m^3/s]	
n	is the porosity	[-]	
L	is the length of the dam	[m]	
W	is Wilkins' coefficient		[0.83566 $m^{0.5}$·s]
m	is the hydraulic mean radius	[m]	
θ	is the angle of the dam toe	[°]	
q	is the discharge per unit length of dam	[m^2/s]	

Hansen *et al.* (2005) note that the true angle of the exit gradient is dependant upon the relative exit height. For non-Darcy flow in a crushed limestone, Hansen (1992) defined a new term, the effective flow angle θ_{ff}, as:

$$\frac{\theta_{ff}}{\theta} = 1.41\frac{y_{exit}}{H} + 0.17 \qquad \textbf{Equation 2.12}$$

where,

θ_{ff} is the angle of the emergent flow field [°]
θ is the angle of the dam toe [°]
H is the height of the dam [m]

Equation 2.12 was found to work best if $y_{exit} < 0.5H$.

2.9 Particle Movement

Near the exit height of a rockfill dam, particles are subject to partially submerged flow through seepage. Particles at the base are submerged and subject to overflow of nearly all the flow conveyed through the structure. Particles in the seepage face between the above two extremes, will be submerged and subject to both overflow and flow through seepage. Hansen *et al.* (2005) postulated that the most unstable particle will reside somewhere within the seepage face. There are three primary forces relevant to this particle: the overflow hydraulic forces, the flow through seepage force and the submerged weight of the particle (Figure 2.5).

The approach taken by Hansen *et al.* (2005) for assessing the possibility of the initiation of motion is based on moment equilibrium of the above-mentioned

forces. Hansen *et al.* (2005) assumes that given the arrangement of particles on the downstream face is quite erratic, no constraint of the particle in question is provided by particles in the same plane. The overall factor of safety (FS) of the particle is

$$FS = \frac{\text{stabilizing moment}}{\sum \text{destabilizing moments}} \qquad \textbf{Equation 2.13}$$

Hansen (1992) identifies seven forces potentially acting on a single rock residing on the downstream face of a flow-through rockfill dam. These are:

i. Shear due to overflow
ii. The force due to seepage
iii. Drag force due to overflow
iv. The buoyant weight of the particle
v. The hydrodynamic lift
vi. The frictional resistance underneath the particle
vii. The constraining effect of adjacent particles.

In his analysis, Hansen (1992), omitted v., vi. and vii.

Hydrodynamic lift is difficult to quantify and Hansen (1992) found that the broad range of lift coefficients, from negative values to values as high as unity, provided no guidance. A basic assumption of Hansen (1992) was that the initiation of motion was by rotation, therefore frictional resistance underneath the particle was not necessary. The constraining by adjacent particles was omitted as the configuration of the rockfill may leave particles unconstrained.

Hansen *et al.* (2005) identified the destabilizing hydraulic forces (F_{hyd}) acting on a single particle within the seepage face as the shear force, the drag force, and the hydrodynamic lift. Hansen *et al.* (2005) neglected the hydrodynamic drag force as small compared to other particle-destabilizing effects and as difficult to quantify. On a rough and irregular rock, with many voids adjacent, hydrodynamic lift effects are highly variable and could possibly be negative or positive. The effects of the shear and drag forces are accounted for in the coefficient C_D in the following expression:

$$F_{hyd} = C_D \rho (L \cdot y_{exit}) \frac{U^2}{2} \qquad \textbf{Equation 2.14a}$$

where,

F_{hyd}	is the hydraulic force	[N]
C_D	is drag coefficient	[dimensionless constant]
ρ	is the fluid density	[1000 kg/m^3]
L	is the length of dam	[m]
y_{exit}	is the seepage face exit height	[m]

$$U = \frac{Q}{(L \cdot y_{exit}) * n} \qquad \textbf{Equation 2.14b}$$

and,

U	is the uniform flow field velocity	[m/s]

If it is assumed that half of the particle in question is completely exposed, the length of the destabilizing moment arm could not be more than $d/2$. The destabilizing hydraulic moment is the product of F_{hyd} and $d/2$.

Hansen *et al.* (2005) define the destabilizing seepage force as:

$$F_{seep} = \forall_p (1+e)\gamma_w i \qquad \textbf{Equation 2.15}$$

where,

$\forall_p$ is the particle volume [m^3]
γ_w is the unit weight of water [kg/m^3]

Hansen *et* al. (2005) rationalize Equation 2.15 as the product of the unit weight of the water moving through the medium and the applicable hydraulic gradient. The term $\forall_p(1+e)$ represents the bulk volume occupied by a particle within the porous medium and must be of a representative size.

The moment arm for the seepage force is

$$L = \frac{d}{2}\sin\xi \qquad \textbf{Equation 2.16}$$

where,

ξ is the angle of the seepage force, measure below the plane of the downstream face [°]

The stabilizing moment for the submerged weight of a particle is

$$M_{stab} = (\gamma_p - \gamma_w)\forall_p \frac{d}{2}\cos\theta \qquad \textbf{Equation 2.17}$$

where,

γ_p is the unit weight of particle [kg/m^3]

Hansen *et al.* (2005) assumes outward rotation about the point of contact, assuming idealized spheres (Figure 2.6), between the particle in question and the one immediately below. Hence there will be no sliding resistance between

the moving particle and adjacent particles. In a flow-through structure, the particle under the seepage-face that has the greatest destabilizing moment induced by the flow through seepage, will generally be the most unstable one (Hansen *et al.* 2005).

Leps (1973) indicated that a minimum downstream slope of 1V:1.4H should be used for impermeable upstream facing rockfill structures. Leps (1973) noted that the amount of flow through the rockfill from overtopping of the impermeable facing did not destabilize the rockfill on the downstream face from observation at a number of existing dams.

Wilkins (1955) completed an analysis of the force on individual rocks and suggested relating piping velocity to the upward velocity required to keep a particle in suspension. Wilkins (1955) completed a limited number of experiments and found that the piping velocity was one half that required to keep a stone in suspension. Wilkins (1955) goes on to say that that the force on a stone varies approximately as the square of velocity and to provide adequate factor of safety (FS) reducing velocity by half, producing an approximate factor of safety of four. Wilkins concludes that there was no experimental evidence for his method.

Deep-seated failures are beyond the scope of this thesis and readers are directed to Garga *et al.* (1995).

2.10 CURRENT RESEARCH

The Research Council of Norway, EBL Kompetanse and a number of other domestic and foreign organizations sponsored the research program "Stability and Breaching of Embankment Dams". Part of the research was integrated with the EU-funded project IMPACT (Investigation of Extreme Flood Processes and Uncertainty). The IMPACT Project has allowed significant advances to be made in the understanding and modelling of a range of extreme flood processes including breach formation, flood propagation, sediment movement, modelling uncertainty and embankment integrity assessment. A description of the field experiments with figures, photos and definition of project objectives is presented in Höeg *et al.* (2004).

Twenty-three scaled model experiments were run in the laboratory and seven experiments on 6-m high embankment dams of different design in the field. The dams varied in cross-sectional geometry and material types, from clean rockfill to zoned earthfill. The field experiments were undertaken downstream of the Rössvatn Dam in Norway. The spillway gates, with a capacity of 450 m^3/s, feed directly into the test dam reservoir and made it possible to maintain a constant reservoir level even after dam breaching had started.

A dimensional analysis was performed by the Norwegian University of Science and Technology (NTNU 2003) producing Equation 2.18.

$$\frac{d_S}{y} = f\left(\frac{q}{\sqrt{gy^3\left(\rho_S - \rho/\rho - 1\right)}}, \frac{y_t}{y}, S_0, \frac{H_d}{y}, \frac{W_c}{y}, \frac{\rho_S}{\rho}, n, C_u, SH, \Phi\right)$$ **Equation 2.18**

NTNU then reduced the number of variables to be practical for the data obtained in their laboratory testing. They argue that the resultant functional relationship still contains the most important variables for defining the flow.

$$\frac{d_S}{y_{exit}} = f\left(\frac{q}{\sqrt{gy_{exit}^3}(S_S - 1)}, S_0, \frac{H_d}{y_{exit}}\right)$$ **Equation 2.19**

where,

d_S	is the rock diameter	[m]
y	is the flow depth	[m]
q	is the flow per unit width	[m^2/s]
g	acceleration of gravity	[m/s^2]
ρ	is the fluid density	[kg/m^3]
ρ_S	is the rock density	[kg/m^3]
y_t	is the tailwater depth	[m]
S_0	is the slope of dam face	[-]
H_d	is the dam height	[m]
W_c	is the dam crest width	[m]
n	is the porosity	[-]
C_u	is the gradation factor	[-]
SH	is the shape factor	[-]
P	is the packing factor	[-]
y_{exit}	is the exit height	[m]

An evaluation of the dimensional analysis was not completed at the time of the report (NTNU 2003) as it was outside of the scope of the project. Instead, an alternate equation, used by others (Abt and Johnson 1991 and Robinson *et al.* 1998) in evaluation of flow over rockfill in a steep chute, is proposed based on best-fit data from the laboratory and field.

$$d_{50,\,critical} = 0.43\, S_0^{0.43}\, q^{0.78} \qquad \textbf{Equation 2.20}$$

where,

$d_{50,\,critical}$	is 50th percentile diameter	[m]
S_0	is the slope of dam face	[-]
q	is the flow per unit width	[m^2/s]

NTNU (2003) conclude from their literature study and dimensional analysis that a parameter depending on a flow depth, e.g. the height of the phreatic surface exit point, should be included.

In the draft Canadian Dam Association (CDA) guidelines, presented at the 2006 CDA conference in Quebec City, rockfill dams are highlighted in Technical Practices T400; Section *2.0 Dam System* and *6.0 Other Dam Types*.

- Subsection *2.1 General*, highlights the basic requirements to ensure satisfactory earth and rockfill structures including deformation, controlling seepage, freeboard and spillway capacity.
- Subsection *2.4.2 Rockfill Dams*, defines rockfill, describes general construction methods and identifies reasons for use. This subsection also distinguishes between a flow-through rockfill dam and a rockfill dam with an impervious membrane.
- Subsection *6.5 Flow-Through Rockfill Dams*, states:

  "Flow through embankment dams are generally used to reduce the peak flow, but they are also used as spillways with various cross-sections including concrete-faced rockfills or in-built rockfills.

  In withstanding the Inflow Design Flood, flow-through rockfill dams should be designed to withstand the combined effects of the action of the flow through seepage emerging from and accumulating on the downstream face, as well as any overflow. The latter is that part

> of the IDF which cannot pass through the rockfill. The dam should withstand the stated combined effects without the movement of rock particles, whether singly or en masse. It is not recommended that the design allow for flow over the crest unless the downstream slope is designed to limit erosion. If the design of the downstream slope involves the use of metal or wire, the effects of the corrosion of the metal or wire on the life-span of the reinforcement must be considered. Allowance should also be made for the possible accumulation, over time, of debris on the upstream face of the dam. If this debris is not removed, it will reduce the quantity of flow that can pass through the embankment and correspondingly increase the flow over it. Frazil ice can have the same effect."

Within Technical Practices T400 are additional guidelines regarding rockfill dams, such as earthquake loading, which was not part of this thesis. Although the proposed guidelines are still in draft form, the capabilities and guidance for design of flow-through rockfill dams appear under-emphasized.

2.11 Justification of Large-Scale Permeameter and Scale Rockfill Dam Testing Program

The literature review indicates that flow through rockfill appears to be above the upper limit of validity of Darcy's law, and therefore an alternate form of velocity-hydraulic gradient relationship would apply. The evaluation of flow through coarse porous media, rockfill up to 150 mm in diameter, requires the use of a large permeameter and associated handling equipment. A number of studies have considered large rock but have been limited in the local material used, duration of test, size of sample volume and direction of flow. All flow through equations listed in this literature review are useful only for the narrow ranges of

particle characteristics and porosities for which they were developed. To obtain the constants required in the flow through equations, testing of local rockfill with a large-scale permeameter is required.

The ability to make predictions of flow rate and hydraulic gradients is required in flow-through rockfill dams. The stability of the rockfill defined as the initiation of particle movement due to flow through and associated wedge of overflow is related to the hydraulic gradient. Several methods for determination of the initiation of particle movement have been proposed, but have limited independent laboratory verification. The testing of laboratory scale dams permits the evaluation of proposed equations as well as assessment of the properties of the local rock.

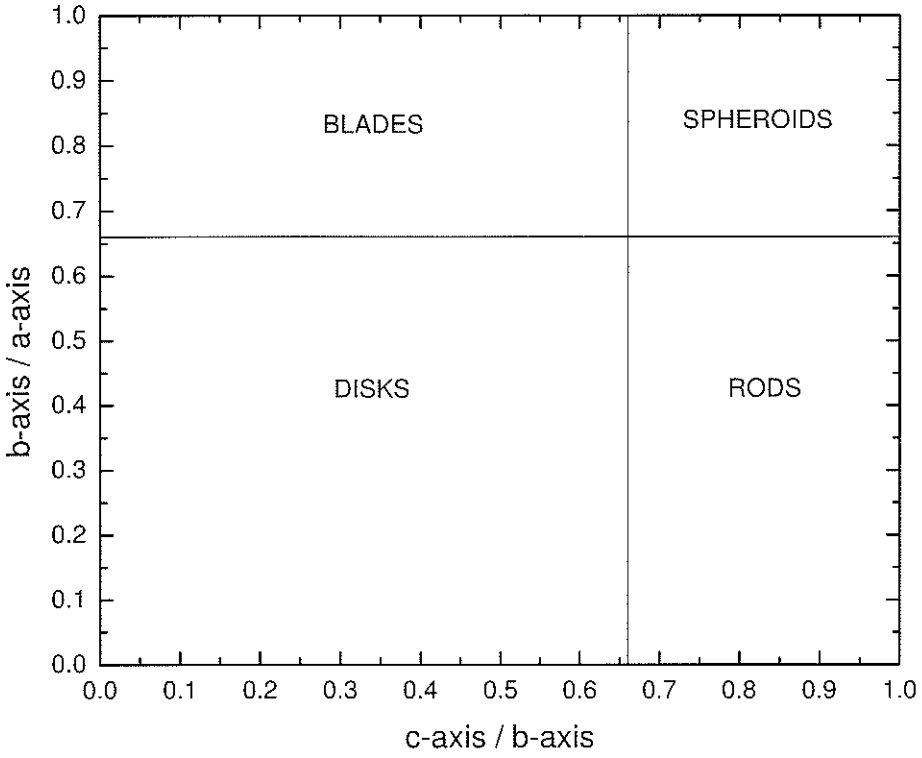

Figure 2.1 – Zingg Diagram (after Garga *et al.* 1991)

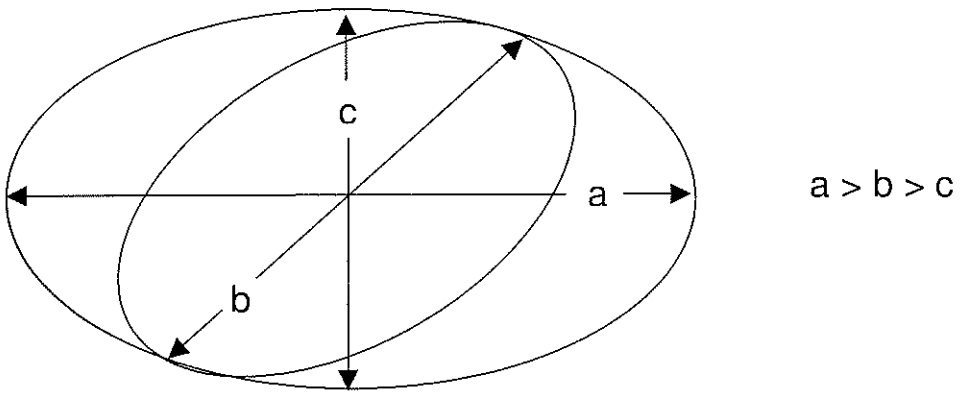

Figure 2.2 – Definition of Particle Axes (after Sabin and Hansen 1994)

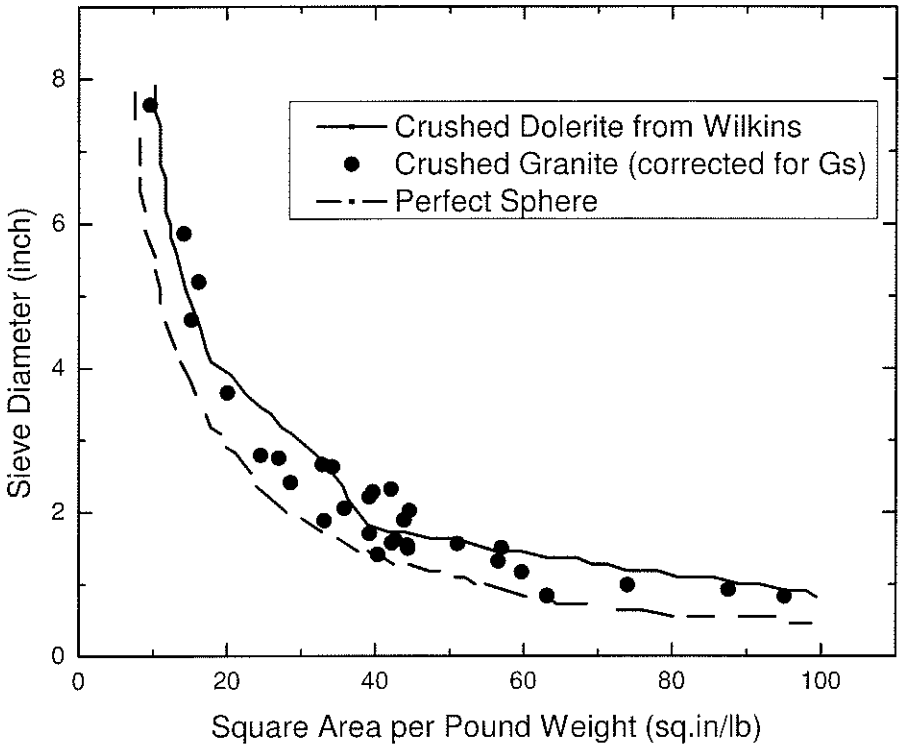

Figure 2.3 – Wilkins Comparative Relationship Surface Area of Angular Rock to Sieve Size

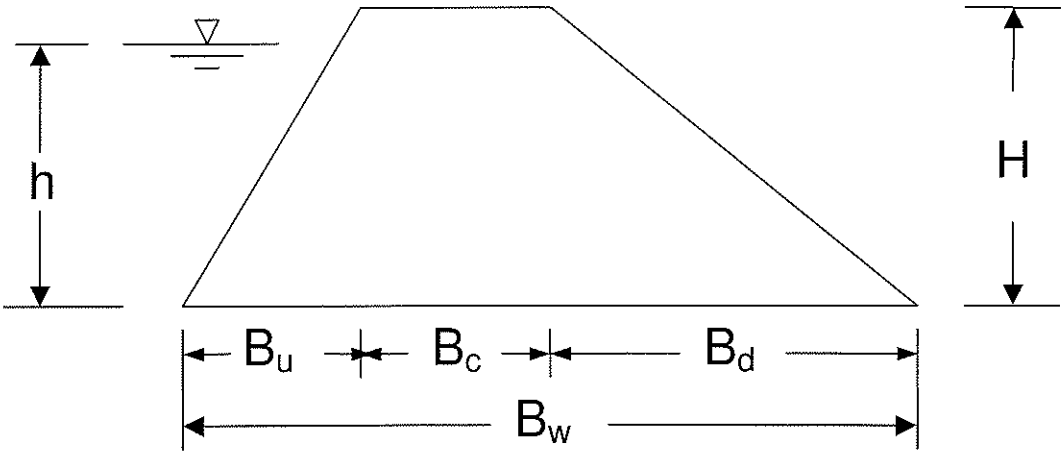

Figure 2.4 – Embankment Dimensions

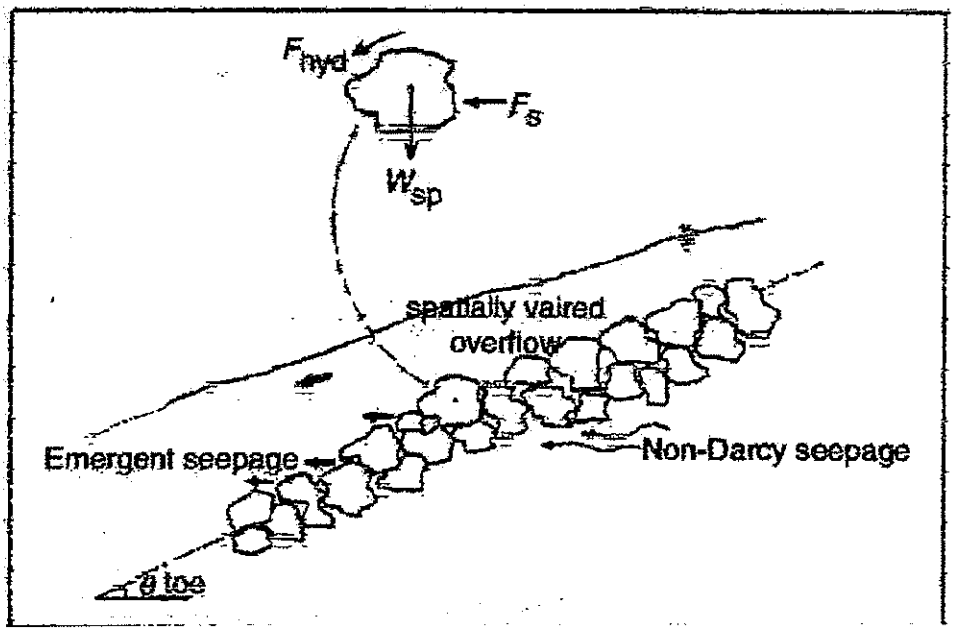

Figure 2.5 – Forces Acting on a Single Particle on the Downstream Face (after Hansen *et al.* 2005)

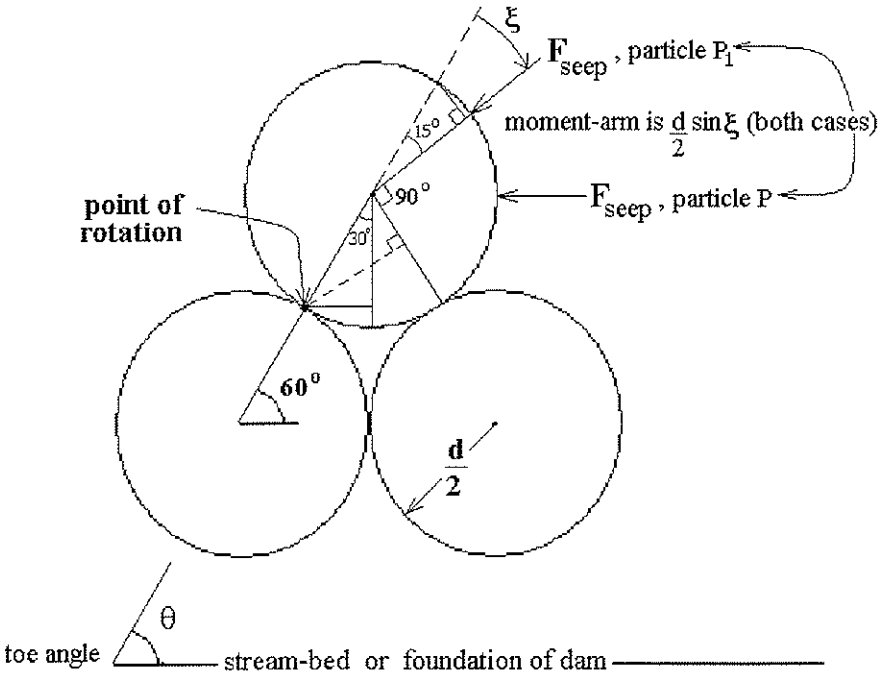

Figure 2.6 – Idealized Particle Position on the Downstream Face (after Hansen *et al.* 2005)

3 COARSE POROUS MEDIA

3.1 MATERIAL USED IN STUDY

The rock selected for the experimental program was granite bedrock from the Canadian Shield near the Winnipeg River in southeastern Manitoba. Manitoba Hydro stockpiled the material during previous construction in which a channel for a generating station was excavated. Figure 3.1 shows the shear wall of a previously blasted rock face in the area. The rock was selected as being representative of existing structures (Figure 3.2) and has potential use in future developments. The granite was excavated using blasting techniques and stored adjacent to the blast site (Figure 3.3). The material was typically angular, with a rough surface and random gradation.

3.1.1 Basic Properties

The rock used in the experimental program contained two distinct granitic materials. They can be identified by their colour: first a peppered black and white, and second a pink colour. As was often the case, individual particles of rock contained both coloured granites. A sample of each material was sent to the X-ray Diffraction Laboratory at the Department of Geological Sciences, University of Manitoba. The peppered black and white rock was a medium-grained rock composed of mainly of quartz, mica biotite and albite. The pink rock was medium-grained granite composed almost exclusively of quartz, microcline and albite.

Observationally, the peppered rock tended to fracture in a platy manner producing flat surfaces that fit in the blades category of the Zingg Diagram. The pink rock fractured in cubic shapes, thus maintaining a spherical shape, as described by the Zingg Diagram.

The basic properties of the granite are noted but only density was considered when comparing the rock and the laboratory results to that of other author's experiments and materials. The basic properties of the granite found in southeastern Manitoba in the Canadian Shield are listed in Table 3.1.

Table 3.1 – Basic Properties of the Granite Used in this Study

Density	2770 [kg/m^3]
Porosity	0.2 - 4 [%]
Absorption	0.1 - 0.4 [%]
Compressive Strength	240 [MPa]
Shear Strength	35 [MPa]
Elastic Modulus	40 - 70
Hardness (Moh's scale)	6.5

3.1.2 Specific Gravity Experiments

When calculating the mean hydraulic radius, the volume of the individual particles being examined was required. One result of this is the calculation of specific gravity using ASTM Standard C127. Using a number of samples the specific gravity of the granite tested was determined to be 2.68.

3.1.3 Scale of Material

To provide material for the laboratory program, a particle size distribution was selected to be representative of typical distributions found in existing rockfill structures operated by Manitoba Hydro. Manitoba Hydro employees measured the diameters of various rocks at and near the surface of a structure in a previous project to obtain the curve shown (Figure 3.4). The particle size distribution to be used in this study was selected to be the same shape as the measured curve while being reduced in scale to 1:10 at any given particle size. The target distribution was therefore simply shifted laterally. This produced a range of particle diameters of 10 mm to approximately 150 mm, as shown in Figure 3.5.

The material available for the research program, stockpiled adjacent to a Manitoba Hydro site, ranged from 10 mm to 1500 mm in diameter; the upper end being too large for laboratory experiments. Therefore, mechanical crushing and screening was completed by an aggregate crushing contractor. A jaw type crusher was used to reduce the material; it was then sorted with a screen system to achieve the specified particle size-distribution. Upon completion and approval via visual inspection, approximately 25 m^3 of rock was delivered to a service yard at The University of Manitoba.

An evaluation of the rock particles for particle shape and angularity, before and after crushing, was conducted using criteria outlined by Sabin and Hansen (1994) to ensure that the geometric properties of the crushed rock were

comparable to the original blast rock. The Zingg diagram, shown in Figure 3.6, was used to compare the shapes of the field observed rock and the laboratory material. The Zingg diagram consists of data for field-measured specimens, located on the downstream face of an existing rockfill structure, and material that had been reduced for the laboratory. Upon removal of some anomalies, the crushed rock conformed well to that of the parent blast rock. The predominant type of anomaly was a blade type particle shape (Sabin *et al.* 1994), which was not as numerous in the blast material. Due to the particle reduction method, a jaw crusher, larger rock particles tend to break down relatively flat. This was unavoidable given current local crushing practices.

3.2 Surface Area and Mean Hydraulic Radius

The surface area of the dominant particle in a flow-through rock mass is used to calculate the hydraulic mean radius. The surface area of an irregularly shaped angular rock particle is difficult to determine without extensive measurements. To develop a relationship between surface area and size of rock particle the Wilkins (1955) method was used. The surface area was sketched on paper and the area was quickly calculated using a drafting program.

To compare the data with the curve provided by Wilkins (1955), the results of this study were shifted to account for the difference in specific gravity (Wilkins-2.87 *vs.* this study-2.68) and then plotted. As shown in Figure 3.7, the surface area per weight of rock, for a given nominal size of stone, are comparable. This

allows quick determination of surface area and enables determination of hydraulic mean radius. The concern with this method as outlined in Garga *et al.* (1991) is the non-inclusion of the shape of the particles. Wilkins requires the assumption that the entire mass of rock involved will have a shape that is typical, *i*.e. few rods and flat discs.

Applying Equation 3.1 to calculate the hydraulic mean radius requires the dominant particle size, and from Figure 3.7 find the surface area per mass of rock (A_{ms}).

$$m = \frac{e}{A_{ms}} \qquad \textbf{Equation 3.1}$$

where e is the void ratio [-]

A_{ms} is the surface area per mass of rock [m^2/kg]

3.3 Drag Tank Analysis

3.3.1 Introduction

To evaluate the combined effects of surface roughness and angularity of individual rocks, a series of drag tank tests were conducted. Individual rock specimens were selected based on variability in size, shape, angularity, and perceived surface roughness. This produced a selection of 10 rocks.

To calibrate the testing, a smooth sphere (10 pin bowling ball) was tested in the same manner as the rocks. Details of the testing methodology and measurements are contained in the following sections.

3.3.2 Drag Tank Apparatus

The drag tank tests took place in the Hydraulic Research and Testing Facility (HRTF) in the variable slope flume. The flume dimensions are 14.0 m long, 0.945 m wide and 0.75 m deep. The maximum flow rate recommended was 0.38 cms. The flume had a floor of galvanized metal and glass sidewalls. Inlet flow was controlled with a butterfly valve while the outlet had motorized louvers. Although not utilized in the testing, the flume had a hydraulically controlled slope that was adjustable from 0.1 to 2%.

The depth of water was controlled with a louvered tailgate at the downstream end. Continuous water supply was provided by the constant head tank (refer to Section 4.2).

To measure velocity of the flow passing the experimental particles in the drag tank, a Kent Miniflo - Type 265 velocity probe was used. The probe was mounted 300 mm upstream of the particle and set at a height corresponding to the center of the particle, shown in Figure 3.8.

To measure the force applied to the particle, a strain gauge was attached at mid length to an aluminium bar. The bar was securely attached to an overhead

heavy steel angle member and extended into the flume. A threaded hole was used to attach the specimen to the end of the bar. Specimens were drilled with a 7 mm diameter hole, into which a 6 mm diameter threaded rod was secured using epoxy glue. As shown in Figure 3.9, the rod extended out of the rock up to 25 mm. This was threaded into the bar creating a rigid connection. With this configuration the specimens were suspended on average 250 mm above the floor of the flume. See Figure 3.8 for a photo layout. The strain gauge was calibrated, creating a linear stress-strain relationship, using a set of calibration weights. The strain gauge was monitored with a Measurements Group Instruments Division P-3500 Strain Indicator as shown in Figure 3.10.

A digital camera with a specially constructed stand was used to capture images of the specimens tested. The images were used to calculate the projected upstream surface of each face of the specimen with the use of the computer software AutoCAD, example shown in Figure 3.11.

3.3.3 Test Procedure

The rock specimens were carefully inspected to assess and label the faces, generally at 60-degree rotations, that would be projected into the flow. During each test the water velocity was altered by controlling the volume flowing through the flume and adjusting the louver gates to maintain water surface elevation. When the velocity and water level reached a steady-state condition, the specimen was rotated to each pre-determined face, and measurements of the

Kent probe and strain gauge were taken. This was completed for a range of velocities. Water height was controlled such that the specimen remained completely submerged during each velocity increment and allowing no more than 25 mm of water height on the strain gauge bar.

To calibrate the test method, apparatus, and test results, a smooth sphere (10 pin bowling ball) was tested. The bowling ball was selected for its spherical shape, polished surface (minimal roughness), similarity of density to that of granite, and the size, approximately 127 mm in diameter, being within the range of the rock specimens tested.

3.3.4 Results and Applications

Upon completion of a test, the measurements were converted using the appropriate calibrations, providing results in terms of velocity (m/s) and force (N). Importing the images of each face into AutoCAD the projected surface area was traced and calculated with the area function. This value was calibrated by the addition of a measuring stick placed next to the specimen for scale is shown in Figure 3.11

Data was plotted between CD and Reynolds number. The Reynolds number for open channel flow passing a particle is:

$$\mathrm{Re} = \frac{L\rho V}{\eta}$$ **Equation 3.2**

where,

Re	is the Reynolds number [-]	
L	is the characteristic length of the body along direction of flow [m]	
η	is the dynamic viscosity of the fluid	[N·s/m^2]
ρ	is the density of the fluid	[kg/m^3]
V	is the velocity	[m/s]

Drag tank testing was carried out on the smooth sphere on two separate occasions for confirmation of repeatability. The diameter and projected surface area of the smooth sphere were known, allowing comparison to the method of finding the projected area using imaging and AutoCAD, proving that the technique was practical.

The results of the smooth sphere are located on Figure 3.13, in terms of Reynolds number (R_e) and drag coefficient (C_D). The trend of the data can be represented as a curve over the region the data is presented. The data, when compared with that of the generally accepted standard drag curve for a sphere (Bailey, 1974), is approximately the same in absolute value and shape of trend. Therefore, the smooth sphere shows that the drag tank tests perform well to standard practice.

The drag coefficient of the angular rock (Figure 3.14) has a range of values, with a trend similar to that of the calibration sphere. Because the rocks are variable in angularity and surface roughness, data points vary over a range of C_D at the

same Reynolds number. The data in Figure 3.14 can be broken into four (4) regions by Reynolds number when comparing to the calibration sphere.

The first region, with data appearing with a black outline and white body, labeled 'Uncertain Data' was generated with measurements from the strain gauge at the extreme low end of the strain gauges measuring range. This condition occurred in only 3 rocks, and it is uncertain whether the plotted results are a function of the inability to accurately measure the strain induced by the force of water on the rocks. These points do not fit the trend of all other data and have been removed from the discussion below.

At low Reynolds numbers, less than 25000, the C_D of the rock generally exceeded the calibration sphere data. The wake of the angular rock in laminar flows (low Reynolds number) will be larger than for a sphere of the same average diameter. This large wake maximizes the region of low pressure and, therefore, results in the maximum difference in pressure between the front and rear faces.

At the larger Reynolds numbers, between 35000 and 55000, data points from the rocks are found on either side of the plotted calibration sphere data. The rocks achieved a turbulent flow regime at lower Reynolds numbers, approximately 35000, decreasing the size of the wake and reducing the C_D. The calibration sphere does not achieve a complete turbulent boundary layer over the range of this test, and as can be seen in Figure 3.13, C_D is still decreasing at

Re = 120,000. Some of the data still plots above the calibration sphere because of the angularity and surface roughness factors attributed to C_D.

At Reynolds numbers greater than 60000, C_D of the rocks is generally greater than that of the calibration sphere. The higher C_D is due in part to the high surface roughness of the rocks and the angularities causing local wakes, relative to the smooth calibration sphere.

The C_D values obtained from this experimentation generally agree with intuition and compare well in magnitude and trend to that of previously published values. When selecting a value of CD for use in analysis of initiation of particle movement (Chapter 7) on the seepage face, the variability of angularity, shape, surface roughness, and local flow velocity requires that a range of C_D be considered to represent the range of particles.

Figure 3.1 – Previously Blasted Rock Face Adjacent to an Existing Rockfill Structure

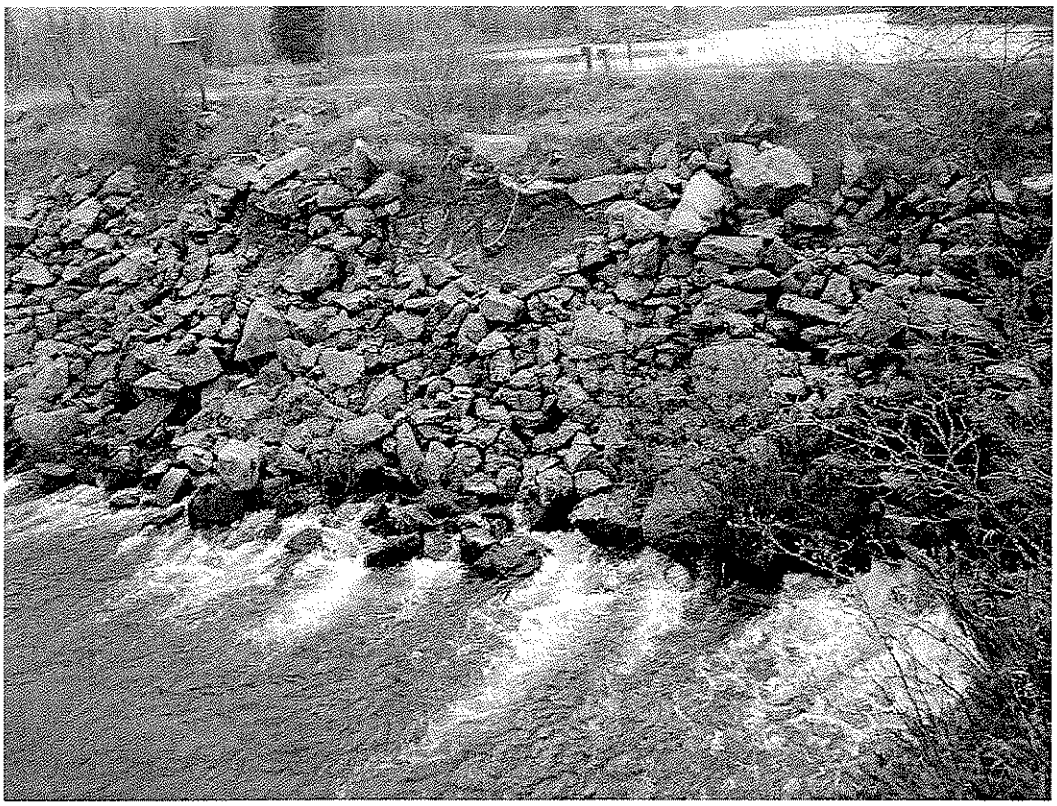

Figure 3.2 – Existing Rockfill Structure

Figure 3.3 – Stockpiled Blast Rock at Manitoba Hydro Site

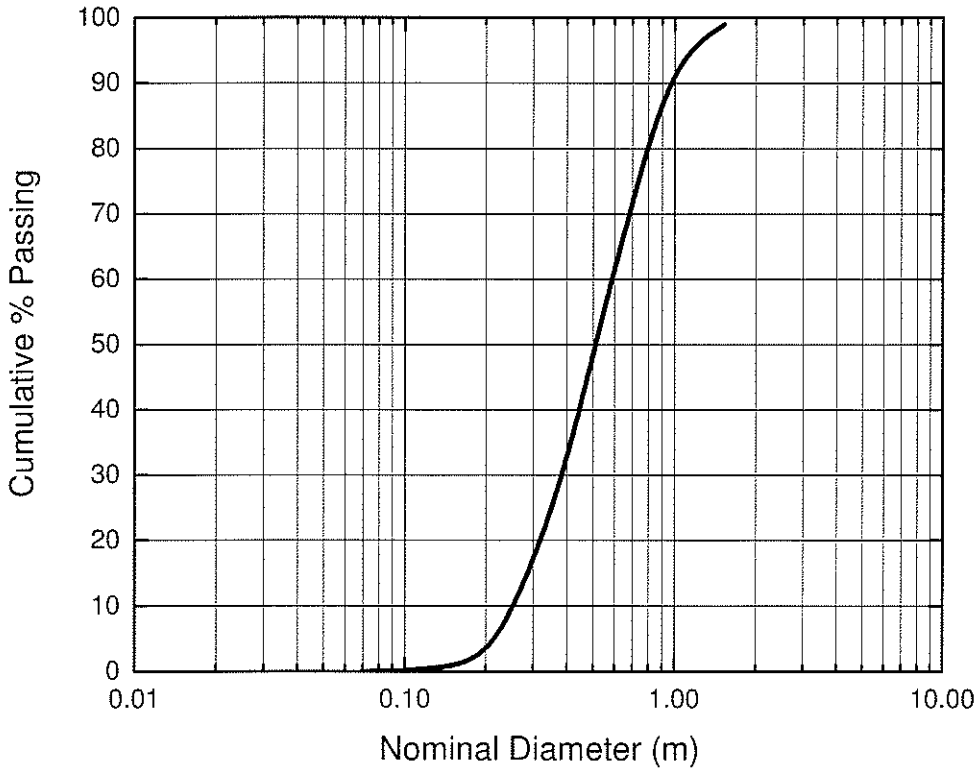

Figure 3.4 – Field Measured Grain Distribution on Downstream Face of Dam

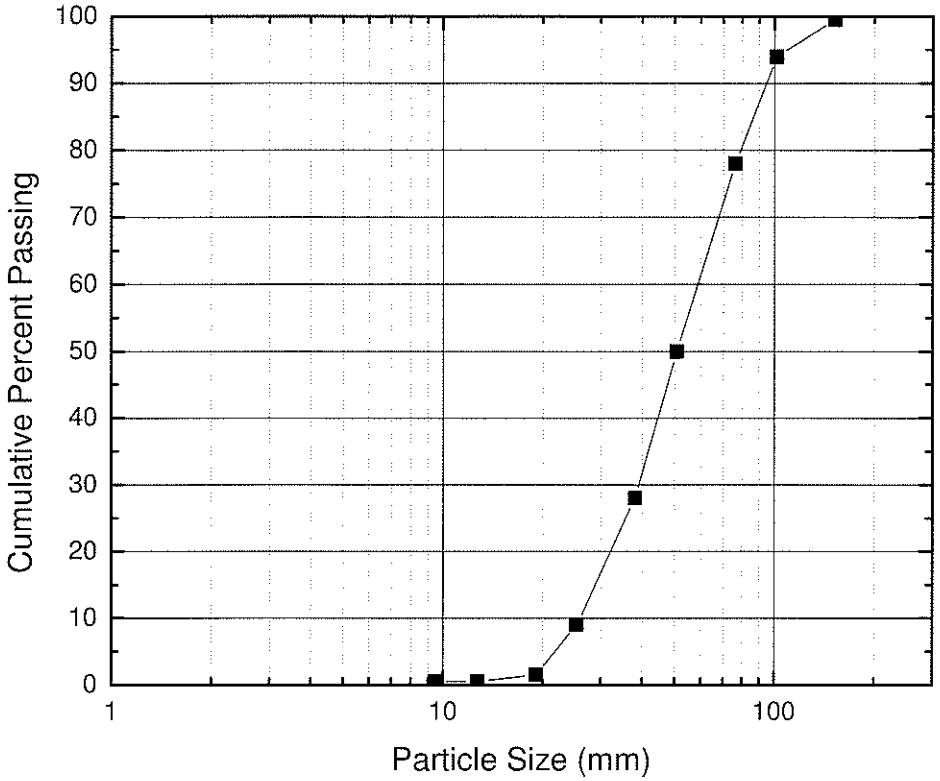

Figure 3.5 – Laboratory Scale Approximation of Field Measured Grain Distribution

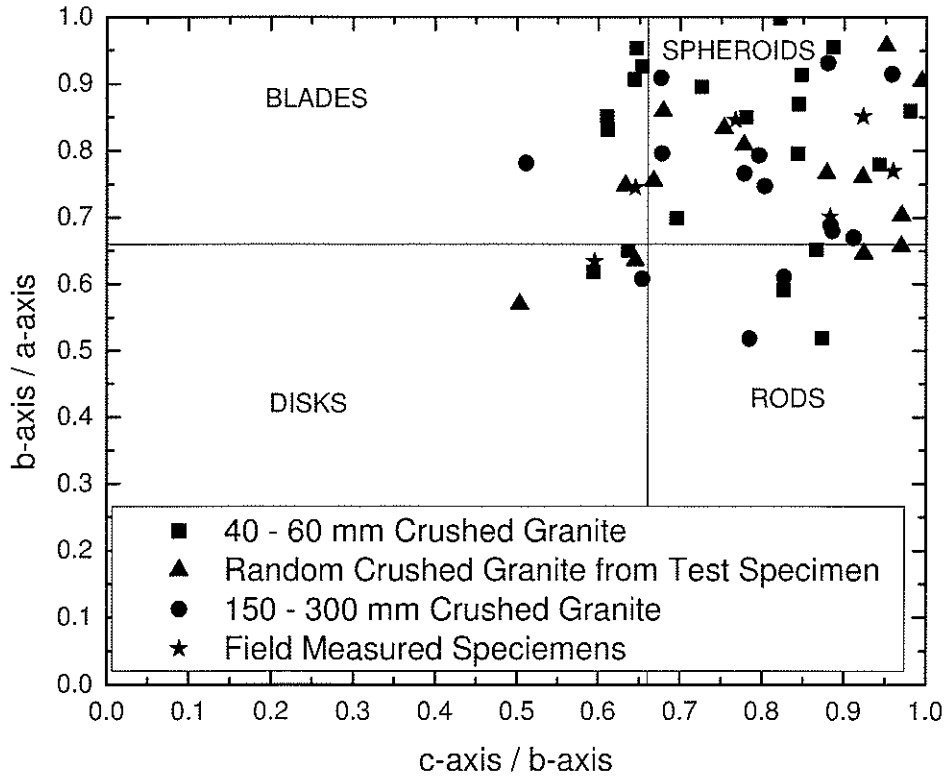

Figure 3.6 – Zingg Diagram for Field Rock and Crushed Laboratory Rock

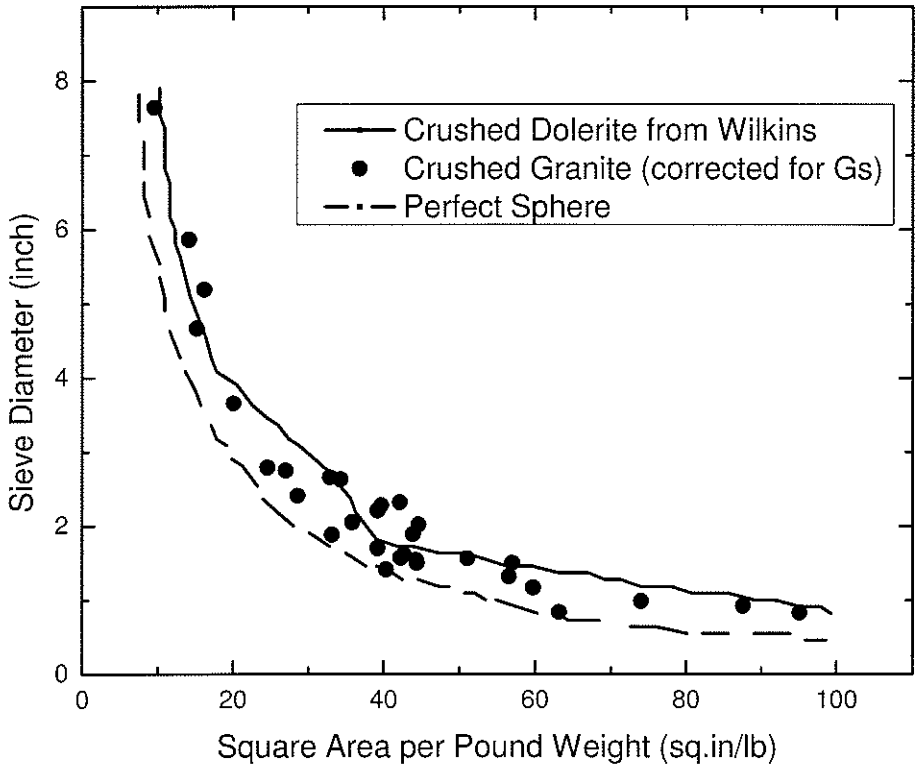

Figure 3.7 – Comparison between Wilkins and this Study

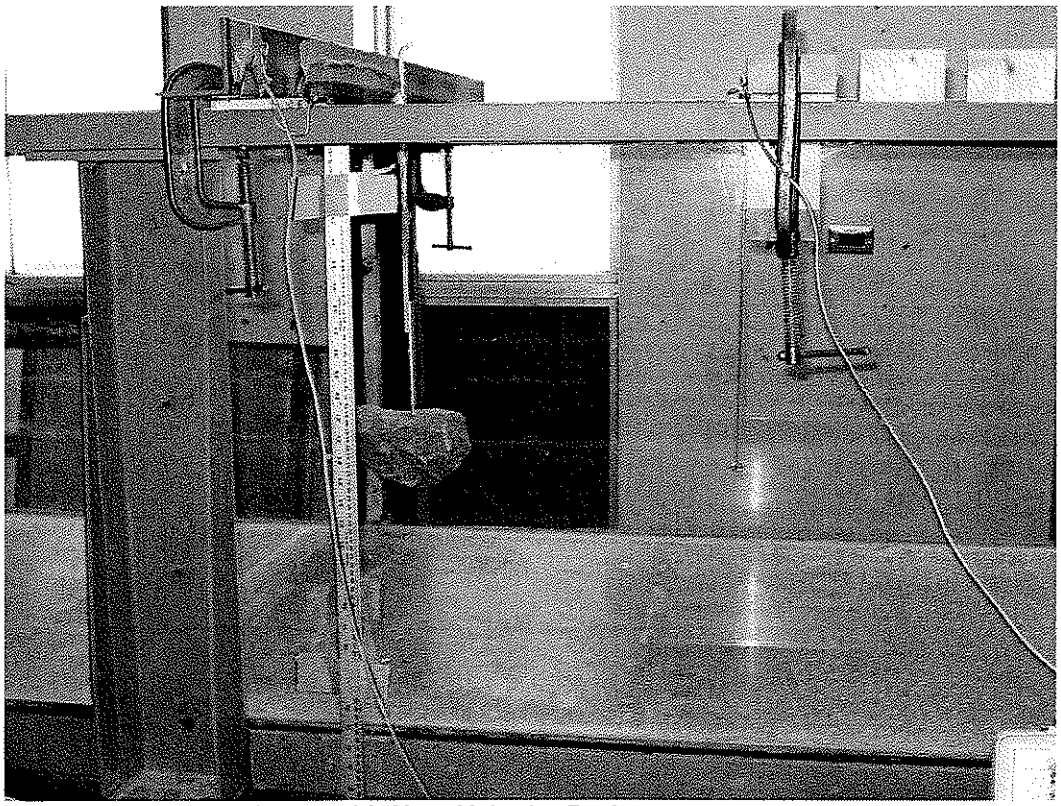

Figure 3.8 – Drag Tank Setup with Kent Velocity Probe

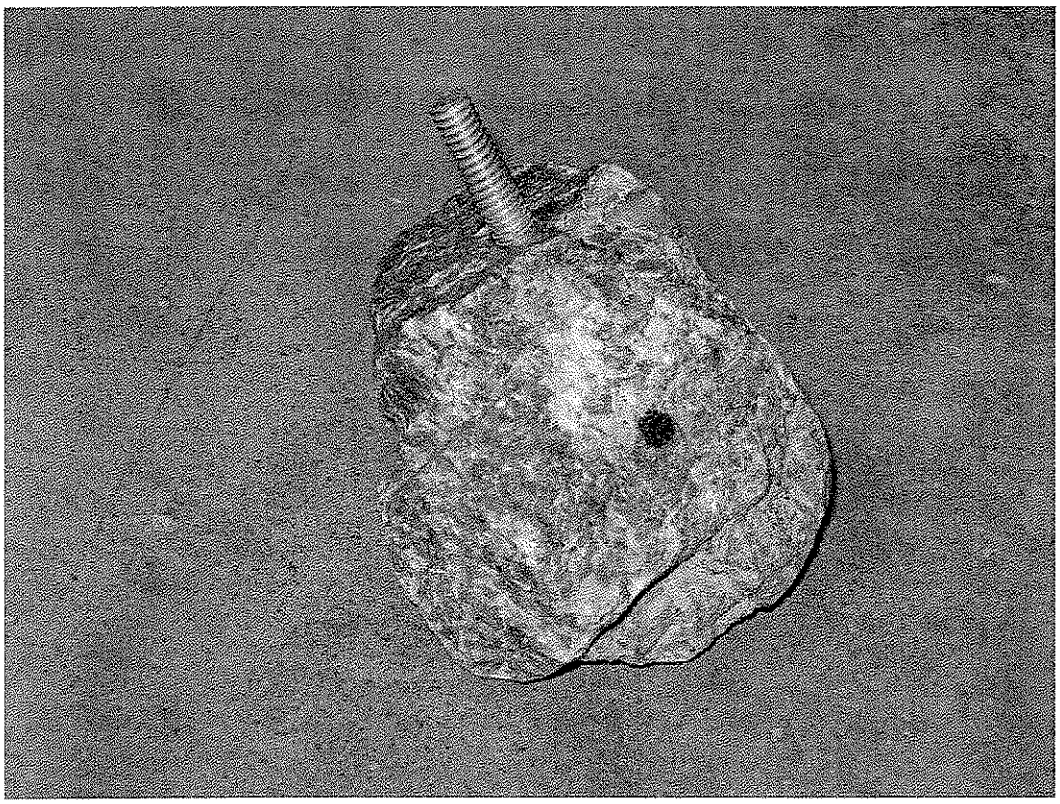

Figure 3.9 – 65 mm Diameter Specimen with Threaded Rod

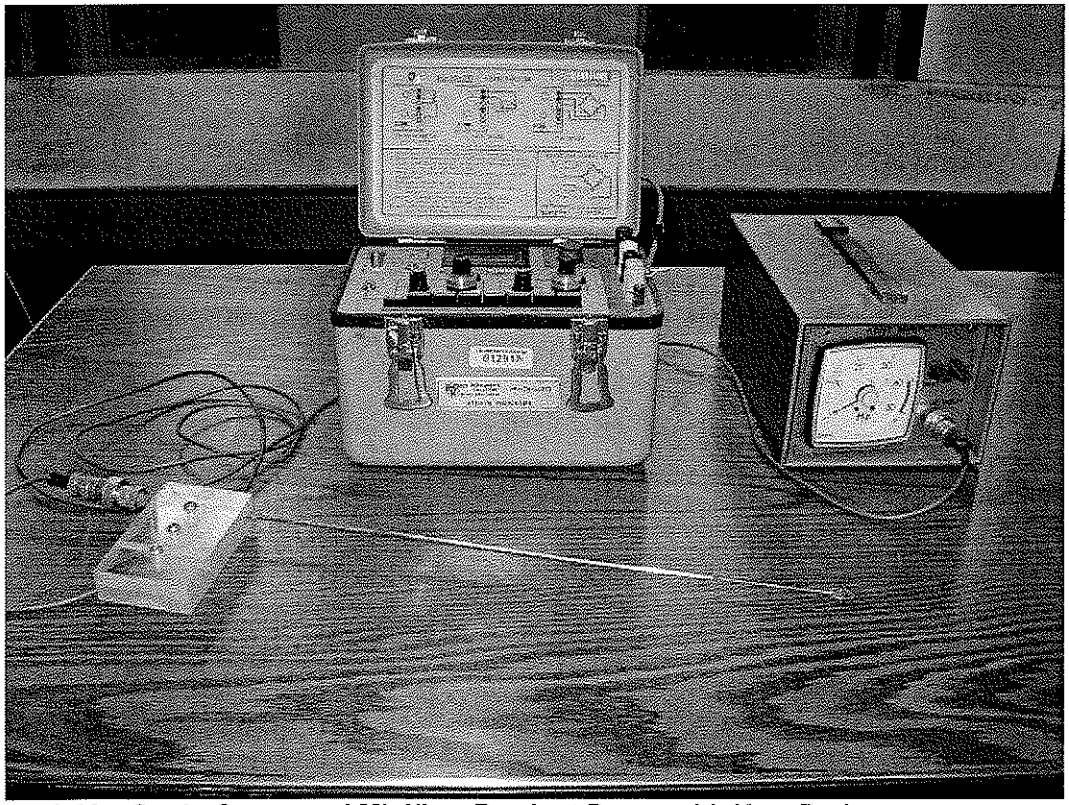

Figure 3.10 – Strain Gauge and Miniflow Readout Boxes with Kent Probe

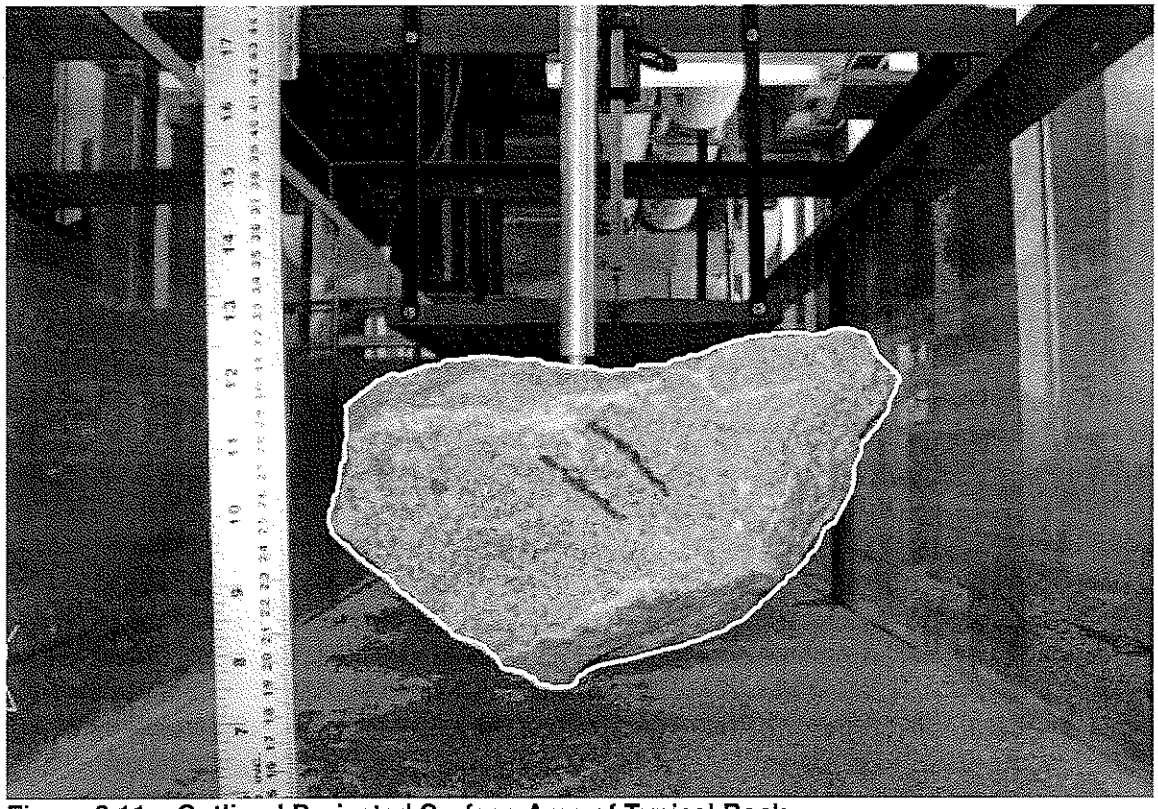

Figure 3.11 – Outlined Projected Surface Area of Typical Rock

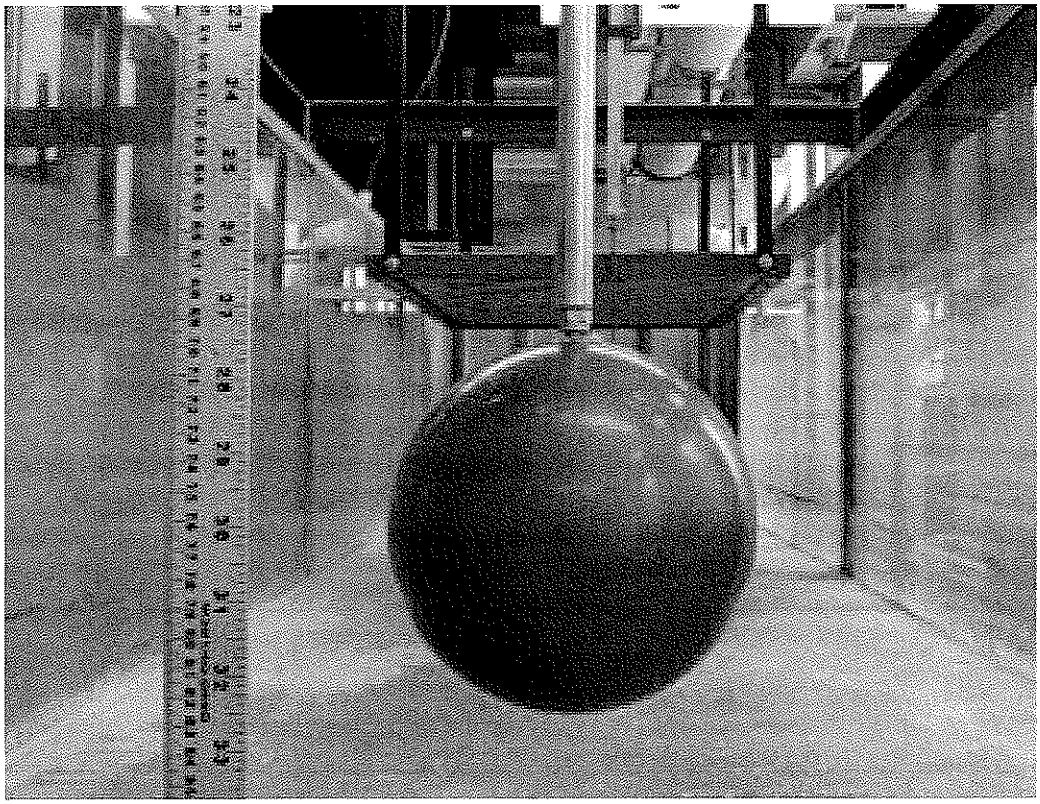

Figure 3.12 – Smooth Sphere for Calibration

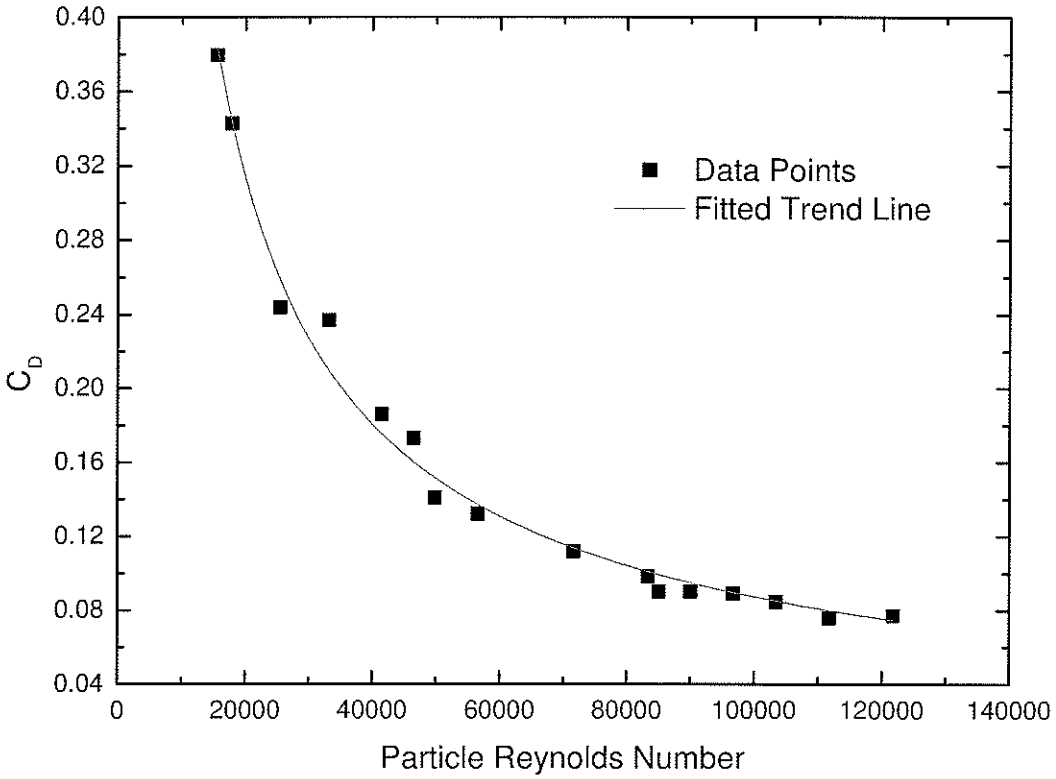

Figure 3.13 – Calibration Sphere Drag Coefficient

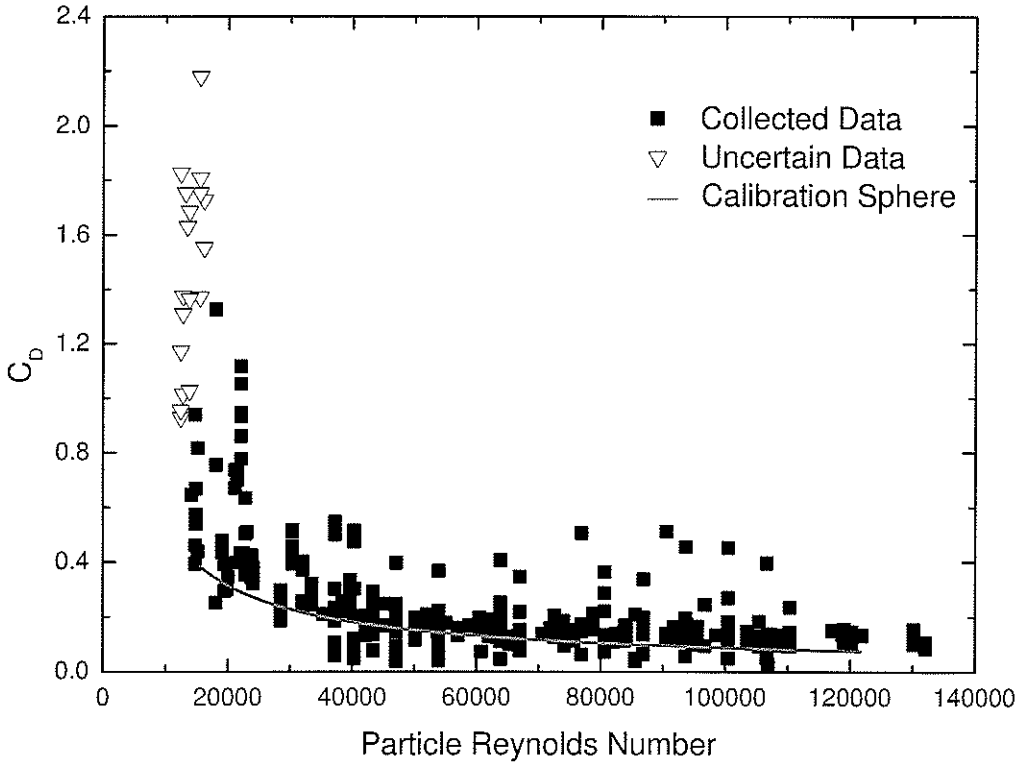

Figure 3.14 – C_D of the Coarse Porous Media in this Study

4 LARGE-SCALE PERMEAMETER

4.1 GENERAL

A permeameter is intended to determine the coefficient of permeability for laminar flow of water through soils. Due to the size and geometric nature of rockfill, the flow of water may not be laminar. The use of a large-scale permeameter permits the assessment of flow through coarse rockfill.

Wilkins (1955), Dudgeon (1964), McCorquodale *et al.* (1978), Martins (1990) and others have undertaken laboratory experimentation to determine the hydraulic properties of coarse rockfill and flow conditions in rockfill dams. Many methods have focused on developing scaling relationships (Venkataraman *et al.* 1998) and numerical models (Scheidegger 1974) for assessing hydraulic properties and flow conditions. Although these studies have provided significant insights into the hydraulic performance of rockfill dams, there is still need for quantitative physical measurements of the hydraulic properties and flow conditions. Few studies (Dudgeon 1965, Wilkins 1955) have used a large-scale permeameter apparatus to determine specific hydraulic properties. This section presents the design and construction of a large-scale permeameter with specific features that allowed evaluation of the hydraulic properties of rockfill up to 150 mm in diameter.

4.2 DESCRIPTION OF THE HRTF

The HRTF is located in the Engineering and Information Technology Complex at The University of Manitoba. With a mezzanine level and lower level, the floor space available for hydraulic models is 650 m^2. All testing detailed in this thesis was conducted in the HRTF. The HRTF had a closed loop water system, with a storage tank, two electric pumps, a constant head tank, PVC pipe distribution, and in-floor return drains. Some of the permanent structures contained within the facility are the volumetric tanks, variable slope flume, random wave-sediment flume, and a counter-rotating ice flume. Temporary structures of interest are the mini dam flume, as well as the scale dam flume. Figure 4.1 shows the HRTF layout with the locations of all listed structures. The water handling equipment is described below, while the different testing structures are described in various chapters where appropriate.

4.2.1 Constant Head Tank

The constant head tank had a capacity of 20 m^3 with excess supply water drained by 80 m of sharp crested weir. Two pumps provide 0.5 cms (500 l/s) of flow, via the storage tank. Flow from the constant head tank was distributed via 350 and 400 mm PVC pipes, and precise adjustments of flow were controlled with butterfly valves. Water not being used and hence circumventing the head tank over the sharp crested weir was diverted through one of two calibrated volumetric tanks and finally to the storage tank.

4.2.2 Volumetric Tanks

When measurement of flow through an apparatus was required, the two volumetric tanks were used. Prior to providing flow to one of the HRTF's testing structures, measure volumetrically the total flow rate of the supply pumps using the volumetric tanks. During testing when water flows through an apparatus, measuring the bypass water volumetrically and subtract this from the total flow rate of the supply pumps, thus establishing the flow passing through the apparatus.

4.3 Description of Large-Scale Permeameter Apparatus

4.3.1 General

The permeameter apparatus was housed within the HRTF. The permeameter was connected to the recirculation system, which allowed experiments to be conducted continuously for several hours.

The design and construction of the large-scale permeameter was completed through an iterative process in cooperation with the research partners. It was designed to meet the following criteria:

1. the ability to carry out permeability experiments on gravel-sized to cobble-sized (150 mm) porous media;
2. the ability to vary the hydraulic gradient and velocities over a broad range, from near-laminar to fully-developed turbulent flow conditions;

3. the ability to monitor initiation-of-particle movement at the top of the packed rock column.

4.3.2 Design and Construction

4.3.2.1 Permeameter Diameter

As mentioned in Section 2.8, ASTM Standard D 2434 outlines specimen cylinder diameter to particle size diameter of approximately 10:1, while research by Dudgeon (1964) suggests wall effects will not be excessive for specimen cylinder diameter to particle size diameter of 5:1. The d_{50} of the rock used in the laboratory experimental program was approximately 50 mm, therefore the minimum diameter of the permeameter, from the ASTM standard, was 500 mm. The upper limit of particle diameter was approximately 150 mm, which at 5:1 called for a permeameter diameter of 750 mm. Based on availability, a 760 mm diameter PVC pipe with a 25 mm thick wall was selected. Originally intended as sewer pipe, the pipe was cut to length with a circular saw removing the belled end. At the other end was a tapered edge that could be considered a sharp-crested weir for calculation of flow.

4.3.2.2 Direction of Flow

When considering flow direction, measurements to be obtained, comparisons to rockfill structures and hydraulically driven particle movement contributed to the decision.

In a flow-through rockfill structure, hydraulic gradients are generally low (less than 1) and the upper limit of the gradient is controlled by the stability of the structure. Therefore, the measurement of hydraulic gradients greater than that found in local rockfill structures was deemed to be unnecessary. The ability to measure movement of rock particles or of the whole rock column would provide an indication of the hydraulic forces acting in and on the rock column. Thus an upward flow direction was selected for the permeameter.

Given that an upward flow direction was selected, consideration was given to ensure that the HRTF laboratory had adequate flow capacity and that a sufficient head difference between the top of the permeameter and constant head tank could be developed. As will be highlighted in the following section, the design of the permeameter considered the head difference, and when constructed the top of the permeameter relative to the constant head tank was able to develop 3.1 meters of head.

4.3.2.3 Rockfill Column Length

The design allowed for a sample length of 1.5 m, which corresponded to approximately 0.7 m^3 of rockfill. The length was selected to be twice the diameter of the pipe while minimizing the weight of rockfill material used in each test. The relatively short length kept the height to a minimum and allowed large gradients to be obtained. Figure 4.2 shows a schematic of the apparatus and

Figure 4.3 shows a photo of the setup, including the inlet connection to the water supply in the HRTF.

4.3.2.4 Internal Sections

As shown in Figure 4.2, the interior of the permeameter was separated into three sections:

1. Inlet Section: Lower 600 mm; containing a baffle that dispersed the inflow entering the 350 mm inlet.
2. Sample Section: Middle 1500 mm; containing porous medium at a length to diameter ratio equal to 2:1.
3. Outlet Section: Upper 600 mm section; containing no material and where water freely spilled over the top at the exit.

4.3.2.5 Sample Support

A support table composed of structural steel was constructed to support the weight of the sample above the inlet section. The tabletop was initially constructed of 25 mm thick PVC plate with 50 mm diameter holes cut at regular spacing. This setup had insufficient flow capacity and caused premature failure of the sample by mass movement. The tabletop was then changed to a grill with 28 mm square openings. The grill was cut to shape from a used sieve recovered from an aggregate crushing contractor. The size of the holes allowed some of the small diameter material to fall through into the inlet section. After completion

of each test, the amount of rock found in the inlet section was measured, and in all tests was found to be insignificant.

4.3.2.6 Permeameter Frame and Gantry

The permeameter was loaded and unloaded approximately 7 meters from the water supply. The procedure for loading and unloading required that the device be vertical for placement of the material and horizontal for removal of the material. A steel frame, shown in Figure 4.3, surrounding the permeameter was used to support the pipe while it was rotated and moved. A rolling gantry with a hoist, also visible in Figure 4.3, was used to manipulate the device during both loading and unloading operations. Using the hoist and gantry the permeameter was moved to the water supply. The base of the permeameter was hinged so that the rigid wall pipe of the permeameter could be lowered onto its side (to horizontal) for unloading. The permeameter frame and gantry consisted of structural steel with bolted and welded joints.

4.3.3 Water Supply

The permeameter received flow from the constant head tank via a 350 mm diameter PVC pipe. The pipe length from constant head tank to the permeameter is 4.5 m vertical downward and 21 m horizontal. Along this length are located 4-90 degree and 1-45 degree joints as well as 1 butterfly valve. Flow capacity available to the permeameter was estimated at 500 L/s. Flow entering

the permeameter was controlled by a butterfly valve and measured as described in Section 4.2. Water entered in the side of the inlet section of the green permeameter via the white saddle-T, as shown in Figure 4.3 and Figure 4.4. Upon entry, the water stream was broken up by a baffle, which was attached to the sample support table. The water then proceeded vertically through the rock column to the outlet section. The water continued upward where it was allowed to freely spill over the top of the permeameter. The water cascaded down the outside of the permeameter and was collected by the flume that the permeameter was contained within. The water was channeled back to the HRTF storage tanks and pumping system to be recirculated.

4.4 INSTRUMENTATION

The instrumentation selection and layout were designed to measure hydraulic gradient and bulk velocity at any time during testing. The permeameter included vibrating-wire piezometers and piezometer tubes to measure pore water pressure at selected points (to infer total head) along the sample. The flow through the apparatus was measured volumetrically using the discharge reservoir of the constant head tank. The movement of specific rocks at the top of the sample was measured using draw-wire extensometers. All electronic devices were monitored using a computer-controlled data acquisition system every 15 seconds. Manual instruments, such as piezometer tubes, were read at predetermined intervals. The manual measurements were designed as a check to validate the output of the electrical sensors.

4.4.1 Piezometer Tubes

Brass tappings were inserted into the wall of the apparatus along the height of the sample at four selected levels. At each level, four tappings were spaced at 90-degree intervals radially to provide a total of 16 tappings along the sample section of the apparatus. The tappings and connected plastic tubes are shown in Figure 4.5. As well, one tapping was placed below the sample, at the height of the inlet section. Plastic tubes were attached to the fittings and extended approximately 2 m above the top of the permeameter to the data collection platform. The water levels that rose up the piezometer tubes, indicated by the bright reflection in the tubes shown in Figure 4.6, required manual measurements (Figure 4.7). The four piezometer tubes at each level allowed for examination of the variability in pore water pressure. They were manually read at each flow rate and at times when conditions were identified as being non-steady or unusual.

4.4.2 Vibrating-Wire Piezometers

Pressure measurements within the permeameter were taken using six vibrating wire piezometers. The vibrating wire piezometers utilized in this experiment were an assortment of 19 mm diameter by 150 mm long GeoKon Inc. and Slope Indicator Inc. brand instruments. One piezometer was placed in the outlet section and one was placed directly below the rockfill specimen (in the inlet

section). Four piezometers were placed within the sample section to measure pore water pressure at approximately the same height as the brass tappings. The black leads from the piezometers can be seen exiting the right hand side of the permeameter in Figure 4.8.

The piezometers were calibrated before and after each test to check for calibration drift, possibly caused by the impact of particles during placement of the rock for each test. A seventh vibrating wire piezometer was placed outside of the permeameter on the data collection platform. This unit measured ambient atmospheric pressure and temperature, which are used to correct the measurements of the piezometers within the permeameter. The piezometers were wired to a Campbell Scientific CS 723X multiplexer that allowed all of the piezometers to be read by the CR23X data acquisition system. Readings were recorded in the CR23X's electronic memory every 15 seconds.

4.4.3 Draw-Wire Extensometers

Draw-wire extensometers were attached to selected rocks at the surface of the sample to record the initiation of particle movement. The draw-wires were electronically monitored every 10 seconds using the data acquisition system. The extensometers used in all experimentations were Micro-Epsilon WPS-MK30 models.

The extensometers were mounted on a sheet of plywood that was attached to the data collection platform. The extensometer draw wire was routed along a PVC channel and through a stop system to arrest movement at its safe stroke distance, as shown in Figure 4.9. Attached to the draw wires was a high strength, near zero stretch polyethylene line that extended beyond the stop system. The lines were near horizontal until passing over a smooth steel rod and descended near vertical into the top of the permeameter. The lines were attached to specific rocks that contained a screw secured with epoxy in a 5 mm deep hole. Six of the twelve extensometers available were used. A photograph of the setup is located in Figure 4.10.

An extensometer receives a voltage input and depending on extension, as related by electrical resistance, outputs a different voltage. The difference in the input and output voltage were recorded with a Campbell Scientific CR23X data acquisition (DA) system. The extensometers were calibrated prior to use in the laboratory and after all the permeameter experiments were complete.

4.5 Operation

The flow generated by the pumps in the laboratory circulation system was constant during the course of each permeameter test. The total flow generated by the circulation system was known during each test and the flow bypassing the permeameter was metered using the volumetric tank.

Each test including setup and disassembly took approximately two days to complete. The following sections describe the procedure for conducting a test using the apparatus.

4.5.1 Safety Procedure

During the operation of the permeameter, loading unloading and testing, safety was a primary consideration. Some actions required the development of a safety procedures document (included in Appendix A), for operation of the large-scale permeameter, and include:

- The movement of rock, individually weighing up to 5 kg and hand buckets of rock in excess of 40 kg required proper safety gear, and safe handling conditions.
- The movement of the permeameter using the rolling gantry. When loaded with rockfill for testing, the gantry lifted approximately 1,400 kg. As well, when the permeameter was lowered from an operational vertical position to an unloading horizontal position, safety procedures were required.
- When testing in full flow conditions, rocks were able to exit the top of the permeameter due to the applied flow. This condition required that personnel would not be allowed near the base of the apparatus during operation.

4.5.2 Loading and Unloading the Permeameter

The permeameter was located on the lower level of the laboratory and when upright extended slightly above the floor of the mezzanine level (Figure 4.4). This enabled workers to load rock into the permeameter from the mezzanine level (Figure 4.11).

The permeameter was loaded in its vertical position by lowering and dumping buckets of rock from a selected height above the already in-place material providing some control of the compactive energy imparted on the in-place rock. This allowed relatively consistent control of the bulk density of the in-place rock sample. Each 5-gallon bucket of rockfill material was weighed before loading and recorded to calculate the total mass of the in-place rock sample. The void ratio was calculated using the mass of in-place rock and the volume that it filled in any given test. Between 900 and 1100 kg of test rock were placed and removed each time the permeameter was loaded and unloaded. During rock placement, the vibrating-wire piezometers were placed within the rock mass at pre-selected target elevations and carefully covered with rock, while maintaining consistent placement conditions (drop height). No other compaction methods were attempted.

Upon completion of a test, the permeameter was detached from the water supply and lowered about its hinges to a horizontal position using the rolling gantry (Figure 4.12). When lowered to the horizontal position, the permeameter was

approximately 100 mm above the floor of the lower level of the hydraulics laboratory, allowing the rock to be removed from the permeameter with minimal lifting.

4.5.3 Pre-Test Procedure

The permeameter was slowly filled to the top with water without overtopping and held constant while the data acquisition system, instrumentation, and piezometer tubes were checked. All measurements were recorded as baseline readings. This process took approximately 10 minutes.

4.5.4 Testing Protocol

After the pre-test procedure, the flow was increased in specified increments. The tests were generally completed with 12 increments in flow, with the readings for each incremental stage of flow requiring approximately 10 minutes. The first increment was targeted to provide a laminar flow condition to allow calculation of a nominal hydraulic conductivity value (k). The flow conditions were allowed to reach steady-state after each increment of flow. Steady-state was considered to be the point where all instrumentation showed constant readings (within a specified range of expected fluctuations), and with no movement of the particles at the top of the porous medium (as measured with the extensometers). The maximum flow achieved in the testing was approximately 300 L/s. Figure 4.13 and Figure 4.14 show the apparatus during low flow and peak flow operation respectively. The flow exiting the apparatus gives an indication of the volume of

water required for these tests. Water spilling over the top of the apparatus was contained below using a flume that directed flow into the laboratory recirculation system.

4.6 COARSE ROCKFILL

An experimental plan was outlined to examine the impacts of gradation and bulk density/porosity on the behaviour of the rockfill media. Four (4) gradations of the rockfill were used in the permeameter experiment (see Figure 4.15). The first rockfill tested was a well-graded 10 to 150 mm nominal diameter material. The range of void ratios developed for testing was 0.7 to 0.82 (porosity of 41% to 45%). The second rockfill sample was a poorly graded nominal 150 mm diameter material with void ratios 0.9 to 1.06 (porosity of 47% to 51%). The third rockfill sample was a poorly graded nominal 50 mm diameter material with void ratios 0.75 to 0.80 (porosity of 43% to 44%) and the fourth rockfill sample was a gap-graded 50 mm and 150 mm diameter material, void ratio varied from 0.65 to 0.70 (porosity of 39% to 41%).

The rockfill was delivered from the storage area to the loading bay adjacent to the HRTF. The well-graded material was drawn directly from the stockpile with care to remove extremely flat particles. The other three gradations required mechanical separation of the rockfill using multiple sieves. Before entering the HRTF, the rockfill was sorted by hand, using large sieves both manufactured in-

house and acquired from a local gravel company, the setup for which is shown in Figure 4.16.

4.7 EXPERIMENTAL RESULTS

4.7.1 General

The measurements taken during the tests were interpreted using an ordinary least-squares regression of log i versus log V, as outlined by Hansen *et al.* (1995) resulting in Equation 2.7a. The gradient (i) and bulk velocity (V) were established from the measured data. In Equation 2.7a, 'a' is a coefficient depending upon the fluid and porous media properties, and 'N' is an index of the level of turbulence, both to be determined experimentally. According to Hansen *et al.* (1995), 'N' ranges from 1.0 to 2.0 as the flow through the porous media moves from laminar to fully turbulent. All testing was designed to achieve fully turbulent flow through the porous media, and success was evaluated based on 'N' approximately equal to 2.0. The measured data shows minimal scatter, giving confidence that the individual measurements were reasonable. The exponent 'N' for almost all of the testing cases (grain size distribution and porosity) was approximately 2.0, indicating that the flow was fully turbulent at generally all but the smallest gradients. This demonstrates that the apparatus was able to induce turbulent conditions within the materials tested, which is consistent with the potential operating conditions of many rockfill dams.

Figures and data for Permeameter Test 1 and 3 are not included in this document. When the experimentation program started, limited literature and experience was available regarding the construction and use of a large-scale permeameter. The first large-scale permeameter test (Test 1) was completed, not to test a rock sample, but to test the large-scale permeameter. Test 1 enabled the author to create guidelines for loading and operation, calibrate and understand the electronic instrumentation and to make adjustments to the apparatus. The flow through data obtained from this test, while recorded, cannot be interpreted. During the Permeameter Test 3, a loss of electrical power within the HRTF occurred three times. Although the power loss was short (less than one second each), the electric pumps would automatically shut down. As well, the memory storage within the data acquisition system did not perform as intended. As such, both the discharge measurements and vibrating wire piezometer data were deemed unusable.

Although not seen in all large-scale permeameter test results, the data did not always fit the trend. At low hydraulic gradients and bulk velocity, the flow through rockfill will behave in a laminar or translational state (N<2). As can be seen in Figure 4.17, the data plots above the fitted curve, representing N=2. During all tests at a hydraulic gradient near 1.0 the rock began to move. Generally, the movement was a rearrangement of particles, creating a preferential flow path. This flow path reduced the flow through the rest of the rockfill, reducing the measured total head. This is observed in Figure 4.19, at a hydraulic gradient of

approximately 1.0 and bulk velocity of approximately 0.3 m/s. These outliers were not included in the calculation of a and N.

4.7.2 Well-Graded 10-150 mm Rockfill

Permeameter Test 2, 4, 5 and 6 used well-graded 10 to 150 mm material. Results of the test are found in Table 4.4 and shown on Figure 4.17 through Figure 4.20. Altering the drop height during placement of rockfill produced two general void ratios, approximately 0.71 and 0.79. All four tests achieved fully turbulent flow, as indicated by N approximately equal to 2.0. When comparing void ratio to the a – coefficient a trend is immediately observed. As void ratio increases, a decreases. This is plotted on Figure 4.21, but the lack of data over a large range of void ratio prevents the author from recommending a relationship between data points.

Table 4.1 – Results of Large-Scale Permeameter
Well-Graded 10 - 150 mm

Test #	Void Ratio	a – coefficient	N - coefficient
Permeameter Test 2	0.717	16.9	2.00
Permeameter Test 4	0.711	17.1	2.00
Permeameter Test 5	0.788	13.0	2.00
Permeameter Test 6	0.706	17.9	2.03

4.7.3 Poorly-Graded 150 mm Rockfill

Four (4) large-scale permeameter tests, Permeameter Test 7 through 10, were completed on 150 mm poorly-graded rockfill. Test results are located in Table

4.2 and on Figure 4.22 through Figure 4.25. The four tests all achieved fully turbulent flow, as indicated by N being approximately equal to 2.0. When comparing void ratio to the a – coefficient (Figure 4.26), no trend is observed. However, the a – coefficient is significantly lower than for the well-graded 10-150 mm rockfill.

Table 4.2 – Results of Large-Scale Permeameter
150 mm Poorly-Graded Rockfill

Test #	Void Ratio	a – coefficient	N - coefficient
Permeameter Test 7	0.97	4.5	2.02
Permeameter Test 8	1.06	7.8	2.00
Permeameter Test 9	0.90	7.1	2.04
Permeameter Test 10	0.92	7.3	2.02

4.7.4 Poorly-Graded 50 mm Rockfill

Three large-scale permeameter tests, Permeameter Test 11 through 13, were completed on 50 mm poorly-graded rockfill. Test results are located in Table 4.3 and on Figure 4.27 through Figure 4.29. The three tests achieved fully turbulent flow, as indicated by N approximately equal to 2.0. The a – coefficient varied from 12.8 to 22.8 over a very small range of void ratio.

Table 4.3 – Results of Large-Scale Permeameter
50 mm Poorly-Graded Rockfill

Test #	Void Ratio	a – coefficient	N - coefficient
Permeameter Test 11	0.76	12.8	2.04
Permeameter Test 12	0.79	19.2	2.05
Permeameter Test 13	0.79	22.8	2.08

When Permeameter Test 11 is plotted on a linear axis as shown on Figure 4.30, it can be seen that the hydraulic gradient values from the vibrating wire piezometers trend away from the open-pipe piezometer data. Generally, the open-pipe piezometers were used to confirm and duplicate the vibrating wire piezometer readings. A review of the data was completed to understand the trend. Unfortunately, the only explanation evident was the placement of the vibrating wire piezometers. Of the 16 large-scale permeameter tests, Permeameter Test 11 was the only one to place the vibrating wire piezometer tips (porous stone covering a void containing sensor) vertically downward, into the direction of flow. As will be described further in Chapter 5, the vibrating wire piezometer measurements of pressure are affected by the velocity of flow when placed into the flow.

Despite the above observation, the vibrating wire piezometer data cannot be ignored. Nor does the observation resolve why the a – coefficient is significantly lower than Permeameter Test 12 and 13.

4.7.5 Gap-Graded 50 and 150 mm Rockfill

Three (3) large-scale permeameter tests were conducted on 50 and 150 mm gap-graded rockfill. Test results are located in Table 4.4 and on Figure 4.31 through Figure 4.33. The three tests achieved fully turbulent flow, as indicated

by N approximately equal to 2.0. The a –coefficient ranged from 15.7 to 19.8 with no clear relationship to void ratio.

Table 4.4 – Results of Large-Scale Permeameter 50 and 150 mm Gap-Graded Rockfill			
Test #	**Void Ratio**	**a – coefficient**	**N - coefficient**
Permeameter Test 14	0.69	18.9	2.07
Permeameter Test 15	0.68	19.8	2.06
Permeameter Test 16	0.77	15.7	2.03

4.7.6 Discussion of Results

When comparing the results of the large-scale permeameter it becomes apparent that the 10 to 150 mm well graded, 50 mm poorly-graded and 50-150 mm gap-graded all behave similarly. This suggests that flow through the rockfill has more to do with the d_{50} of the material than the gradation. However, this statement isn't exclusively true, as the amount of fine material within a coarse porous media has been found, in previous studies, to potentially control flow. As is evident on Figure 4.15, the three above mentioned gradations all have a d_{50} of 50 mm.

Although it is argued that only two representative diameters of rockfill have been tested, a number of observations are made regarding the a-coefficient from the power-law equation (Equation 2.7a). As can be seen on Figure 4.34, a is inversely proportional to d_{50} (or alternatively m, Figure 4.35) which is in agreement with the testing completed by Hansen (1992). As well, although

possibly obscured by three outliers, a linear relationship between a and void ratio could be inferred on Figure 4.36.

It is apparent from the literature review and the results of the laboratory testing that increased diameter of rockfill allows an increased velocity of flow for a given hydraulic gradient. Hansen (1992) reported that for a diameter greater than 20 mm, N would typically be equal to 2.0. Although not exclusively tested in this experiment, all tests including those with a d_{50} of 50 mm, achieved fully turbulent flow.

The large-scale permeameter data was used to evaluate Equation 2.10 (Wilkins 1955). Figure 4.37 shows Permeameter Test 8 and Test 10, both using the 150 mm poorly-graded rockfill, along with the curves obtained from Wilkins' equation. The curves are nearly coincident and within 15% of the experimental data. Figure 4.38 shows Permeameter Test 4, well-graded 10 to 150 mm diameter rockfill, along with the curve from Wilkins' equation. Wilkins' equation over predicts the hydraulic gradient, for a given bulk velocity, by up to 50%. This result is consistent for all three d_{50} = 50 mm gradations.

The large-scale permeameter data was used in the evaluation of Equation 2.8a. The value of turbulent hydraulic conductivity (k_t), Equation 2.8b, was calculated from the void ratio of the permeameter tests, hydraulic mean radius (calculated either from Equation 2.2 or 2.4) and the particle size distributions on Figure 4.15.

The inverse of k_t was compared to a, knowing that Equation 2.8a only considers fully turbulent flow, and that the a-coefficient was calculated with fully turbulent flow data. The Norwegian proposed representative diameter (1.22 d_{20}) was found to produce a turbulent hydraulic conductivity generally within 20% of a. However, the a-coefficient of the 150 mm poorly-graded rockfill does not compare well to the estimation of k_t. Figure 4.39 shows the laboratory obtained a-coefficient and the calculated k_t plotted against hydraulic mean radius.

As was completed above, the data and turbulent flow power-law coefficients (a and N) obtained from the large-scale permeameter, can be used for the further evaluation of existing gradient-discharge relationships. As well, the a and N – coefficients will be used in future chapters to estimate flow through scale rockfill structures constructed in the laboratory. With the flow through the rockfill known, estimation of discharge height, exit gradient, and initiation of particle movement can be completed.

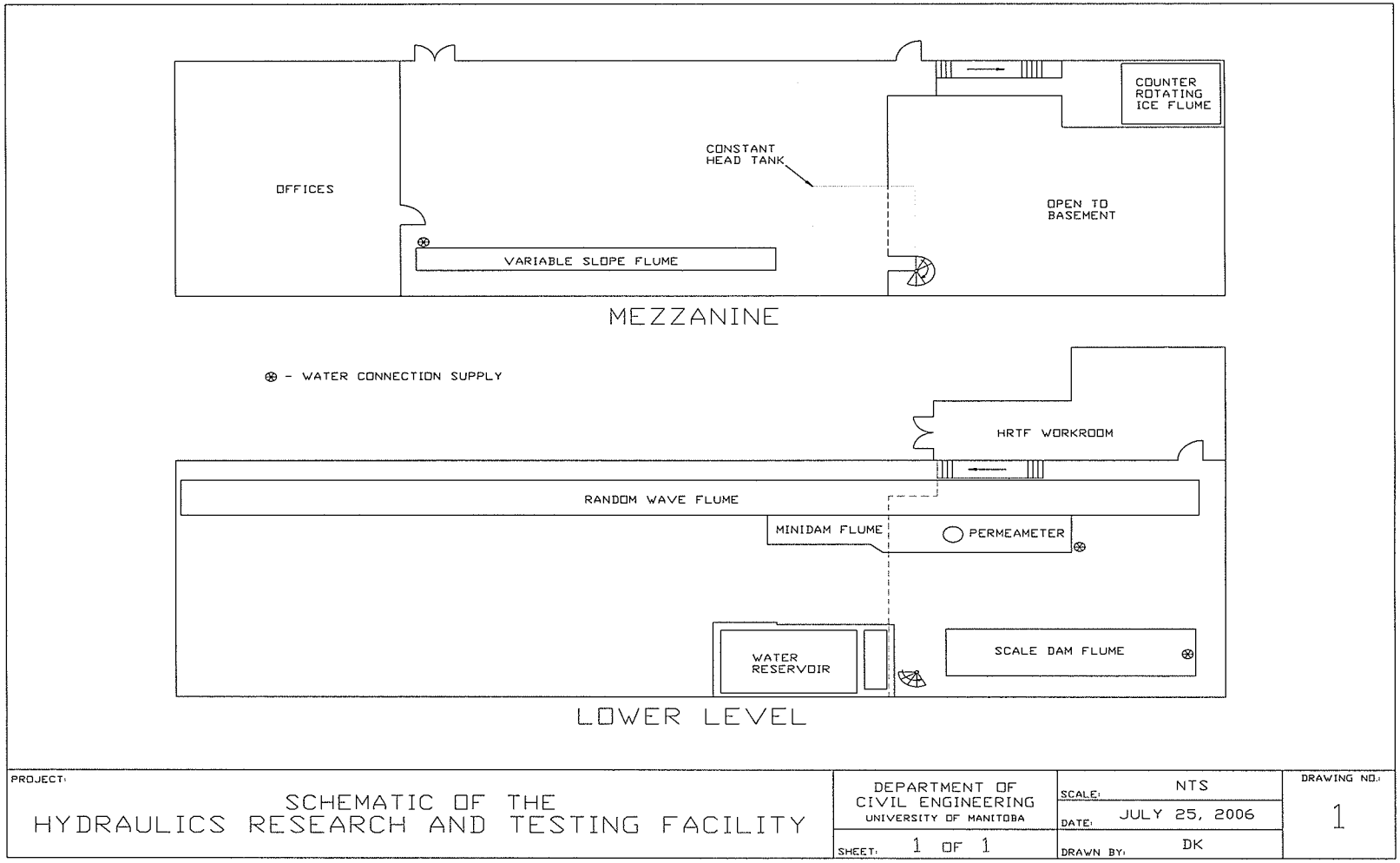

Figure 4.1 – Schematic of HRTF Laboratory

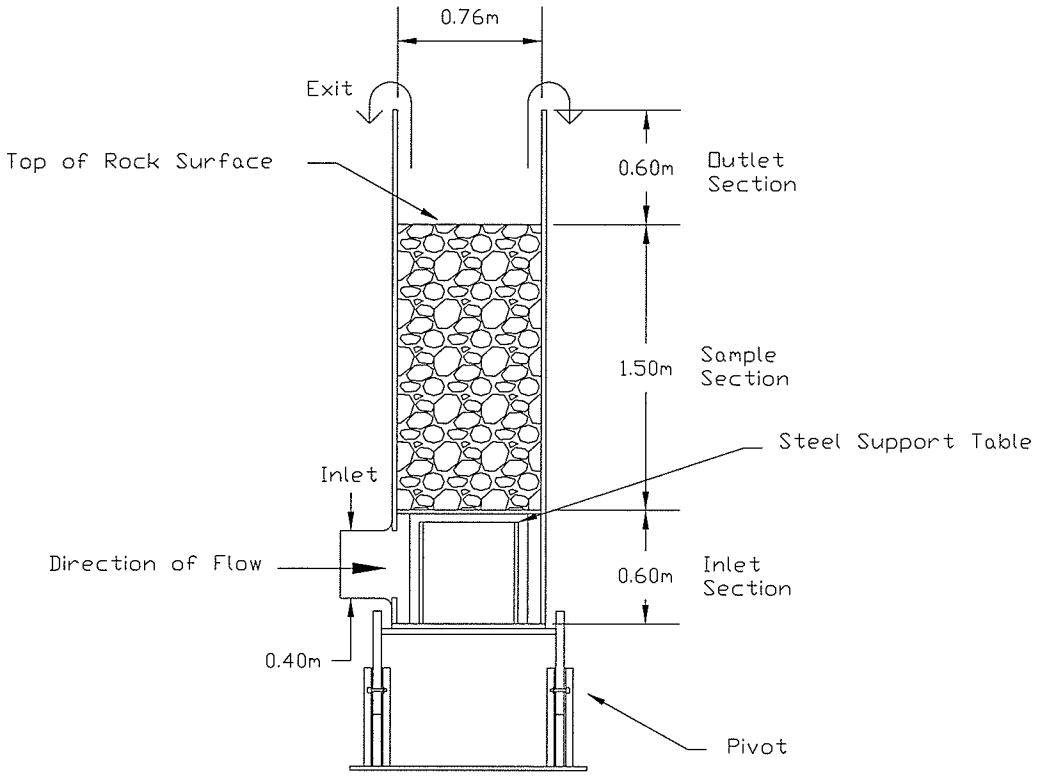

Figure 4.2 – Schematic of Large-scale Permeameter

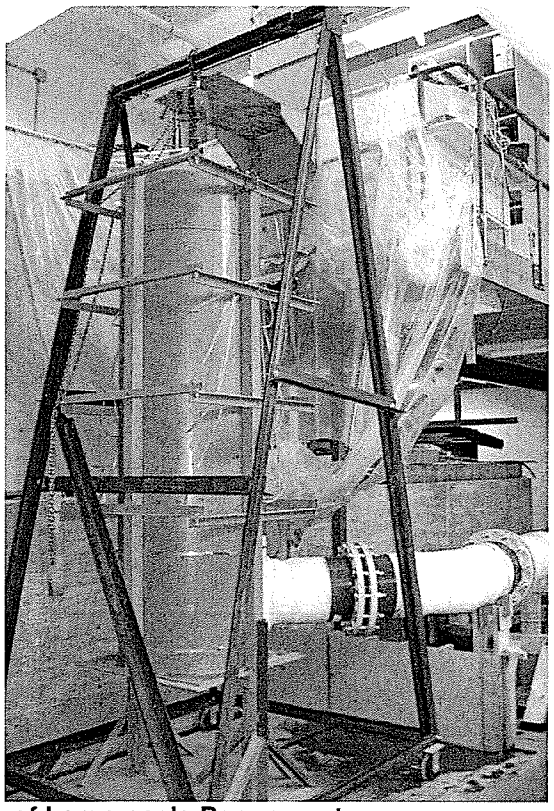

Figure 4.3 – Photograph of Large-scale Permeameter

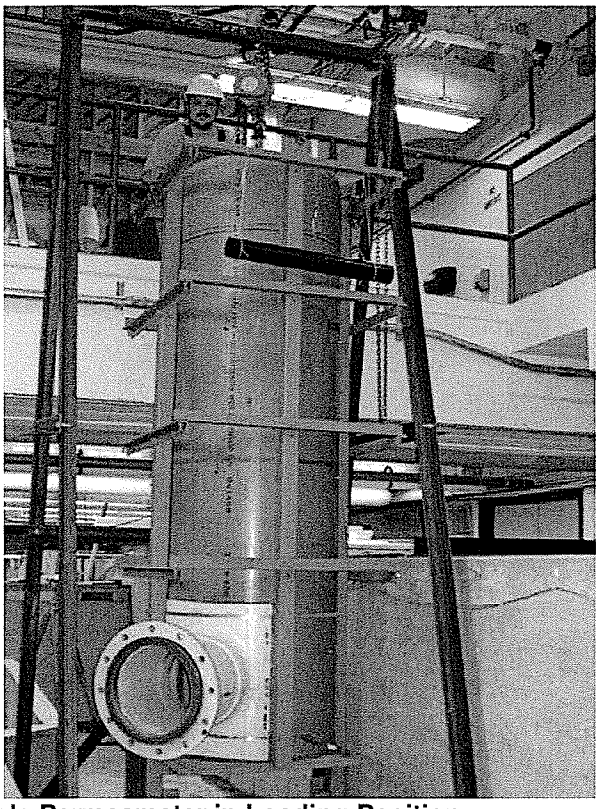

Figure 4.4 – Large-Scale Permeameter in Loading Position

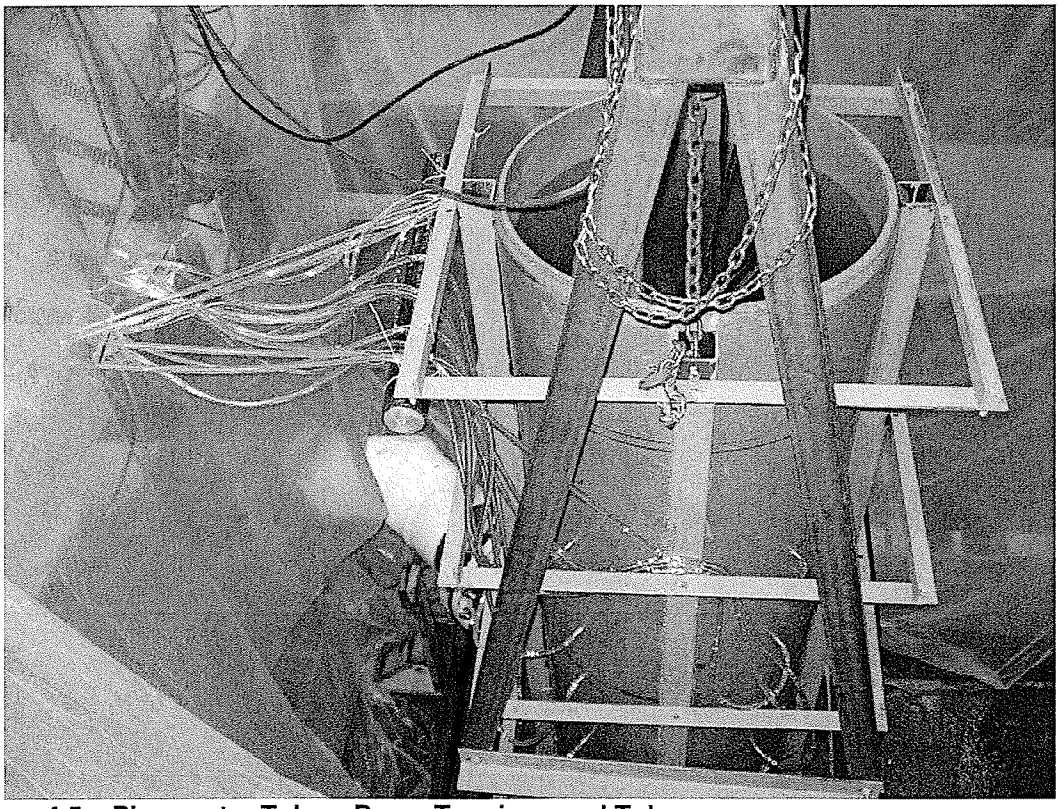

Figure 4.5 – Piezometer Tubes, Brass Tappings and Tubes

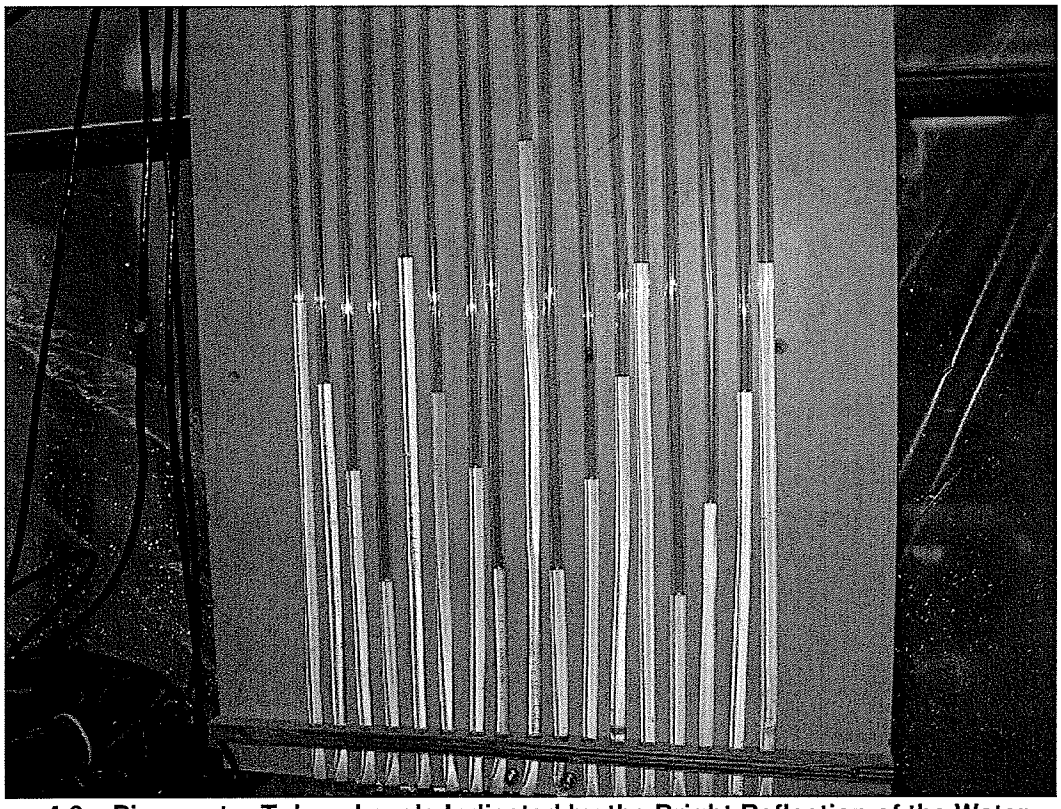

Figure 4.6 – Piezometer Tubes, Levels Indicated by the Bright Reflection of the Water

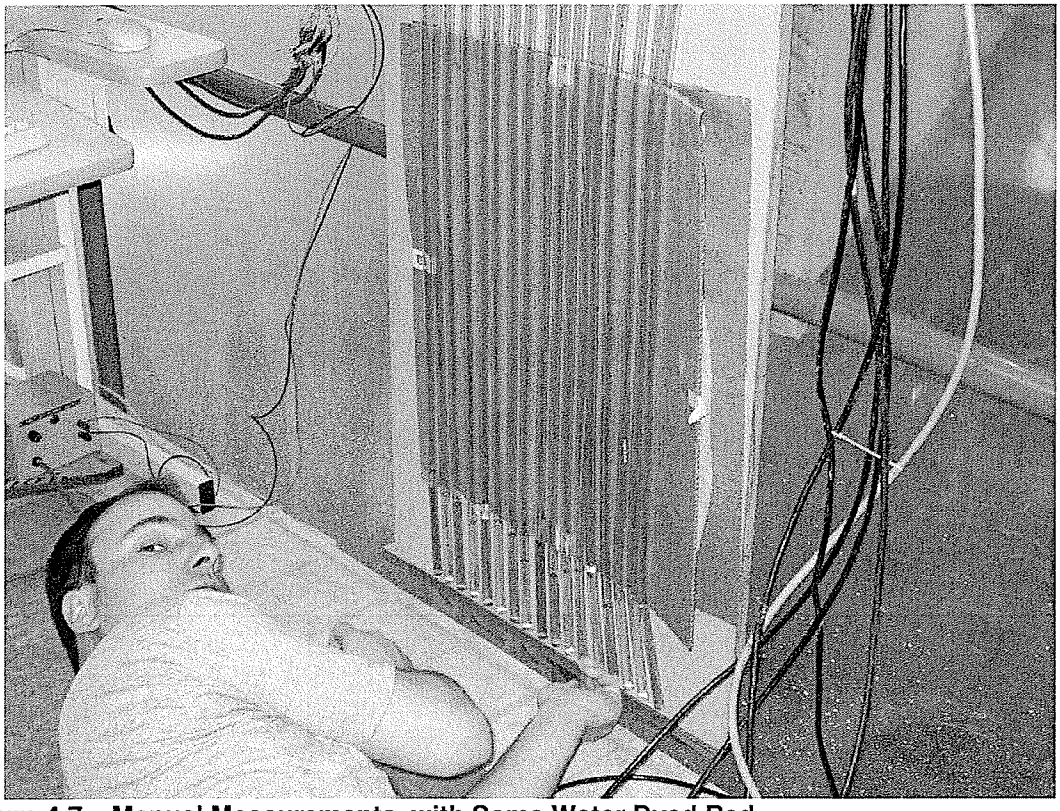

Figure 4.7 – Manual Measurements, with Some Water Dyed Red

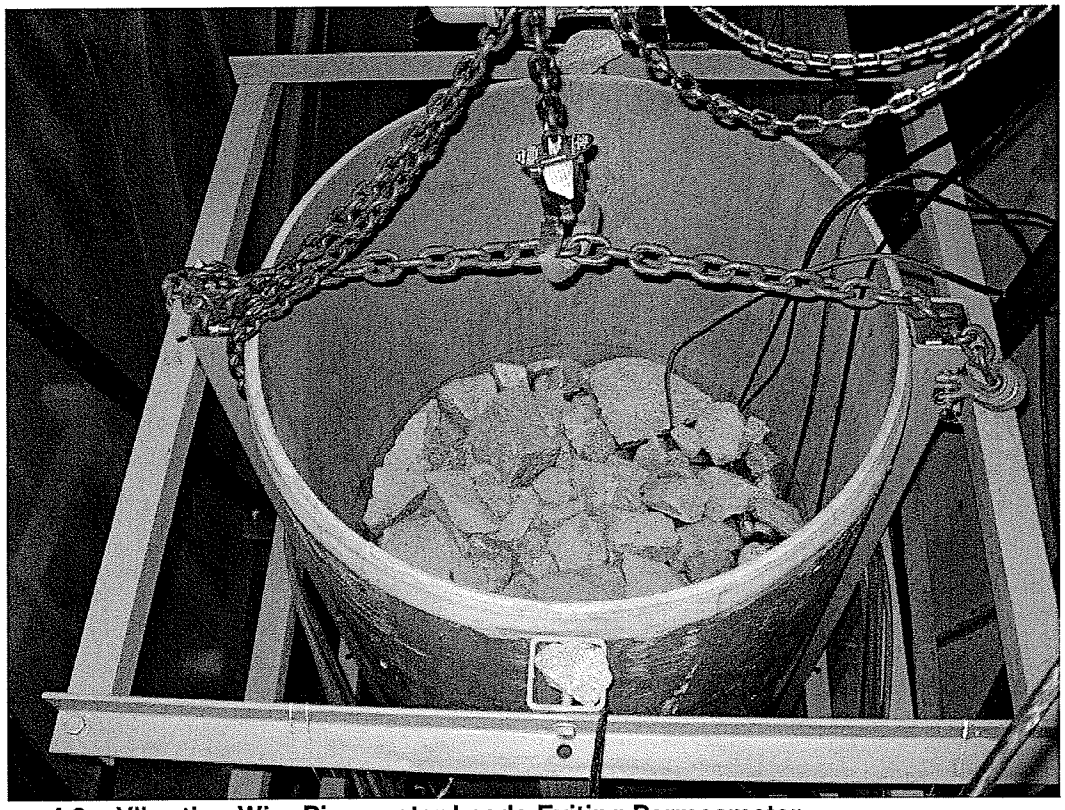

Figure 4.8 – Vibrating Wire Piezometer Leads Exiting Permeameter

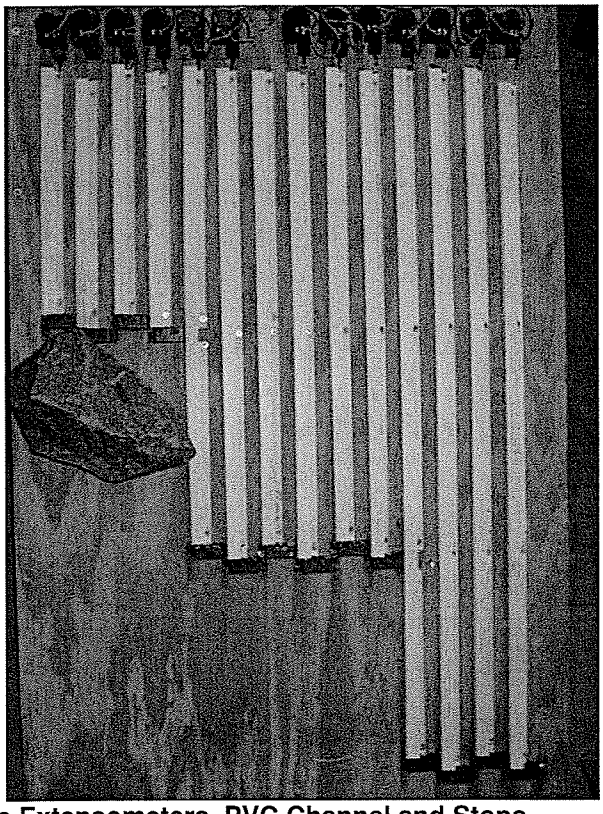

Figure 4.9 – Draw-wire Extensometers, PVC Channel and Stops

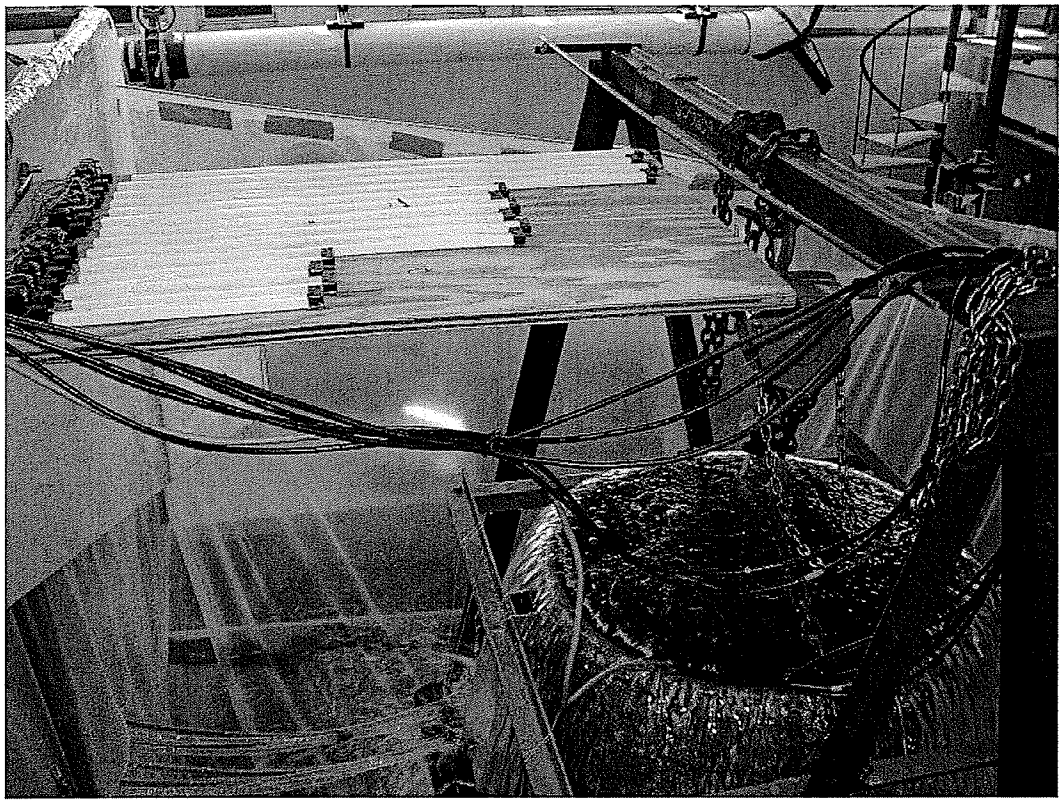

Figure 4.10 – Draw-wire Extensometer Setup

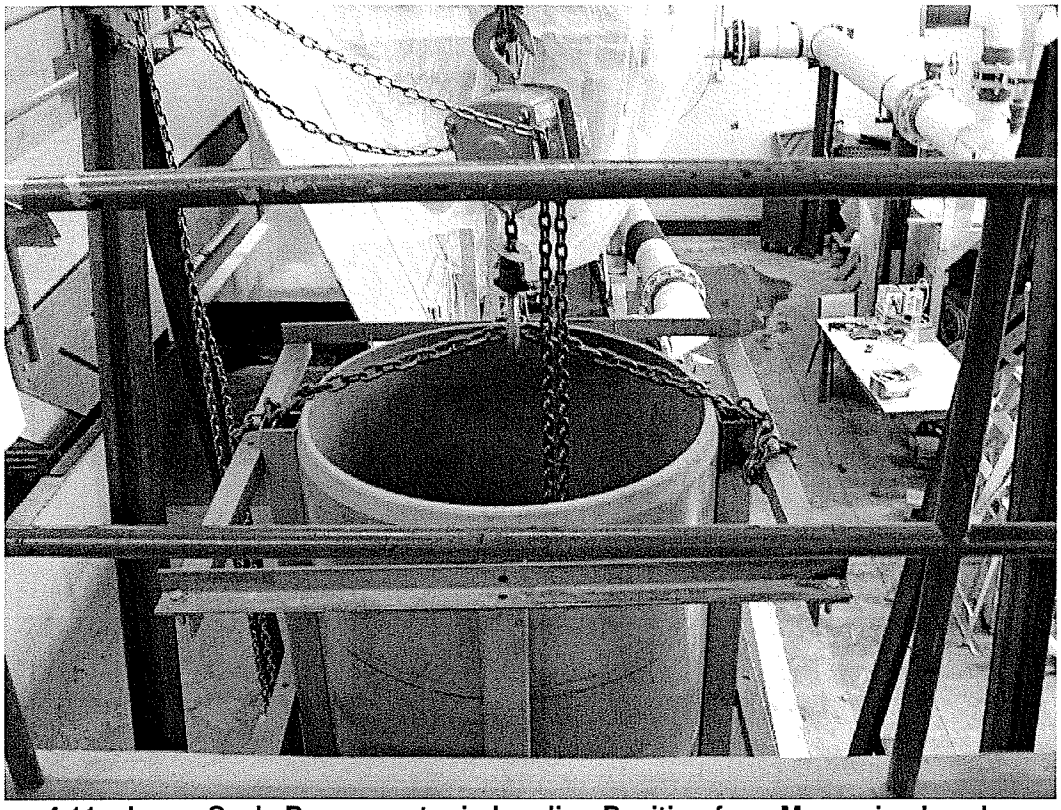

Figure 4.11 – Large-Scale Permeameter in Loading Position from Mezzanine Level

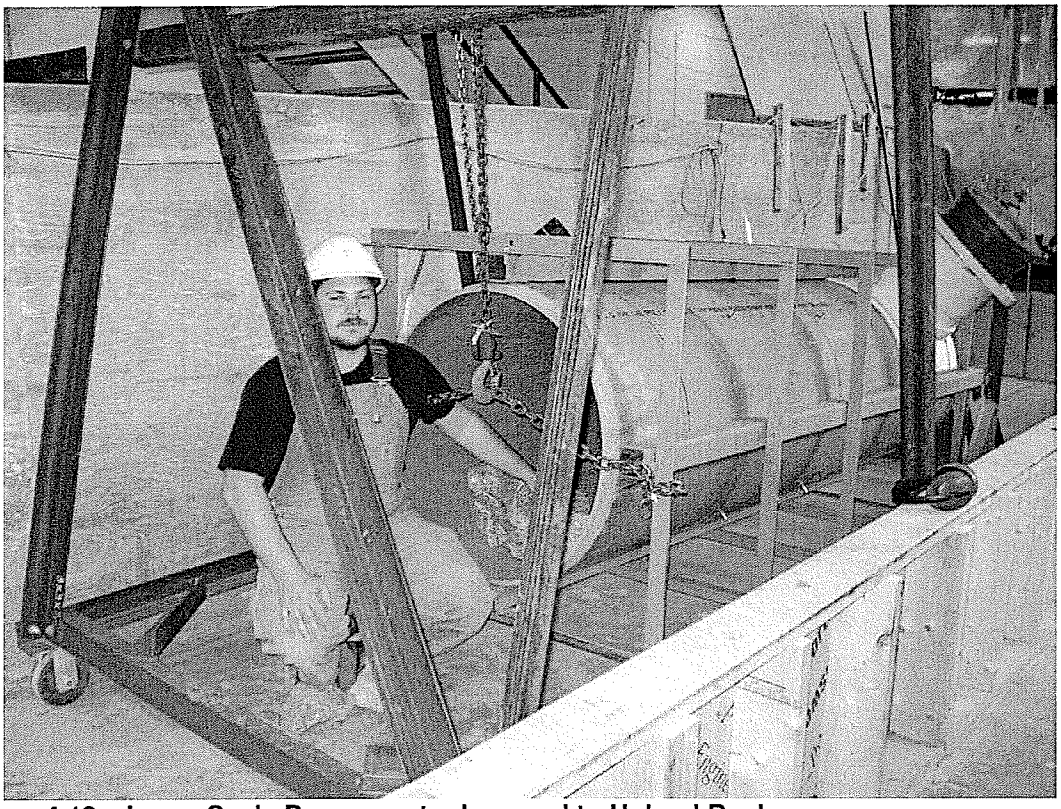

Figure 4.12 – Large-Scale Permeameter Lowered to Unload Rock

Figure 4.13 – Large-Scale Permeameter during Low Flow Conditions

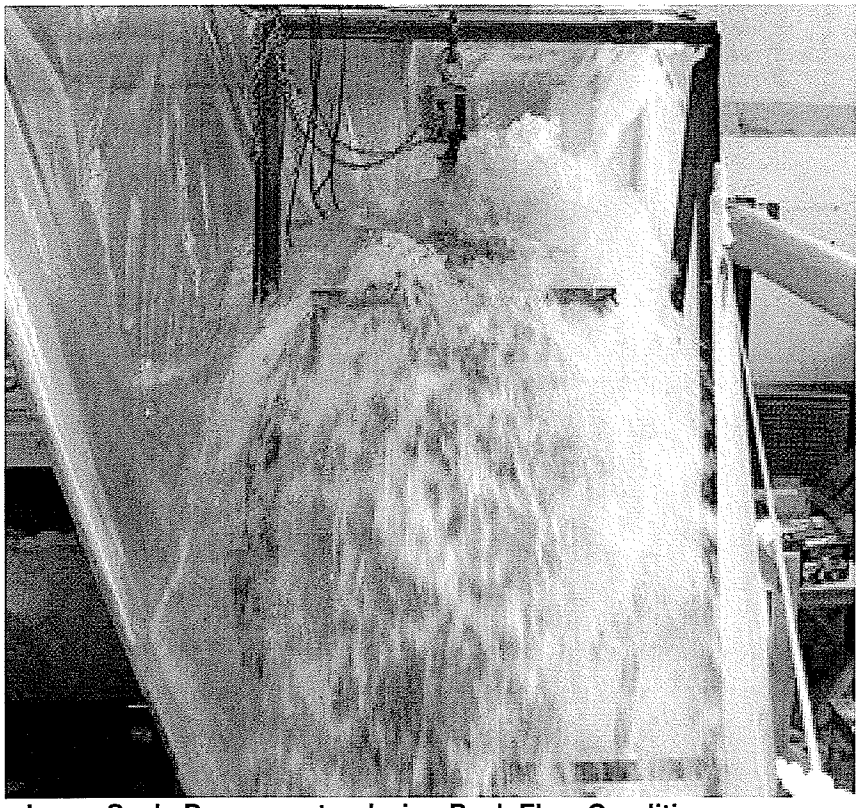

Figure 4.14 – Large-Scale Permeameter during Peak Flow Conditions

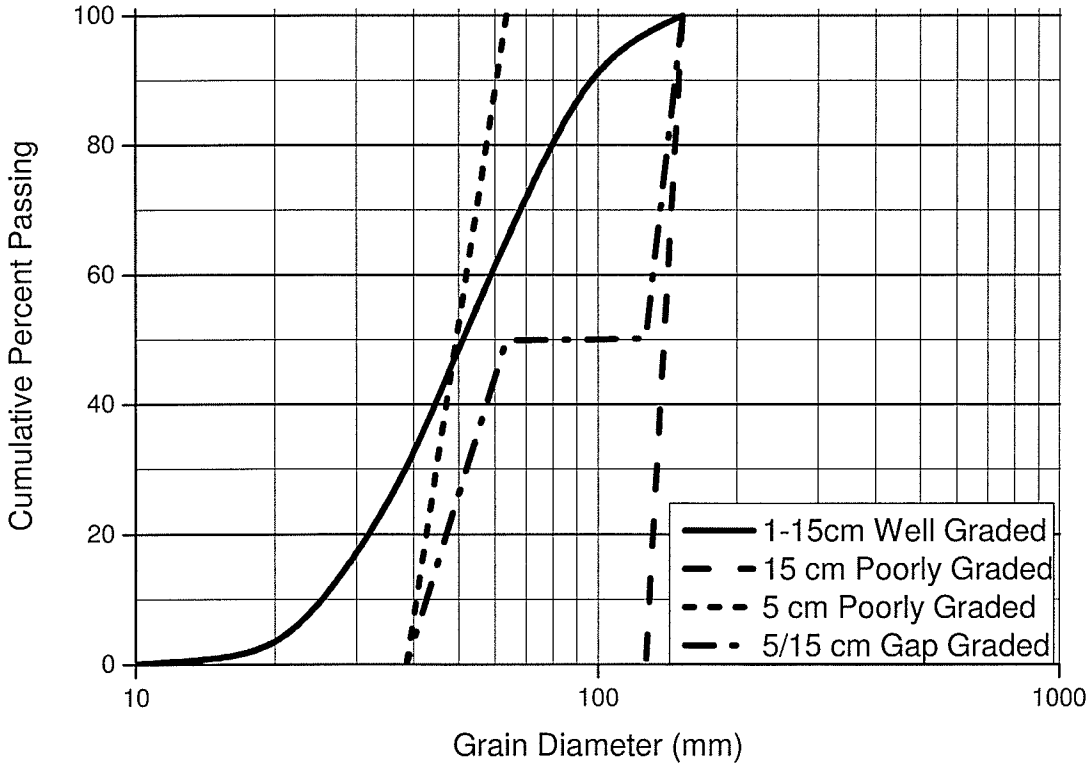

Figure 4.15 – Particle Size Distribution

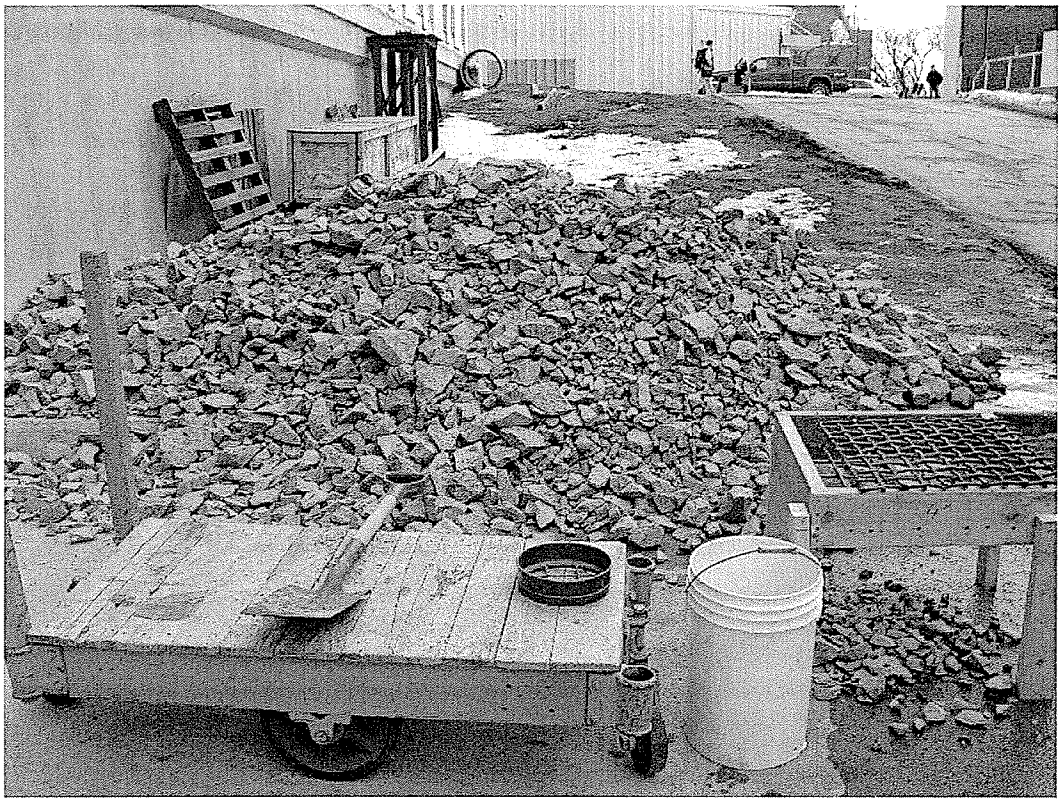

Figure 4.16 – Mechanically Separating the Rockfill

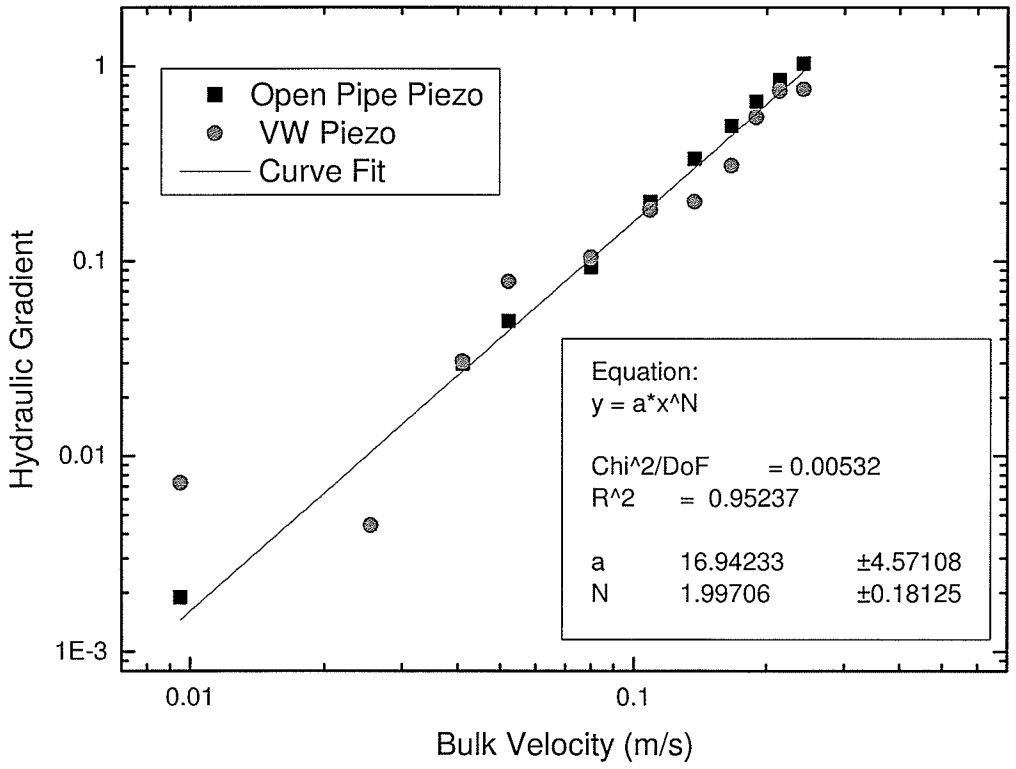

Figure 4.17 – Permeameter Test 2

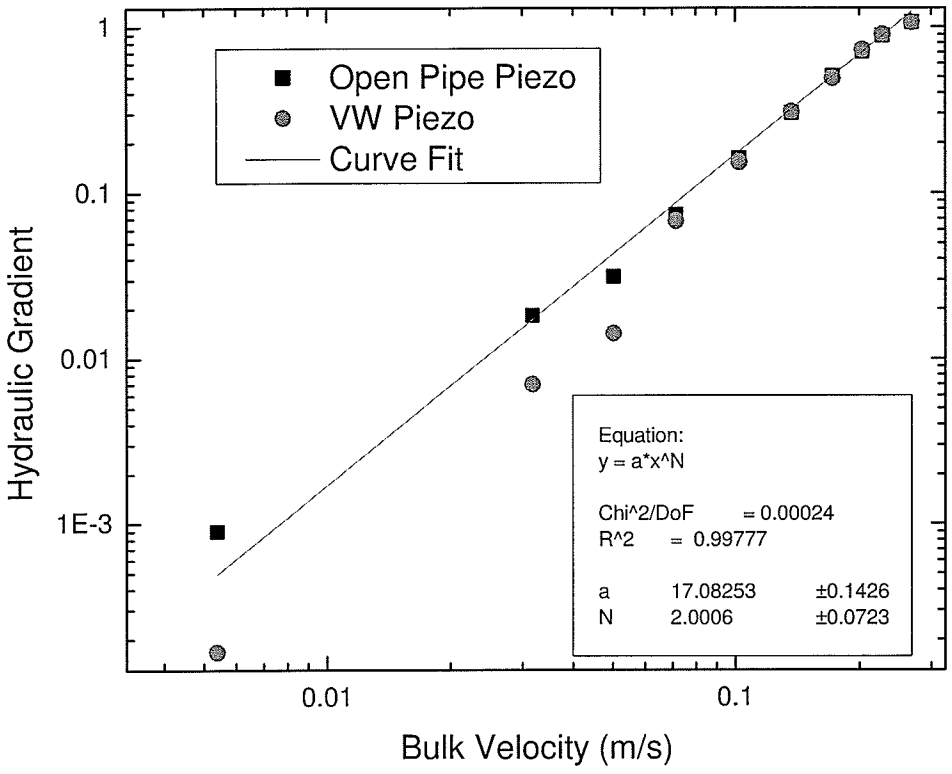

Figure 4.18 – Permeameter Test 4

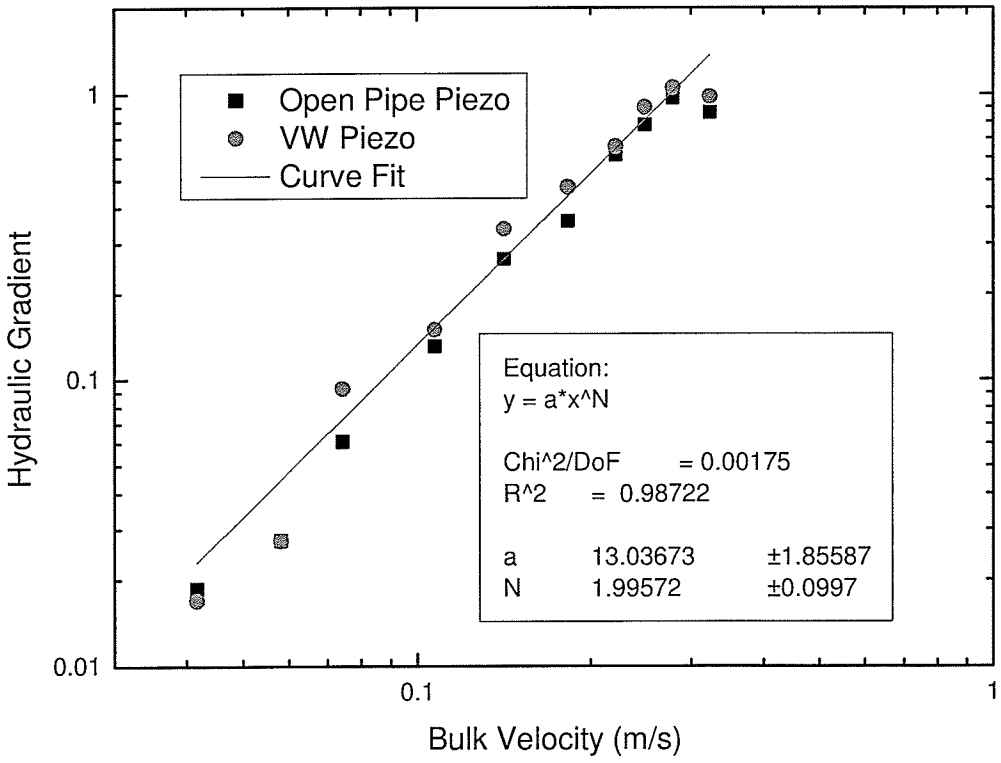

Figure 4.19 – Permeameter Test 5

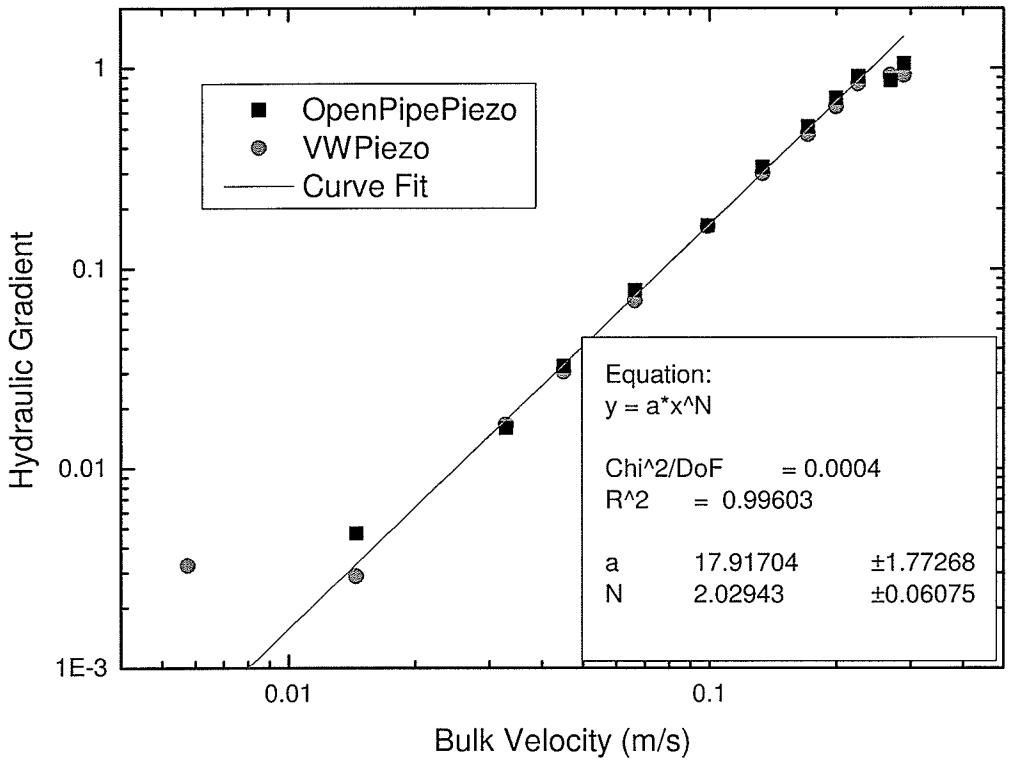

Figure 4.20 – Permeameter Test 6

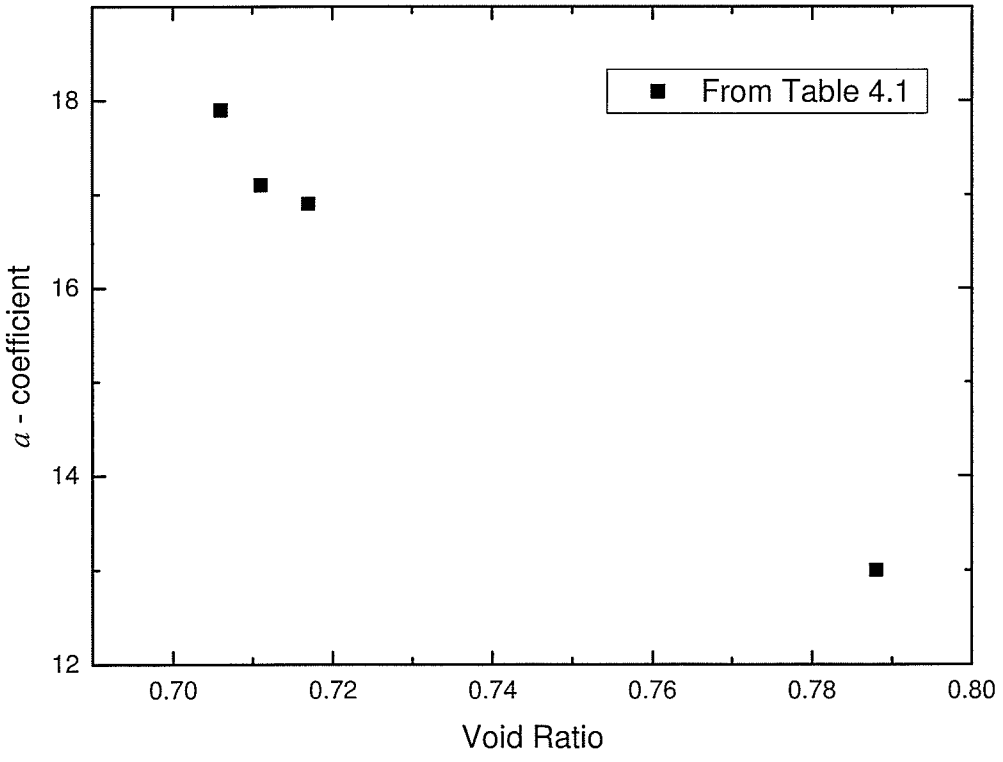

Figure 4.21 – Void Ratio versus a-coefficient, Well-Graded 10-150 mm Rock

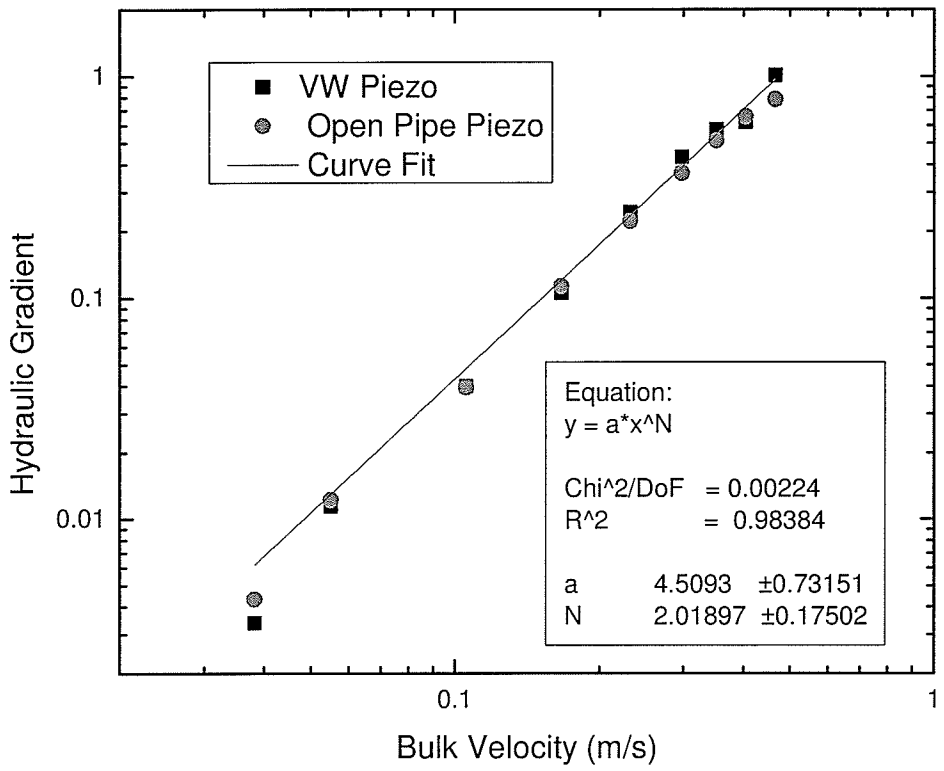

Figure 4.22 – Permeameter Test 7

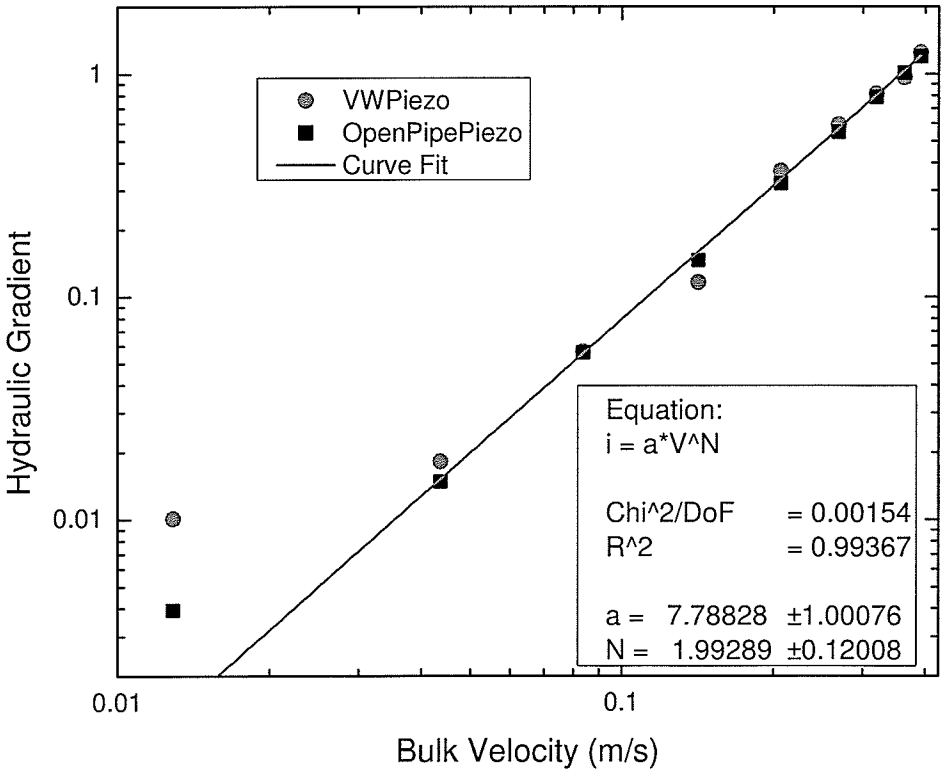

Figure 4.23 – Permeameter Test 8

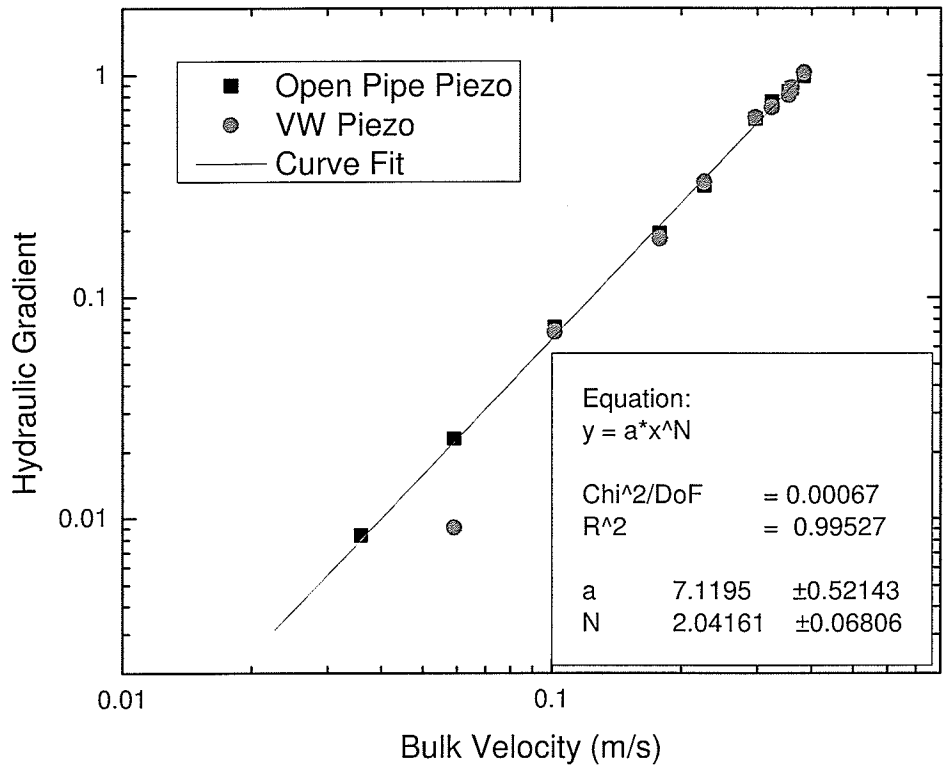

Figure 4.24 – Permeameter Test 9

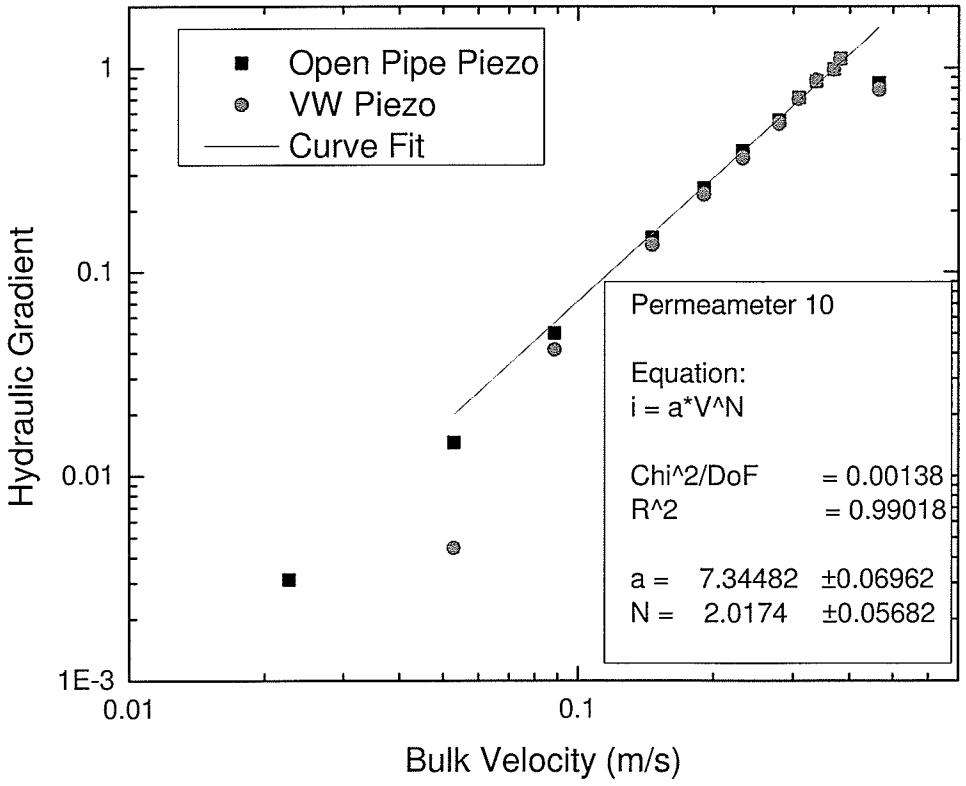

Figure 4.25 – Permeameter Test 10

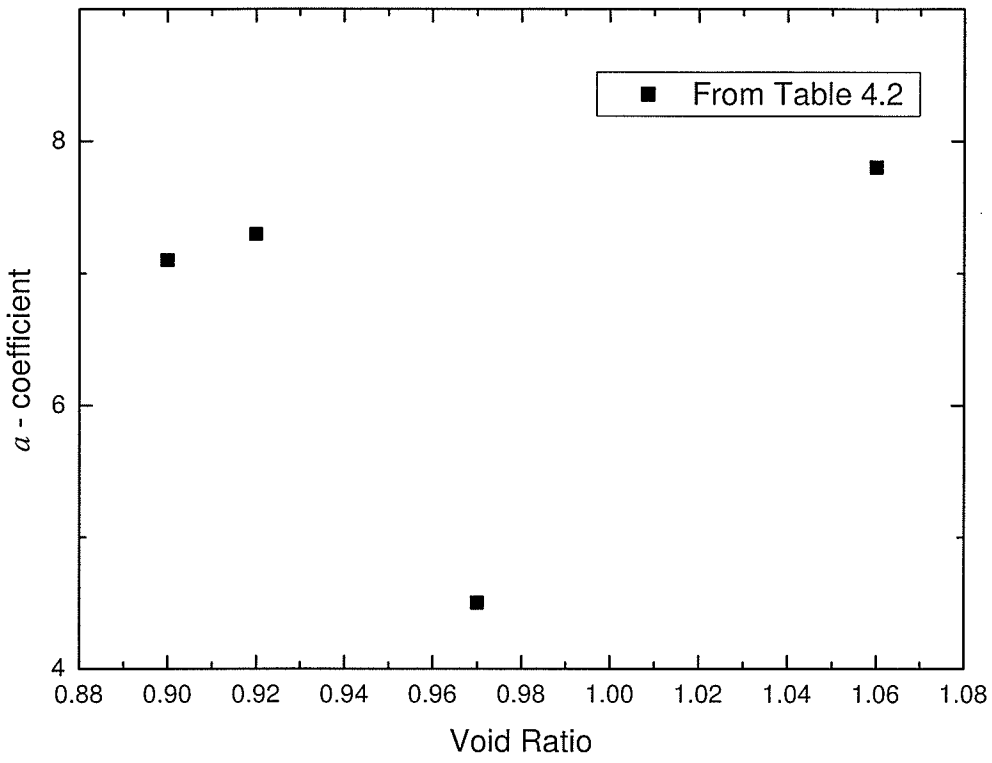

Figure 4.26 – Void Ratio versus a - coefficient, 150 mm Poorly Graded Rockfill

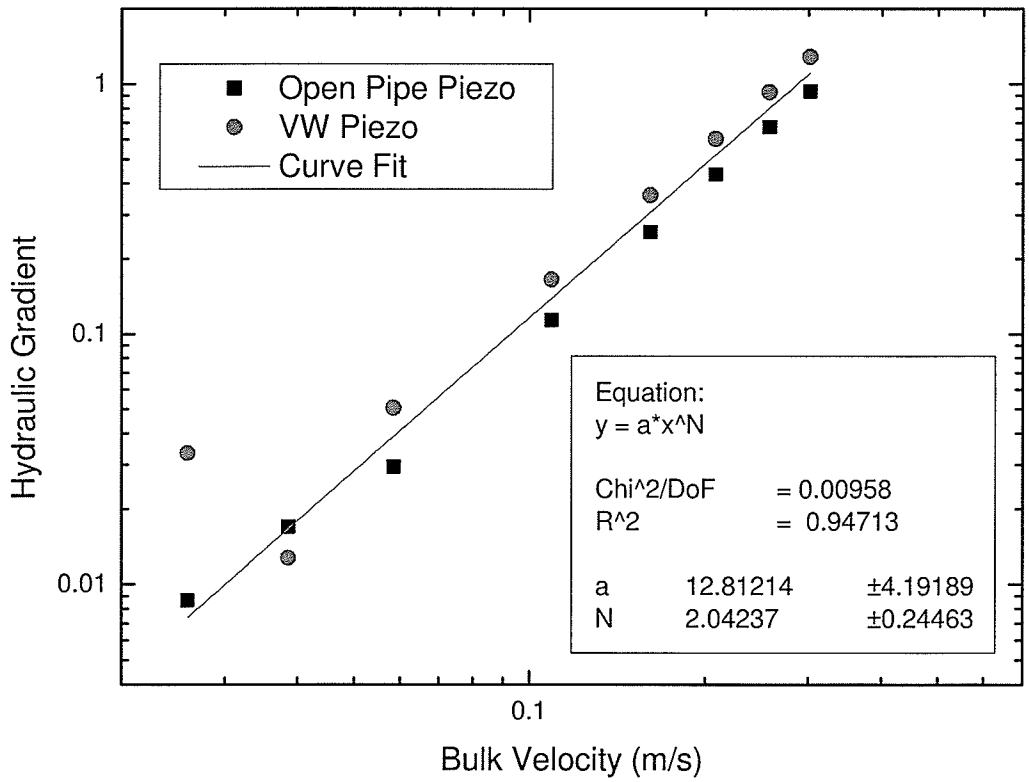

Figure 4.27 – Permeameter Test 11

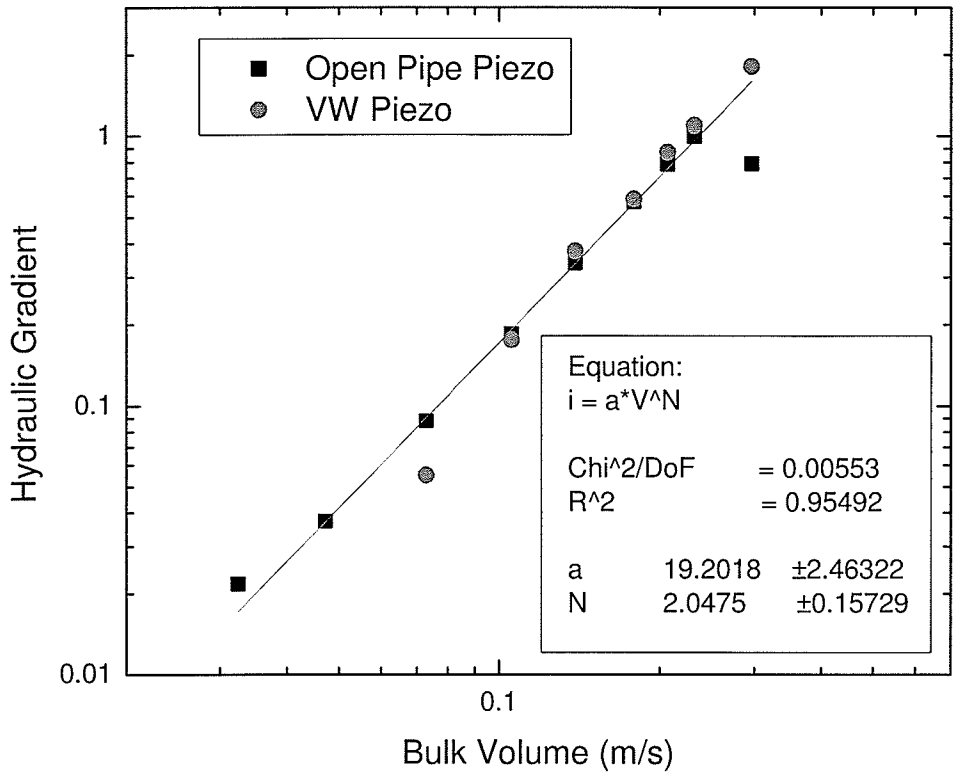

Figure 4.28 – Permeameter Test 12

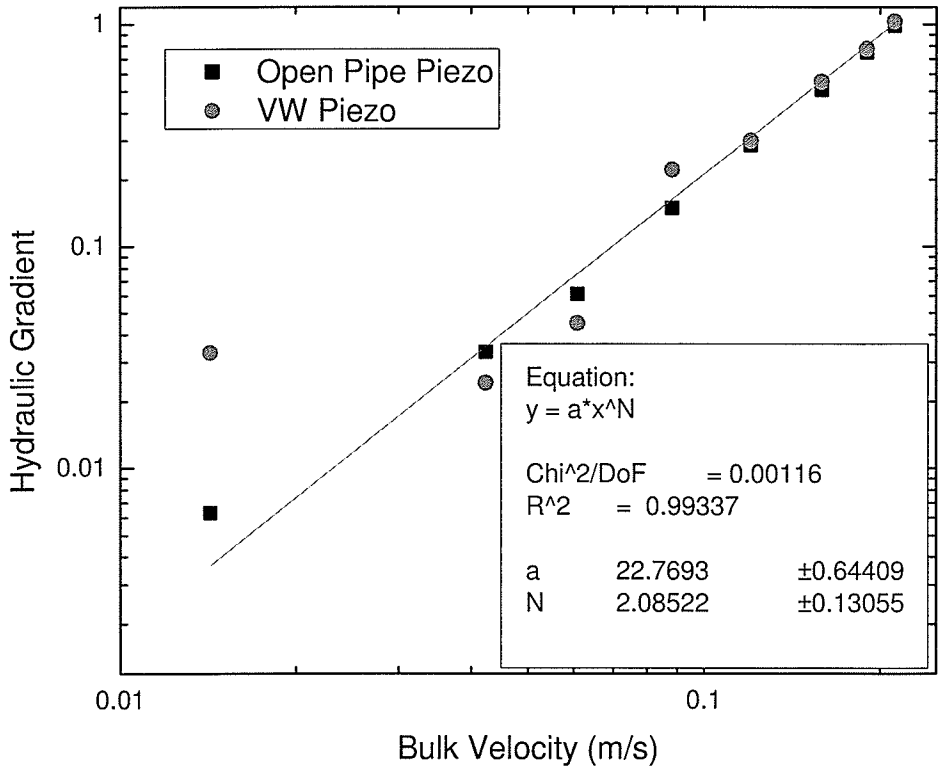

Figure 4.29 – Permeameter Test 13

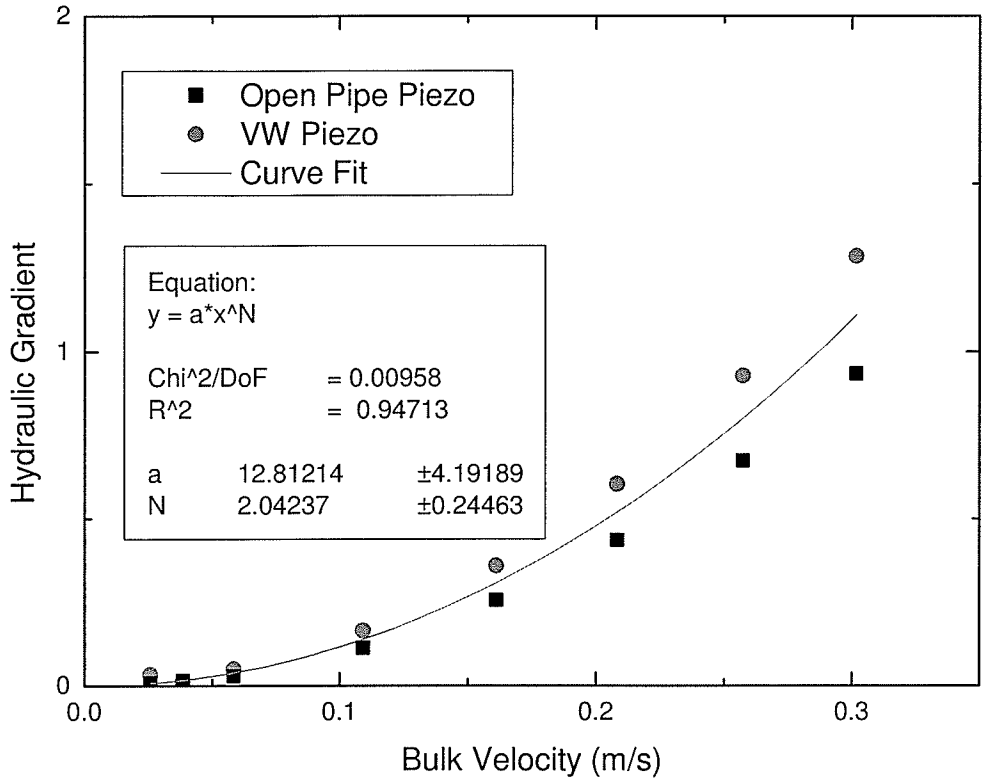

Figure 4.30 – Permeameter Test 11, Shown on Linear Axis

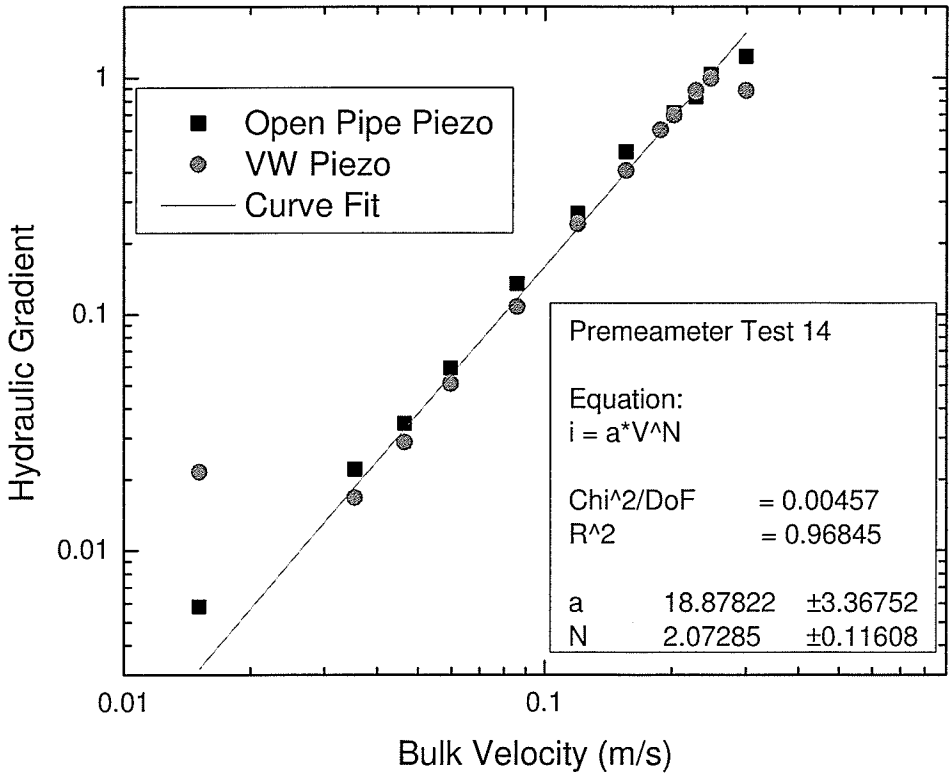

Figure 4.31 – Permeameter Test 14

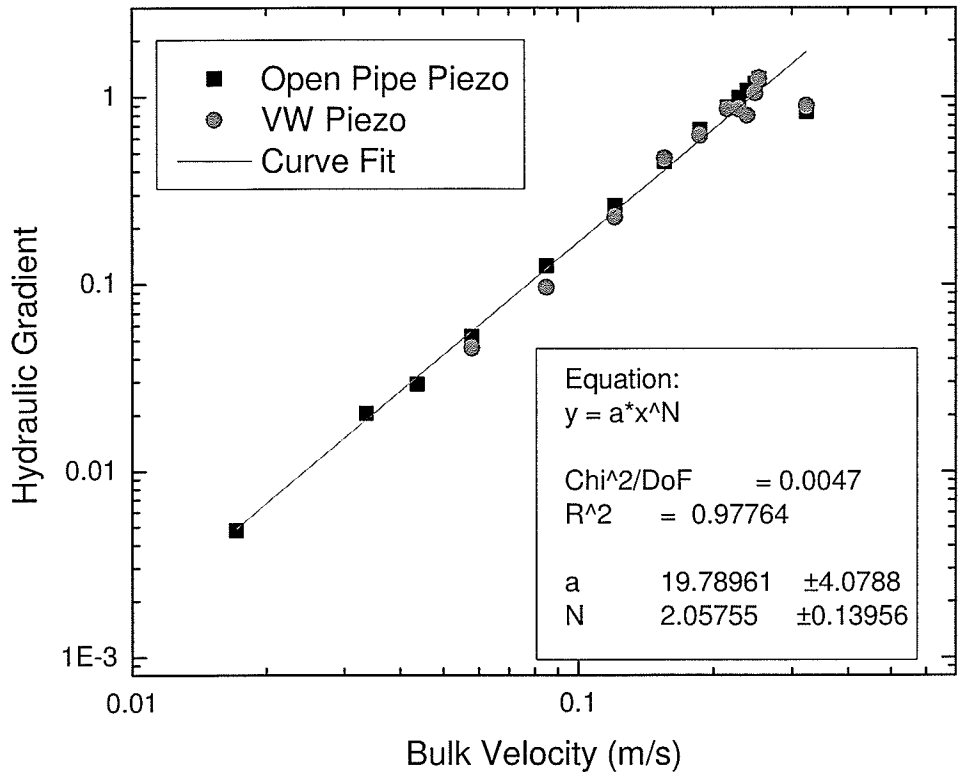

Figure 4.32 – Permeameter Test 15

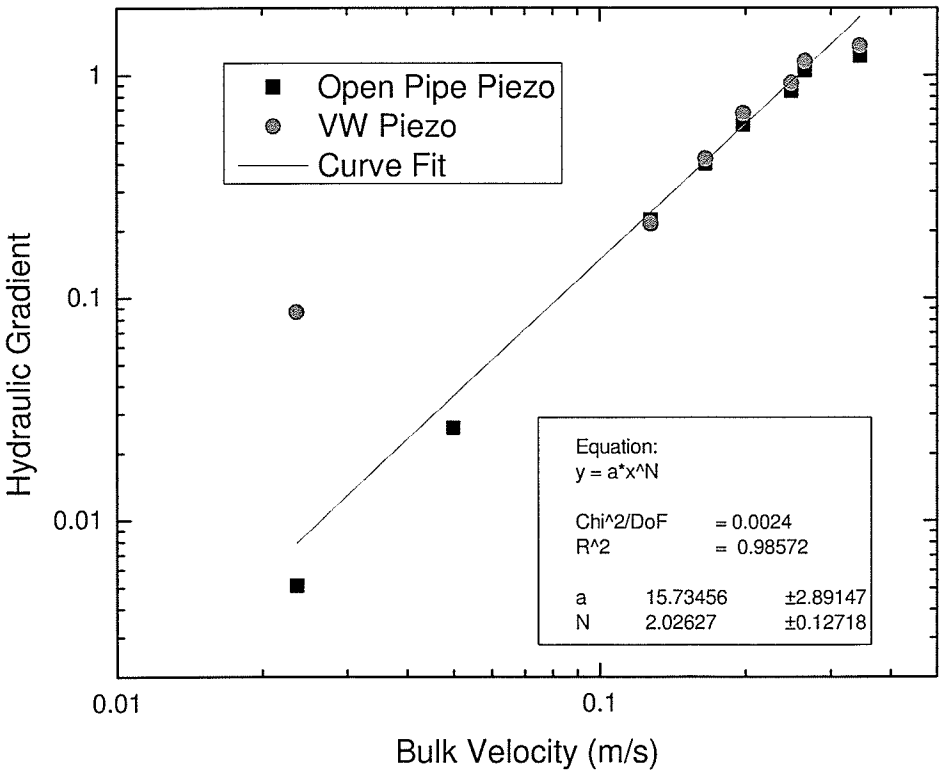

Figure 4.33 – Permeameter Test 16

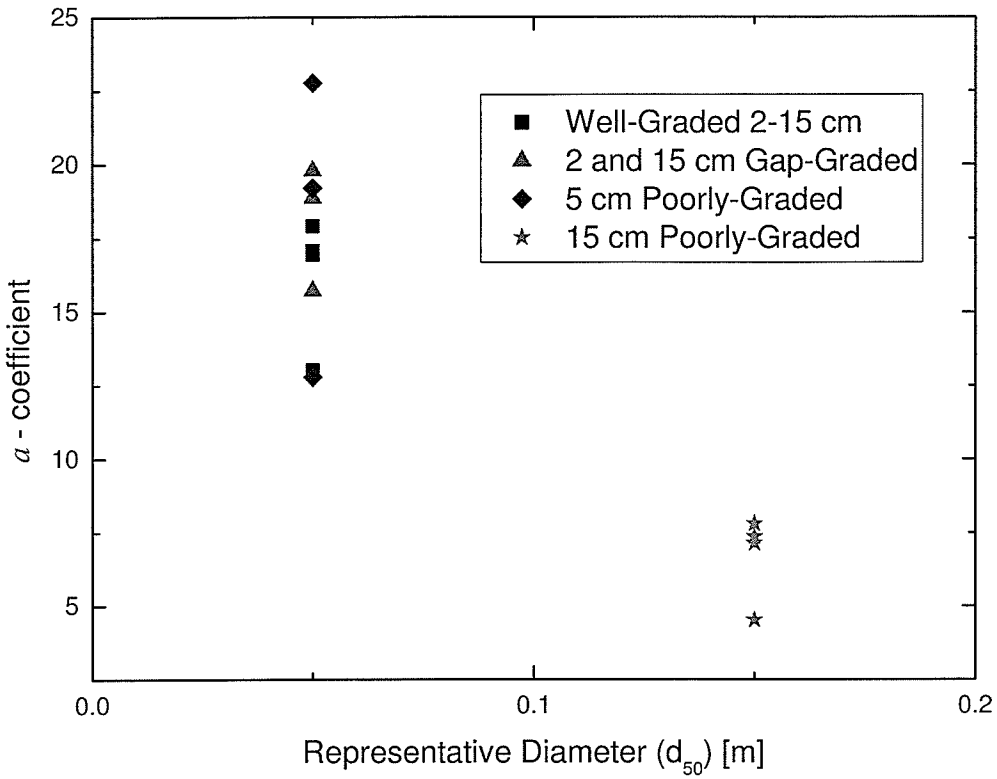

Figure 4.34 – d_{50} versus a-coefficient, All Permeameter Tests

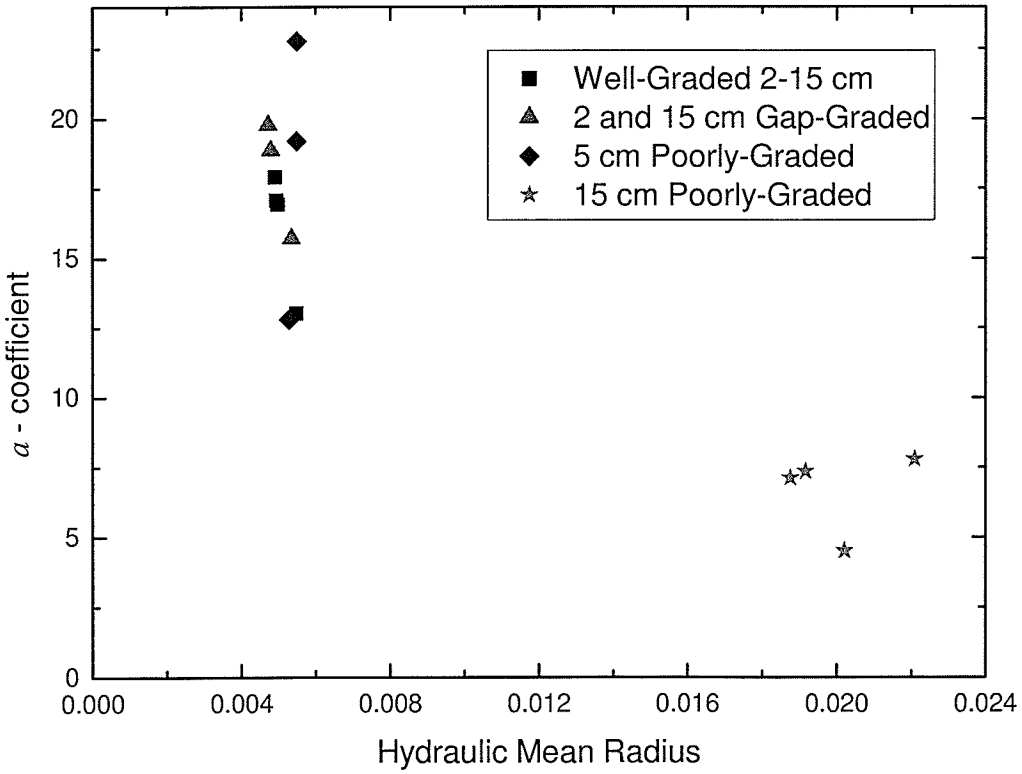

Figure 4.35 – Hydraulic Mean Radius versus a-coefficient, All Permeameter Tests

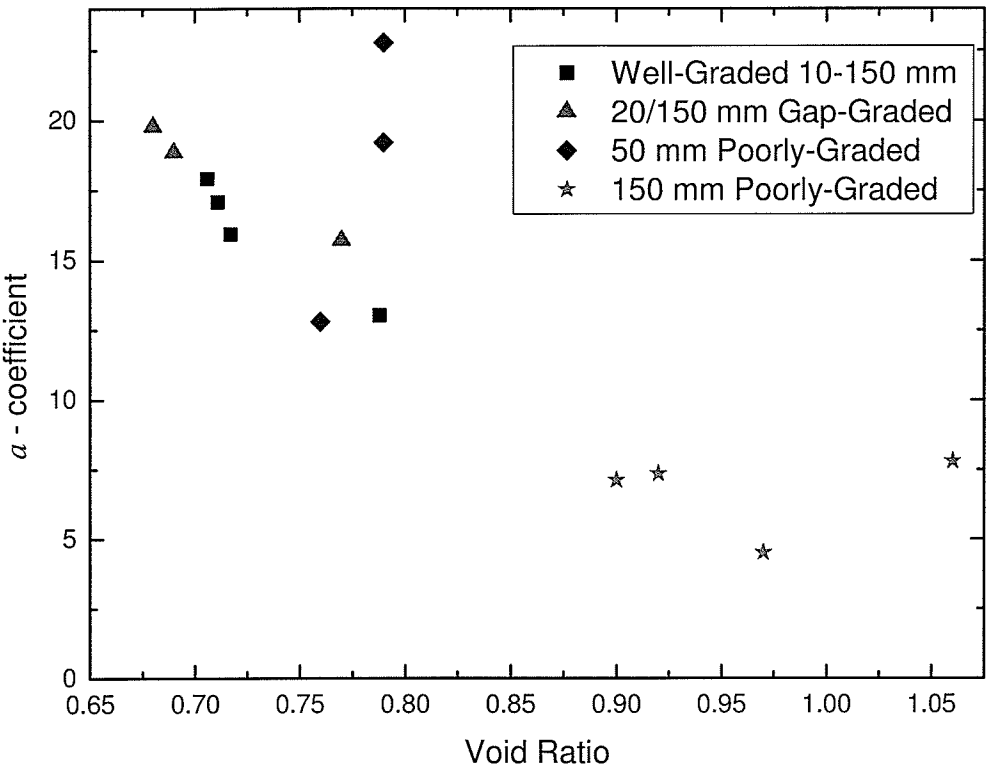

Figure 4.36 – Void Ratio versus a-coefficient, All Permeameter Tests

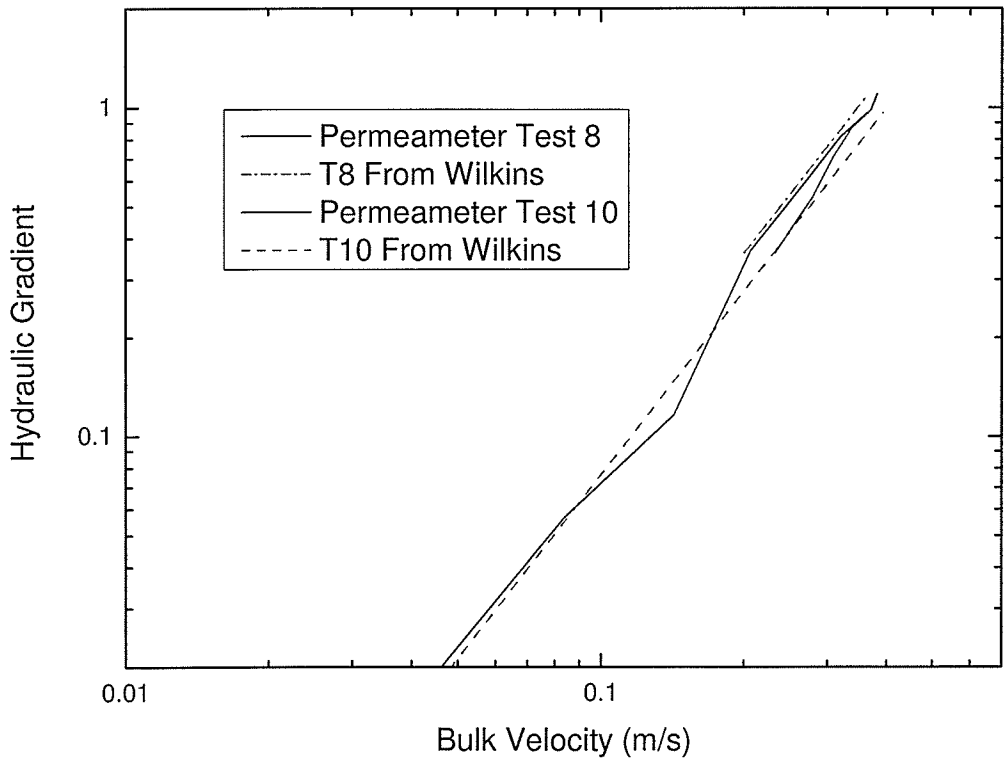

Figure 4.37 – Evaluation of Wilkins' Equation

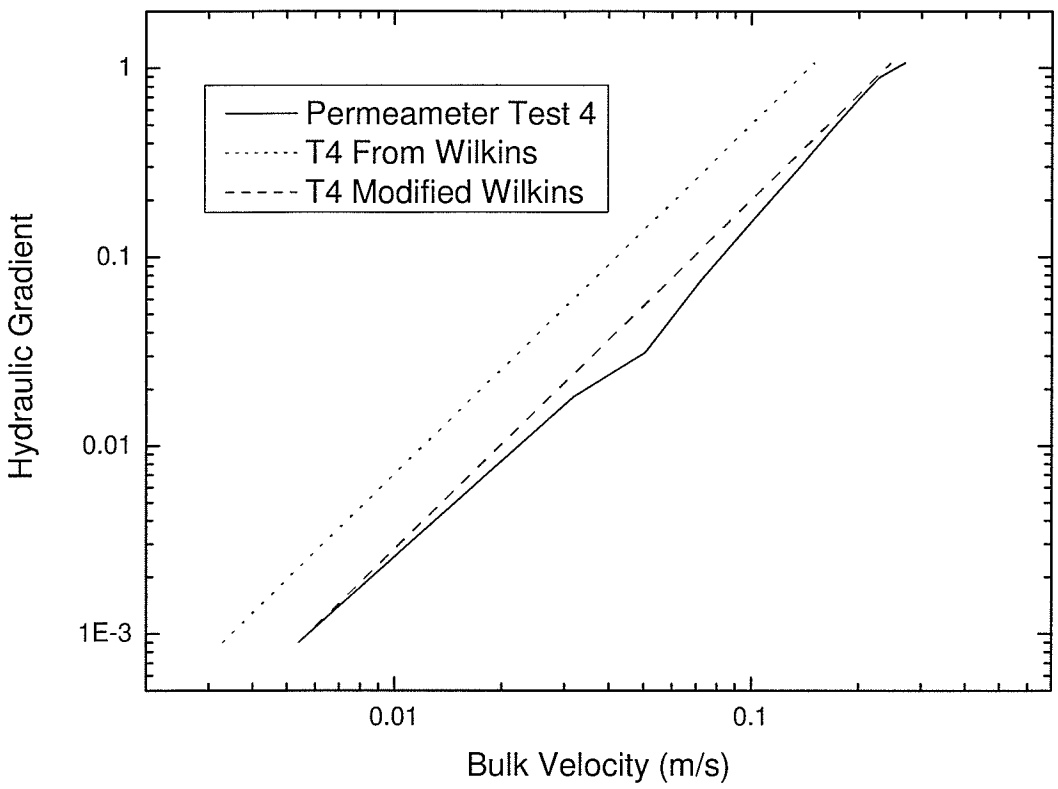

Figure 4.38 – Evaluation of Modified Wilkins' Equation

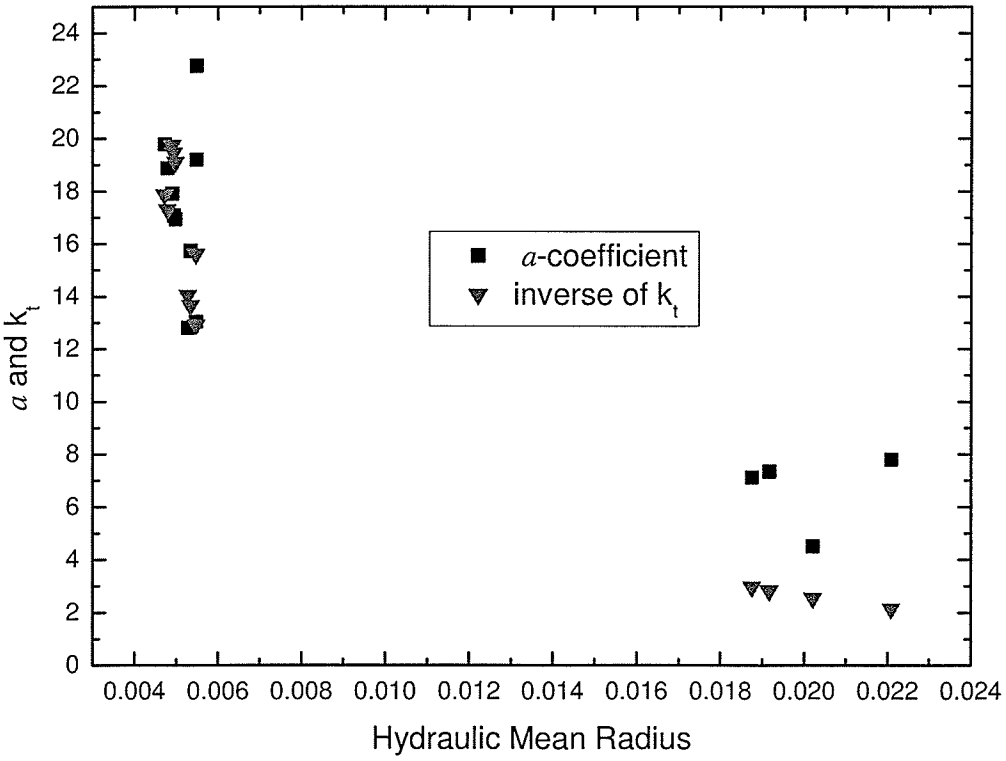

Figure 4.39 – Comparison of a and k_t, versus Hydraulic Mean Radius

5 MINI DAMS

5.1 GENERAL

Fifteen miniature dams were constructed and tested to provide sensitivity studies for geometric properties to aid in the design of the scale dam experiment (described in Chapter 6). The miniature structures were referred to as mini dams (notation: MD1 through MD15) as they were notably smaller than the planned scale dams. The scope of the mini dam experiments was to identify areas of concern during construction and operation for the planned scale dams, to confirm the flow through properties of the rockfill, and to test the initiation of particle movement with the variables of downstream slope angle, compaction, and gradation.

5.2 MINI DAM TESTING FLUME

The mini dams were constructed in the water return flume used for the large-scale permeameter. Originally designed as a flow diversion channel for the large-scale permeameter, the mini-dam flume (Figure 5.1) was upgraded to allow the testing of the small structures. The flume was approximately 18 m long, 0.65 m tall, and had two widths 1.9 m and 1.5 m with a linear transition between the two sections. The flume floor was the laboratory floor, consisting of smooth concrete with some minor abrasions and having negligible slope. One wall was the existing outside of the concrete random wave-sediment flume. The second wall was wood framed with engineered plywood sheathing along the length except at the location of the mini-dam, which was fitted with a clear acrylic panel.

5.3 DAM CONSTRUCTION

Each mini dam was constructed 0.5 m tall, 1.45 m wide, with a 1 vertical to 1 horizontal (1V:1H) upstream face. The downstream face varied between tests, the three slopes selected for testing were 1V:1H, 1V:1.5H, and 1V:2H. Figure 5.2 shows the geometry of a 1V:1H mini dam.

Placement of the rockfill was completed using a bucket dumping technique from a predetermined height for compaction. Some hand placement of rockfill was required to maintain control of the dimensions and therefore the volume of the dam. The mass of rock in each dam varied depending on the use of compaction and particle gradation. Table 5.1 provides details of the construction of each dam, including the mass of rock used as well as the bulk void ratio of the structure. The column labeled 'Compacted' refers to the use of a standard compaction method (described later). Toe reinforcement refers to the use of a rockfill blanket placed at the toe of the dam to prevent erosion of the toe.

Table 5.1 – Mini Dam Construction Information					
Test #	**Downstream Slope**	**Mass of Rock (kg)**	**Void Ratio**	**Compacted**	**Toe Reinforcement**
150 mm Poorly Graded					
MD1	1V:1H	-	Low	-	-
MD2	1V:1H	-	High	-	-
50 mm Poorly Graded					
MD3	1V:1H	771	0.825	-	-
MD4	1V:1H	771	0.825	-	-
MD7	1V:1H	812	0.734	Standard	-
MD10	1V:1H	773	0.819	-	Rock at toe
MD11	1V:1H	853	0.65	Standard	Rock at toe
MD5	1V:1.5H	871	0.904	-	-
MD6	1V:1.5H	871	0.904	-	-
MD8	1V:1.5H	941	0.762	Standard	-
MD12	1V:1.5H	954	0.738	Standard	Rock at toe
MD13	1V:2H	1031	0.803	Standard	Rock at toe
MD9	1V:2H	1065	0.792	Standard	Rock at toe
10-150 mm Well Graded					
MD14	1V:1H	870	0.574	Standard	Rock at toe
MD15	1V:1.5H	999	0.616	Standard	Rock at toe

To vary the porosity of the mini dams while maintaining all other variables, compaction using a standard method was completed for some tests. The method was as follows:

1. Fill bottom of standard 5-gallon bucket with 5 kg of 2" diameter rock.
2. Place an even 15 cm layer of rock using the standard bucket dumping method.

3. Hold the compaction bucket 15 cm from the rock surface; drop such that it hits the surface evenly.
4. Repeat this motion, moving the bucket in the upstream to downstream direction, so that the rock surface is impacted by 1/3 more of the bucket width per impact.
5. When the upstream to downstream line has been completed, move adjacent to the first line and repeat steps 3 and 4.
6. Continue until the entire layer has been compacted.

5.4 Measurements And Instrumentation

During construction of each mini dam the mass of rock used in the dam was measured. As well, the size and shape of the dam was strictly maintained for ease of calculating the volume of the structure. Using the mass and volume, the bulk void ratio was calculated for each dam.

Although the number used in each test varied, vibrating wire piezometers were placed upstream, downstream and within the dam to provide point measurements of pore water pressure. The piezometers were the same ones used in the large-scale permeameter testing. The main goal of installing the piezometers was to test their abilities within a rockfill structure.

During operation of the mini dams the discharge, upstream water level, downstream water level, phreatic surface and water exit height were measured. The discharge was measured with the method described in Section 4.2.

Upstream and downstream water levels were measured using an aluminium measuring stick, as well as vibrating wire piezometers. The phreatic surface was observed through the clear acrylic wall (see Figure 5.3), observed as the height of wet rock and was traced on to the acrylic at several stages. The water exit height, the greatest height at which water exits the face of the dam, was observed and measured both on the face of the dam and on the acrylic wall.

5.5 OBSERVATIONS

5.5.1 Vibrating Wire Piezometers

It was observed during testing of the mini dams that the vibrating wire piezometers produced readings that did not match readings manually measured. Further tests within the dam and independent tests conducted in an open flume found that the velocity of water passing the piezometer affected the readings. When the piezometer tip, porous stone and sensor, was placed facing into the direction of flow, the measured head was up to 15% greater than the measured depth, over the velocities tested. When the piezometer tip was placed perpendicular to the flow, no appreciable difference between measured head and measured depth was observed. When the piezometer tip was placed in the downstream direction with the flow, the measured head varied slightly from the measured depth.

5.5.2 Dam Contact Surfaces

Particle movement occurred in a number of dams at flow rates and upstream water levels lower then anticipated. Many of these movements occurred at the edge of the dams at the rockfill-acrylic wall interface. It was assumed that the smoothness of the acrylic did not provide enough friction to support the structure. As well, it was observed in three dams that the entire structure had shifted downstream. Due to the unexpected nature of the latter movement, no measurements or observations were made of this phenomenon during the first 9 tests. The greatest movement occurred on a poorly graded, compacted, 1V:1.5H dam. The structure adjacent the acrylic wall moved approximately 20 mm over the course of the test. The magnitude of the movement was observed on the upstream mid-slope, upstream crest and downstream crest. Unfortunately, the downstream slope was not monitored for this movement.

Another movement, which occurred frequently, was the erosion of the downstream toe. This movement occurred within the first few flow increments at low discharge, and was considered premature failure to what would occur in a full-scale structure. The rock to flume floor interface friction was considered to be less than the conditions found in full-scale structures and therefore improving the friction interface or restraint of the erosion movement was required. To restrict the toe rocks, a downstream rock blanket at the toe was introduced for MD8 through MD15. This solution did not address the fundamental problem of the

flume floor frictional resistance, but did accomplish the task of restricting the movement of toe material.

During previous testing at The University of Manitoba, researchers encountered issues with premature failure of an experimental water retention structure due to low wall to structure interface friction. Therefore, to ensure that undesirable movement of the scale dams did not occur, measures were undertaken to increase the frictional resistance of the surfaces of the scale dam flume.

5.6 TEST RESULTS

The description of results of the mini dam experiment is located in the following paragraphs, and includes a summary of the data collected in Table 5.2.

The flume utilized in this experimental program was originally intended to direct water exiting the large-scale permeameter and as such, unregulated seepage occurred under the wooden wall. No attempt was made to quantify the amount of seepage, as it was dependant on the upstream water level in the flume, as well as the state of the seal underneath the wall, which was deteriorating during each test and being repaired between each test. As such, only the magnitudes of measured discharges through the dam will be referenced.

5.6.1 MD1 and MD2

The first two mini dams completed (MD1, MD2) were not extensively monitored, as their primary goal was to test the flume and gain insight into the water

retention abilities of the rockfill. The material used in these first two tests was 150 mm poorly graded rockfill. The first test (MD1) was constructed with a downstream slope of 1V:1H using the bucket placement method and although not measured, was considered to have a lower void ratio than MD2. MD1, shown in Figure 5.4, was operated until the upstream water level reached 40 cm with a discharge through the structure in excess of 80 l/s. At that point the dam was partially dismantled to reduce the upstream water level, as improvements to the flume for conducting the mini dam test had not been completed.

MD2 was constructed at 1V:1H by hand placing rockfill on the existing partially dismantled MD1. The hand placement was intended to increase the void ratio and potentially induce a flow-through failure. Failure from flow through causing reduction of crest height and inducing overtopping, shown in Figure 5.5, was noted at upstream water levels less than the maximum of MD1; as well the discharge at failure was less than 80 l/s.

After the second test the 150 mm particle gradation was no longer employed. The dimensions of the rockfill to that of the dimensions of the dam, was not scale representative of actual structures. As well, with the limited upstream water level available, void ratios required to induce flow through particle movement would not be representative of that found in the field.

5.6.2 MD3 to MD8

The rockfill used in tests MD3 to MD8 was 50 mm poorly-graded material. These tests were constructed with the bucket dumping method and compaction was completed on MD7 and MD8. No toe stabilization was employed during the testing of these dams. An example, MD7, is shown in Figure 5.6.

MD3 and MD4 were constructed as a 1V:1H downstream slope dams, with no compaction. Both used approximately the same mass of rock, and therefore the same void ratio. All variables in the dam construction were repeated from MD3 to MD4 to test for repeatability. Comparing the phreatic surfaces from MD3 (Figure 5.7) and MD4 (Figure 5.8), the height of the phreatic surfaces for a given discharge are similar, as are the slope of the surfaces. In comparing the failure mechanisms, listed in Table 5.2, both dams experienced toes sliding at low discharge rates. This effected later slides, which are noted to have different discharge rates at movement. However, the final overtopping failures occur at similar discharge rates. From comparison of MD3 and MD4, the repeatability of the mini dam tests appears to be good.

MD5 and MD6 were constructed with 1V:1.5H downstream slopes with no compaction. To reduce void ratio, both MD7 at 1V:1H and MD8 at 1V:1.5H were compacted. In Figure 5.9 through Figure 5.12, representing MD5 through MD8 respectively, the magnitude and slope of the phreatic surfaces appear similar. The failure mechanisms of all 6 dams, MD3 through MD8, occurred in a similar

manner and at similar discharges as noted in Table 5.2 under the column 'Flow Through Movement Comments'. First to occur was toe sliding, as observed in Figure 5.20, which led to a steepening of the downstream slope. The second movement, although not observed in all tests was movement of individual particles which were not interlocked on the surface of dam. Next was a large movement of several particles, extending from two-thirds up the downstream face to near the toe. This movement and subsequent depression was difficult to capture in a photograph, as it tended to blend in with the surrounding material. Later in the test, further movement of particles on the downstream face tended to cause a reduction in height of the downstream crest, as observed on the right hand side of MD7 and shown in Figure 5.21. This caused overtopping, shown in Figure 5.22 and Figure 5.23, at an elevation lower than the constructed crest height.

5.6.3 MD9 to MD13

Mini dams MD9 to MD13 were constructed with 50 mm diameter poorly-graded rockfill, employed a downstream toe blanket constructed as a single layer of 150 mm rockfill from the stockpile. The blanket prevented toe erosion in the early stages of a test and observed movement occurred at increased discharge, when compared to the mini-dams without a blanket, as can be seen in Table 5.2. The phreatic surfaces of MD9 to MD13 are located on Figure 5.24 to Figure 5.28 respectively.

To evaluate the effects of the downstream blanket on the discharge through the mini dams as well as the phreatic surface a comparison between two like dams was completed. MD10 was the first dam with a downstream toe blanket that could be compared to that of a mini dam with no blanket, MD3. At a discharge of 0.013 $m^3/s/m$, for both MD3 (Figure 5.7) and MD10 (Figure 5.25), the upstream level is a little over 20 cm and the exit height is approximately 10 cm. As well, the slopes of the phreatic surfaces are similar. At a larger discharge, Q=0.034 and Q=0.038 $m^3/s/m$ for MD3 and MD10 respectively, the upstream water levels are at similar elevation, while the exit heights are approximately 20 cm (MD3) and 25 cm (MD10). This can be explained by noting that a large number of particles moved at 0.034 $m^3/s/m$ near the center of MD3, reducing the seepage path and therefore energy dissipation, causing a preferential flow path and reducing flow at the edge of the dam. Also note the increased upstream water level (10%) and discharge (50%) at observed movement in MD10 over MD3, indicating failure may be premature in MD3 due to the low friction interface between rockfill and concrete floor (Table 5.2).

MD9 and MD13, the 1V:2H dams, had reductions in crest widths due to particle movement induced by flow through. However, the crest heights of both dams were not reduced by the failures on the seepage face, unlike all other 50 mm poorly graded dams. Catastrophic failure did not occur until the water reached maximum crest height when overtopping occurred.

5.6.4 MD14 and MD15

The gradation used for MD14 and MD15 was well-graded 10 to 150 mm rockfill, the same as was utilized in the large-scale permeameter. The particle gradation distribution can be found in Figure 3.5.

The well-graded material produced low void ratios making it difficult to compare with the 50 mm poorly-graded material. However, Table 5.2 shows that movements in the well-graded tests occurred at larger discharges than the 50 mm poorly graded rockfill, even though the smallest particle in the well-graded rockfill was less than 20 mm in diameter. The slope of the phreatic surfaces for both MD14 and MD15 (Figure 5.29 and Figure 5.30) are shallower through the dams than that of the 50 mm poorly graded dams. This represents a lower hydraulic gradient and therefore lower velocity through the well-graded dams. Also observed in MD14 and MD15 was the lack of significant reduction of crest height that was observed in the 50 mm poorly graded dams. This suggests that the structure of the well-graded rockfill was more stable than that of the 50 mm poorly graded rockfill.

Table 5.2 – Test Results of the Mini Dams

Test #	Downstream Slope	Void Ratio	Q @ movement [l/s/m length]	Upstream Water Level [m]	Flow-through Movement Comments	Overtopping Comments
150 mm Poorly Graded						
MD1	1V:1H	Low	-	-	No movement	Dam was not overtopped
MD2	1V:1H	High	< 80	-	Several rocks washed downstream	Dam was not overtopped
50 mm Poorly Graded						
MD3	1V:1H	0.825	33.9	37.5	Toe slide at 12.5 l/s/m. First slide at 33.9 l/s/m.	Crest lowered, overtopping (@42 cm) > 50 l/s/m
MD4	1V:1H	0.825	28.9	29.6	Significant sliding of toe on concrete at 11 l/s/m.	Crest lowered, overtopped (@40 cm) > 60 l/s/m
MD7	1V:1H	0.734	38.2	40	Toe slide at 12 l/s/m. First movement at 28 l/s/m. First slide at 38.2 l/s/m.	Total of 5 slides before overtopping at 48 cm, at 57 l/s/m.
MD10	1V:1H	0.819	< 53	~ 41	Single rock at 38 l/s/m. Several slides at < 53 l/s/m.	Crest lowered, overtopped at 65 l/s/m
MD11	1V:1H	0.65	53.3	46.6	First mvmt at wall at 46 l/s/m. First slide at center.	Crest lowered, overtopped at < 65 l/s/m
MD5	1V:1.5H	0.904	24.5	27.1	Toe slide at 12 l/s/m. First movement at 20 l/s/m.	Crest lowered to 43 cm, at 51 l/s/m then overtopped
MD6	1V:1.5H	0.904	28.6	32.2	Toe slide at < 14 l/s/m.	Maintained U/S crest at 46 cm
MD8	1V:1.5H	0.762	38.5	42.9	First movement at 29 l/s/m. Sliding along wall.	Crest lowered, @ 46 cm, at 61 l/s/m
MD12	1V:1.5H	0.738	51.2	49.4	First movement at 43 l/s/m.	Crest lowered and overtopped at 62 l/s/m. Failure at 73 l/s/m
MD9	1V:2H	0.792	52.6	50.5	First movement at 32 l/s/m.	Overtopped at 73 l/s/m
MD13	1V:2H	0.803	51.8	51.6	First movement at 27 l/s/m.	Overtopped at > 73 l/s/m
25-150 mm Well Graded						
MD14	1V:1H	0.576	58.2	45.7	Shift was first movement.	Overtopping at > 80 l/s/m
MD15	1V:1.5H	0.616	66.1	51.5	First movement at 45 l/s/m.	At 66 l/s/m particle shift induced overtopping but not collapse

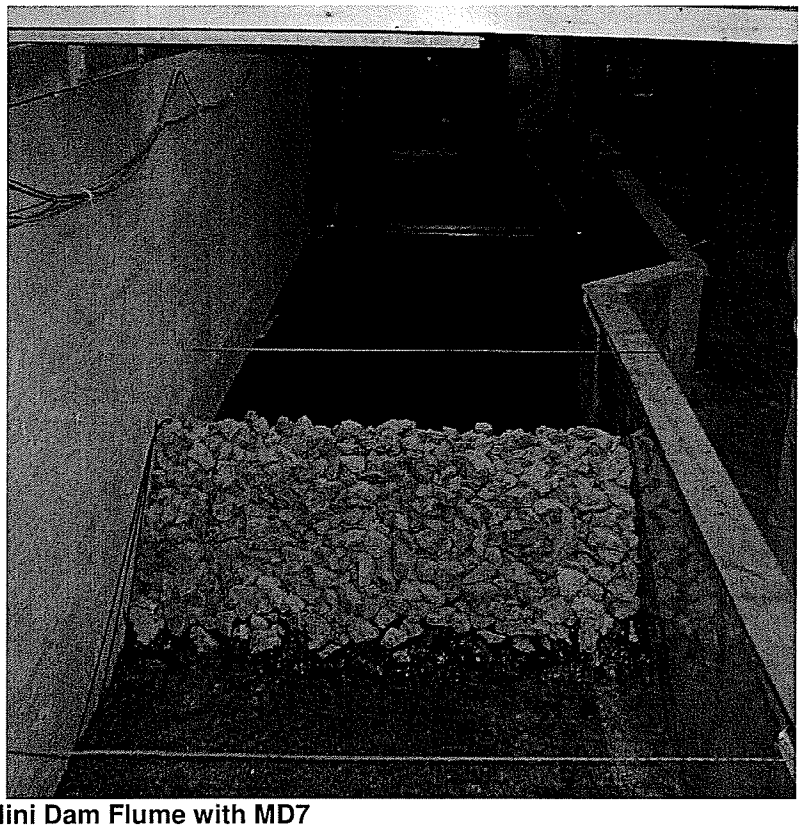

Figure 5.1 – Mini Dam Flume with MD7

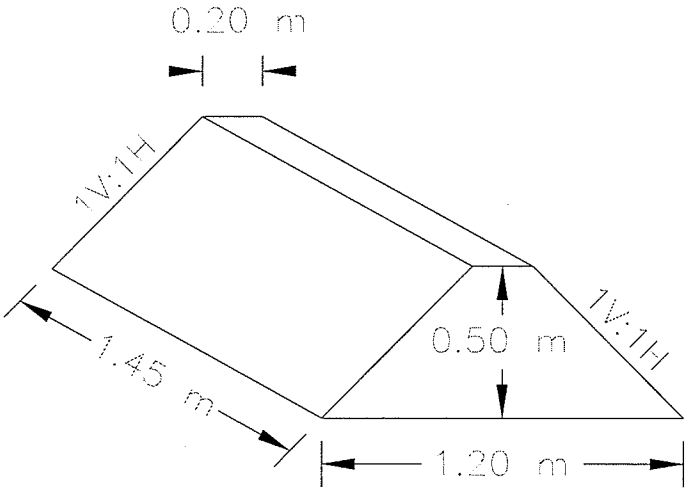

Figure 5.2 – Schematic of Mini Dam with 1V:1H Downstream Slope

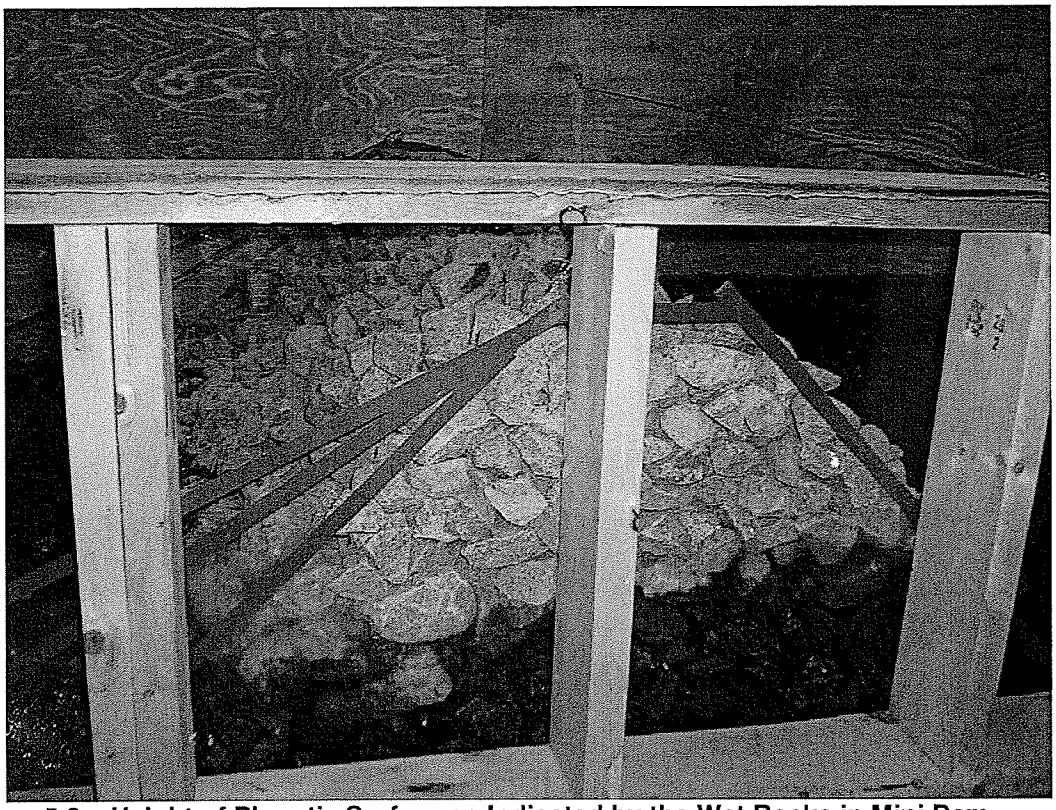

Figure 5.3 – Height of Phreatic Surface as Indicated by the Wet Rocks in Mini Dam

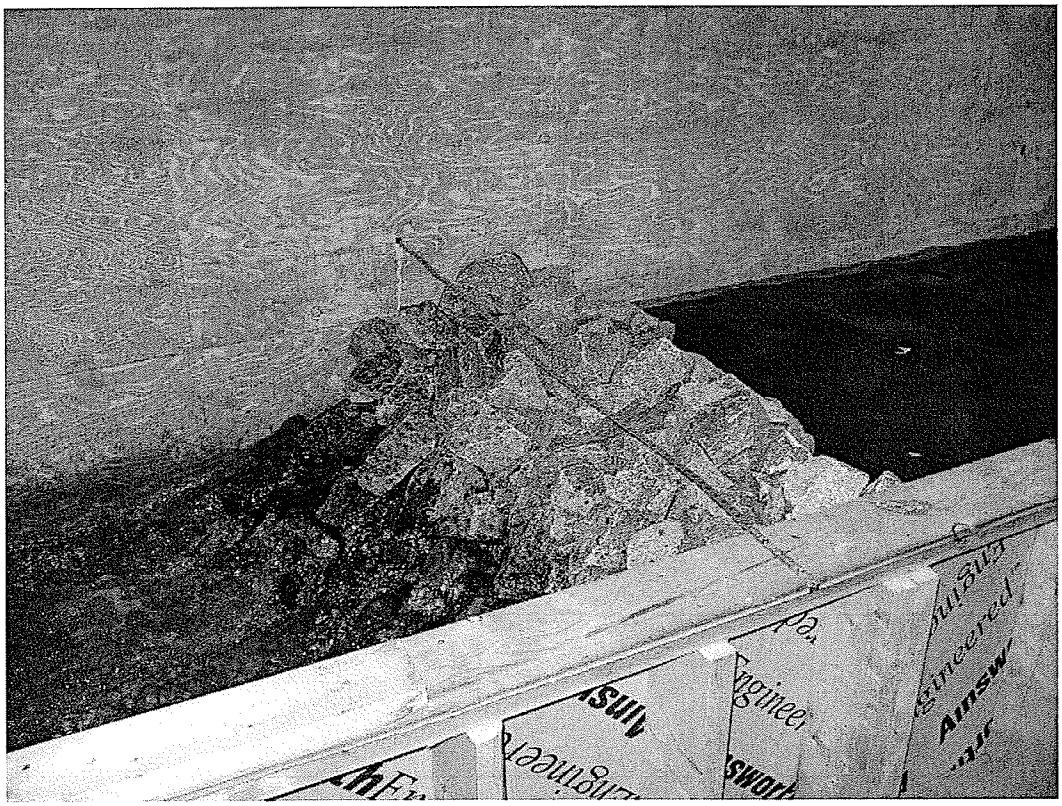

Figure 5.4 – MD1, Upstream Water Level at 35 cm

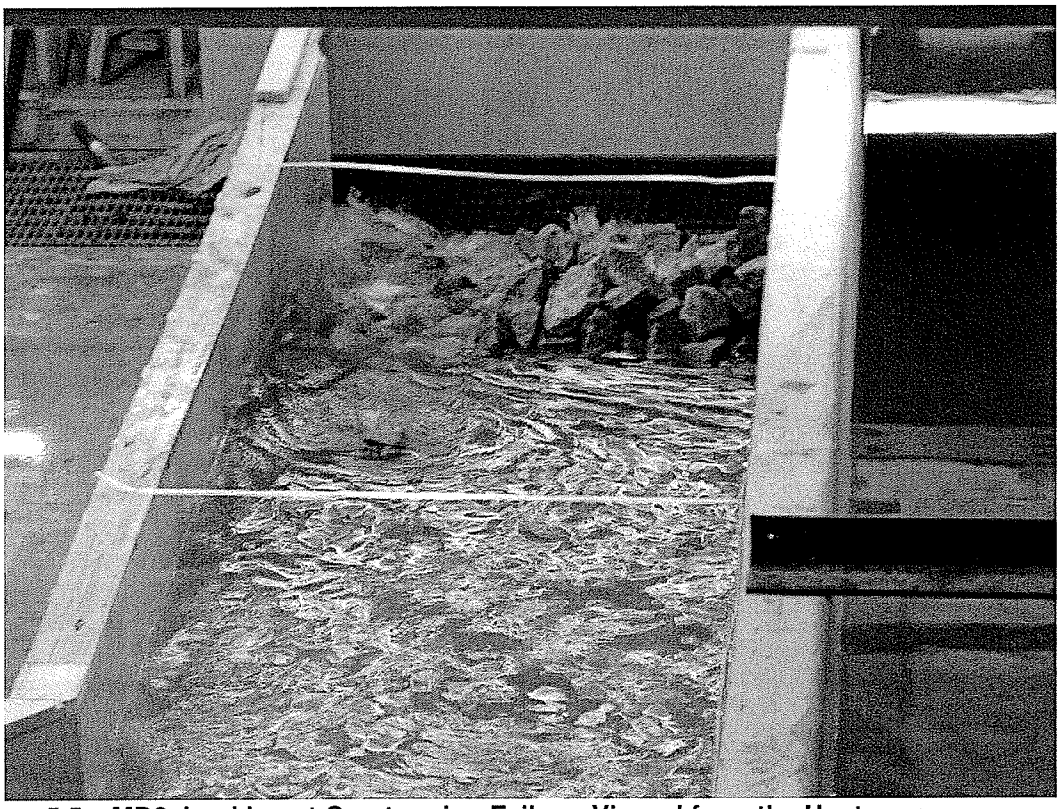

Figure 5.5 – MD2, Looking at Overtopping Failure, Viewed from the Upstream

Figure 5.6 – MD7 Prior to Testing

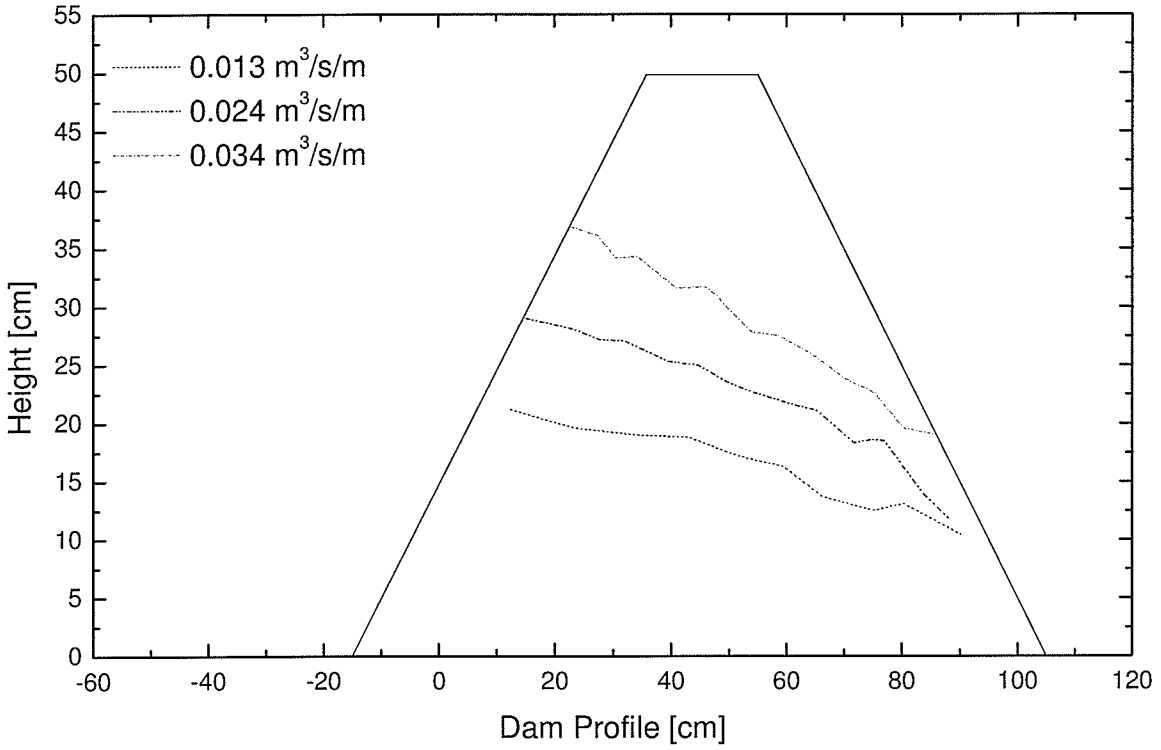

Figure 5.7 – MD3 Measured Phreatic Surfaces

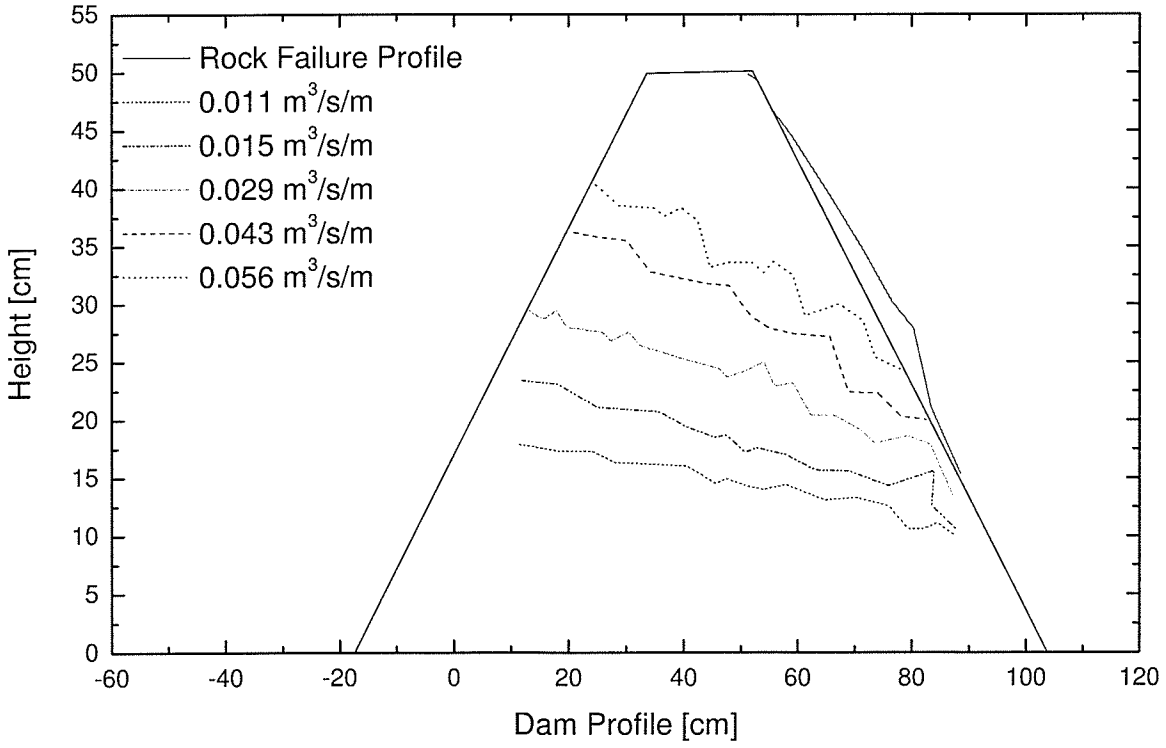

Figure 5.8 – MD4 Measured Phreatic Surfaces

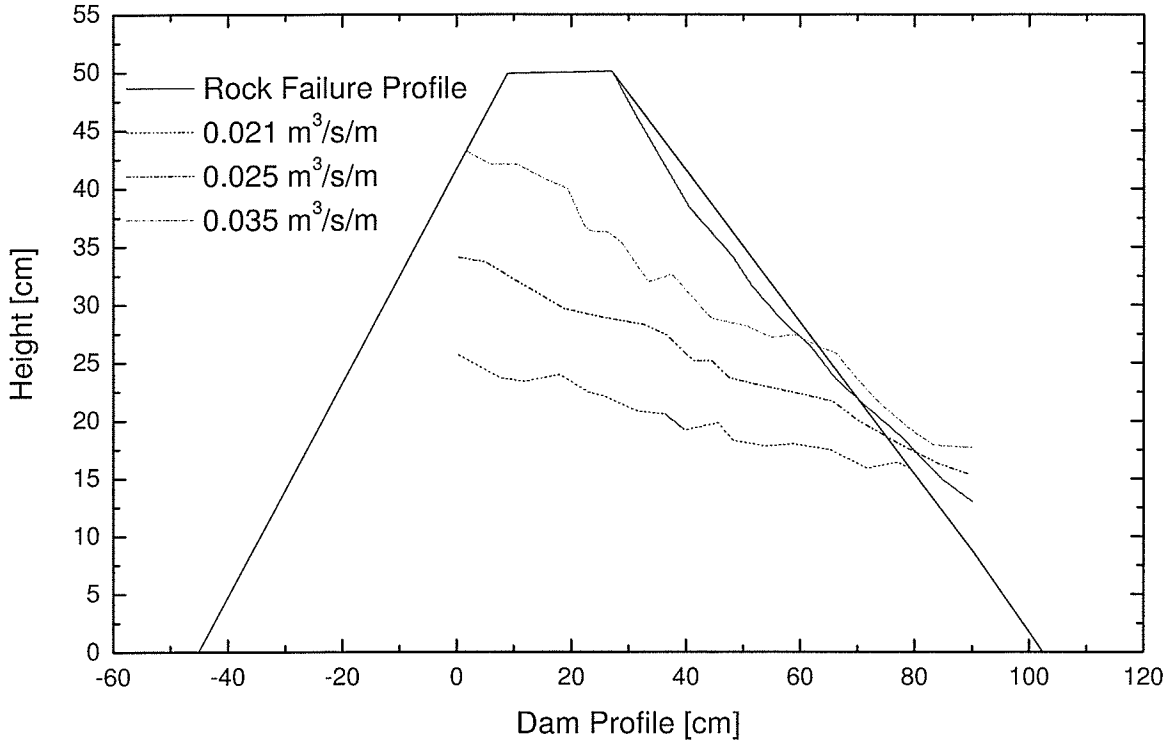

Figure 5.9 – MD5 Measured Phreatic Surfaces

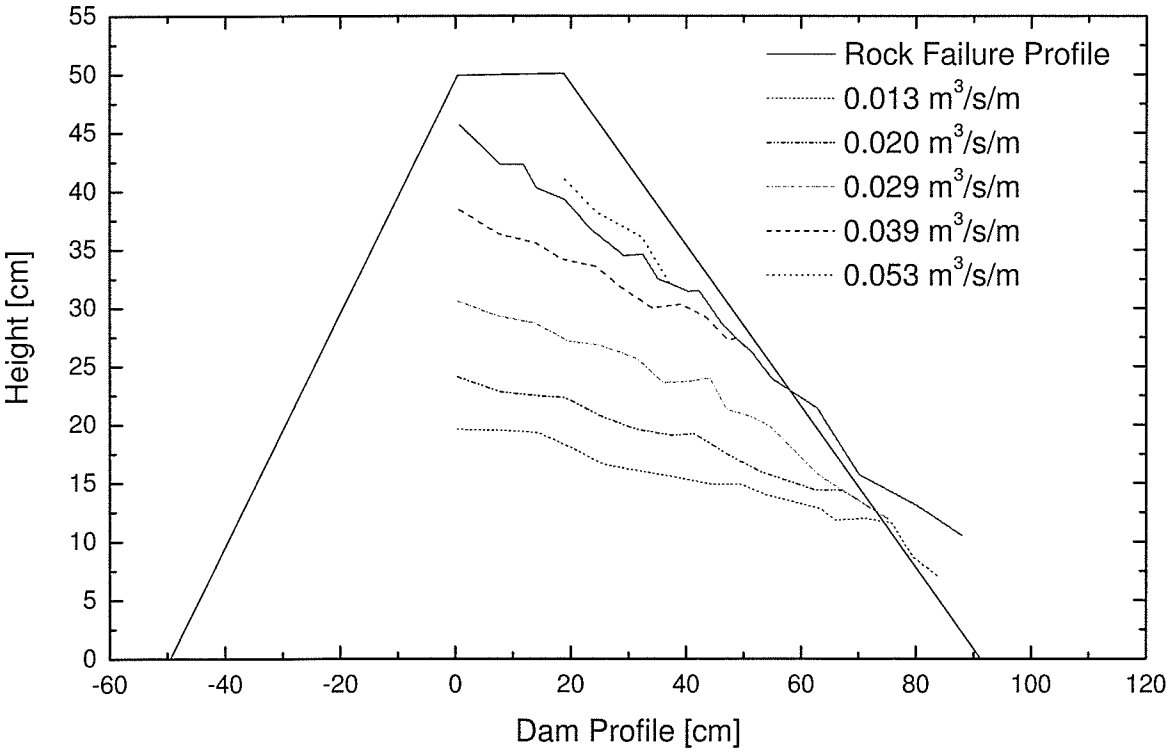

Figure 5.10 – MD6 Measured Phreatic Surfaces

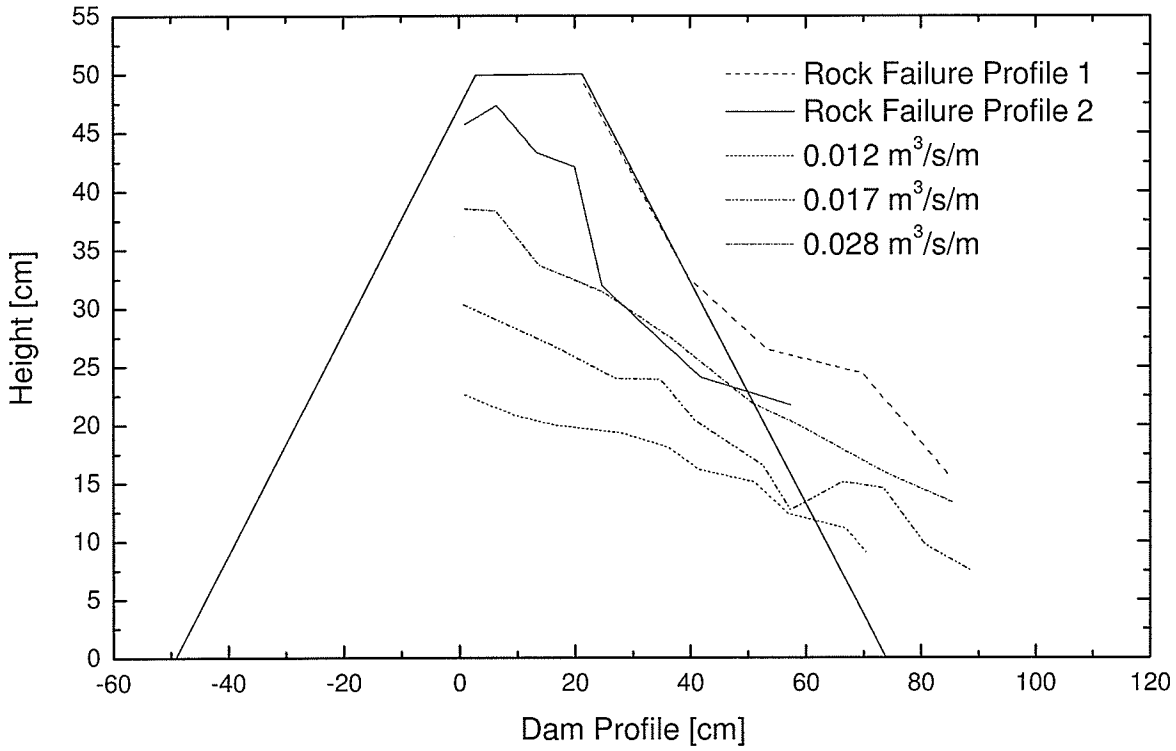

Figure 5.11 – MD7 Measured Phreatic Surfaces

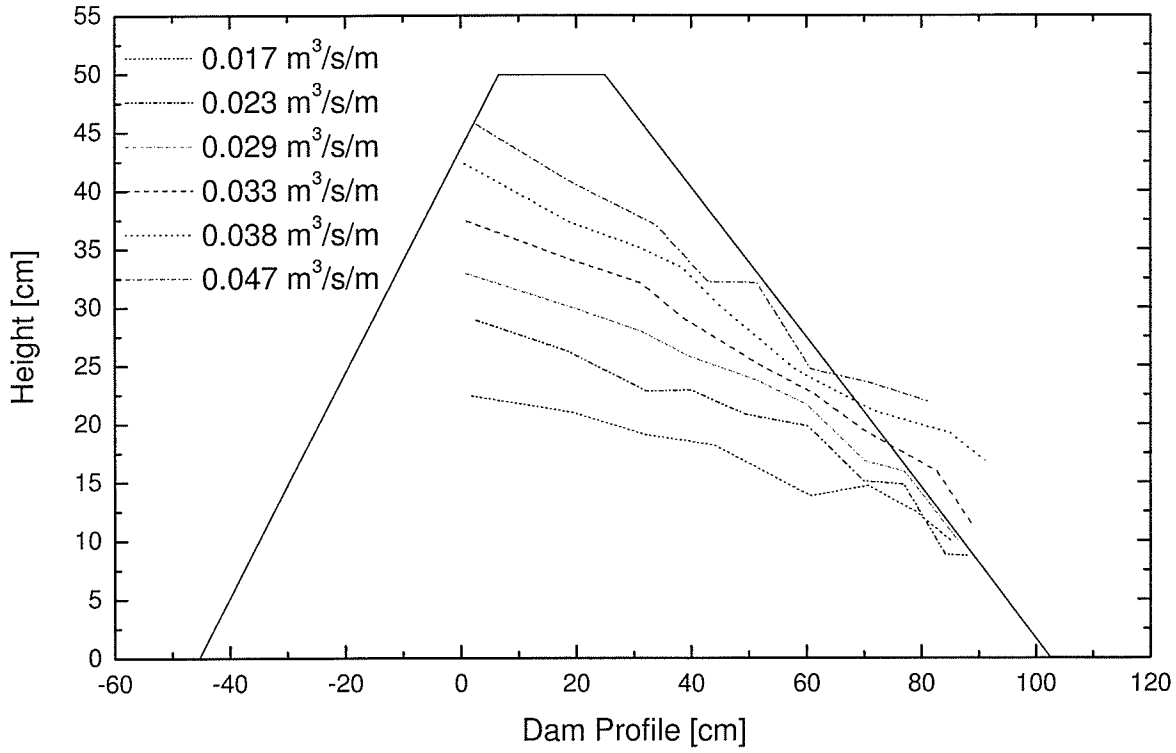

Figure 5.12 – MD8 Measured Phreatic Surfaces

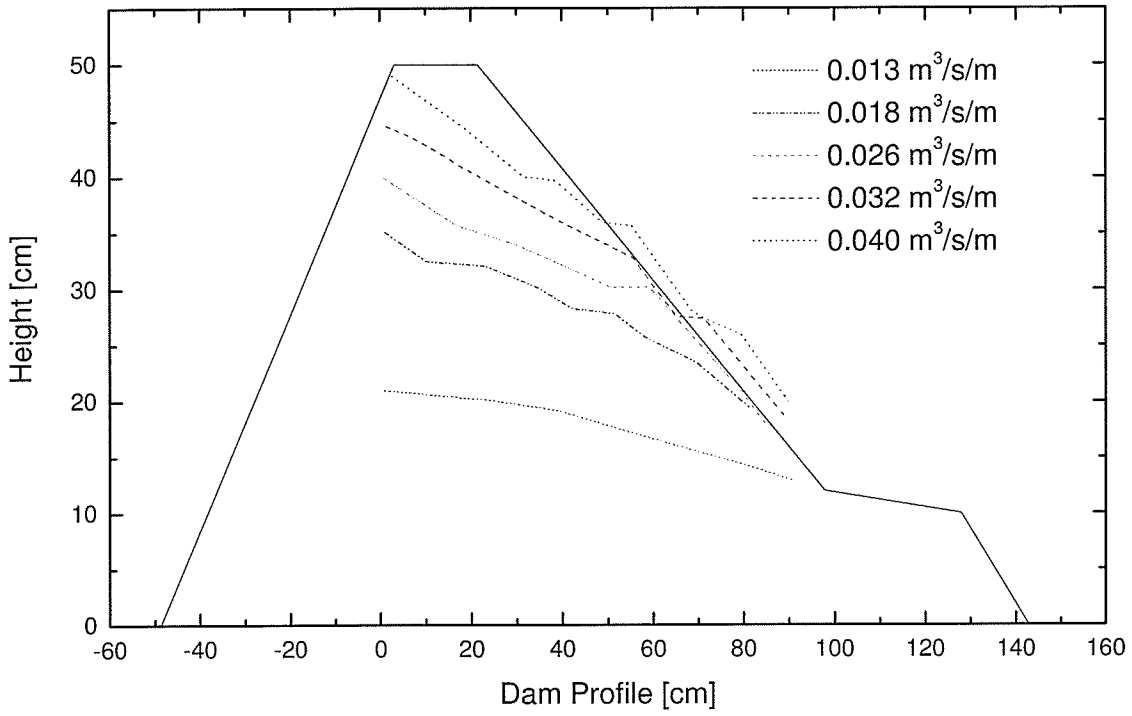

Figure 5.13 – MD9 Measured Phreatic Surfaces

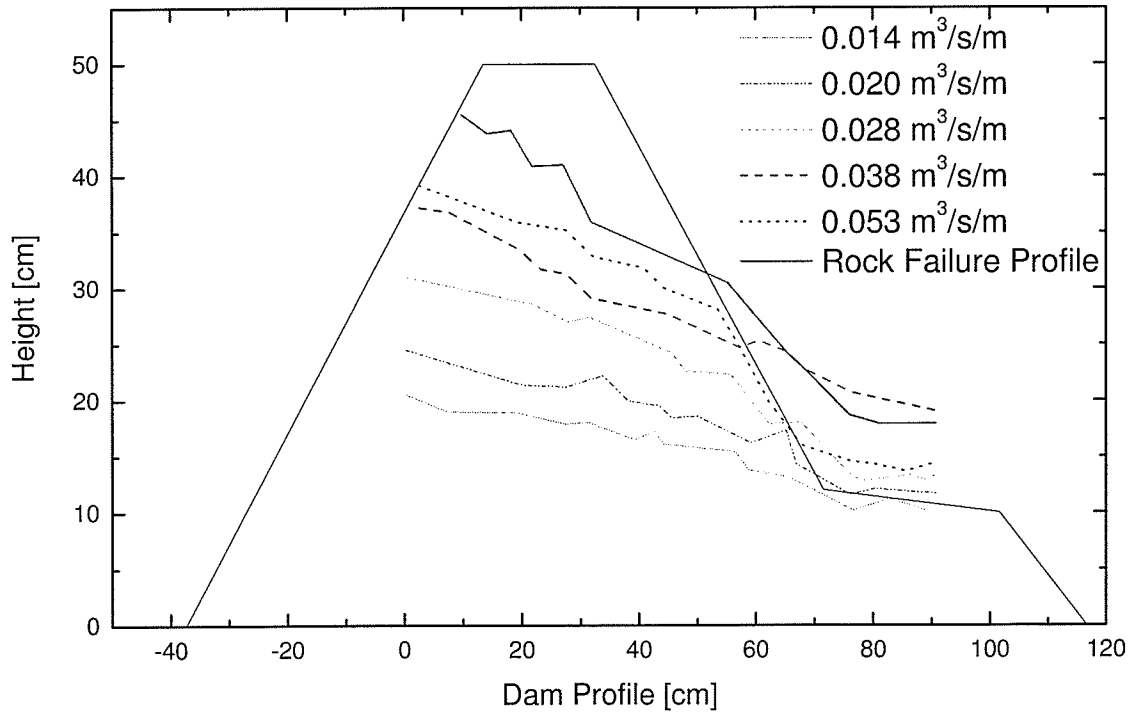

Figure 5.14 – MD10 Measured Phreatic Surface

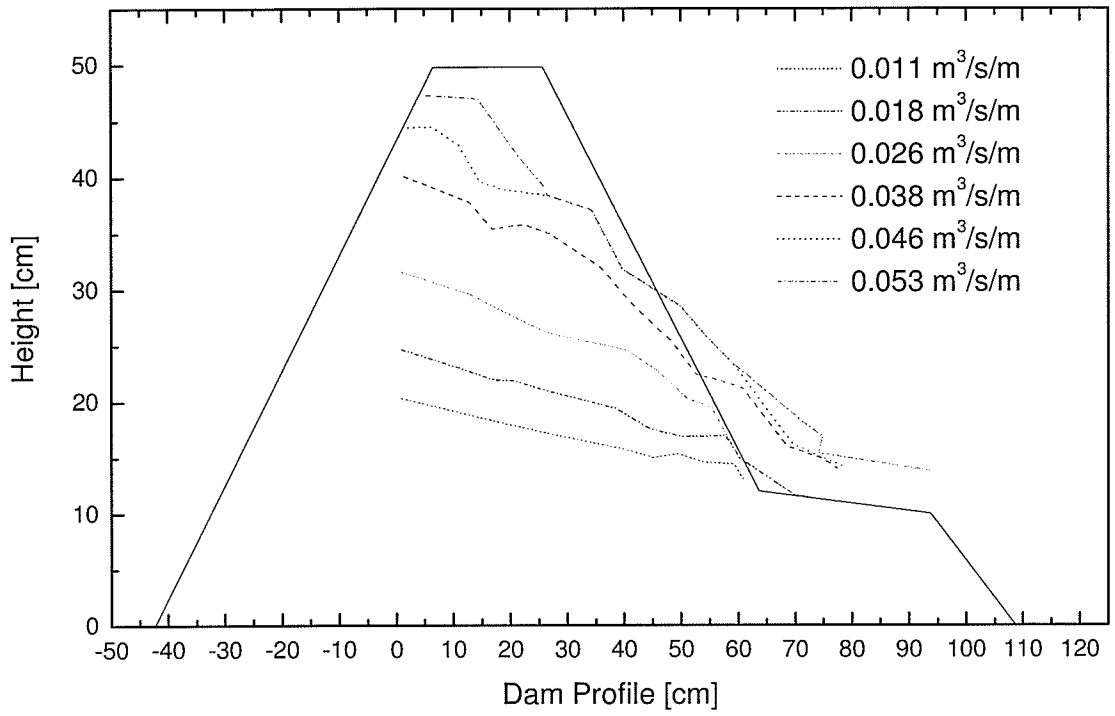

Figure 5.15 – MD11 Measured Phreatic Surfaces

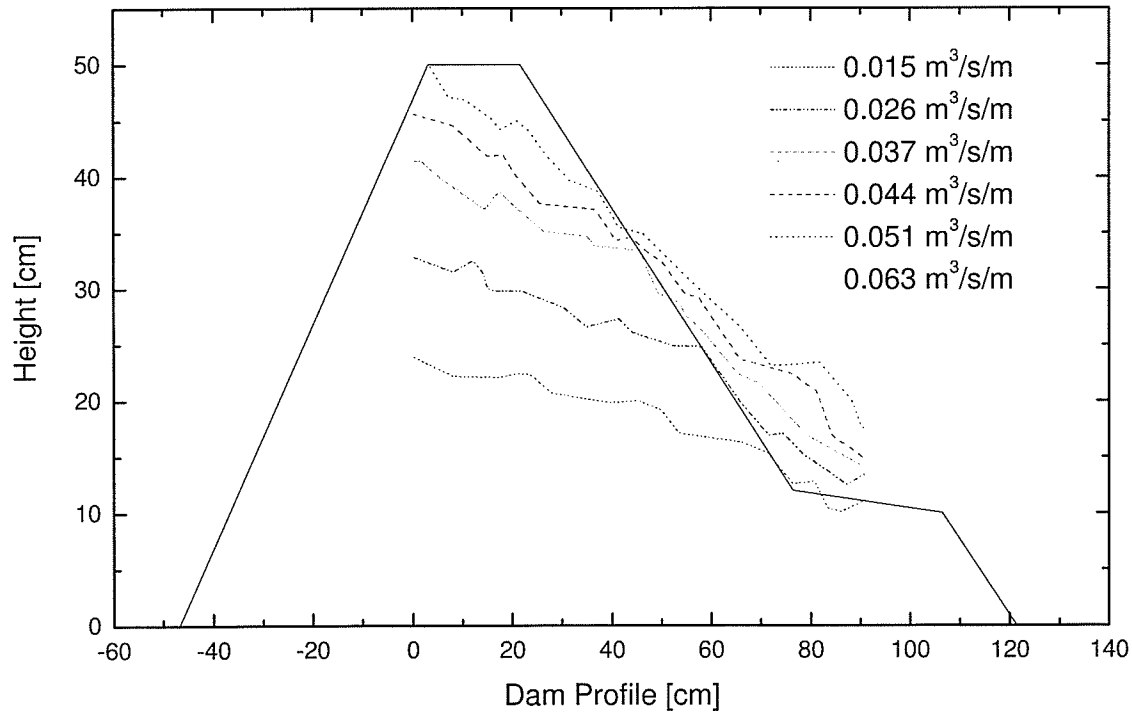

Figure 5.16 – MD12 Measured Phreatic Surfaces

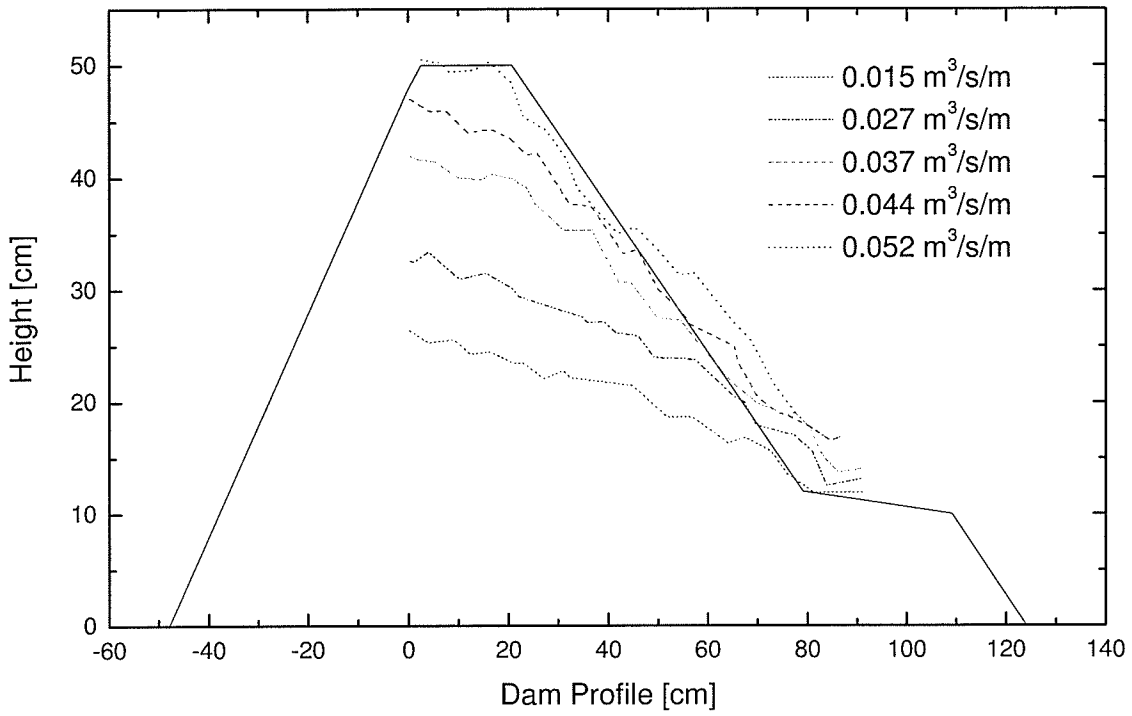

Figure 5.17 – MD13 Measured Phreatic Surfaces

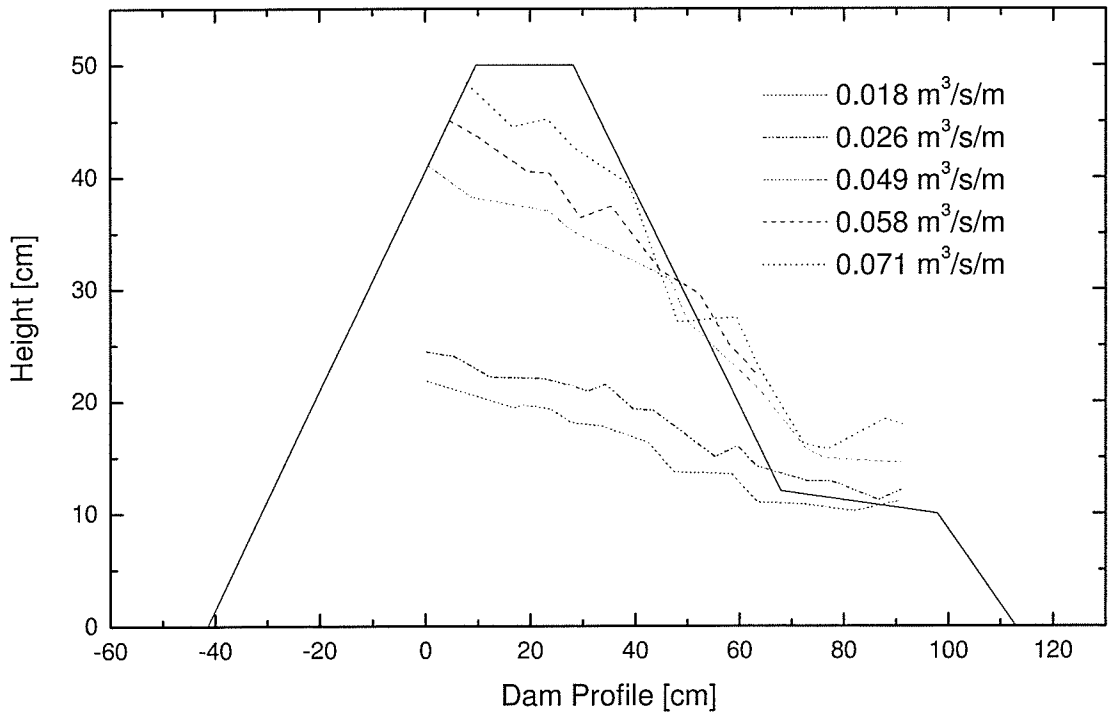

Figure 5.18 – MD14 Measured Phreatic Surfaces

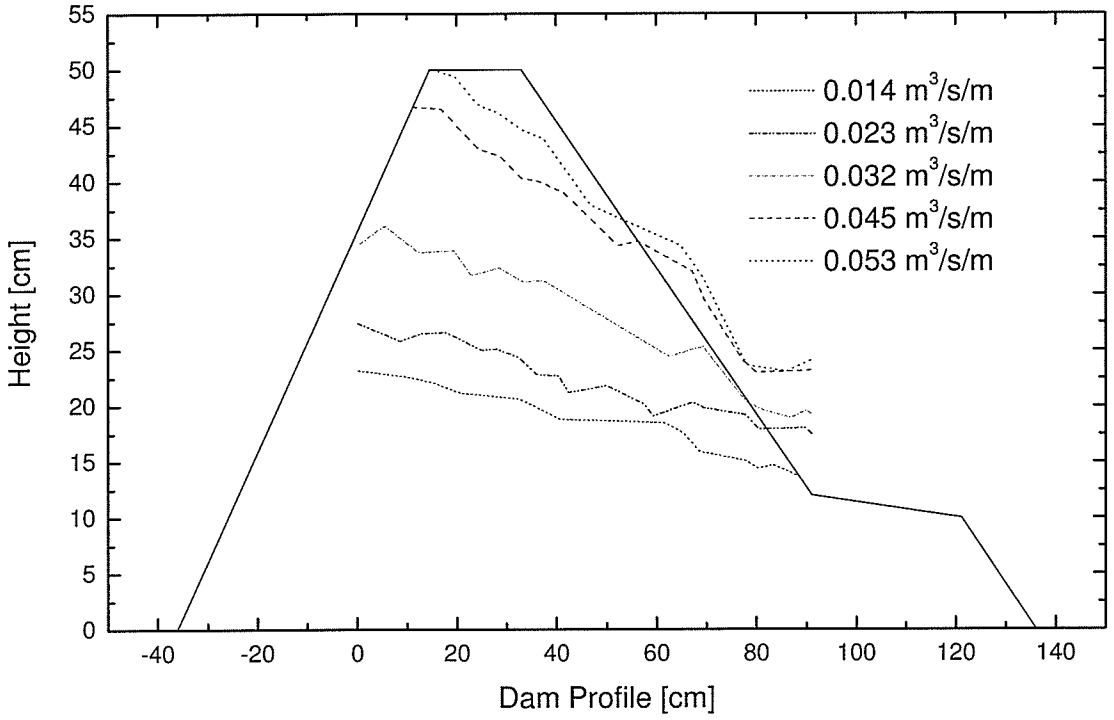

Figure 5.19 – MD15 Measured Phreatic Surfaces

Figure 5.20 – MD7 Toe Sliding

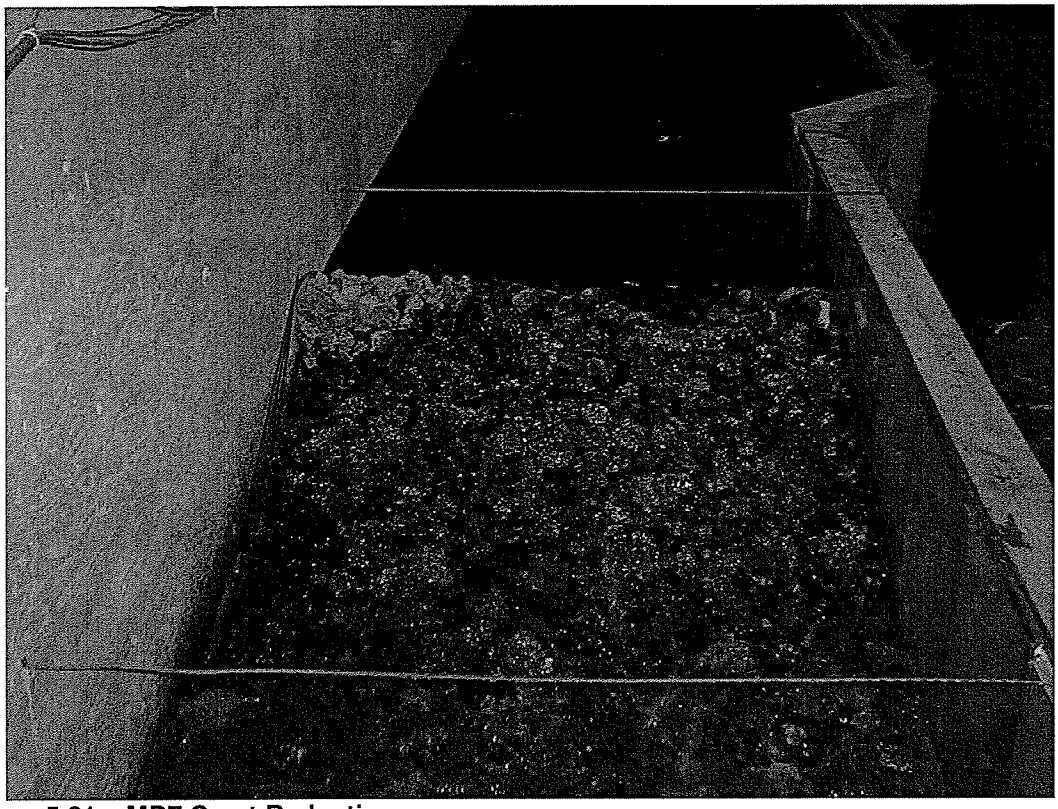

Figure 5.21 – MD7 Crest Reduction

Figure 5.22 – MD7 Overtopping Failure

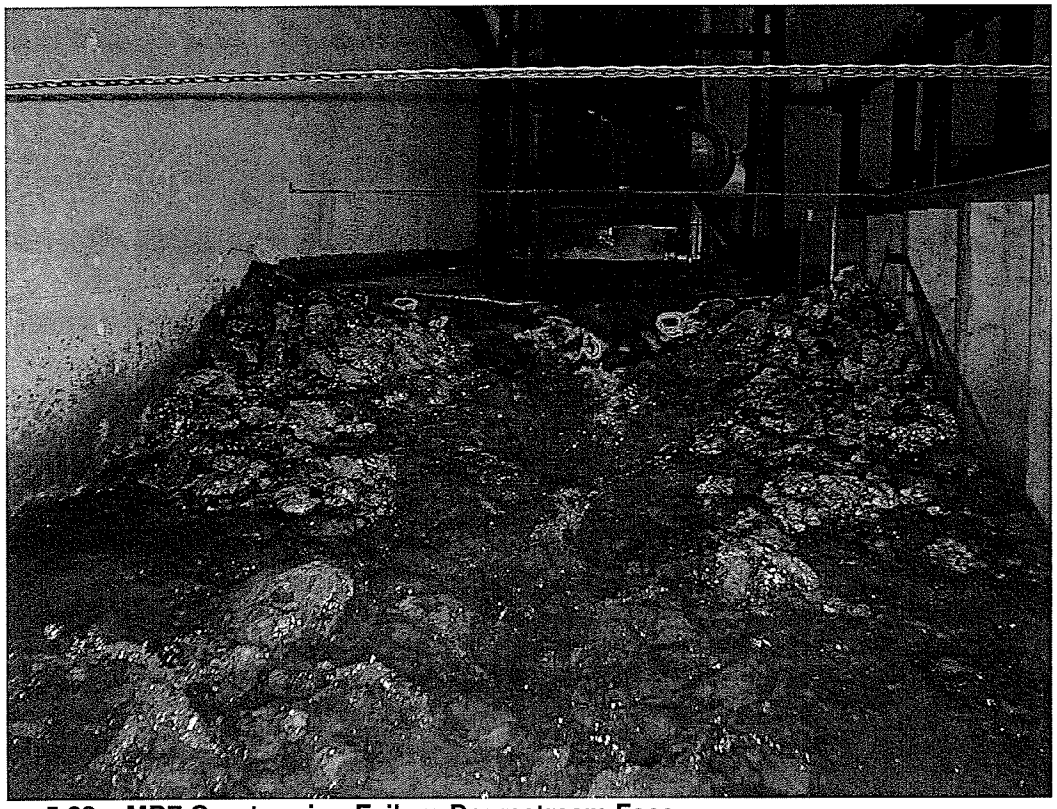

Figure 5.23 – MD7 Overtopping Failure Downstream Face

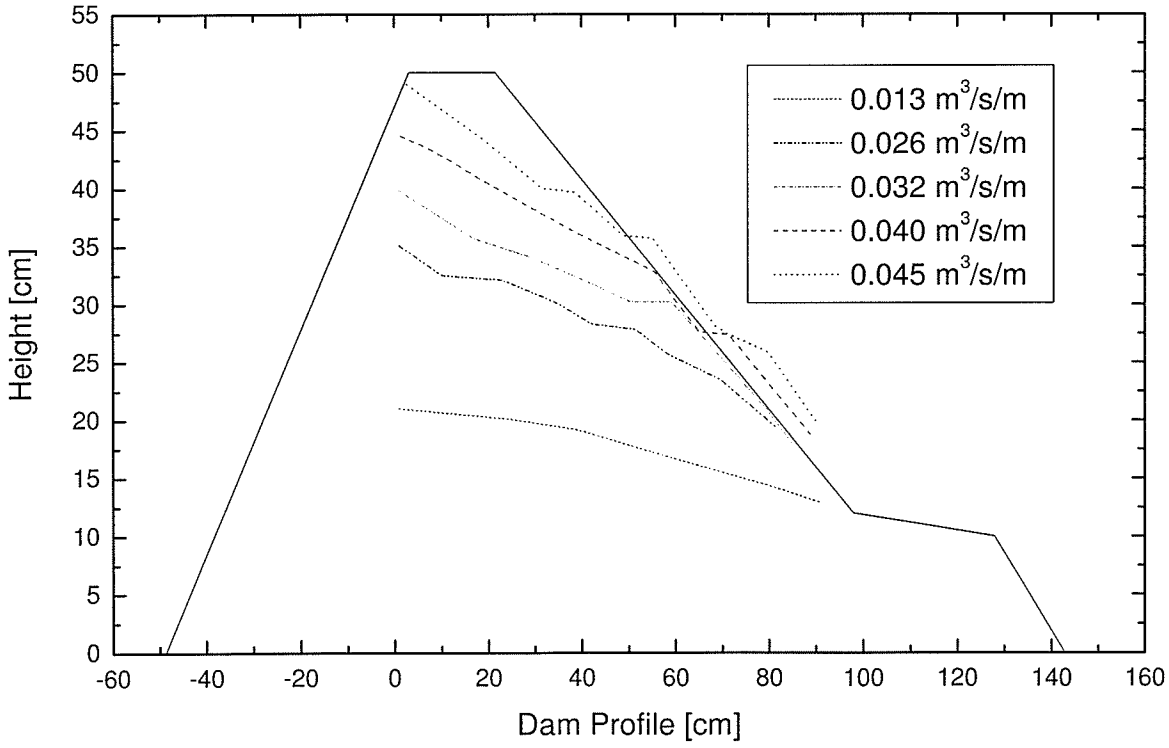

Figure 5.24 – MD9 Measured Phreatic Surfaces

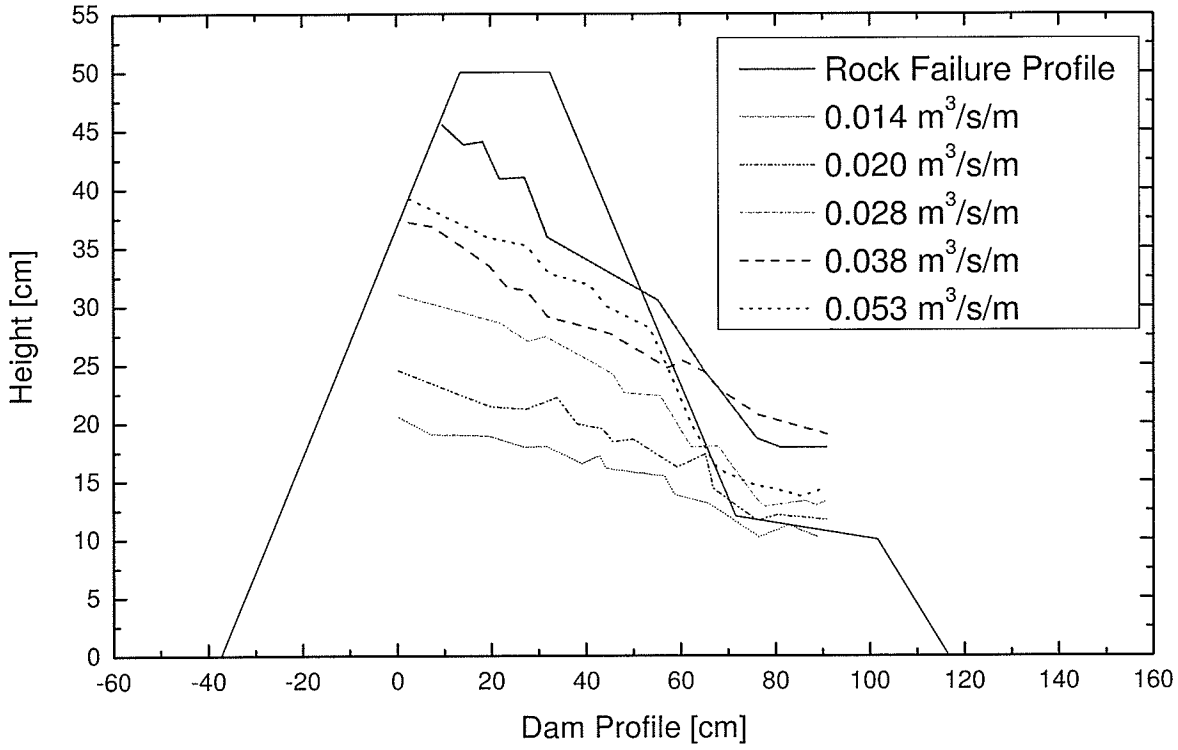

Figure 5.25 – MD10 Measured Phreatic Surfaces

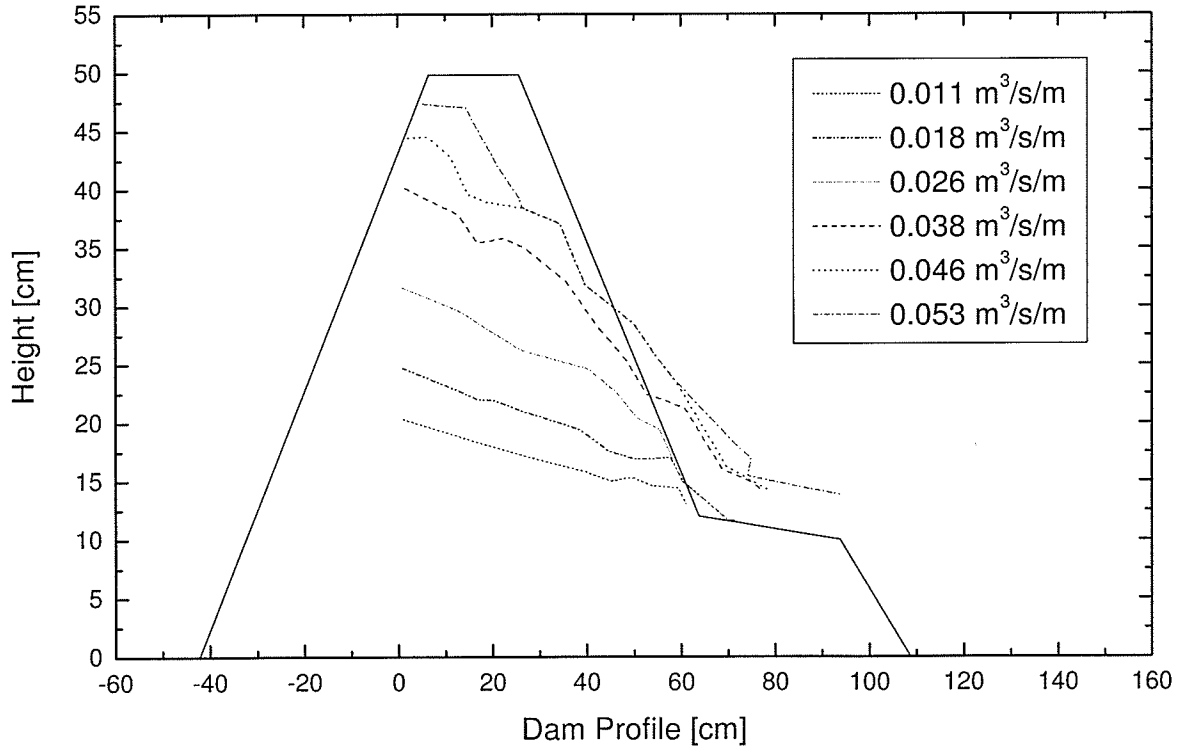

Figure 5.26 – MD11 Measured Phreatic Surfaces

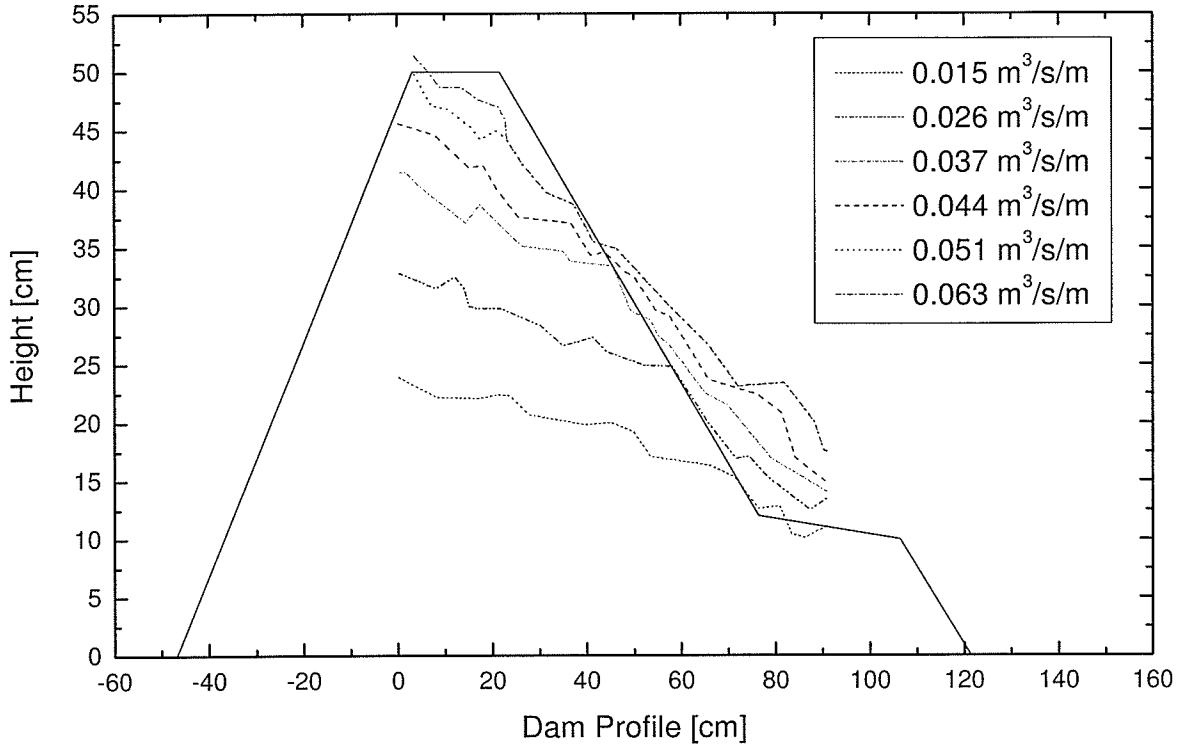

Figure 5.27 – MD12 Measured Phreatic Surfaces

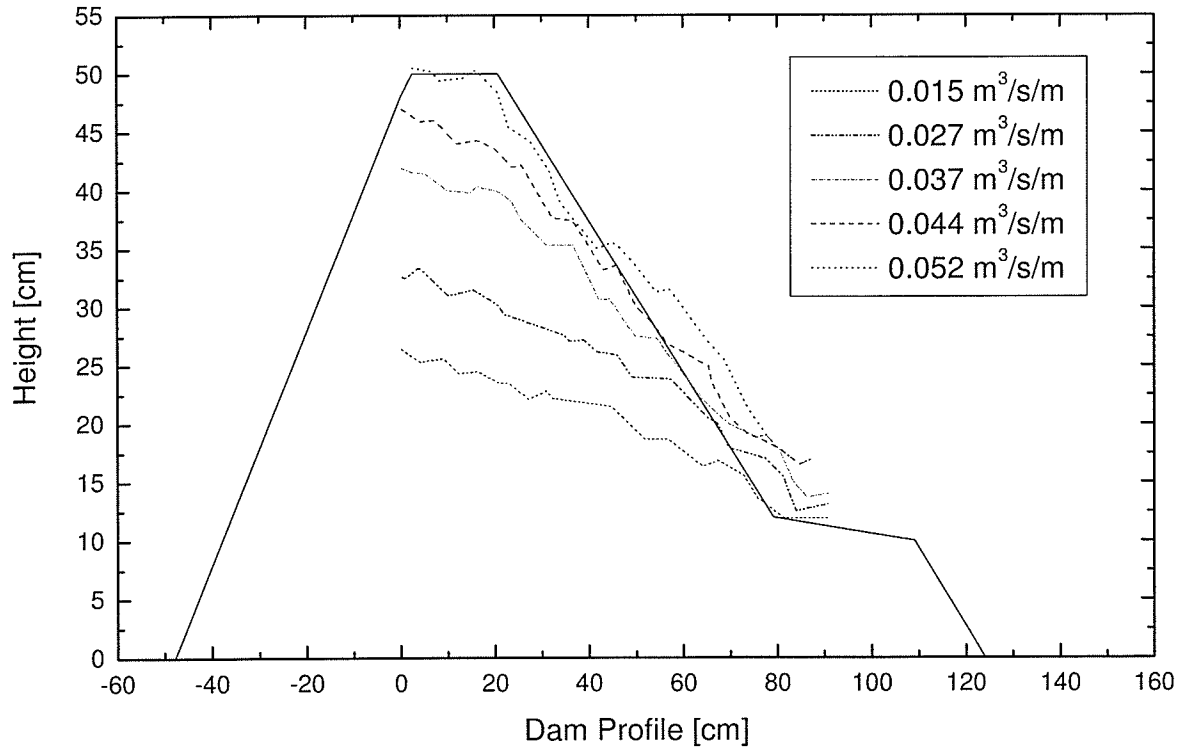

Figure 5.28 – MD13 Measured Phreatic Surfaces

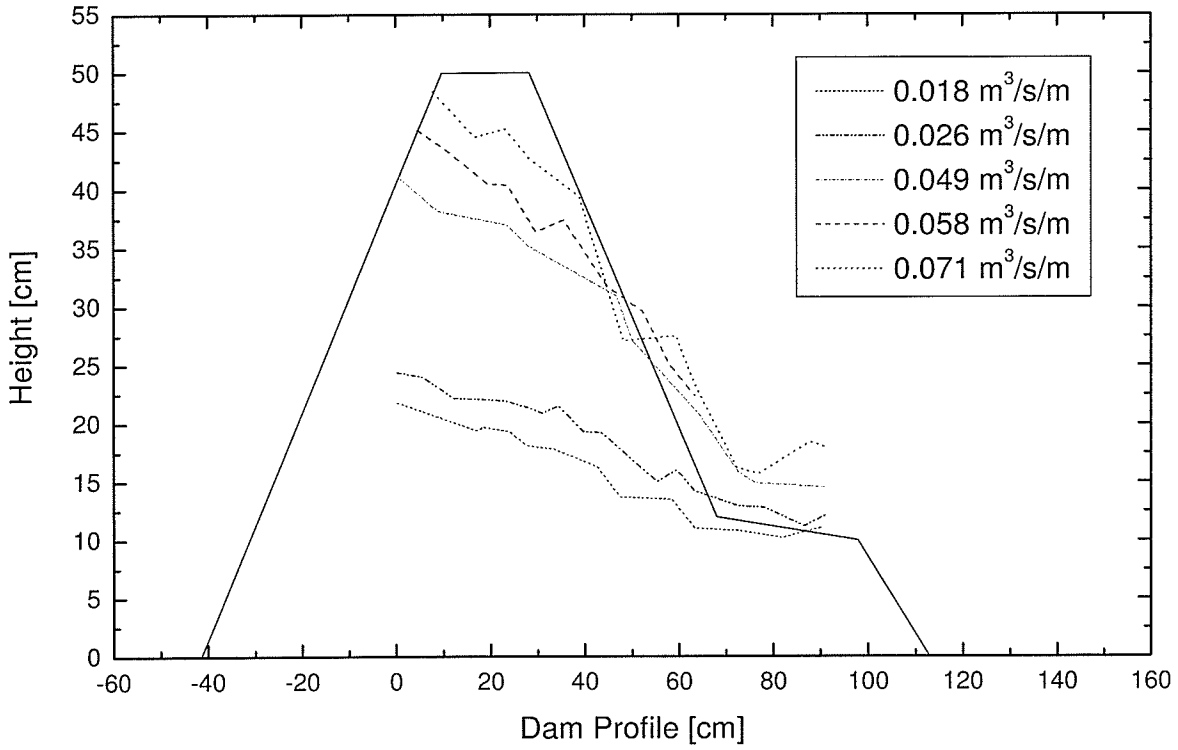

Figure 5.29 – MD14 Measured Phreatic Surfaces

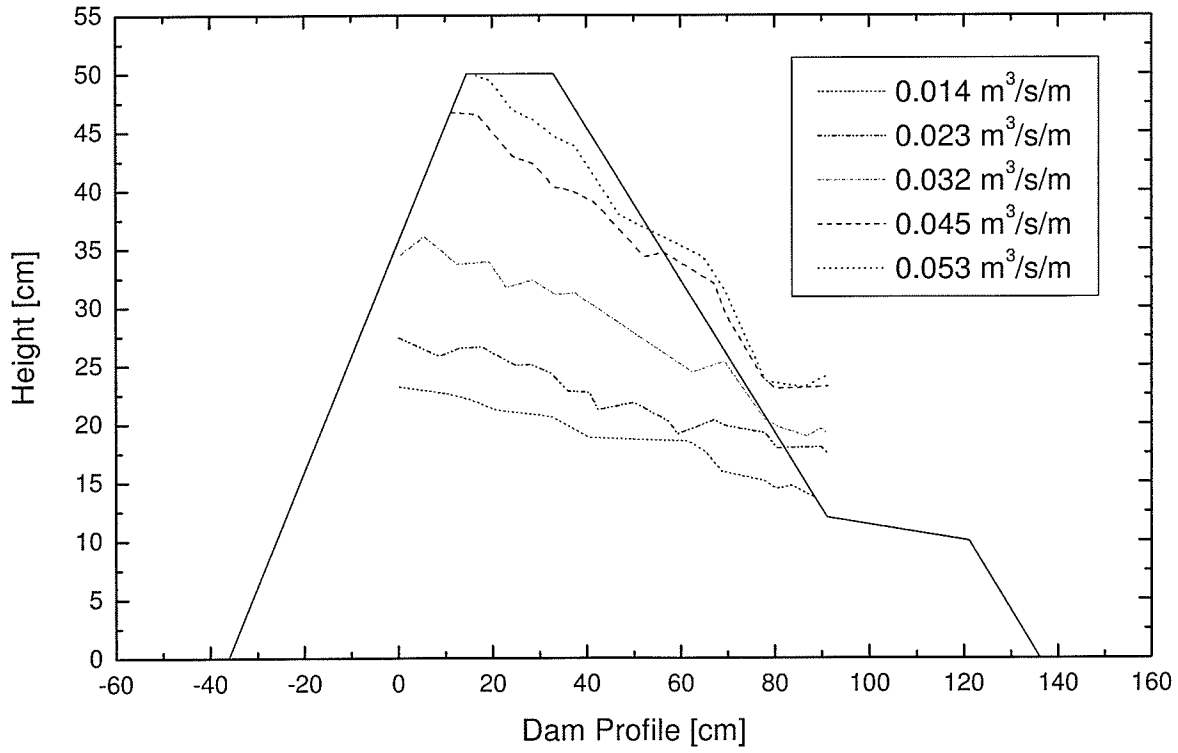

Figure 5.30 – MD15 Measured Phreatic Surfaces

6 SCALE DAMS

6.1 GENERAL

Construction and testing of two dams was completed between June 25 and July 6, 2006. Testing was completed in the HRTF Laboratory under controlled conditions in a large flume. To distinguish these experimental dams from the mini dam experiment and existing operational structures, the experimental structures were referred to as the scale dams. The two scale dams were identified as Scale Dam 1V:1H and Scale Dam 1V:1.5H. Both dams had similar dimensions except for the downstream face, the slope of which is identified in their respective names. The scale dam experimental program was intended to evaluate existing predictive tools: flow through conditions and initiation of particle movement. Given the limited number of scale dam tests and therefore the limited ability to effectively alter parameters of the structures, the Mini Dam experimental program described in Chapter 5 was undertaken to complement the scale dams.

6.2 SCALE DAM TESTING FLUME

The dams were constructed in an engineered plywood flume located in the lower level of the HRTF (see Figure 4.1). The flume was 11 m long, 1.8 m tall, and 2.42 m wide. It was constructed of 2" by 6" stud framing and ¾" plywood that was coated with a rubberized paint. The inlet was located at the east end of the flume, while a gated outlet at the west end returned water to the HRTF closed

system. The gated outlet was 0.66 m by 0.46 m. A flow straightener system was incorporated into the inlet. The flow capacity of the flume was equal to the maximum capacity of the HRTF pump system. A section of the flume wall was modified to be removable, which allowed walk-in access to the interior of the flume during construction of the dams. During testing this section was sealed in-place.

As described in Section 5.7.2, the rockfill was observed to have moved along both the concrete and acrylic surfaces of the mini dam flume during testing. To address this in the scale-dam flume, the flume surfaces were modified. The existing floor and one wall of the scale-dam flume was plywood coated with a rubberized paint, 1 to 2 mm thick, while the other wall combined both plywood with rubberized paint and a clear acrylic pane. A section of plywood from the original flume was replaced with the clear acrylic and was positioned to allow observation of the crest and downstream slope of both scale dams, as shown in Figure 6.1. The rubberized paint provided an improved frictional interface compared to smooth concrete, but was considered to be insufficient. As shown in Figure 6.2, a section of chain link fence, extending from the upstream toe to the downstream toe of either scale dam was fastened to the floor of the flume to improve frictional resistance. As well, strips of wood, 4.5 by 4.5 cm square, 1.2m tall were fastened to both walls of the flume at 40 cm spacing along the length of the dam.

During the Scale Dam 1V:1H test, the downstream water level was elevated due to insufficient outflow capacity at low levels. The flume was modified while the test was in progress, after the flow through became constant and measurements were taken, however the increased outlet size generated little change in the downstream elevation. The modification was expanded between Scale Dam 1V:1H and Scale Dam 1V:1.5H with improved results.

Walkways were installed on either side of the flume as well as on top of the flume, above the upstream side of the dam. This allowed personnel to access and monitor the flow conditions and failures on the downstream face of the dam during operation.

6.3 INSTRUMENTATION

The scale dam instrumentation plan was designed to monitor total head at discrete locations, discharge through the rockfill, and rock movements. Vibrating wire piezometers and open-pipe piezometers were utilized to measure head variations within the rockfill, which were resolved to produce the hydraulic gradient. A clear acrylic wall exposing the cross-section of the scale dams allowed for the measurement of phreatic surface, which was used in the calculation of hydraulic gradient. The HRTF volumetric tanks were used to measure the discharge through the rockfill. Draw-wire extensometers were used to monitor the movement of discrete particles on the downstream face of the structure. Video and still photographs were captured of the dams during

operation for a visual record of particle movement. The entire structure was monitored for movement using conventional surveying techniques.

6.3.1 Vibrating Wire Piezometers

The vibrating wire piezometers used in the scale dam testing were a combination of Geokon Inc. Model 4500S, Figure 6.3, and Slope Indicator Inc. 19 mm, Figure 6.4, and Slope Indicator Inc. push-in piezometers, Figure 6.5. A total of twelve vibrating wire piezometers were located within the dam along two sections through each scale dam, as shown for Scale Dam 1V:1H in plan on Figure 6.6 and in cross-section on Figure 6.7. The vibrating wire locations of Scale Dam 1V:1.5H are shown in plan and cross-section in Figure 6.8 and Figure 6.9. Along each of the two vibrating-wire sections, three vibrating-wires were located in the lower part of the dam, between the crest and the downstream toe; two were placed directly below mid-height of the dam; one vibrating-wire located near the anticipated peak phreatic surface. The lower level piezometers captured pressure readings throughout the test, while the middle level was not active until approximately the fourth discharge when the water level reached mid-height of the dam (above the level of the piezometers), finally the top piezometer acquired readings near the end of the test just prior to flow-through failure. Vibrating wire piezometers were also located in the flume to monitor both upstream and downstream water levels.

The Campbell Scientific CR23X data acquisition system was used to monitor and record the vibrating wire piezometers. The piezometers were monitored every 10

seconds throughout the test. During each increment readings were also manually recorded to ensure the data would not be lost due to electronic malfunction.

Vertical spikes in the piezometer data occurred in the large-scale permeameter and were expected to occur in the scale dams. These anomalies were attributed to electronic "noise" in the instrumentation and only the sustained changes in trend were used in the interpretation.

6.3.2 Open-pipe Piezometers

The open-pipe piezometers were intended to confirm the readings of the vibrating wire piezometers.

Six open-pipe piezometers were located in a line on the floor of the flume approximately 30 cm from the acrylic wall. The first open-pipe piezometer was located under the crest of the dam and adjacent open-pipe piezometers continued downstream in a row with 20 cm spacing between. To construct each open-pipe piezometer, copper pipe was extended up through the floor of the flume and bent 90 degrees such that the pipe opening faced in the downstream direction. Plastic tubing was connected to the copper pipe, extended out from under the flume and attached to the side of the flume where measurements could be conducted. Prior to the scale dam experiments, the open pipe piezometers were tested, confirming that minimal variation was encountered due to the effects of water velocity.

In addition to the six floor open-pipe piezometers, four open-pipe piezometers were installed within the dam structure. During construction, plastic tubes were laid amongst the rockfill and extended to the acrylic wall. The tubes were carefully hand placed to minimize perching of the tube on the sharp angular edges of the rockfill. To avoid impacting the construction and the homogeneity of the dam, rockfill material was placed over the tubes in the standard manner as described in Section 6.4.

6.3.3 Clear Acrylic Wall

The acrylic wall was 2.4 m long and 1.2 m high, which provided a cross-sectional view of both dams. The acrylic wall was positioned such that the crest of the dam and the downstream slope could be viewed. This allowed observation of the exit height and phreatic surface. To structurally support the rockfill and match the rest of the wall, the acrylic was 19 mm thick. The flow through the rockfill was observed during the testing and the phreatic surface was recorded.

6.3.4 Flow Rate

The discharge through the dam was measured at every increase in flow using the methodology outlined in Section 4.2.

6.3.5 Draw-wire Extensometers

Draw-wire extensometers were attached to pre-selected rocks that had been geometrically characterized along the downstream face. The rocks were placed in approximately the middle third of the downstream face, the area believed to be highly susceptible to flow-through initiation of particle movement. Within the middle third the rocks were randomly placed and compacted at the same time as the rest of the dam face. The draw-wires were electronically monitored every 10 seconds using the CR23X data acquisition system. The draw-wires were intended to record the initiation of particle movement with regards to time and magnitude.

The draw-wires were also monitored for indications of bulging of the downstream face during experimentation. Significant bulging would indicate improper dam construction and be considered the first failure mechanism of the dam.

6.3.6 Video and Still Camera Monitoring System

A digital video camera was used to capture the upstream water level, downstream face of the dam and downstream water level. Recording time was synchronized with the data acquisition system, allowing recorded visual confirmation of the upstream and downstream water levels, as well as initiation of particle movement. To enhance the visibility of the downstream face, individual rocks randomly selected along the length of the face were painted. The dam

face was divided into four vertical levels. Each level received a different paint colour applied to the selected rocks.

A hand held digital camera was used to take photographs of the downstream face of the dams. The face was divided into quadrants and a photograph was captured for each. During the experiments, photographs from previous flow rate were compared with the current flow rate to identify rock particle movements.

6.3.7 Downstream Surface Measurements

During construction, a total station was used to capture the dimensions of each dam. Throughout testing the downstream face was visually monitored, and when movements were observed the total station was used to record the location and approximate size. After flow through failure and overtopping the final dimensions of the dam were captured.

The total station used was a Topcon GTS-605AF. All readings were recorded in the instruments electronic database and downloaded after the dam experimentation was complete.

6.4 Dam Construction

Each scale dam was constructed 1.2 m tall, 2.42 m long, with a 0.6 m crest width, and a 1V:1H upstream slope. The downstream face was altered for each

test based on the specified design. Figure 6.10 shows the geometry of Scale Dam 1V:1H, while Figure 6.11 shows Scale Dam 1V:1.5H.

During the initial stockpiling of rockfill in the laboratory for construction of the rockfill scale dams, all material was weighed. The weight combined with the dimensions of the scale dam was used to calculate the bulk porosity.

Both of the two scale dams were built in the same manner. Appropriate rock gradation was confirmed using sieve analysis of a random sample. The material was stockpiled within the flume, loaded into buckets using shovels and the buckets were lifted up onto a platform, which rested on already in-place rockfill, as shown in Figure 6.12. The material was then placed using bucket dumping from a predetermined height. Typically the material was placed from upstream to downstream in a 60 cm wide section.

Compaction methods for construction of small full-scale rockfill structures generally apply large quantities of water and traverse the material with a large tracked bulldozer. To simulate this a simple method was followed. Upon placing a 20 cm layer of rock, compaction was completed using a weighted bucket. Water from a small hose was sprayed over the dam during construction and a bucket with 25 kg (245 N) of rock was used to compact each layer of material. The bucket was dropped from a height of 20 cm, to create an impact. A complete methodology is listed below.

1. Place an even 20 cm layer of rock, dumping from 20 cm above the existing level;
2. Hold the compaction bucket 20 cm above the rock surface, drop such that it hits the surface evenly;
3. Repeat this motion, moving the bucket one third of a bucket width upstream to downstream, so that the rock surface is impacted 3 times;
4. When the upstream to downstream line has been completed, move adjacent to the first line and repeat;
5. Continue until the entire layer has been compacted.

Surveying using the total station was conducted to produce the proper shape of each dam. The total station was also used to document the locations of the vibrating wire piezometers and open-pipe piezometers. Extreme care was taken to produce a downstream face that was smooth and straight. The limitations of precise placement during bucket placement and the impact of compaction caused variations in both the upstream and downstream faces. Additional rock was dumped on the downstream face in locations of depressions and some hand placement was used along the flume walls. To achieve a compaction level on both the upstream and downstream faces comparable to the rest of the structure, a unique method was used. A square wooden plate with a long handle was built expressly for scale dam face compaction. Water was sprayed over the face of the dam while the wooden plate was used to tamp the face.

A rockfill blanket was placed at the downstream toe of both scale dams to prevent toe erosion similar to that observed in the mini dam tests. As described in Section 5.5.2, when the rockfill dam to floor interface was concrete, material on the downstream toe tended to erode in the early stages of testing. A rockfill blanket was introduced in the mini dam testing and was found to have minimal affect the downstream water levels while dramatically decreasing premature failure of the structure due to toe erosion. The blankets in the scale dams were hand placed using a single layer of 15 cm rocks acquired from the excess stockpile. The blanket rested on the wire fencing on the floor of the flume (Section 6.2), and was not included in the scale dam mass or volume calculations.

In Figure 6.12 summer students are hard at work shoveling rock into buckets with personnel on the base of the 1V:1H dam to place material. All rock was stockpiled, shoveled into buckets and placed randomly to decrease the chance for zones of like dimension of rock to be created within the dam.

6.5 Pre-Test Procedure

After completion of the construction of the scale dam, the flume was sealed to minimized leakage. The flume was then filled with water entering at the inlet, which is on the upstream side of the dam. Flow through the dam occurred while the flume was being filled, but the flow velocity through the dam was controlled

and kept at a minimum. The water level was raised over a 6-hour period, up to 1.2 m depth, completely submerging the dam. The 1.2 m level was maintained for approximately 2 hours. During the time to fill and the time maintaining the maximum level, the vibrating wire piezometers and open-pipe piezometers within the dam were tested and calibrated. Any calibration required in the vibrating wires was due to an intercept shift in the initial calibration curve. This was likely caused by the impact of adjacent rocks on the piezometer during placement and compaction. The water level was lowered over a 4 to 6 hour period, until fully drained. During the draining, a sheet of plastic was laid over the dam to maintain a high relative humidity and keep the porous stones of the vibrating wire piezometers damp.

After the construction and prior to filling the flume, a topographical survey of the dam was conducted using a total station. Key locations such as the upstream and downstream toe, and upstream and downstream crest were surveyed. After completing the filling and draining of the flume, the survey was re-conducted to capture any vertical settlement or horizontal movement of the dam due to submergence.

6.6 Test Protocol

The testing procedure was developed from the testing procedure of the large-scale permeameter and modified based on observations from the mini dam testing. A general overview of the testing procedure is outlined in this section.

To control the discharge through the rockfill, a butterfly control valve was manipulated. The discharge started at zero flow and was increased in intervals until the rockfill structure collapsed. Each interval allowed time for flow through the rockfill to stabilize, which was indicated by the upstream water level becoming stable. When stabilized, the following was recorded manually: discharge through the dam, upstream water level, downstream water level, water level in the open-pipe piezometers, phreatic surface and surface movements. A digital camera captured photographs of the downstream face of the dam. The electronic instrumentation: vibrating wire piezometers, draw-wires, and video camera, were monitored continuously throughout the test. When movements of the rockfill occurred, personnel identified the type, marked the location and measured the size of movement.

This process was repeated until the water retaining abilities of the rockfill dam was lost. This was observed when the dam was overtopped either from a reduced crest height or from discharge capacity through the rockfill being exceeded.

6.7 Predictive Design

Both scale dams used the same gradation of material, were constructed with the same methodology and had the same geometry except for the slope of the

downstream face. As such, the methodology for design discussed in this section is relevant to both Scale Dam 1V:1H and Scale Dam 1V:1.5H.

The predictive design methodology was intended to utilize the known characteristics of a dam and predict failure due to initiation of particle movement on the downstream face. The predictive design was completed, producing the stage-discharge rating curve through the rockfill, as well as the difference in head that will cause the initiation of particle movement. The predictive design was not used in the selection of any of the critical parameters of the dam, only to predict the results as they pertained to failure.

6.7.1 Stage-Discharge Rating Curve

6.7.1.1 Parameters

The critical parameters that make up the dam were selected independently and often were a result of available conditions. The critical parameters include: the specific gravity of the rock particles, the dominant particle size of the rockfill, the gradation and shape of the rockfill particles, relative density of the rockfill, and inclination of the downstream slope (Leps 1973). Table 6.1 lists the parameters used in the predictive design, while the following paragraph provides reasoning for the parameter selection.

Table 6.1 – Design Parameters		
	Scale Dam 1V:1H	**Scale Dam 1V:1.5H**
Specific Gravity [-]	2.68	2.68
Dominant Particle [mm]	50	50
Gradation of Rockfill	10-150 mm Well-Graded (Figure 3.5)	10-150 mm Well-Graded (Figure 3.5)
Rockfill Shape	Angular	Angular
Relative Density [Void Ratio]	0.72	0.72

The specific gravity of the rock particles used in this experimentation is typical of Canadian Shield granite found in the Winnipeg River area and was confirmed in the laboratory. An ongoing discussion exists to define the dominant particle size, but most authors agree that if there are limited fines content (<10%), d_{50} may be considered representative (Leps 1973). The gradation used for the scale dams was the same as in the Large-scale Permeameter Tests 1 through 6, Figure 3.5. The shape of the rockfill used in this experimentation, regarding angularity and typical dimensions is described in Chapter 3. The relative density of the rockfill refers to the void ratio or porosity of the structure. Based on compaction tests, results from the permeameter tests, and that of the mini dams a void ratio of 0.72 was selected to be representative of what may occur.

6.7.1.2 Rating Curve Calculations

Leps (1973) identified the discharge and maximum gradient as critical flow-through parameters. The discharge can be found as part of the rating curve developed for this predictive design. Using Equation 2.9 to calculate effective

gradient and Equation 2.7a to determine bulk velocity, and hence discharge, a stage-discharge rating curve can be obtained.

Referring to Section 2.5.2, the relationship for flow through coarse porous media can be expressed as Equation 2.7a. With the expectation of a void ratio of 0.72, the a and N parameters can be determined from the Large-Scale Permeameter Tests 2, 4, and 6. From Table 4.1 the a parameter is between 17 and 18, while N is 2.0. An average value of 17.5 for a was selected for design. It is assumed that the flow through the scale dam will approach fully turbulent flow, therefore N will equal 2.0.

Equation 2.7a, V, the bulk velocity [in m/s], can be expressed in terms of Q, the total discharge [in m^3/s], by applying the length of the scale dams, 2.42 m, and the height of the flow as approximated by the upstream water level, h. For a particular h-value, Equation 2.9 solves for a hydraulic gradient, which is applied to Equation 2.7a to solve for a bulk velocity and hence the total discharge.

Figure 6.13 shows the predicted rating curve for Scale Dam 1V:1H, and for Scale Dam 1V:1.5H. Both curves can be represented by power functions; 1V:1H has the form $Q = 274.15 \times h^{1.7}$ and for 1V:1.5H the relationship is $Q = 250.97 \times h^{1.7}$, where h is in meters and Q is in liters per second.

6.7.2 Initiation of Particle Movement

6.7.2.1 Uppermost Unstable Particle

The uppermost unstable particle, as defined by Hansen *et al.* (2005), is a single particle located within the seepage face to which we design. The three primary forces identified by Hansen *et al.* (2005) are the overflow hydraulic force, the seepage force, and the submerged weight. The first two forces are destabilizing forces while the submerged weight is a stabilizing force.

The design begins with identifying the known and assumed parameters of the dam. These parameters include the gradation of rockfill, void ratio and diameter of representative particle, potential upstream water level (for calculation of discharge), the downstream slope and the length of the dam (perpendicular to flow).

Table 6.2 – Parameters for Initiation of Particle Movement in Scale Dams

Dominate Particle Size	d_{50} (m)	0.05
Porosity	n	0.42
Void Ratio	e	0.72
Length of dam	Width of the flume (m)	2.42
Downstream Slope Angle	θ (°)	45 or 33.7

The three unknowns in this analysis are the discharge, the exit height and the exit gradient. The variables associated with this analysis are coefficient of drag (C_D), and the angle of the emerging seepage gradient. The analysis assumes a factor of safety of unity for initiation of particle movement.

Using the stage-discharge rating curves obtained in Section 6.7.1.2, discharge is calculated for several upstream water levels (initially increment Δh = 0.1 m). The associated exit heights for the discharge are calculated with Equation 6.1, from Hansen *et al.* (2005), which uses Wilkins' (1955) relationship for turbulent flow. An assumption to this equation is that the hydraulic gradient may be adequately approximated by the angle (θ) of the toe of the dam (Hansen *et al.* 2005).

$$y_{exit} = \frac{Q}{nLWm^{0.5}(\tan\theta)^{0.54}} = \frac{q(\cot\theta)^{0.54}}{nWm^{0.5}} \qquad \textbf{Equation 6.1}$$

where,

y_{exit}	is the seepage face exit height	[m]
Q	is the total discharge	[m^3/s]
n	is the porosity	[-]
L	is the length of the dam	[m]
W	Wilkins' coefficient	[0.83566 $m^{0.5}$·s]
m	is the hydraulic mean radius	[m]
θ	is the angle of the toe of dam	[°]
q	is the discharge per unit length of dam	[m^2/s]

Wilkins' defines an empirical constant W (5.243 $m^{0.5}$/s) and uses the hydraulic mean radius (m). It has been suggested by a number of authors (Wilkins 1955, Garga *et al.* 1995) that the diameter used in calculating m for a graded material could be defined as the 50th percentile diameter (d_{50}). From Figure 3.5 the d_{50} is 0.05 m, and applying to Equation 2.4, m is 0.00462 for the assumed void ratio.

The equation proposed by Hansen *et al.* (2005) for the destabilizing hydraulic force (F_{hyd}) due to flow down the face of the dam, Equation 6.2, requires the coefficient of drag of a particle (C_D). From experimentation in the drag tank,

Section 3.3, C_D was found to range from a value of 0.1 to 1.0 (Figure 3.14). When considering C_D, multiple values are possible and are dependant on the shape, angularity, projected surface area of the rock, velocity and level of turbulence of the flow. Three values of C_D (0.1, 0.4, 1.0) will be used in the calculations and will be carried through to the end of the analysis. The velocity of flow over the rock is not known for this situation and therefore a value equal to the exit velocity of the voids is calculated (Equation 6.3) and considered to be conservative.

$$F_{hyd} = C_D \gamma_W (L \cdot y_{exit}) \frac{U^2}{2} \qquad \textbf{Equation 6.2}$$

where,

U	is the void velocity (m/s)
Q	is the discharge (m^3/s)
L	is the length of dam (m)
y_{exit}	is the exit height of the seepage face (m)
n	is the porosity
C_D	is the coefficient of drag
γ_w	is the unit weight of water (kN/m^3)

and U can be calculated as:

$$U = \frac{Q}{(L \cdot y_{exit}) * n} \qquad \textbf{Equation 6.3}$$

The unknown in Equation 6.2 and 6.3 is the void velocity. The moment arm of the hydraulic force (F_{hyd}) is assumed to be the one-half of the representative diameter of the particle.

The force exerted on a unit bulk volume of porous medium, a product of the unit weight of the fluid moving through the medium and the applicable hydraulic gradient, is defined by Hansen *et al.* (2005) as the destabilizing seepage force (F_{seep}). The volume of an individual particle is required in this analysis; as the material is well-graded, the d_{50} particle will be selected as representative to maintain consistency with all other calculations in this section. Also required in this analysis is the hydraulic gradient. The destabilizing seepage force is:

$$F_{seep} = \forall_p (1+e)\gamma_w i \qquad \textbf{Equation 6.5}$$

where,

$\forall_p$ is the particle volume [m^3]
γ_w is the unit weight of water [kg/m^3]
e is the void ratio

The moment arm for the seepage force is the product of one-half the diameter of the representative particle and the angle of the seepage vector, as measured below the plane of the downstream face (Figure 2.6). For Scale Dam 1V:1H the downstream face is at an angle of 45°, and measuring down, a horizontal seepage vector would be at 45°. For Scale Dam 1V:1.5H, the downstream slope angle is 33.7°. Hansen *et al.* (2005) suggest that due to the flow on the face of the dam, the seepage exiting would act at some angle other than horizontal. As a conservative estimate, a horizontal seepage vector (45°) is used in the following calculations. As well, a seepage vector at 15° (30° to the horizontal) is calculated for comparison.

Finally the submerged weight of a particle, the only stabilizing moment in this analysis, is calculated as the product of the submerged weight of the particle and the moment arm of one-half the diameter at the angle of the downstream face.

$$M_{stab} = (\gamma_p - \gamma_w)\forall_p \frac{d}{2}\cos\theta \qquad \textbf{Equation 6.6}$$

where,

γ_p is the unit weight of rock [kg/m^3]

The overall factor of safety (FS) of the uppermost unstable particle is:

$$FS = \frac{M_{stab}}{M_{hyd} + M_{seep}}. \qquad \textbf{Equation 6.7}$$

The discharge and exit height used in this analysis were developed from the stage-discharge relationship and are directly related. As such, hydraulic gradient and void velocity calculations are not unique. Therefore, Hansen *et al.* (2005) define the effective angle of the emergent seepage face as:

$$\frac{\theta_{ff}}{\theta} = 1.41 \cdot \frac{y_{exit}}{H} + 0.17 \qquad \textbf{Equation 6.8}$$

where,

θ_{ff} is the effective angle of the emergent flow field within the toe

θ is the angle of toe of dam
y_{exit} is the exit height [m]
H is the height of the dam [m]

Hansen *et al.* (2005) found this equation worked best if $y_{exit} < 0.5\ H$. Using Wilkins' (1955) equation, where i is replaced with $\tan\theta_{ff}$, F_{hyd} and F_{seep} can be

estimated. By setting FS to 1.0 (incipient failure) in Equation 6.7, the three moments can be compared to determine the critical discharge, exit height and upstream water level. The example of the analysis is documented in Table 6.3.

Table 6.3 – Sample Calculations for Initiation of Particle Movement

h [m]	Q [m^3/s]	y_{exit}	M_{hyd}	M_{seep}	$M_{hyd} + M_{seep}$	M_{stab}
0.4	0.058	0.159	0.003	0.010	0.013	0.021
0.6	0.115	0.318	0.005	0.013	0.018	0.021
0.7	0.150	0.413	0.006	0.014	0.021	0.021
0.8	0.188	0.518	0.008	0.016	0.024	0.021
1.0	0.274	0.757	0.013	0.020	0.033	0.021

Table 6.3 represents Scale Dam 1V:1H with CD = 0.4 and ξ= 45°. At an upstream water level approximately 0.7 m, and discharge of 0.150 m^3/s, the two destabilizing moments approximately equal the stabilizing moment producing a factor of safety near 1.0.

Table 6.4 contains a summary of the calculated flow parameters for Scale Dam 1V:1H and Table 6.5 contains a summary of the calculated flow parameters for Scale Dam 1V:1.5H. Sensitivity plots for Scale Dam 1V:1H are shown on Figure 6.14, and Figure 6.15. On Figure 6.14, plotting the flow parameters versus C_D, the slope of the best-fit linear line, for upstream water level, is approximately 0.65, suggesting that the initiation of particle movement analysis is sensitive to C_D and careful selection is required. Plotting flow parameters versus ξ on Figure 6.15, the slope of the best-fit linear line is approximately 0.013.

Table 6.4 – Summary of Calculated Flow Parameters for Initiation of Particle Movement					
Scale Dam 1V:1H					
C_D	ξ	h [m]	Q [m^3/s]	y_{exit}	Notes
0.1	15	1.283	0.419	1.157	$h > H$
0.4	15	1.020	0.283	0.783	
1.0	15	0.707	0.152	0.420	
0.1	45	0.901	0.23	0.634	
0.4	45	0.700	0.150	0.413	
1.0	45	0.488	0.081	0.224	

Table 6.5 – Summary of Calculated Flow Parameters for Initiation of Particle Movement					
Scale Dam 1V:1.5H					
C_D	ξ	h [m]	Q [m^3/s]	y_{exit}	Notes
0.1	15	1.620	0.620	1.710	$h > H$
0.4	15	1.310	0.437	1.206	$h > H$
1.0	15	0.970	0.260	0.719	
0.1	45	1.235	0.390	1.084	$h > H$
0.4	45	0.990	0.270	0.745	
1.0	45	0.756	0.170	0.471	

Several of the upstream water levels found in Table 6.4 and 6.5 are greater than the height of the dam (H = 1.2 m) and are considered unfeasible. These values will be revisited after testing of Scale Dam 1V:1H and Scale Dam 1V:1.5H.

6.7.2.2 Deep-seated Failure

To induce deep-seated movements, surface erosion must be resisted. It was anticipated that the scale dams would fail due to surface erosion prior to deep-seated movements. As such, design for deep-seated movements were not conducted.

6.7.3 Pore Pressure

To analyze rotational deep-seated stability of the rockfill dams, pore pressure distribution and associated hydraulic gradients are required. A seepage analysis of Scale Dam 1V:1.5H was completed as part of the predictive design of the structure. Using the finite element modeling computer software GeoStudio, developed by Geo-Slope International Ltd., and in particular the Seep/W package, the flow through the structure and piezometric head were analyzed. The software was designed and intended to use Darcy's Law, and hence are valid only for a laminar flow regime. As the flow through rockfill is laminar only at very small flow rates, this computer program will not accurately forecast flow through rockfill under turbulent conditions. However, the difference in pore pressures between non-Darcy and laminar flow is in the order of 10% (Hansen 1995). As such, the pore pressures calculated by Seep/W are useful as a rough design tool.

The geometry for the Scale Dam 1V:1.5H was selected prior to the initiation of this computer modeling, and modeled in Seep/W. From the large-scale permeameter at low flow rates (k) was approximated as 1.0 m/s and was inputted into the program. The other main input into the model was the applied boundary conditions. As would be expected, no flow (Q_T=0) will enter the structure from the bottom, as well the upstream slope will have a condition that the total head (H) is equal to the height of water being impounded. For the downstream face, two approaches were tested. The first approach was the application of a fixed

downstream water elevation to match that expected in the experiment. The second boundary attempted was a review boundary, which allowed the program to develop a computed downstream water elevation. The downstream boundary ultimately selected was the review boundary, as the predicted exit height of the flow was above the downstream water level. Figure 6.16 shows both the Seep/W predicted total head, and the total head measured in Scale Dam 1V:1.5H.

6.8 Experimental Results

The improvements made to the scale dam flume, most significantly the floor and wall sliding resistant measures were considered to be a success. No sliding movement was measured by the draw-wire extensometers. Although capable of passing the flows required, the outlet artificially raised water levels more than expected. The information gathered from the experiment was affected by the elevated downstream water level and affected the posttest interpretation. The results of the both Scale Dams are discussed below.

6.8.1 Scale Dam 1V:1H

6.8.1.1 General

Scale Dam 1V:1H was completed on June 26, 2006, supervised by the author and three summer students. Eighteen stages were tested for flow through the rockfill dam, while a nineteenth stage produced overtopping of the structure and complete unraveling. Shown in Table 6.6 are the stage number, upstream water level, downstream water level, and discharge through the structure.

Table 6.6 – Scale Dam 1V:1H, Stage Summary			
Discharge Stage	**Upstream Water Level (m)**	**Downstream Water Level (m)**	**Discharge through dam (m^3/s)**
Stage 1	0.117	0.020	0.0140
Stage 2	0.152	0.040	0.0189
Stage 3	0.261	0.062	0.0311
Stage 4	0.290	0.067	0.0355
Stage 5	0.363	0.105	0.0472
Stage 6	0.426	0.115	0.0578
Stage 7	0.497	0.123	0.0708
Stage 8	0.574	0.154	0.0838
Stage 9	0.643	0.169	0.1002
Stage 10	0.714	0.208	0.1162
Stage 11	0.785	0.220	0.1351
Stage 12	0.857	0.234	0.1535
Stage 13	0.916	0.250	0.1720
Stage 14	0.975	0.270	0.1926
Stage 15	1.040	0.295	0.2121
Stage 16	1.090	0.320	0.2314
Stage 17	1.150	0.360	0.2540
Stage 18	1.170	0.360	0.2739
Stage 19*	-	-	0.2926
*Overtopping occurred during Stage 19			

6.8.1.2 Instrumentation

An issue encountered with the instrumentation was noted early in the experimentation; none of the open-pipe piezometers located within the rockfill worked properly. The water levels within the pipes did not change with increasing upstream water level until water was manually drawn into the pipe,

and even then the values recorded do not fit that recorded in all other methods. It is thought that the pipes, being flexible, were pinched within the rockfill and the hydraulic head was not sufficient to force water through.

6.8.1.3 Bulk Void Ratio

During construction of Scale Dam 1V:1H the mass of rock used was weighed. The dimensions and volume of the dam were confirmed using the total station. Table 6.7 shows the above-mentioned values, as well as the calculated bulk void ratio and porosity.

Table 6.7 – Scale Dam 1V:1H

Volume of Dam [m^3]	5.292
Mass of Rock [kg]	8167
Bulk Void Ratio	0.74
Porosity	42.4%

6.8.1.4 Pore Pressure Data

Figure 6.17, 6.18, and 6.19 are the total head values acquired every 15 seconds by the vibrating wire piezometers throughout the full 8 hours of the experiment. Ignoring the vertical spikes in the data, Figure 6.17 shows the total head from piezometers 1A and 1B. These piezometers were located approximately 0.9 m above the floor of the flume, while upstream water level was greater than 0.9 m for stages 14 through 18 before overtopping failure. Piezometer 1A appears to

have produced no usable data, while 1B captured 3 stages (14, 15, 16) before mass movements affected the location and operation of the piezometer.

Figure 6.18 shows the total head from piezometers 2A & B, and 3A & B. With the lowest at 40 cm and the highest at 57 cm, the middle set of piezometers began capturing data between stage 6 and 7.

Figure 6.19 shows the total head from piezometers 4A & B, 5A & B, and 6A & B. The height of the piezometers ranged from 20 to 30 cm and captured data for 16 stages (3 to 18).

The common trends and data grouping between numerical pairs (i.e. 4A and 4B), demonstrates that the vibrating wire piezometers located at different positions along the length of the rockfill dams measured similar pore pressures, and changes in pore pressure. Note that the upstream piezometers 4A and B have a significantly higher total head than 5A and B, which in turn are greater than 6A and B. This demonstrates that the piezometers are registering head loss through the rockfill.

Figure 6.20 is a cross-section of Scale Dam 1V:1H showing the total head through the dam at various stages of the experiment. Within each stage the individual data points represents the reading from a vibrating wire piezometer.

Although the open-pipe piezometers in the rockfill did not operate properly, the flume floor mounted open-pipe piezometers worked perfectly. Figure 6.21 shows select stages of the upstream and downstream water levels with the total head collected from the open-pipe piezometers. This data compares well to that observed in the piezometer data in Figure 6.20, confirming the successful operation of the vibrating wire piezometers.

6.8.1.5 Phreatic Surface

Figure 6.22 shows select phreatic surfaces collected during Scale Dam 1V:1H experiment. The phreatic surface is a location of zero pressure head and is referenced to the experiment datum; therefore the figure shows the results in total head. When visually comparing the curves between that of the vibrating wire piezometers (Figure 6.20) and open-pipe piezometers (Figure 6.21), the phreatic surface follows the same trends.

6.8.1.6 Discharge

Included in Table 6.6 is the monitored discharge for each stage of the Scale Dam 1V:1H experiment. Figure 6.23 contains both the predicted stage-discharge curve, as developed earlier in this chapter, and the measured stage-discharge from the experiment. Figure 6.24 and Figure 6.25 show flow exiting the structure at moderate and high level respectively. As will be discussed in Chapter 7, the predicted and the measured flow are not the same. The discrepancy between the predicted and measured flow rate increases with increasing head, which

indicates that the slope of the predicted flow is incorrect. The slope of the predicted trend is controlled by N, the exponent of Equation 2.7a, which is a measure of the turbulence of flow.

6.8.1.7 Downstream Slope Movements

At Stage 13, prior to reaching steady-state flow through the dam, two movements occurred. The movements were located approximately 1.0 m apart and acted independently. The first movement was 3 to 4 rocks sliding approximately 4 cm along the face of the structure. The rocks were relatively flat and were completely inundated at the exit of the phreatic surface when movement occurred.

The second movement involved, at first, just one rock rolling forward until it was supported by the next lower rock. The slope remained stable until the upstream level was increased. During the increase of flow and upstream level, exit water completely inundated an adjacent rock, which rolled. This immediately led to the unraveling of several (10 or more) other rocks. This second rock, which induced the movement, was approximately 0.2 m long and 0.1 m diameter with a shape similar to that of an ellipsoid. The long dimension faced into the flow, and the rock was nearly inundated at the exit of the phreatic surface, when it moved. One of the subsequent rocks to move was attached to the draw-wire extensometer electronic monitoring system and was observed visually and on the computer. In Figure 6.26, the draw-wire rock in question can be seen hanging by

the draw-wire on the yellow grid marking, in the lower left corner of the photograph. The draw-wire rocks former location was below and to the right of the green rock directly above the current position. The area of the movement is not easily visible, but is located in the same quadrant as the hanging rock, as outlined by the yellow rope.

At Stage 15, a sequence of unraveling occurred on the downstream face. The movement was observed from near the midpoint of the dam and to the right. This area was approximately 1 m wide and included the earlier slide. The movement extended from the crest to above the downstream water level. The shape of the failure was a teardrop.

During the increase in loading for Stage 16 another mass movement occurred. This may be considered a progressive movement, as it occurred at the same location as the Stage 15 movement. The movement occurred deeper into the crest of the structure and included rockfill from the Stage 15 movement. Associated with this movement was an increased elevation of the exit height within the movement zone. As the flow path was decreased in length by the loss of material, the energy dissipation through the structure at that point decreased, leading to the rise in exit height and increase in energy at the exit point, causing greater instability.

A second movement occurred at Stage 16 after the progressive movement detailed above. This movement occurred on the left side of the dam, but may have been made more susceptible by the previous movements. A mass movement similar to that described for Stage 15 occurred during the steady-state flow conditions through the dam.

The above-mentioned Stage 16 movements and the Stage 17 progressive mass movements, both unraveling and surface sliding produced a lowered crest height, and a narrowed crest width with a near vertical face in excess of 0.3 m high. The displaced material flattened the slope below the near vertical face. The narrowest crest width at the beginning of Stage 18 was on the right hand side, and had the highest water exit height. During the loading of Stage 18 the right hand side neared overtopping as shown in Figure 6.27, but on the left hand side an unraveling movement was initiated. This movement built momentum as material dropped from the crest and impacted onto the material below. This caused a continuous movement, which led to breach of the crest of the structure and subsequent overtopping.

The overtopping carved a flow channel in the downstream face as shown in Figure 6.28. The flow through the structure was dramatically reduced and the exit height on the right hand side was no longer visible on the face of the structure.

Upon completion of the test a survey using the total station was conducted to obtain the shape of the structure at failure. Figure 6.29 shows an AutoCAD reproduction of the surface of the structure prior to testing, while Figure 6.30 shows post failure.

6.8.2 Scale Dam 1V:1.5H

6.8.2.1 General

Prior to construction of Scale Dam 1V:1.5H a second outlet was added to the flume to increase outflow and reduce the impounded downstream water level. An exit was created in the side of the flume, along with a gate to control the amount of water exiting this portal. The increased outlet capacity was successful in reducing the downstream water level, but impounded water levels still occurred. Concern was raised that flow through the structure would be impacted, by preferential flow to one side of the dam, if the outlet on the side were to change flow patterns. To address the possibility of the new outlet creating differential flows through the dam, a wing-wall directing flow was added to the outlet.

The test was completed on July 6, 2006, supervised by the author and three summer students. Seventeen stages, distinguished by different discharge rates, were tested for flow through the rockfill dam, while a eighteenth stage was in progress when the test was shut down due to a technical difficulty. Before Stage 18 could stabilize and allow measurements to be taken, the flow straightener

used in the scale dam flume detached from the flume wall causing a wave to overtop the dam. The damage caused by the wave was irreversible and forced the premature termination of the experiment.

Shown in Table 6.8 are the stage number, upstream water level, downstream water level, and discharge through the structure.

Table 6.8 – Scale Dam 1V:1.5H, Stage Summary

Discharge Stage	Upstream Water Level (m)	Downstream Water Level (m)	Discharge through dam (m^3/s)
Stage 1	0.318	0.086	0.0293
Stage 2	0.347	0.086	0.0337
Stage 3	0.410	0.086	0.0450
Stage 4	0.480	0.100	0.0547
Stage 5	0.550	0.100	0.0682
Stage 6	0.633	0.100	0.0842
Stage 7	0.705	0.130	0.1006
Stage 8	0.776	0.148	0.1160
Stage 9	0.852	0.148	0.1357
Stage 10	0.922	0.148	0.1538
Stage 11	0.992	0.210	0.1736
Stage 12	1.054	0.207	0.1944
Stage 13	1.110	0.220	0.2315
Stage 14	1.150	0.245	0.2286
Stage 15	1.195	0.260	0.2510
Stage 16	1.228	0.275	0.2712
Stage 17	1.249	0.275	0.2840
Stage 18*			

*Stage 18 ended before readings could be recorded

6.8.2.2 Instrumentation

Measures were taken to resolve the problem with the open-pipe piezometers within the rockfill. Unfortunately, once again the results of the open-pipe

piezometers within the rockfill were suspect. The water levels within the pipes did not change with increasing upstream water level until water was manually drawn into the pipe, and did not fluctuate with changing water levels.

6.8.2.3 Bulk Void Ratio

Table 6.9 shows the mass and volume of dam, as well as the calculated bulk void ratio and porosity.

Table 6.9 – Scale Dam 1V:1.5H	
Volume of Dam [m^3]	6.174
Mass of Rock [kg]	9817
Bulk Void Ratio	0.68
Porosity	40.4%

6.8.2.4 Pore Pressure Data

Figure 6.31, 6-33, and 6-34 show the total head values acquired every 15 seconds by the vibrating wire piezometers throughout the full 8 hours of the experiment. Refer to Figure 6.8 and Figure 6.9 for the locations of the vibrating wire piezometers.

Figure 6.31 shows the total head from Piezometers 1A and 1B. These piezometers were located approximately 45 cm above the floor of the flume. The upstream water level was greater than 45 cm for 13 stages (5 to 17) before overtopping failure.

Figure 6.32 shows the total head from piezometers 2A & B, and 3A & B. With the lowest at 24 cm and the highest at 32 cm, this middle set of piezometers was able to capture all but the first stage.

Figure 6.33 shows the total head from piezometers 4A & B, 5A & B, and 6A & B. The heights of the piezometers are approximately 10 cm, which was the lowest position they could be placed without affecting the construction of the dam. This lowest set of piezometers was able to capture all 17 stages, although due to the inherent instability of flow during progressive failures it becomes difficult to distinguish each stage near the end of the experiment.

Note the common trends and data grouping between numerical pairs (i.e. 4A and 4B), this demonstrates that vibrating wire piezometers located at different positions along the length of the rockfill dams produce similar pore pressures, and pore pressure changes. Also note that the upstream piezometers 4A and B have a significantly higher total head than 5A and B, which in turn are greater than 6A and B. This demonstrates that the piezometers are measuring head loss through the rockfill.

Figure 6.34 is a cross-section of Scale Dam 1V:1.5H showing the total head through the dam at various stages of the experiment. This data was obtained from the vibrating wire piezometers and each data point represents the reading

from a piezometer. In some instances adjacent data points on the graphs are nearly vertically separated. This may be a function of the local flows paths through the rockfill and precision of the measurement of the height of piezometer tip.

Figure 6.35 shows select stages of the upstream and downstream water levels with the total head collected from the in-floor open-pipe piezometers. The slope of the total head through the dam increases with increasing discharge, which is a comparable result to that observed in the piezometer data in Figure 6.34.

Figure 6.16 shows the predicted pressure plus elevation head, calculated using Seep/W as outlined in Section 6.7.3, and the pressure plus elevation head measured by the vibrating wire piezometers. When comparing between predicted and measured pressure plus elevation head, the maximum difference observed is less than 5 cm, less than 10% of the measured value.

6.8.2.5 Phreatic Surface

Figure 6.36 shows select phreatic surfaces collected during the Scale Dam 1V:1.5H experiment. The phreatic surface is a location of zero pressure head and is referenced to the experiment datum; therefore the figure shows the results in total head. When visually comparing the curves between that of the vibrating wire piezometers and open-pipe piezometers, the phreatic surface follows the same trend.

6.8.2.6 Discharge

Discharge was monitored for each stage of the Scale Dam 1V:1.5H experiment, included in Table 6.8. Figure 6.37 contains both the predicted stage-discharge relationship, as detailed earlier in this chapter, and the measured flow from the experiment. As will be discussed in Chapter 7, the predicted and the measured discharge are in close proximity, although the slope of the predicted does not match that of the measured.

6.8.2.7 Downstream Slope Movements

During Stage 11, three rocks were observed to have moved. The first two rocks, one being a painted index rock, shifted approximately 30 mm, and maintained position. The third rock, which was monitored by draw-wire, shifted shortly after, but in a separate location suggesting the incidents were independent of each other. Two of the initial three rocks that moved were indexed rocks and raises some suspicion regarding the validity of the movement with regards to the initiation of particle movement analysis. Unlike the first test, not all indexed rocks, those painted for visual observation and those attached to the draw-wires, were placed during initial compaction. Since the rocks had already been measured and recorded, they were kept separate from the construction of the second dam until near completion, when they were individually placed on the face of the dam and compacted. This can be considered different to the placement of rock for infilling lows on the face during construction, which was

completed by bucket placement of multiple rocks and compacted as a group. It is postulated that these index rock movements do not accurately represent the stability of the rockfill due to flow through the structure.

At Stage 14 a slide movement occurred along the right hand wall. This movement was limited to between the wooden uprights, and is therefore considered to have been caused by the limited friction between the rock and the wall.

During the steady state conditions of Stage 15, a surficial shift occurred near the center of the dam. The movement was less than 3 cm and involved 8 rocks.

During the increase in flow to Stage 16, a mass movement occurred at the center extending 0.8 m to the right. The movement extended from the crest to well below the flow-through exit height. Although the movement did not lower the crest height, it did reduce the crest width by approximately 0.1 m (16%). This produced an elevated exit height, approximately 0.15 m greater than where no movement had been observed.

At Stage 17 movement at the left wall was observed. This movement was initiated by particles moving at the wall due to the low friction between the wall and the rock. Immediately following the wall movement, rock extending out 0.5 m from the wall shifted slightly.

During the increase in discharge from Stage 17 to Stage 18 a large unraveling of the downstream face occurred. The entire width of the dam experienced movement. This movement led to a reduction in height of the crest of the dam, producing near overtopping at the center of the structure. The crest had previously been reduced in width during Stage 16 and with the latest movement a significant amount flow began to exit the upper portion of the dam, with a noticeable decrease in flow through the main body of rockfill. As mentioned previously, before Stage 18 could stabilize, the flow straightener used in the scale dam flume detached from the flume causing a wave to overtop the dam causing unraveling. This damage was irreversible and forced the premature termination of the experiment.

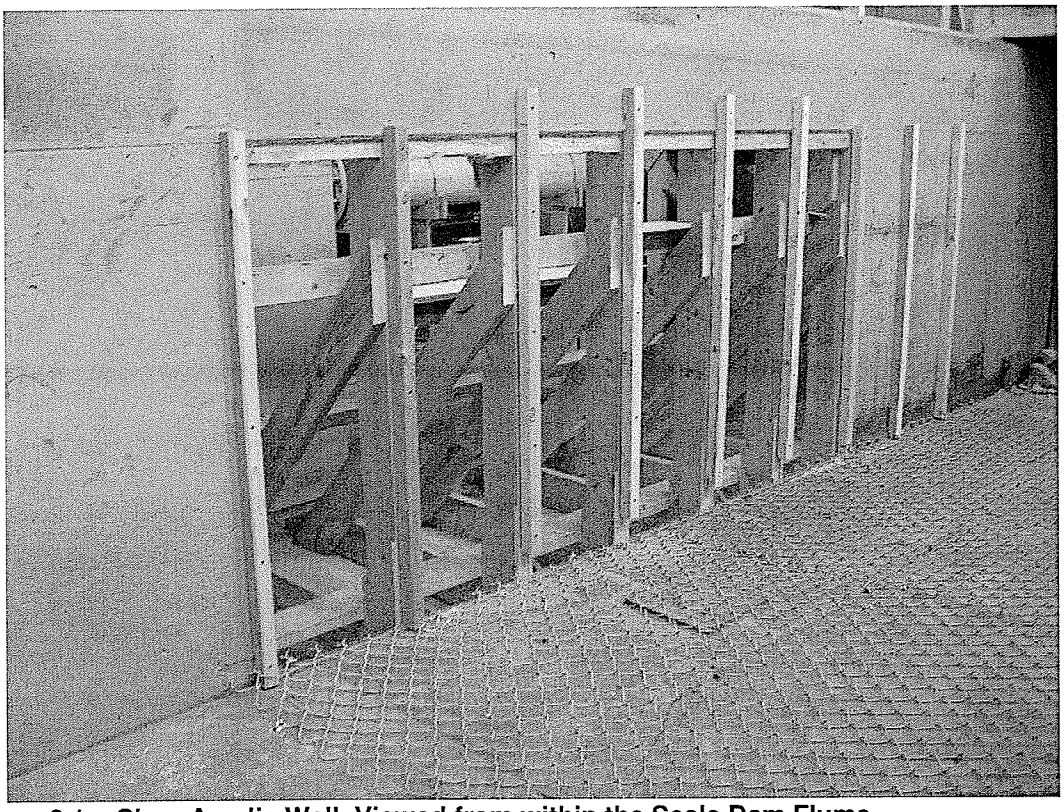

Figure 6.1 – Clear Acrylic Wall, Viewed from within the Scale Dam Flume

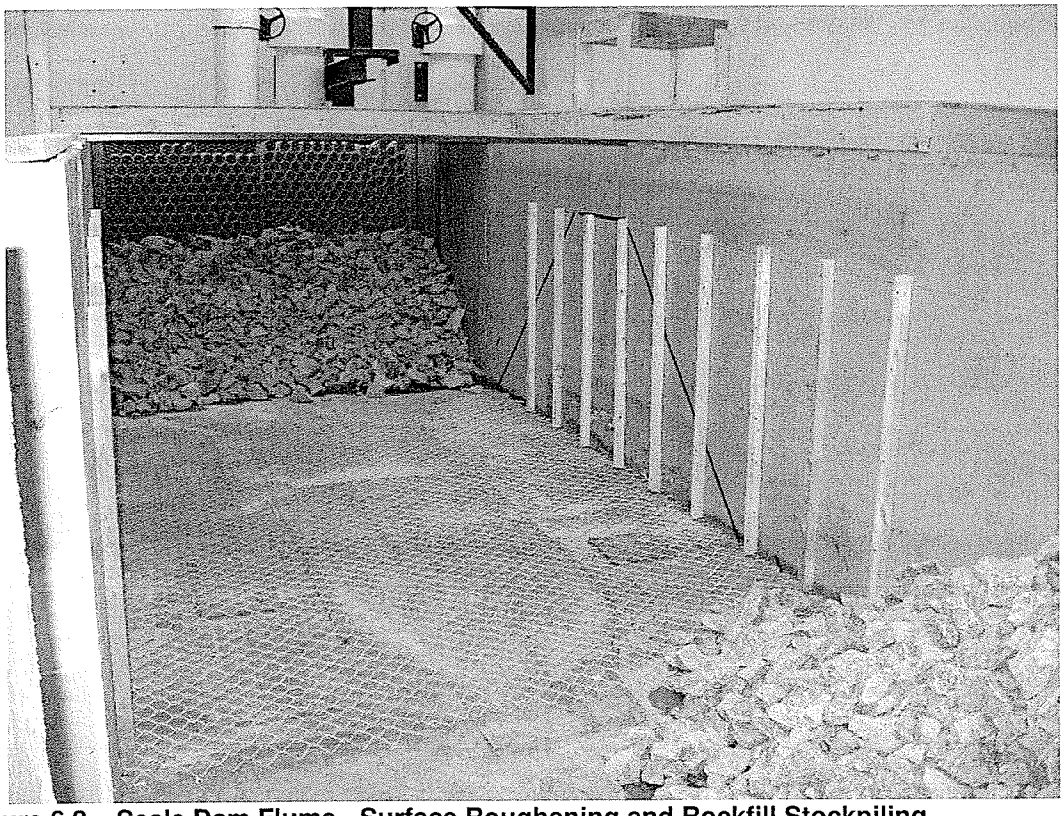

Figure 6.2 – Scale Dam Flume - Surface Roughening and Rockfill Stockpiling

Figure 6.3 – Geokon Inc. Model 4500S Vibrating Wire Piezometer

Figure 6.4 – Slope Indicator Inc. 19 mm Vibrating Wire Piezometer

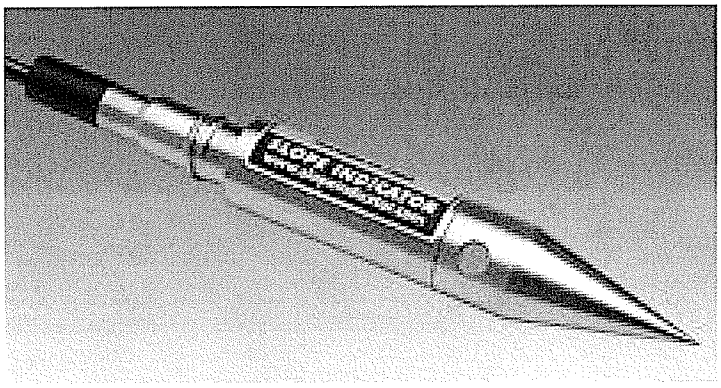

Figure 6.5 – Slope Indicator Inc. Push-in Vibrating Wire Piezometer

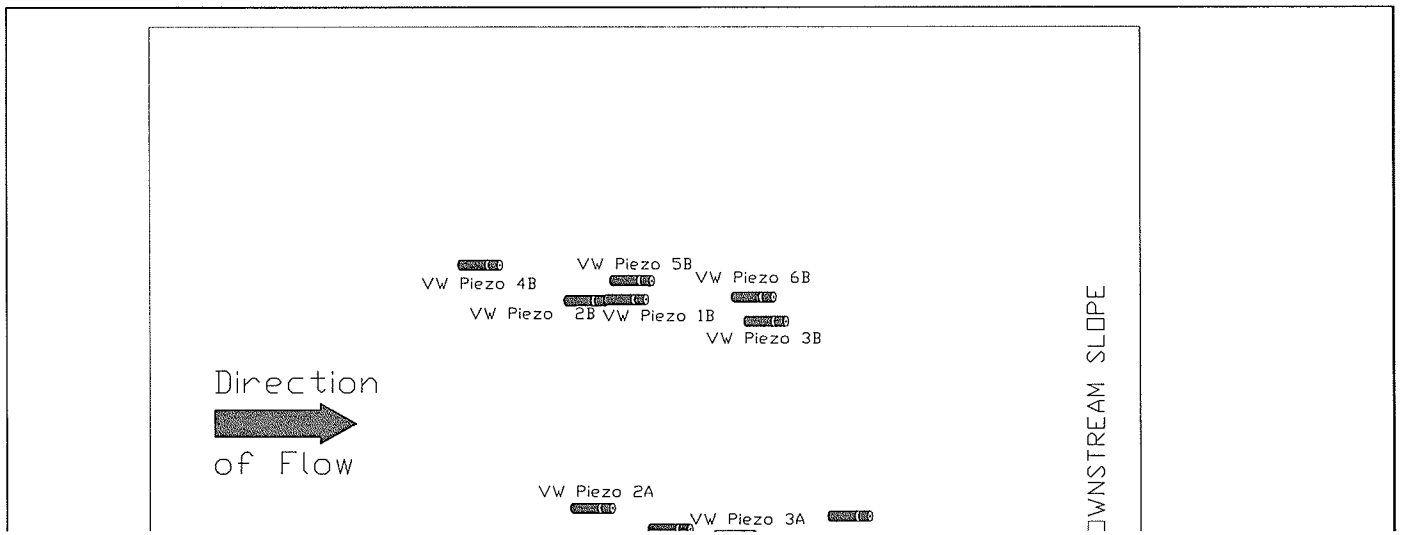

Figure 6.6 - Scale Dam 1V:1H, Plan with Locations of Vibrating Wire Piezometers

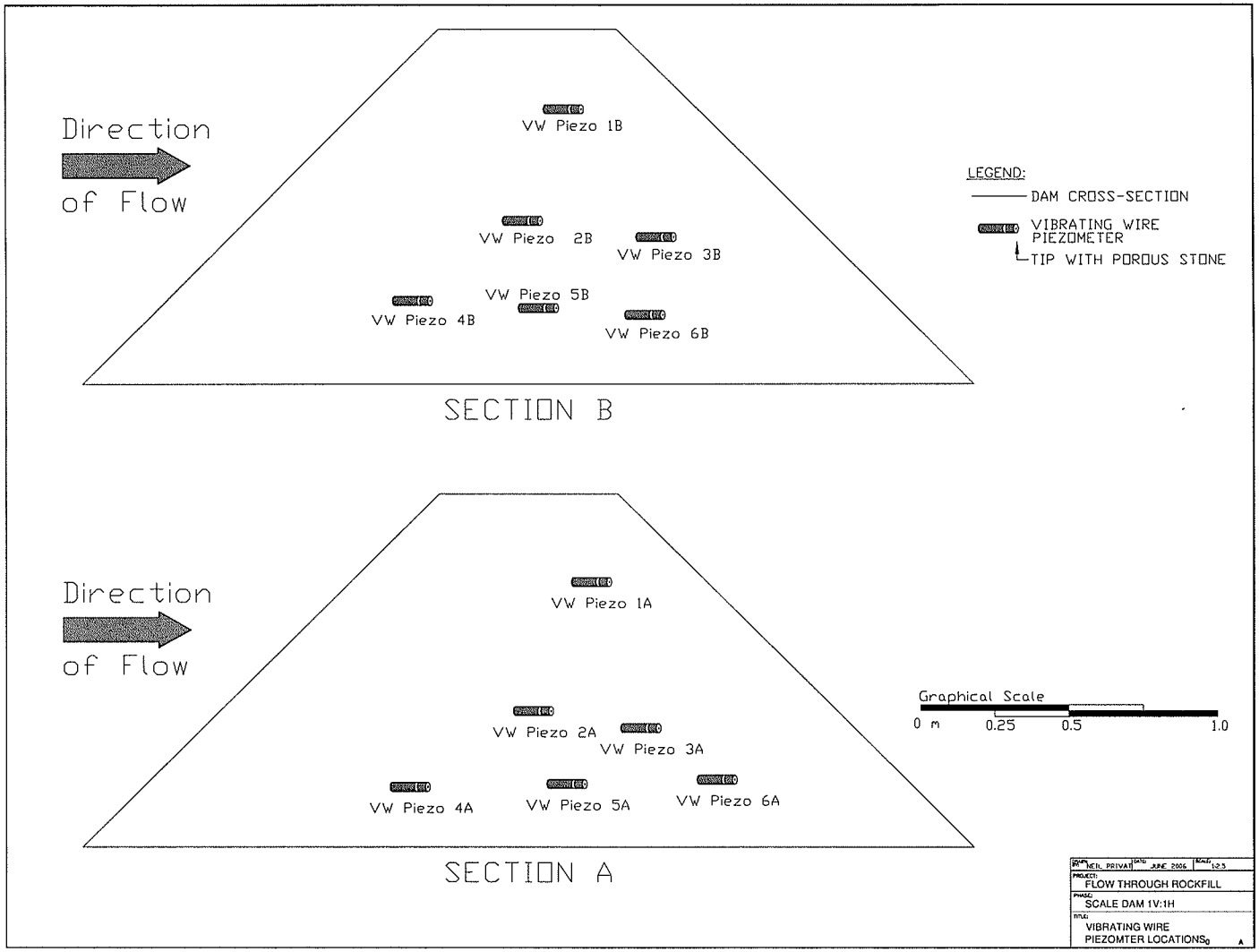

Figure 6.7 – Scale Dam 1V:1H, Cross-sections with Locations of Vibrating Wire Piezometers

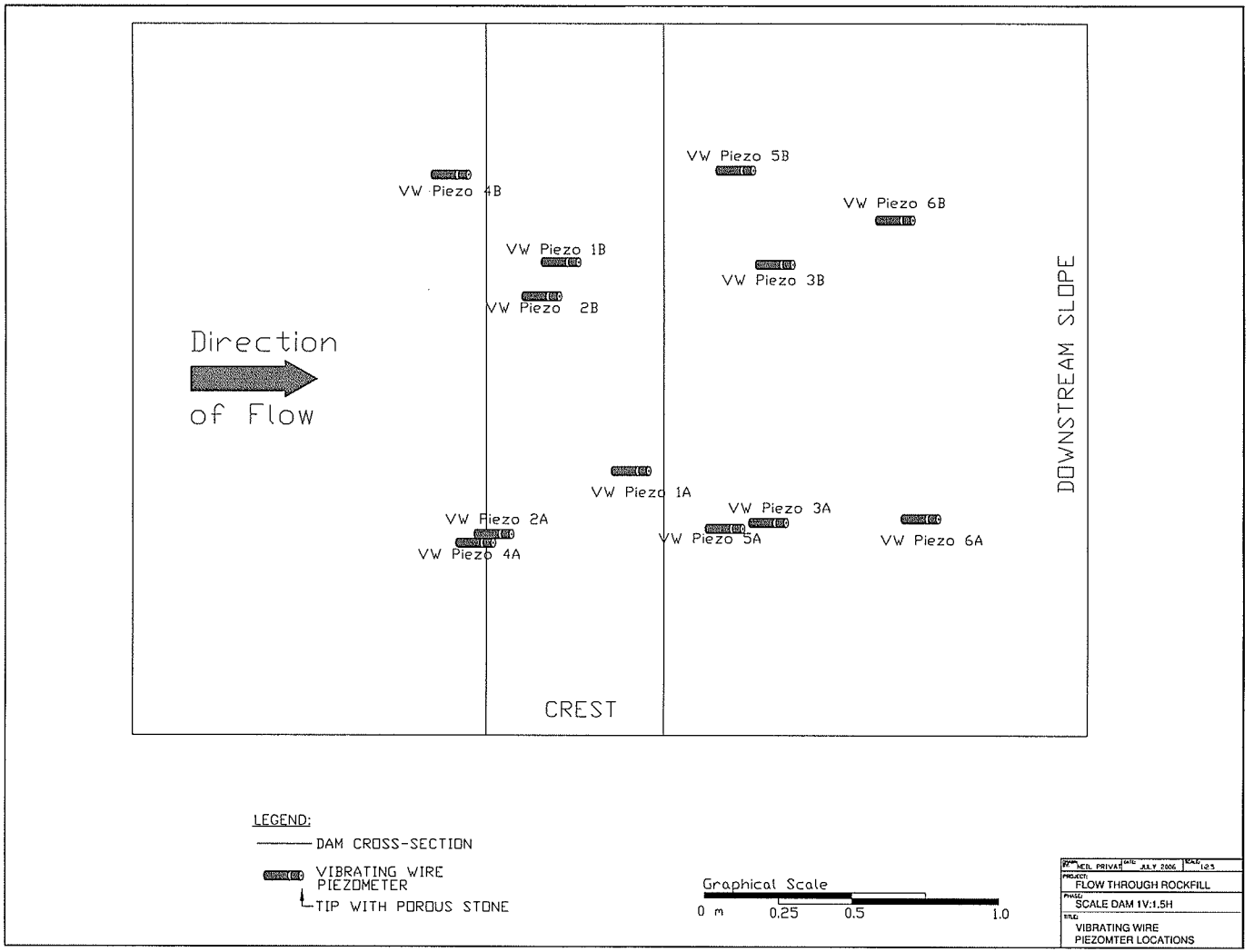

Figure 6.8 – Scale Dam 1V:1.5H, Plan with Locations of Vibrating Wire Piezometers

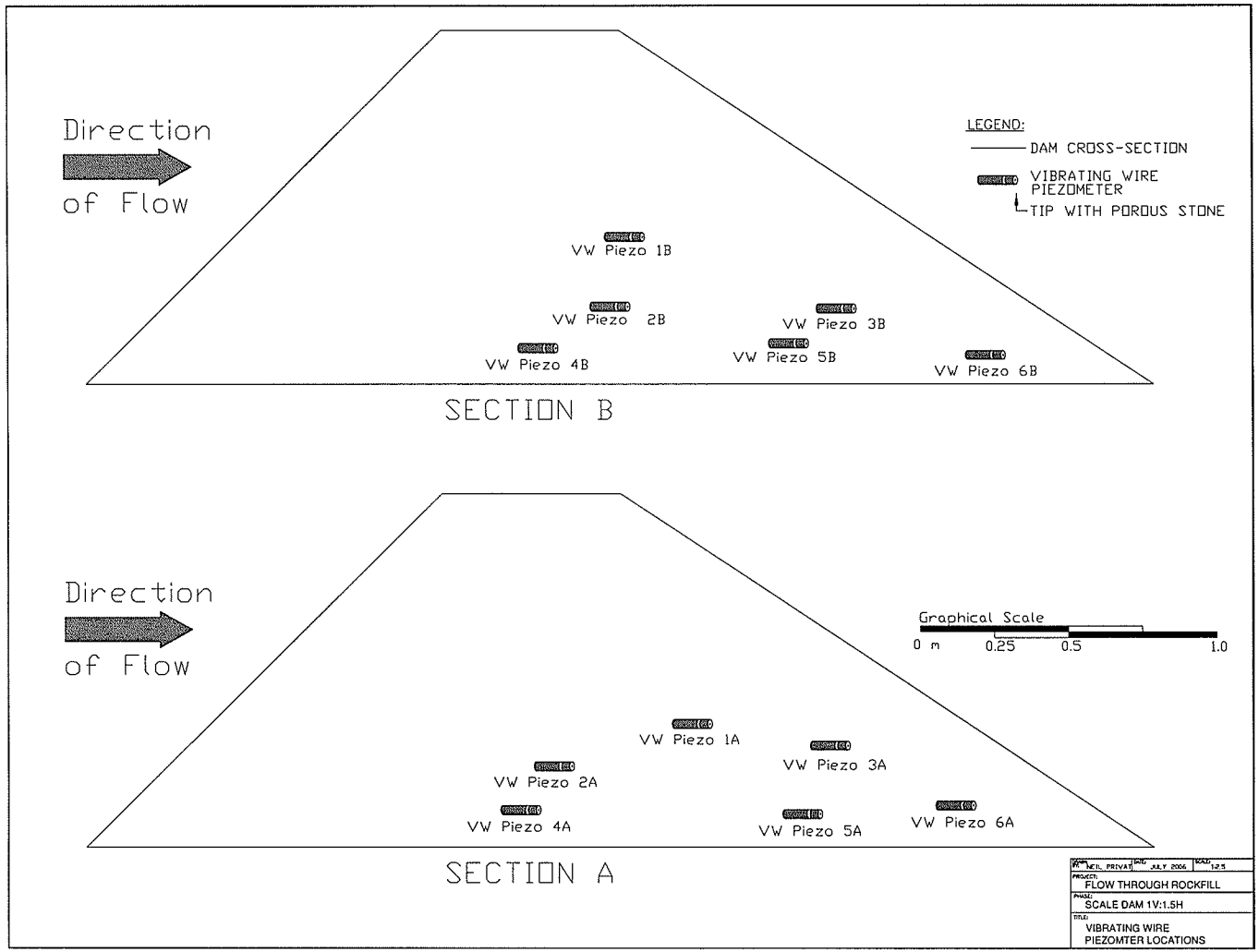

Figure 6.9 – Scale Dam 1V:1.5H, Cross-section with Locations of Vibrating Wire Piezometers

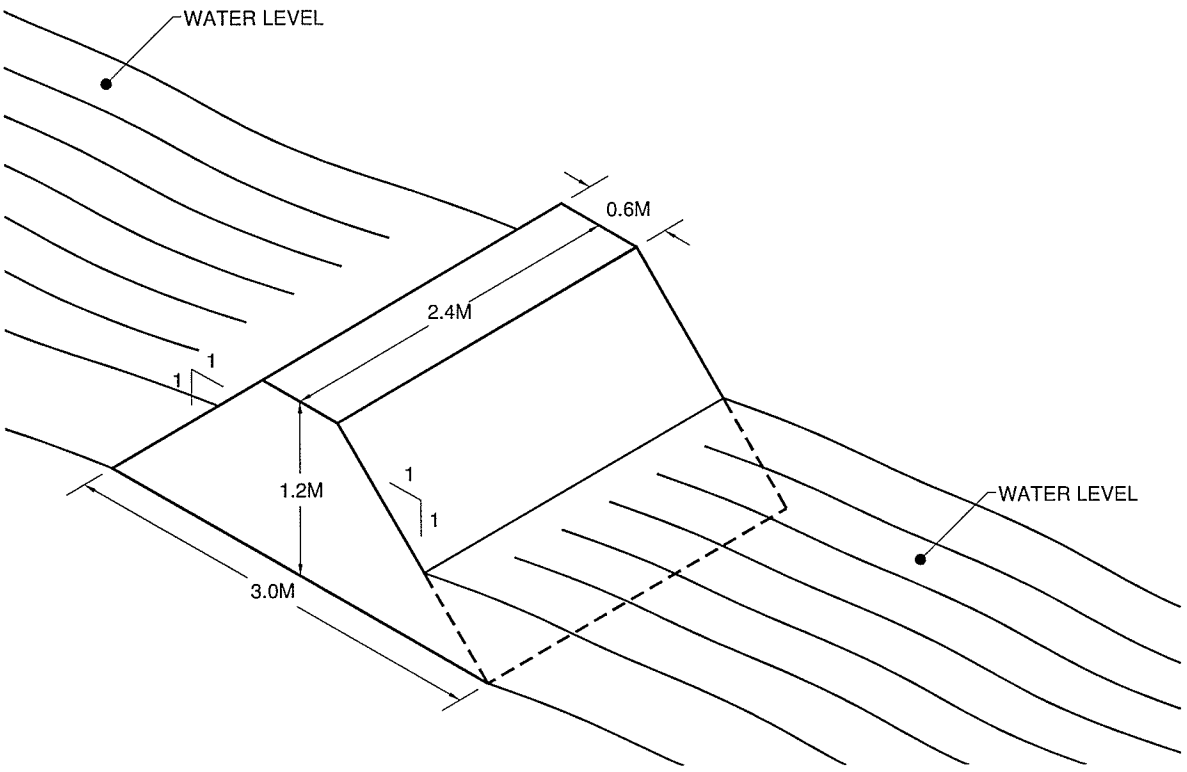

Figure 6.10 – Scale Dam 1V:1H, Geometry

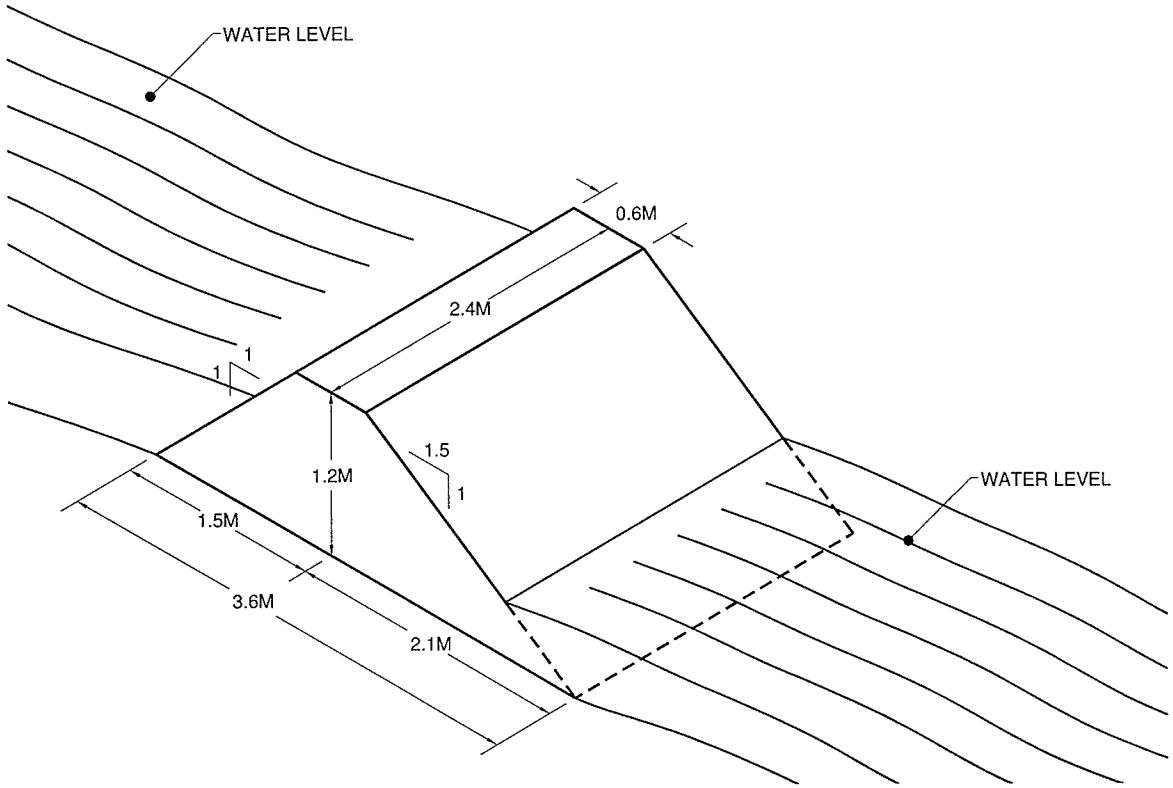

Figure 6.11 – Scale Dam 1V:1.5H, Geometry

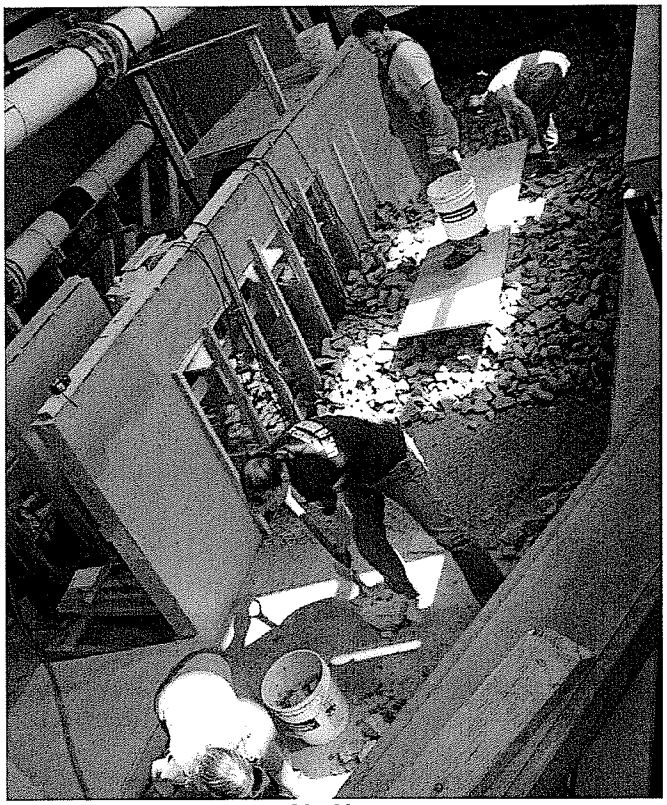

Figure 6.12 – Construction of Scale Dam 1V:1H

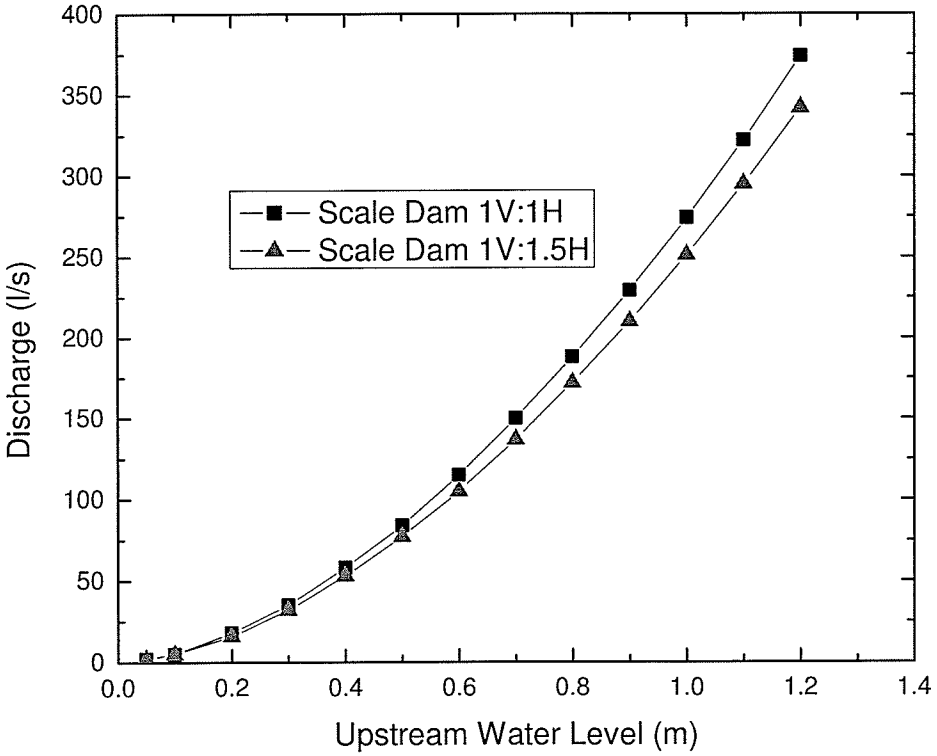

Figure 6.13 – Scale Dam 1V:1H and 1V:1.5H, Predicted Stage-Discharge Rating Curves

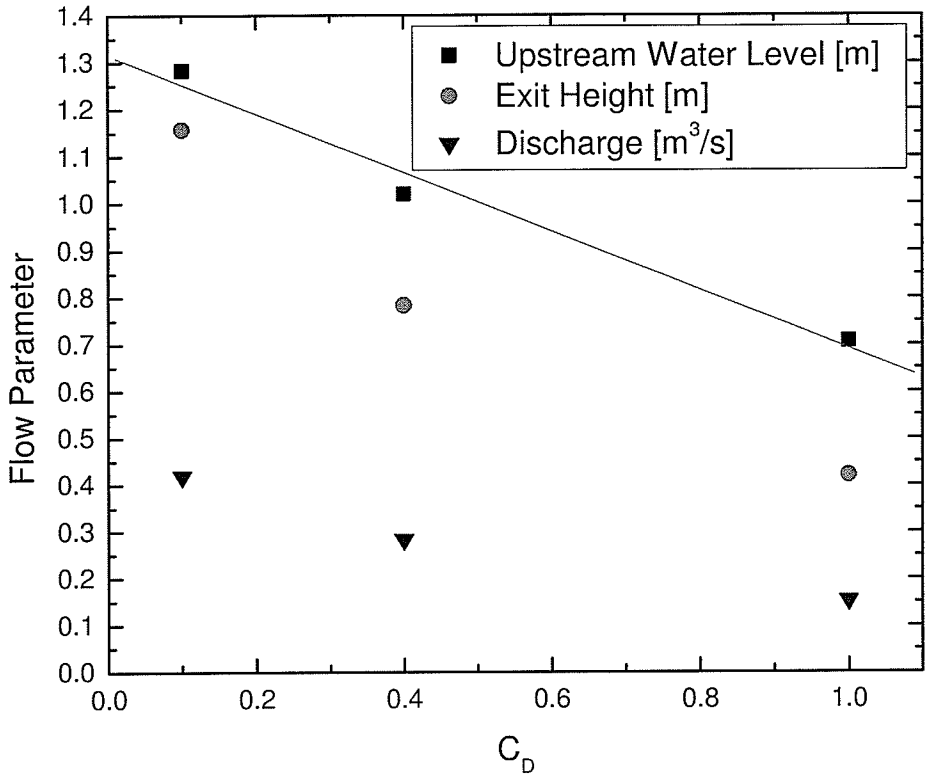

Figure 6.14 – Sensitivity Plot, C_D

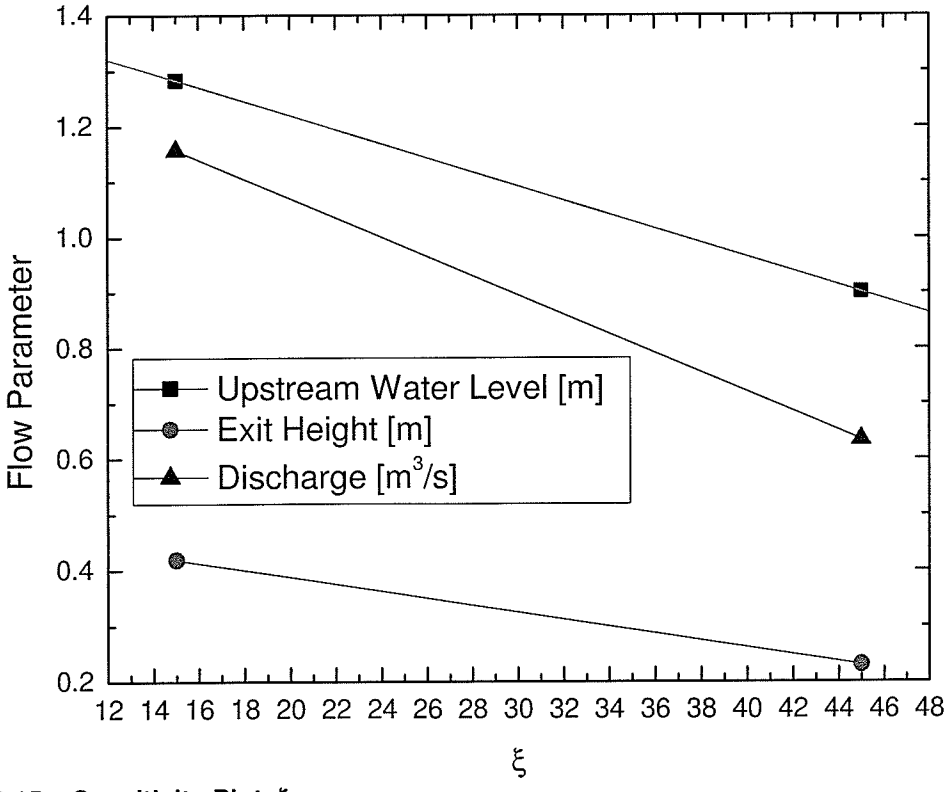

Figure 6.15 – Sensitivity Plot, ξ

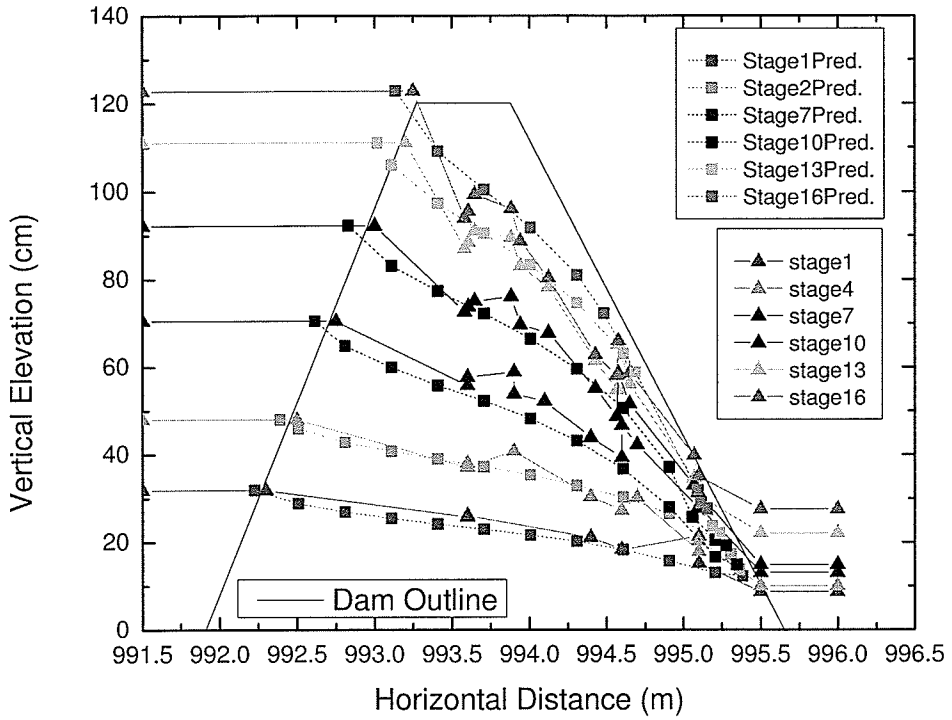

Figure 6.16 – Scale Dam 1V:1H, Comparison of Predicted and Measured Pressure plus Elevation Head

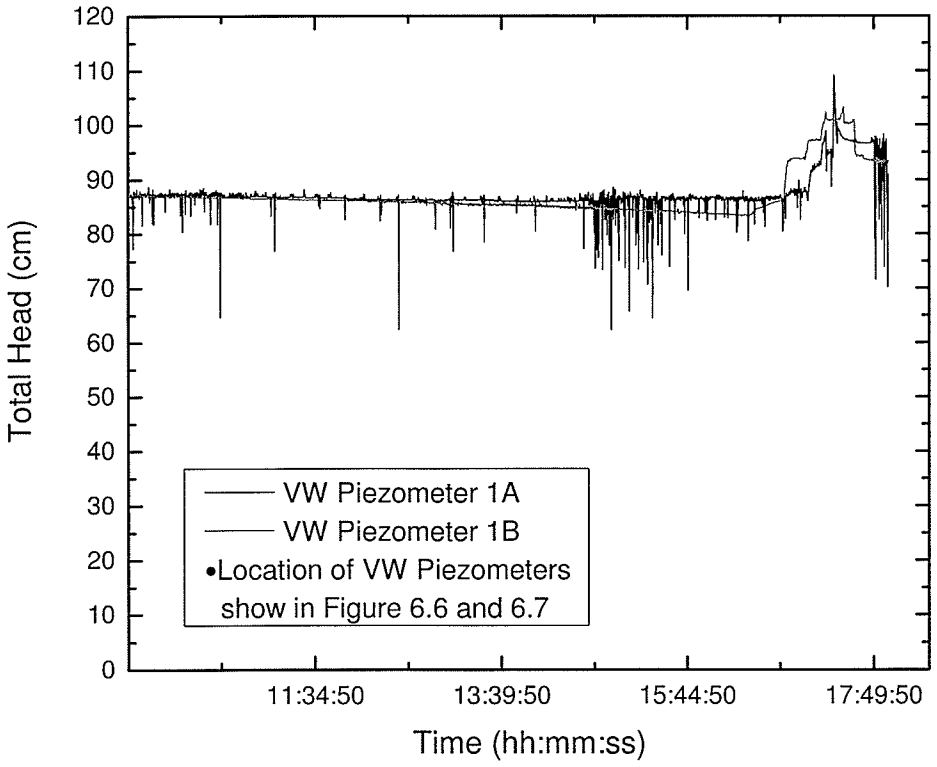

Figure 6.17 – Scale Dam 1V:1H, Total Head, Upper Level Vibrating Wire Piezometer

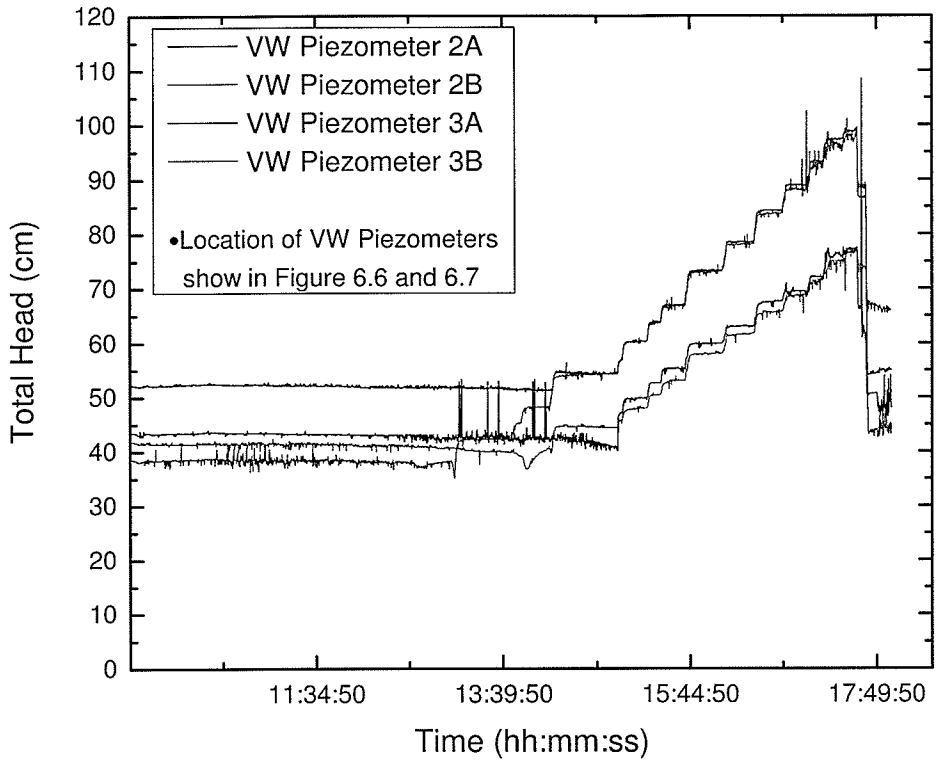

Figure 6.18 – Scale Dam 1V:1H, Total Head, Middle Vibrating Wire Piezometers

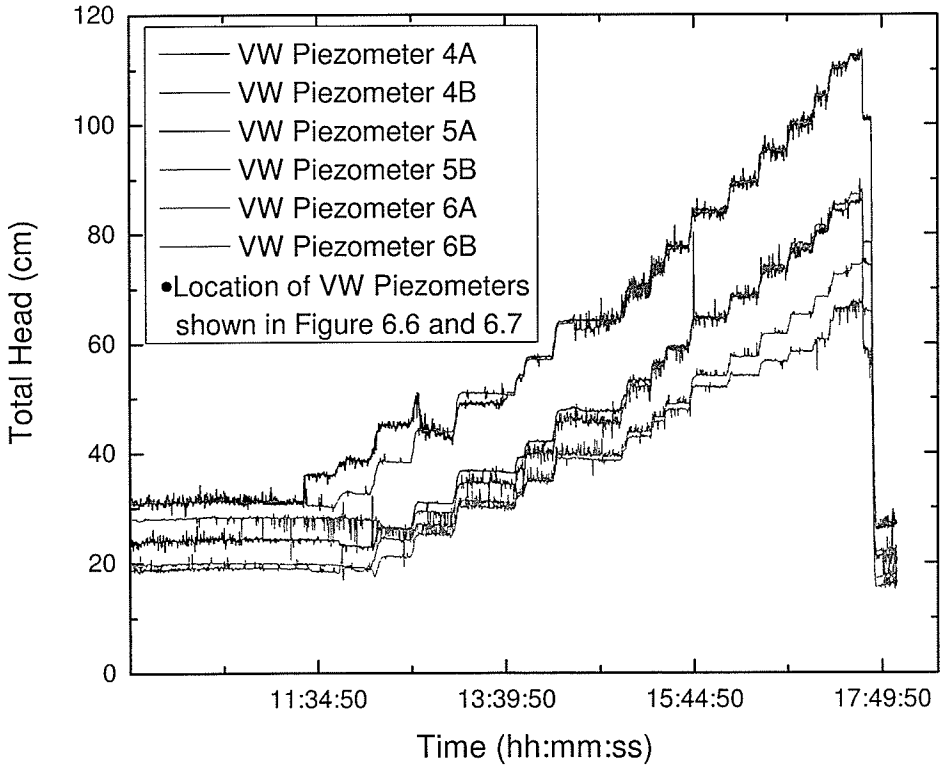

Figure 6.19 – Scale Dam 1V:1H, Total head, Lower Vibrating Wire Piezometers

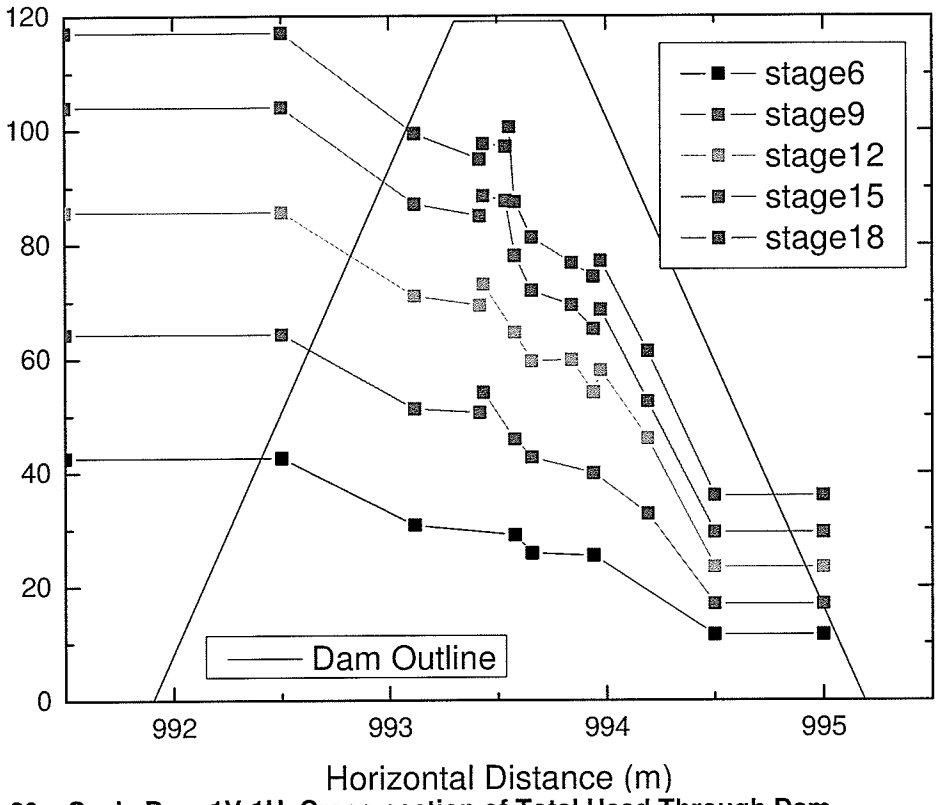

Figure 6.20 – Scale Dam 1V:1H, Cross-section of Total Head Through Dam

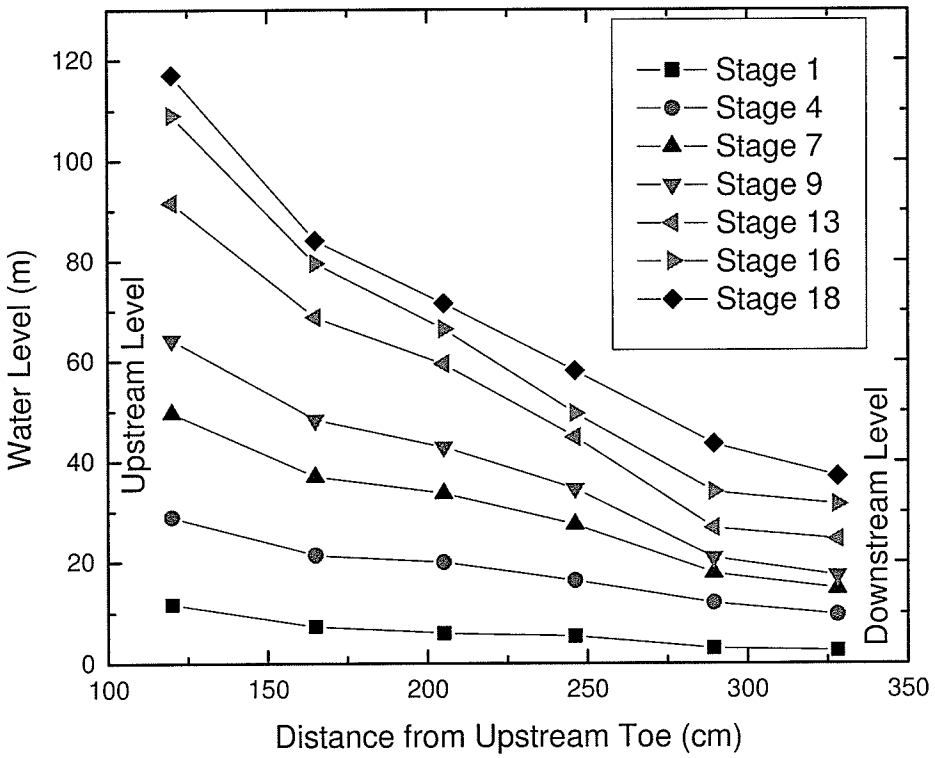

Figure 6.21 – Scale Dam 1V:1H, Pressure plus Elevation Head from Open-pipe Piezometers

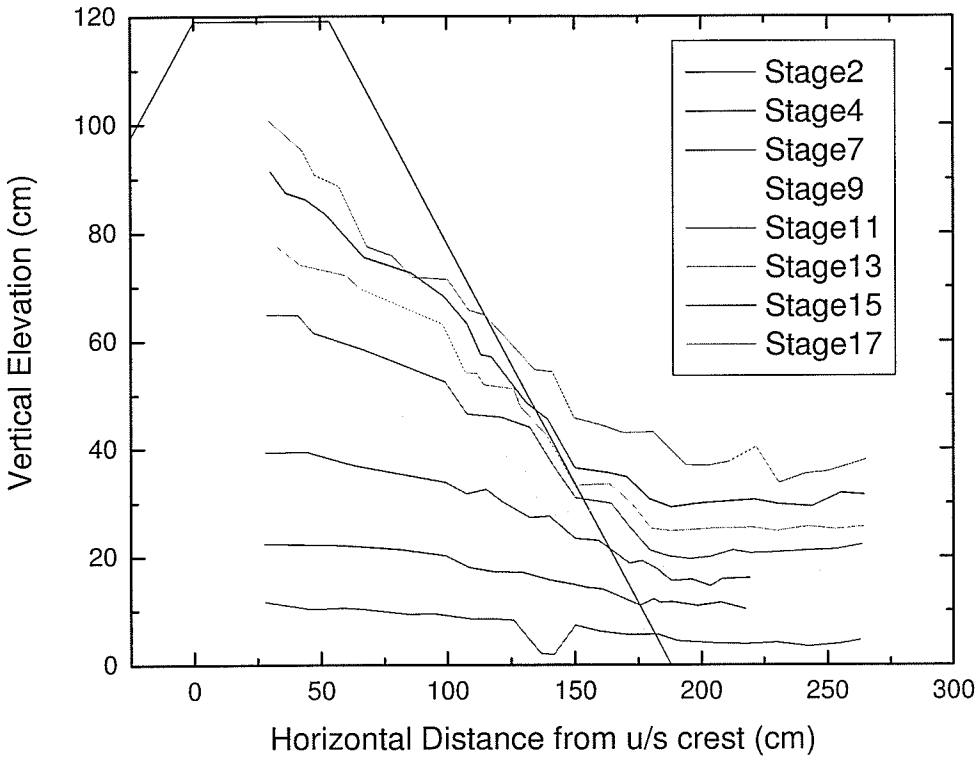

Figure 6.22 – Scale Dam 1V:1H, Select Phreatic Surfaces

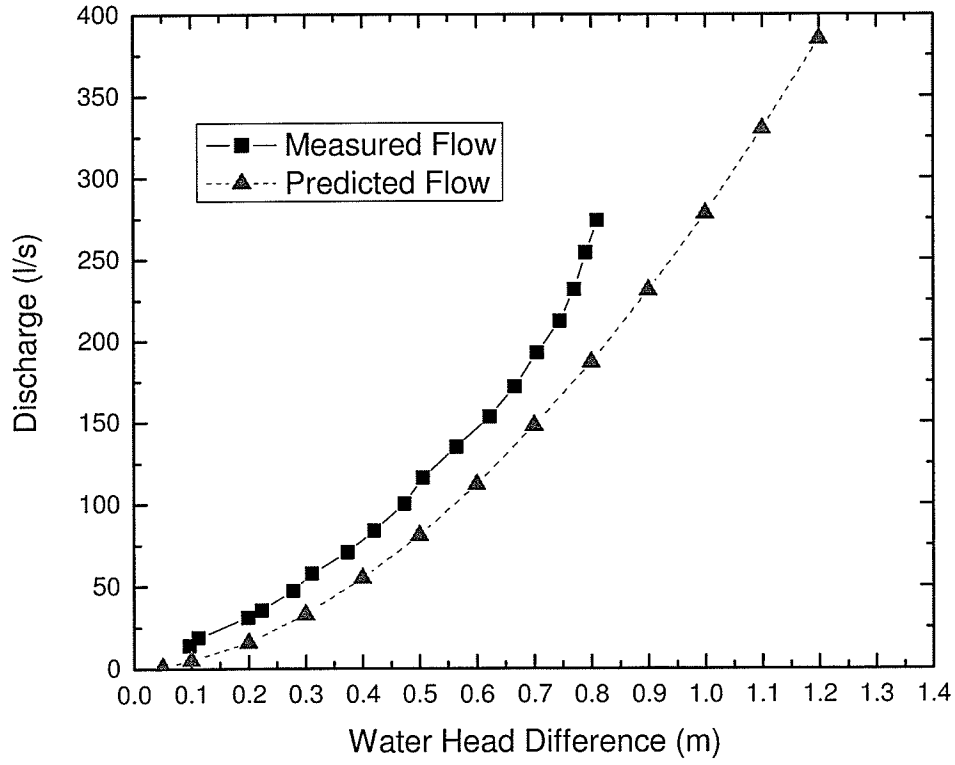

Figure 6.23 – Scale Dam 1V:1H, Measured and Predicted Stage-Discharge Rating Curve

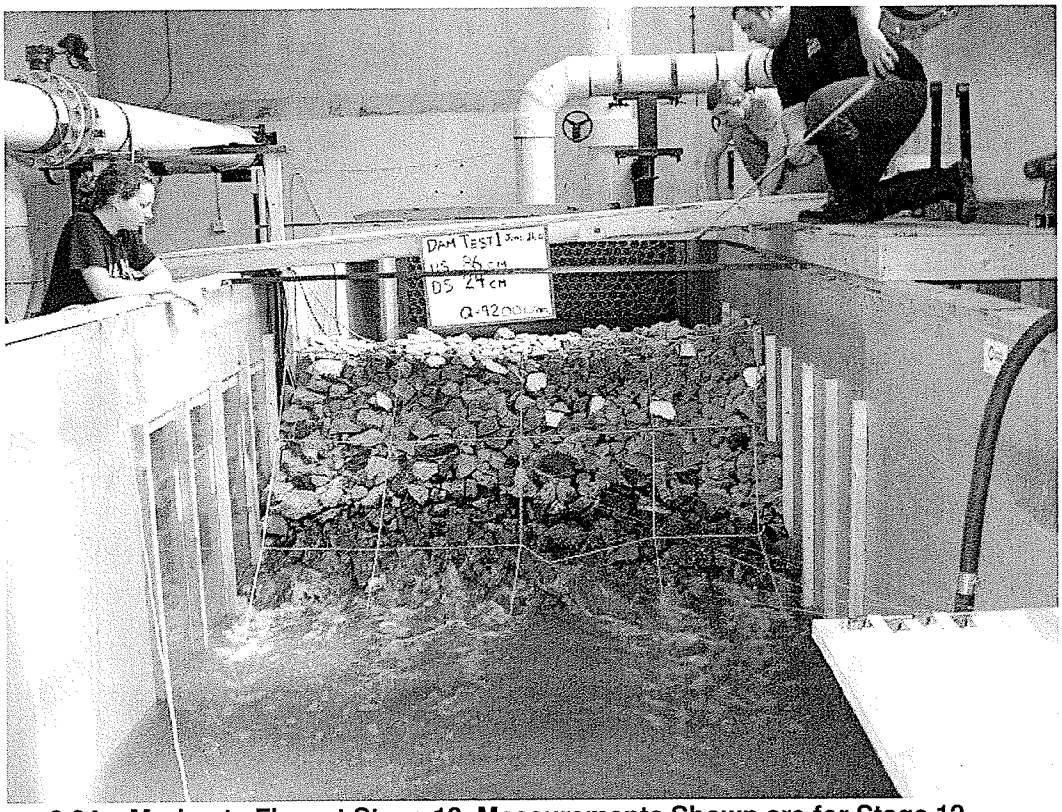

Figure 6.24 – Moderate Flow at Stage 13, Measurements Shown are for Stage 12

Figure 6.25 – High Flow Exiting Structure

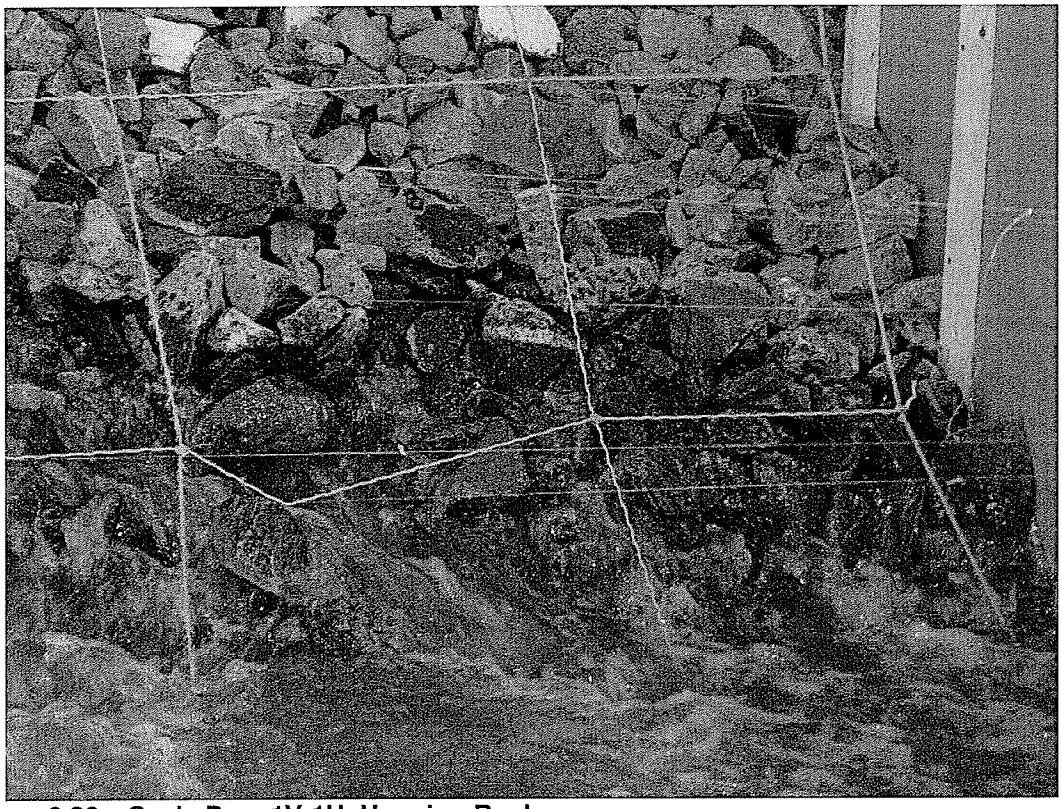

Figure 6.26 – Scale Dam 1V:1H, Hanging Rock

Figure 6.27 – Near Overtopping, Scale Dam 1V:1H

Figure 6.28 – Overtopping of Scale Dam 1V:1H

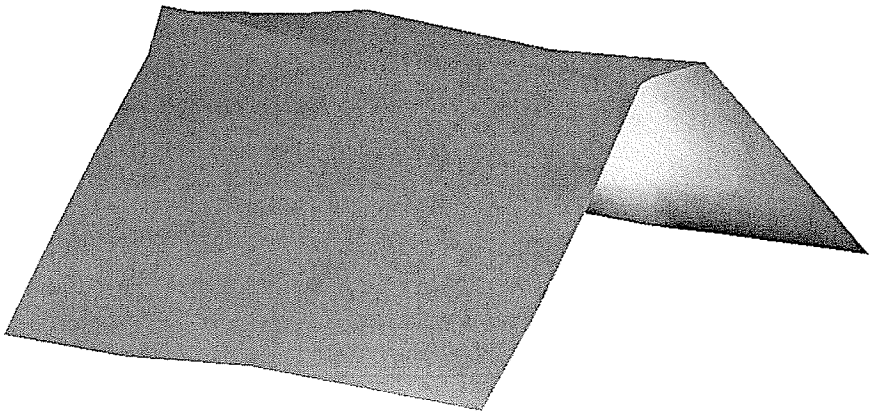

Figure 6.29 – Pre-Test AutoCAD Reproduction of Scale Dam 1V:1H

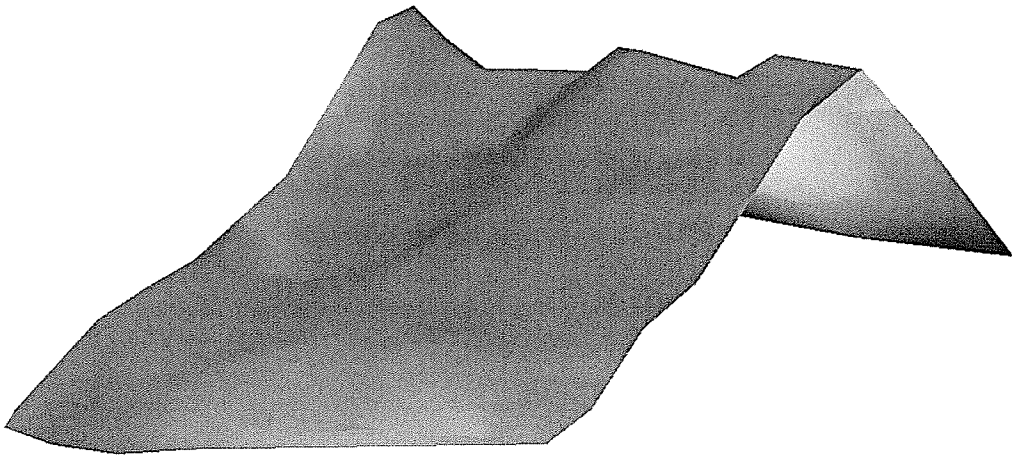

Figure 6.30 – Post Test AutoCAD Reproduction of Scale Dam 1V:1H

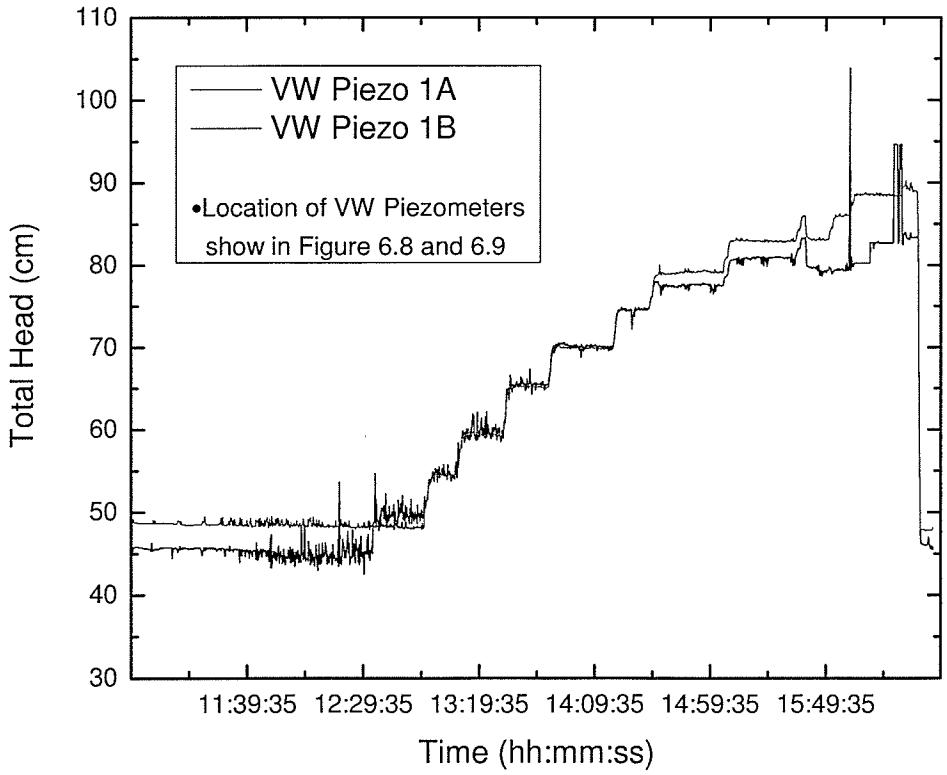

Figure 6.31 – Scale Dam 1V:1.5H, Upper Vibrating Wire Piezometers

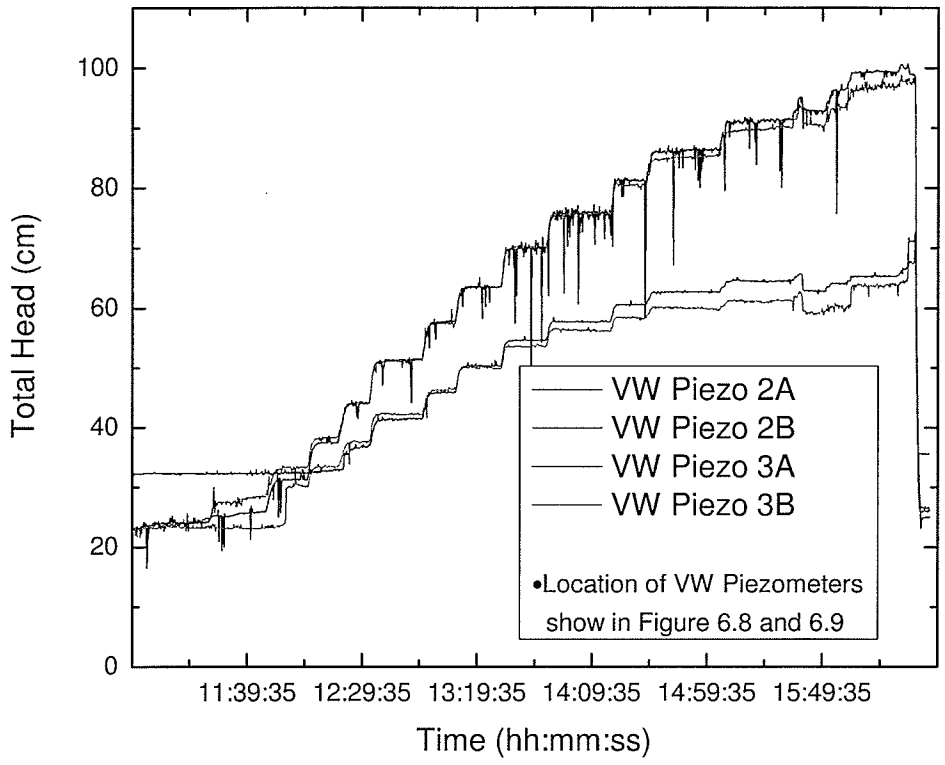

Figure 6.32 – Scale Dam 1V:1.5H, Mid-Level Vibrating Wire Piezometers

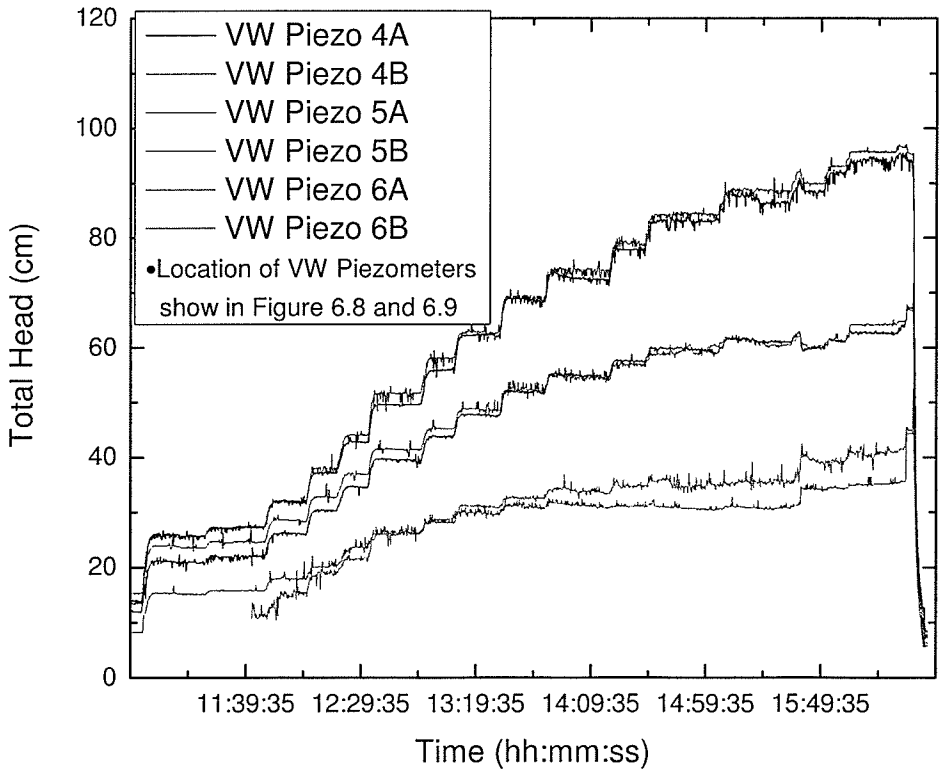

Figure 6.33 – Scale Dam 1V:1.5H, Lower Level Vibrating Wire Piezometers

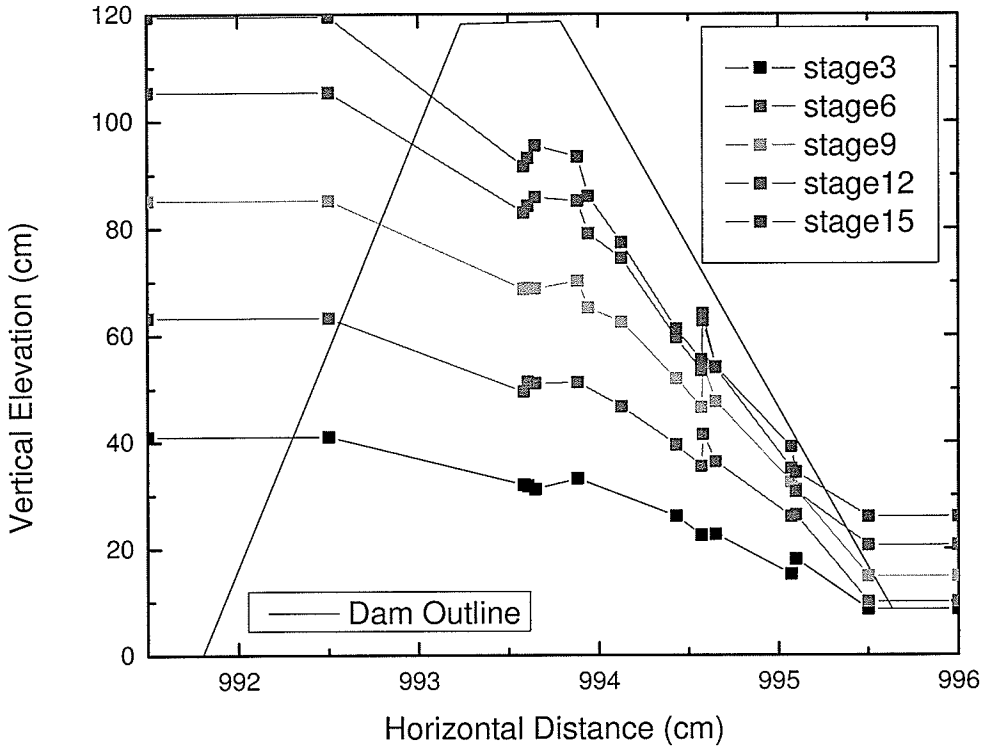

Figure 6.34 – Scale Dam 1V:1.5H, Cross-section of Total Head Through Dam

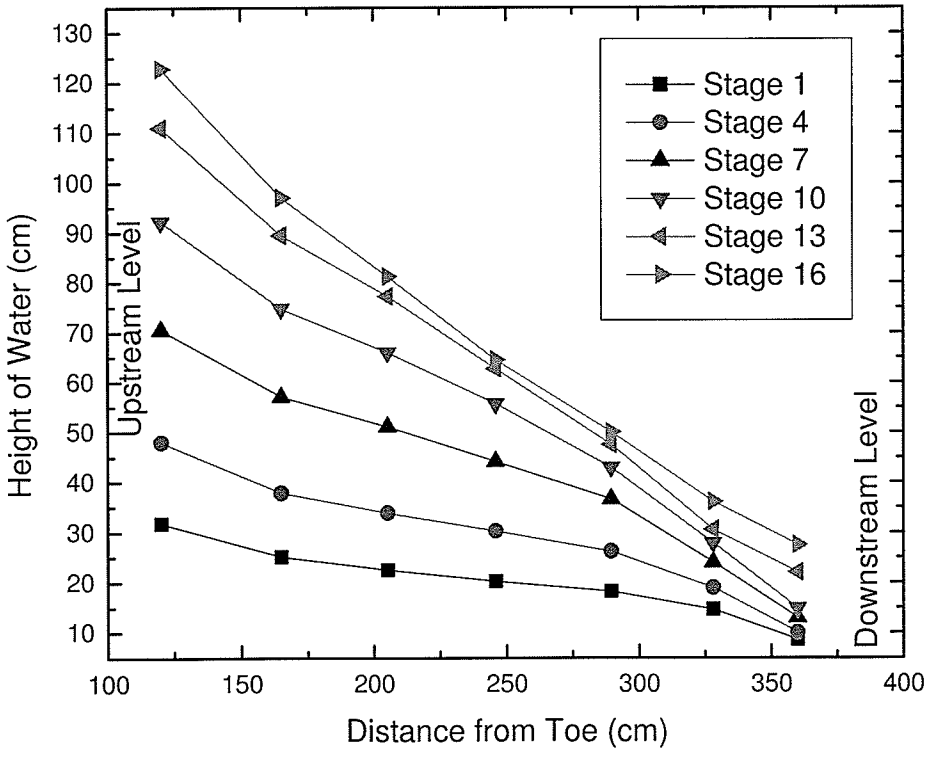

Figure 6.35 – Scale Dam 1V:1.5H, Total Head Measured by In-Floor Open-pipe Piezometers

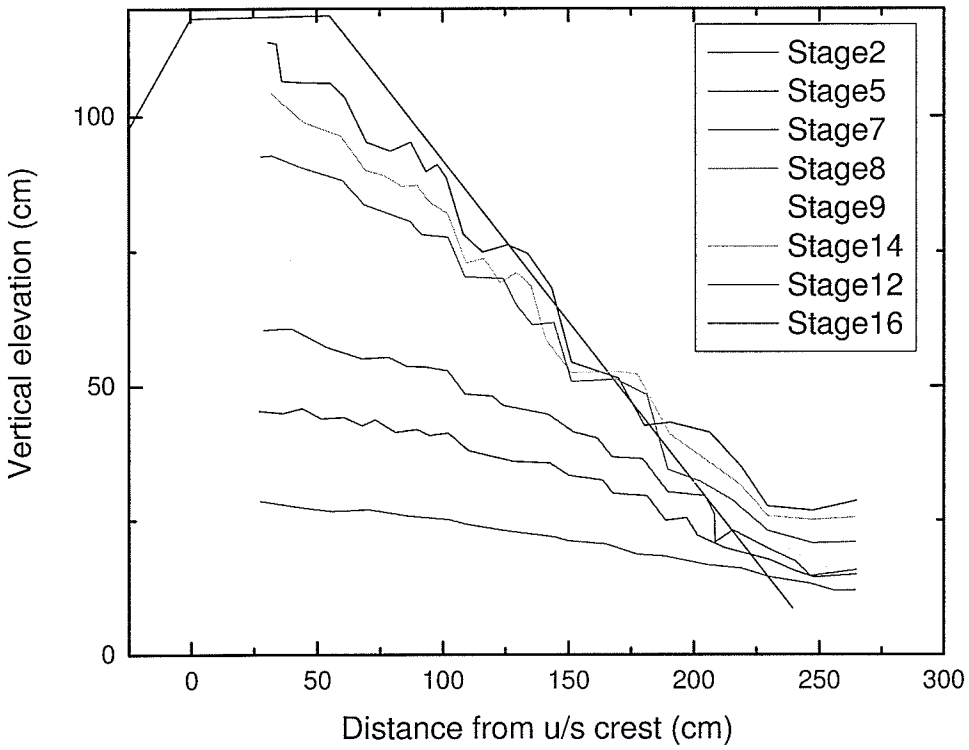

Figure 6.36 – Scale Dam 1V:1.5H, Select Measured Phreatic Surfaces

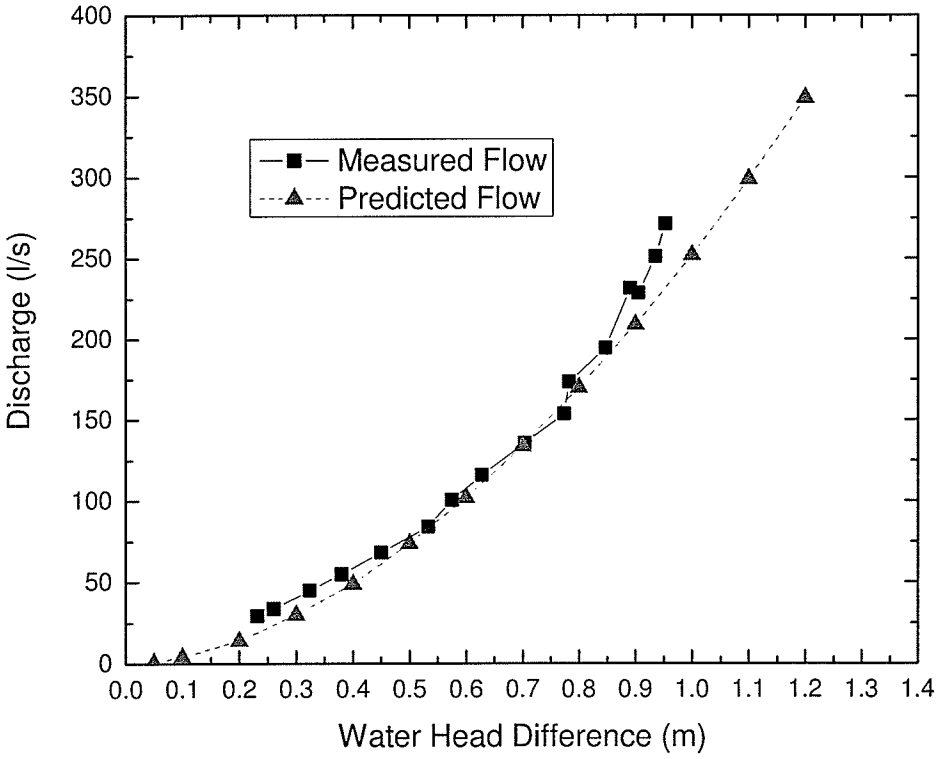

Figure 6.37 – Scale Dam 1V:1.5H, Measured and Predicted Discharge

7 INTERPRETATION OF RESULTS

7.1 FLOW THROUGH ROCKFILL

7.1.1 Discussion of Rockfill Parameters

7.1.1.1 Dominant Particle Size and Gradation

The hydraulic mean radius is calculated from the representative particle size and void ratio of the flow-through coarse porous media. In a well-graded rockfill, selection of a representative particle size for the hydraulic mean radius is difficult, as the dominant particle size affecting flow is not known. Leps (1973) suggested that selection be based on the ability of smaller particles to fill the larger voids thus effectively creating a porous media of smaller diameter. The gradation of the material obviously relates to the dominant particle size but also relates to the permeability. Well-graded materials placed under ideal conditions have a lower permeability than uniformly graded materials that have the same dominant particle size (Leps 1973).

In the 10 to 150 mm well-graded porous media used in Mini Dam tests MD14 and 15, the dominant particle size was estimated as the d_{50} of the gradation and was interpreted as 50 mm (Figure 7.1). Test MD14 is compared to MD11, a 50 mm poorly graded dam, which had the same downstream slope and similar void ratios (0.58 and 0.65 respectively). For any given stage the well-graded dam had less discharge. As well, the first particle movement observed on the well-graded dam was at a greater discharge. This suggests the dominant particle size, for the well-graded rockfill, for flow characterization should be reevaluated.

7.1.1.2 Void Ratio (Porosity)

As described in Chapter 4 regarding the Large-scale Permeameter experiments, void ratio (e) affects several aspects of the flow. MD10 and MD11 were constructed with 50 mm poorly-graded rockfill, with a downstream slope of 1V:1H. The void ratios of the two were 0.82 and 0.65 respectively. As can be seen on Figure 7.2, for a given upstream water level MD10 had a discharge 4 l/s per m length of dam greater than MD11. Similarly, as shown in Figure 7.3, MD6 (e=0.9) has a 5 l/s per m length greater discharge for a given upstream water level than MD12 (e=0.74). Both MD6 and MD12 were constructed with 50 mm poorly-graded rockfill and had 1V:1.5H downstream slopes. It can be concluded that compaction of the rockfill to reduce the bulk void ratio would reduce the flow and hydraulic gradient.

7.1.1.3 Downstream Slope Angle

MD10, MD8 and MD12 are compared in Table 7.1 with data from Table 5.2 and the phreatic surfaces, Figure 5.14, Figure 5.12, and Figure 5.17 respectively. For comparable void ratios and varying downstream slope geometries the exit height of the seepage face will generally be higher on a dam with a shallower downstream slope. Table 7.1 demonstrates this statement for one discharge stage, but the trend was observed throughout the data. An argument as to the affect of the void ratio of MD8 may be made, but the general trend between downstream slope and upstream water level is observed.

Table 7.1 – Comparing Downstream Slope Angle					
Test	Void Ratio	Downstream Slope	Discharge [$m^3/s/m$]	Upstream Water Level [m]	Exit Height [m]
MD10	0.82	1V:1H	0.38	0.37	0.25
MD8	0.76	1V:1.5H	0.38	0.42	0.25
MD13	0.8	1V:2H	0.37	0.44	0.29

7.1.2 Stage-Discharge Curve Analysis

Mass surface movements occurred on the downstream face of Scale Dam 1V:1H during Stage 15 and Scale Dam 1V:1.5H during Stage 13. When the downstream face experienced sliding and unraveling, leading to a loss of material, the flow-through length within the rockfill was decreased. Therefore, comparisons between the predicted and measured discharge will be limited to the stages prior to the first significant movement.

7.1.2.1 Scale Dam 1V:1H

As shown in Figure 6.23, the difference in the calculated discharge and the measured discharge for a given head, ranges from 14 to 40 l/s (5.2 to 16.4 l/s per m length). In the development of Equation 2.9, Hansen *et al.* (1995) ignored the depth and effect of the downstream water level, stating that it was less than 10 percent of the upstream water level. In Scale Dam 1V:1H experiment, the downstream water level varied approximately 2 times that reported in Hansen *et al.* (1995), from less than 20 percent at low discharge up to approximately 30

percent at peak discharge. To account for the reduction in discharge relate to the height of the downstream water level, the post experiment curve fitting took h, initially defined as the upstream water level from Equation 2.9, as the upstream level minus one-half the downstream level. When plotting, as on Figure 7.4, the y-axis remains the upstream water level (h) as measured.

A curve fitting procedure was conducted to fit the measured data with the equation for turbulent flow (Equation 2.7a), with a and N as the unknowns. The fitted curve represents the measured data well, as shown in Figure 7.4. In the fitting process, the trend of the data was matched as the shape of the curve with the hydraulic gradient versus bulk velocity parameters a equals 21.8 and N equal to 2.0. To overlay the curving matching to the measured data a vertical shift of 10 l/s was required. This represents a consistent under prediction of discharge and a non-zero discharge at zero head. This phenomenon can be explained with the consideration of the following two factors. First, the flume upstream of the dam was known to have a minor leak, and during the test the amount of leakage was not monitored. Secondly, noted during the pre-test submerging of the dam was flow on the flume floor representing a preferential flow path, avoiding flow through the rockfill (tortuosity, angularity and surface roughness). Observations of the two factors suggest the second factor would be the greater contributor to the continuous discrepancy between the measured discharge and the curve fitting.

The curve fitting of Scale Dam 1V:1H results produced values of 21.8 and 2.0 for a and N respectively. The large-scale permeameter tests, Table 4.1, with a void ratio of 0.74, would suggest a lower value of a for this test. Leps (1973) reported that other researchers have found the need to increase a when comparing between vertical permeameter testing and horizontal rockfill flume flow.

7.1.2.2 Scale Dam 1V:1.5H

As shown in Figure 7.5 the predicted discharge diverges from the measured discharge for increasing discharge. This corresponds to the slope of the predicted curve being different than the measured discharge data. A change to the a-value will change the slope of the curve such that they are parallel. The vertical shift, which was applied for Scale Dam 1V:1H was applied to the curve fitting for Scale Dam 1V:1.5H as well. Using curve fitting and the 10 l/s vertical shift, an equation can be applied to the measured data. In matching the shape of the curve a equals 30 and N is 2.0.

The vertical shift for the non-zero reading was observed in both scale dam tests, providing confidence that the shift is a function of the test procedures (apparatus) and not representative of the flow-through properties of the rockfill.

7.1.3 Alternate Predictive Models

As outlined in Hansen *et al.* (1995) several existing equations provide a close approximation for flow through packed columns of granular material with Wilkins' equation (Wilkins 1956) having been used extensively in Canada. Wilkins'

equation (Equation 2.7a) is an empirical relationship between velocity and hydraulic gradient and can be used when flow data is not available. Wilkins' requires the hydraulic mean radius of the flow-through material. This can be difficult to interpret due to the non-uniform gradation of the material.

Using the specific surface area graph (Figure 2.3) and associated Equation 7.1 proposed by Wilkins (1955), hydraulic mean radius can be calculated. For Scale Dam 1V:1H m equals 0.00461 compared to 0.00474 using Equation 2.2 (Garga *et al.* 1991). For Scale Dam 1V:1.5H m equals 0.00447 compared to 0.00436.

$$m = \frac{V_B n}{A_{ms} M_R}$$ **Equation 7.1**

where
V_B is the bulk volume of the rockfill
A_{ms} is the mass specific surface area
n is the rockfill porosity
M_R is the mass of the rockfill

The stage-discharge relationship is produced by combining Equation 2.10, proposed by Wilkins (1955), and Equation 2.9, developed by Hansen *et al.* (1995). Wilkins (1963) later reported that W (Wilkins coefficient) was found to be 6.693 in a flume. Figure 7.7 and Figure 7.8 shows the measured data, calculated results from the originally reported W and of the 1963 W. The original W under predicts the curve while the '1963' W over predicts but is generally good.

7.2 FLOW-THROUGH MOVEMENT IN ROCKFILL

7.2.1 Mini Dam Observations

Table 7.2 lists mini dams MD9 through MD15 and provides information on the flow through conditions at the moment of initiation of flow-through particle movement.

Table 7.2 – Details of Initiation of Particle Movement MD9 through MD15

	Downstream Slope	Void Ratio	Discharge [l/s/m length]	Upstream Water Level [cm]	Exit Height [cm]
MD9	1H:1V	0.79	52.6	50.5	35
MD10	1H:1V	0.82	53	41	28
MD11	1H:1V	0.65	53.3	46.6	34
MD12	1V:1.5H	0.74	51.3	47.4	39
MD13	1V:1.5H	0.80	51.8	49.5	45
MD14	1H:1V	0.57	58.2	43.6	31.5
MD15	1V:1.5H	0.62	66.1*	51.5*	46*

*MD15 did not experience particle movement until overtopping occurred.

7.2.1.1 Erosion of Downstream Toe

As described in Chapter 5, erosion of the downstream toe of the dams occurred in MD3 through MD8 at low flows. No restriction was placed on the downstream toe of these dams. The resistance to movement was provided by the friction interface between the concrete flume floor and rockfill. The movement of the toe allowed premature headward erosion. This observation of MD3 though MD8 is supported in Table 5.2 by the lower discharge at first mass movement compared to the later tests (MD9-MD15).

7.2.1.2 Downstream Slope Inclination

The exit height of the seepage face at initiation of particle movement are higher for the mini dams with the 1V:1.5H slope (Table 7.2). Decreasing the angle of the downstream slope tended to increase the exit height for a given discharge. Decreasing the slope angle reduces flow length and head loss through the dam, typically meaning a reduced hydraulic gradient. As mentioned previously the exit hydraulic gradient is an important factor in determining particle movement. The impact of slope inclination is dependant on the geometry of the dam, including crest width and height.

When considering individual particle movement, as well as mass sliding or unraveling, stability is increased by a decrease in downstream slope angle. However, (Hansen 1992) idealized the motion of a particle on the surface of the downstream face of the dam as a rotational movement. Rotational movements of individual rocks are not greatly affected by the angle of the slope. In a deep-seated mass movement the downstream slope inclination plays an important roll. Surface erosion must be resisted to induce deep-seated movements and therefore deep-seated movements are beyond the scope of this research.

7.2.1.3 Initiation of Particle Movement

Even at low discharge the low frictional resistance of rockfill to concrete interface led to premature failure of the laboratory rockfill dams. The limited surface contact due to the angularity of the rockfill along with the smoothness of the

flume floor contributes to low frictional resistance. It is possible that a similar situation could occur in the field. Although it is already considered in most dam construction, treatment of the foundation material is important to the stability of rockfill. Wilkins (1955) and others have developed recommendations and design criteria for the prevention of toe movement. Some of the alternates recommended include placement of oversized rock at the toe of the slope (Wilkins 1955), steel bar mesh with anchor bars (Wilkins 1955), wire mesh with anchors (Leps 1973) and a low concrete retaining wall (Hoeg *et al.* 2004).

First movements in the mini dams with a toe blanket tended to be individual particles rolling down the downstream face of the dam. Generally, adjacent rocks would shift immediately after the first particle began moving. This movement mechanism indicates that due to the erratic arrangement of particles on the downstream face, no constraint of the initial particle is provided by adjacent particles. In the analysis of movement of the most unstable particle, Hansen *et al.* (2005) state that it is conservative to assume that there is no constraint of said particle. Hansen *et al.* (2005) speculate that an unconstrained particle may strike a constrained particle causing it to become dislodged, thus promoting unraveling.

7.2.2 Initiation of Particle Movement

A review of the prediction made in Section 6.7.2.1 will be completed. As well, a back analysis of the initiation of particle movement for both Scale Dam 1V:1H

and Scale Dam 1V:1.5H are completed with the data collected from the experimentation.

7.2.2.1 Scale Dam 1V:1H

The known parameters of the dam and the stage at which particle movement occurred is located in Table 7.3 below. Particle movement was first observed during Stage 13 of the Scale Dam 1V:1H experiment. A detailed description of the movement is found in Section 6.8.1.7.

Table 7.3 – Known Parameters for Initiation of Particle Movement in Scale Dam 1V:1H

	Unit	Measurement
Time of Observed movement	Stage	13
Discharge	Q (m^3/s)	0.172
Downstream Exit height	y_{exit} (m)	0.44
Porosity	n	0.42
Void Ratio	e	0.74
Length of dam	Width of the flume (m)	2.42
Downstream Slope Angle	θ (°)	45

During the prediction for initiation of particle movement several assumptions were made including the void ratio, the stage-discharge relationship, and exit height. The two extremes of C_D and ξ (0.1,15 and 1.0,45) appear to bound the problem. All other combinations found in Table 6.4 are potential failure parameters and must be considered. When comparing with the data obtained from the test, two C_D, ξ combinations are close (1.0,15) and (0.4,45) having almost the same prediction. The failure exit height was within 5%, discharge was

within 12%, however upstream water level was under predicted by 30%. The prediction of upstream water level may be affected by the over prediction of the stage discharge rating curve, and the impounding of water on the downstream side of the dam.

As the initial step in a back analysis the exit height can be calculated from Equation 6.3, and using Equation 2.4, m is 0.00474 for the above known void ratio. The calculated exit height is 0.475 m and is within 8% of that measured during the experimentation (Table 7.3).

The factor of safety can be calculated in a similar manner to that of Section 6.7.2.1. The void velocity (U) can be calculated with Equation 6.3 using the measured data and applied to Equation 6.2 to calculate the destabilizing hydraulic force and moment arm (Table 7.4). Three different values of C_D are used in the calculations to provide a comparison with the predicted values in Section 6.7.2.1. Equation 6.4 was used to calculate the destabilizing seepage force. The seepage moment M_{seep} was calculated with two seepage vectors (ξ = 15 and 45°) and included in Table 7.4. The stabilizing moment, the submerged weight of a particle, will be unchanged from the predictive analysis completed in 6.7.2.1 and is carried forward in this analysis. The overall factor of safety (FS) of the uppermost unstable particle is a ratio of the stabilizing moment versus destabilizing moments and is calculated using Equation 6.6. A summary of the analysis is found on Table 7.4 below.

Table 7.4 – Back Analysis for Initiation of Particle Movement Scale Dam 1V:1H						
CD	ξ	M_{hyd}	M_{seep}	$M_{hyd} + M_{seep}$	M_{stab}	FS
0.1	15	0.0017	0.0054	0.0071	0.0207	2.92
0.4	15	0.0068	0.0054	0.0122	0.0207	1.70
1.0	15	0.0169	0.0054	0.0223	0.0207	**0.93**
0.1	45	0.0017	0.0148	0.0165	0.0207	1.25
0.4	45	0.0068	0.0148	0.0215	0.0207	**0.96**
1.0	45	0.0168	0.0148	0.0317	0.0207	**0.65**

From the back analysis three failure scenarios are produced. As argued earlier the extreme C_D and ξ (1.0,45) is a possible lower bound, and the two other FS less than unity demonstrates a numerical confirmation of failure.

7.2.2.2 Scale Dam 1V:1.5H

The same method of calculation of safety factors for Scale Dam 1V:1H was completed for Scale Dam 1V:1.5H. The parameters utilized, as well as the results are listed below in Table 7.5 and Table 7.6. A complete description of Scale Dam 1V:1.5H is found in Section 6.8.2.

Table 7.5 – Scale Dam 1V:1.5H, Measured Parameters		
	Unit	**Measurement**
Time of Observed movement	Stage	15
Discharge	Q (m/s)	0.251
Downstream Exit height	y_{exit} (m)	0.65
Porosity	n	0.40
Void Ratio	e	0.68
Length of dam	Width of the flume (m)	2.42
Downstream Slope Angle	θ (°)	33.7

When comparing the prediction of particle movement with the data obtained from Scale Dam 1V:1.5H the failure exit height was within 12%, discharge was within 6% and the upstream water level was under predicted by 18%. The prediction of upstream water level may be affected by the over prediction of the stage discharge rating curve, and the impounding of water on the downstream side of the dam.

The exit height was calculated from Equation 6.3, and using Equation 2.4, m is 0.00436 for the above known void ratio. The calculated exit height is 0.746 m and is within 15% of that measured during the experimentation (Table 7.5).

Table 7.6 – Back Analysis for Initiation of Particle Movement Scale Dam 1V:1.5H

CD	ξ	M_{hyd}	M_{seep}	$M_{hyd} + M_{seep}$	M_{stab}	FS
0.1	15	0.0019	0.0058	0.0077	0.0243	3.16
0.4	15	0.0075	0.0058	0.0133	0.0243	1.83
1.0	15	0.0187	0.0058	0.0245	0.0243	**0.99**
0.1	45	0.0019	0.0158	0.0177	0.0243	1.37
0.4	45	0.0075	0.0158	0.0233	0.0243	**1.04**
1.0	45	0.0187	0.0158	0.0345	0.0243	**0.70**

Although the fifth FS in Table 7.6 is greater than 1.0, Hansen *et* al. (2005) state that any value of FS just above unity should be considered unsafe because of the turbulent nature of the flow and the inherent random component to the behaviour of rockfill.

7.2.3 Summary of Results

The rockfill used in the scale dam experiments was well-graded, ranging from 0.01 to 0.15 m in diameter. However, the analysis of particle movement required that a single diameter be selected as representative. From previous researchers (Wilkins 1955, Leps 1973, Garga 1995), the 50^{th} percentile diameter (d_{50}) of 0.05 m was selected. This representative diameter was used throughout the analysis.

The initiation of particle movement analysis as outlined by Hansen *et al.* (2005) produced a number of factors of safety, which varied gradient slope and C_D to the variability of some of the estimated parameters. In both Scale Dam 1V:1H and Scale Dam 1V:1.5H the scenario that produced a safety factor near unity was the combinations of drag coefficient C_D and horizontal seepage vector ξ of 1.0, 15 and 0.4, 45. As estimated from drag tank testing, the upper limit of C_D lies somewhere between 0.4 and 1.0. From Hansen *et* al. (2005) ξ generally lies somewhere between the extremes of 15 and 45°.

The method for estimating initiation of particle movement from Hansen *et al.* (2005), successfully estimated a factor of safety near unity in the prediction of particle movement and in the back calculating movement from the observed conditions at particle movement in the scale dam tests.

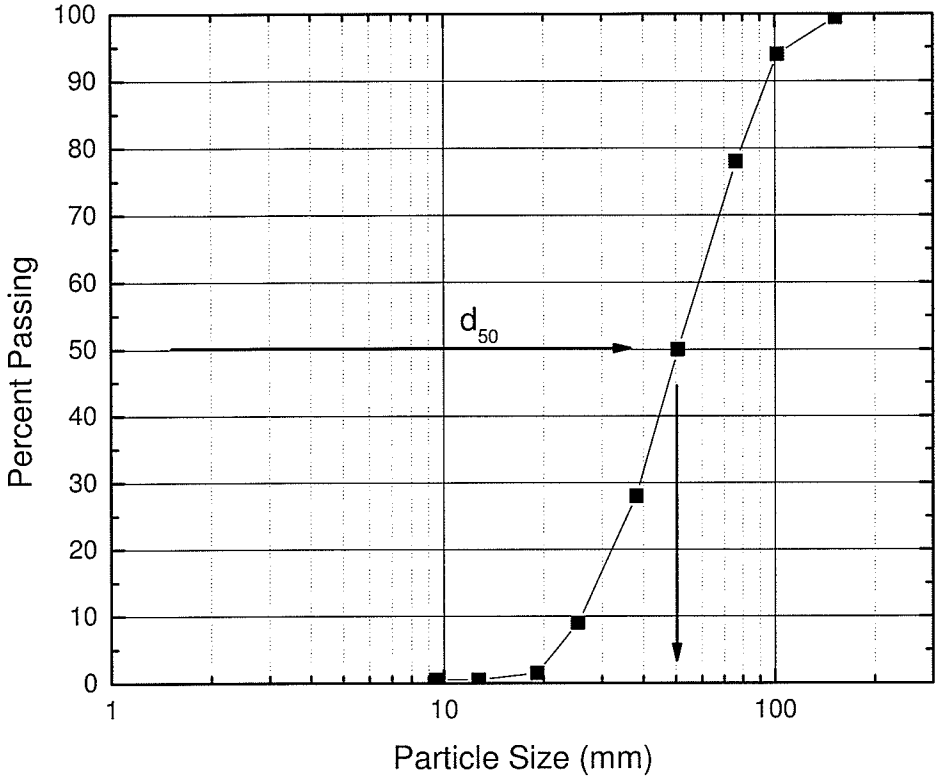

Figure 7.1 – Laboratory Scale Approximation of Field Measured Grain Distribution

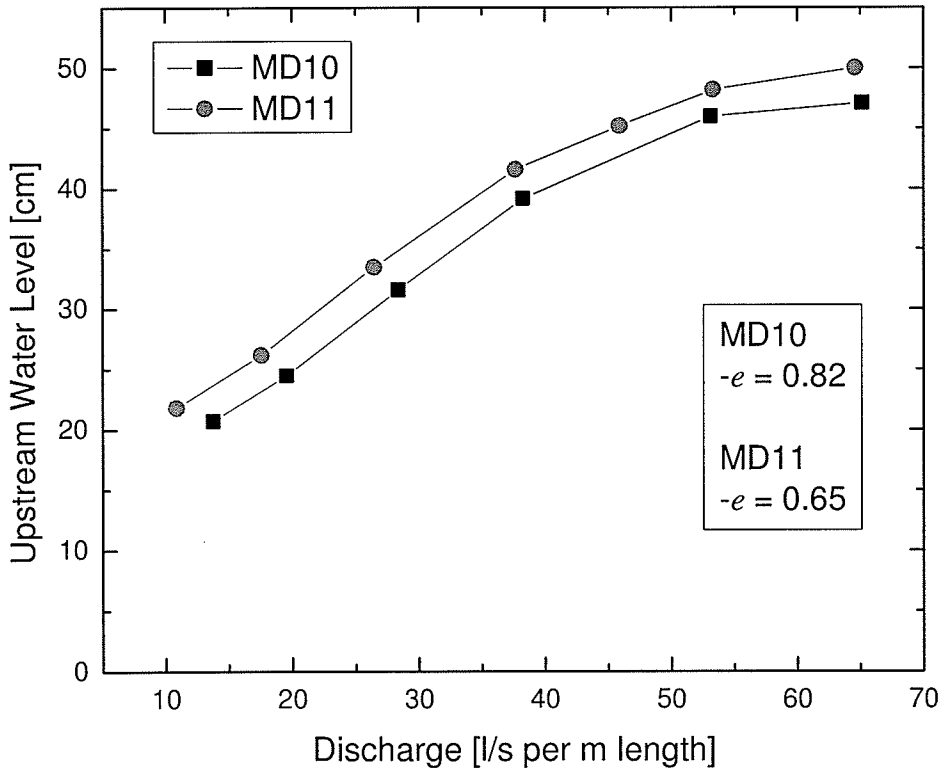

Figure 7.2 – Comparison of Void Ratio, MD10 and MD11

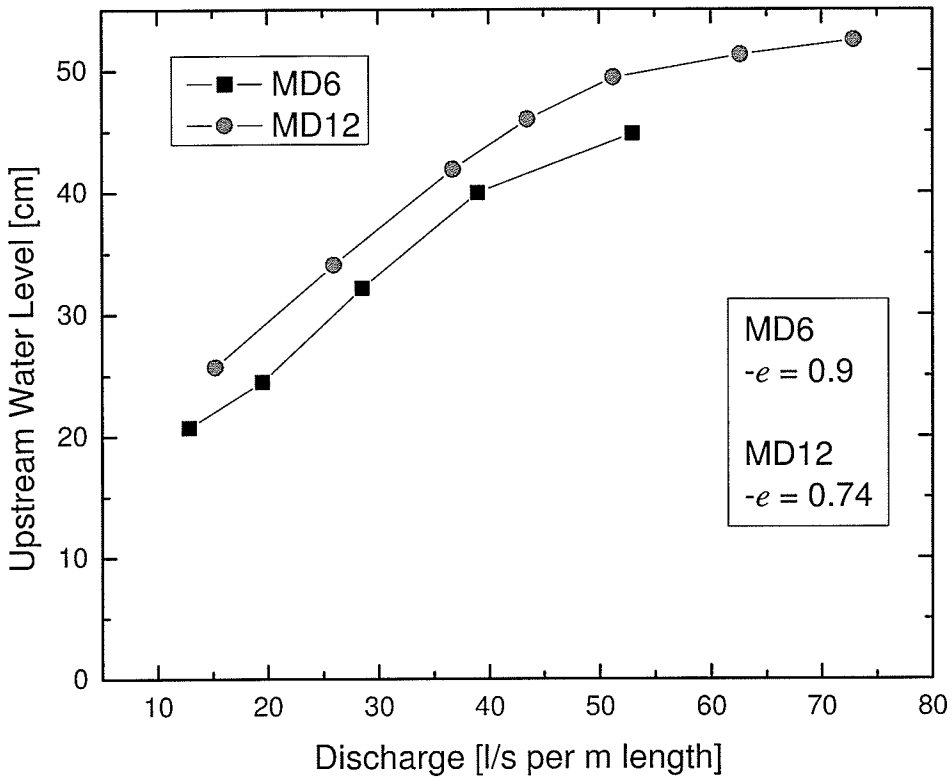

Figure 7.3 – Comparison of Void Ratio, MD6 and MD12

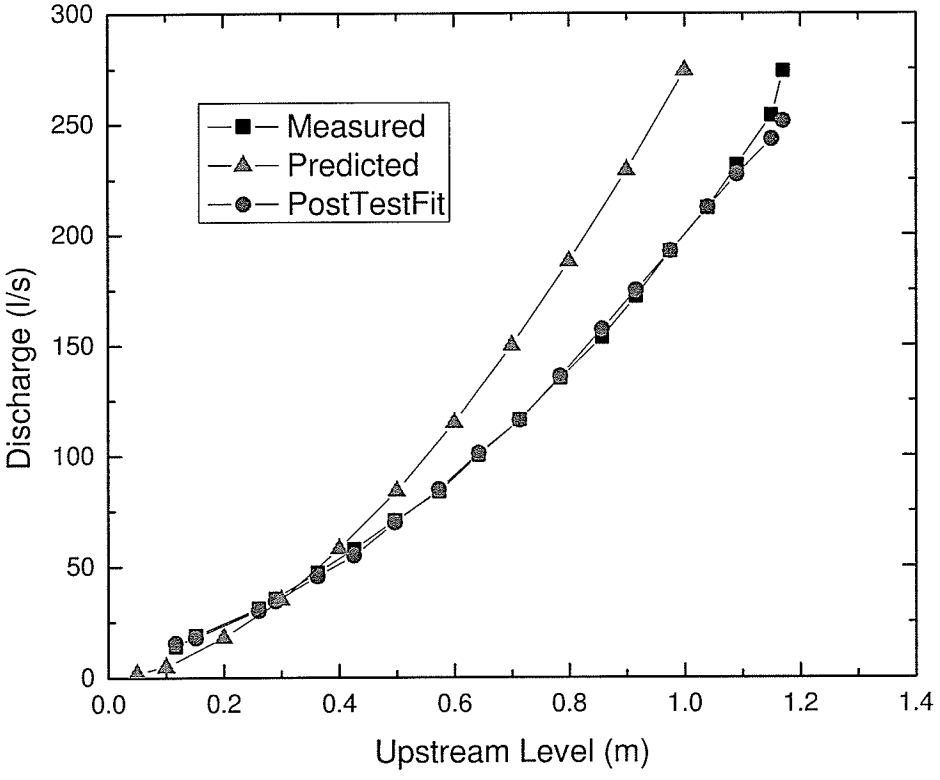

Figure 7.4 – Scale Dam 1V:1H, Post experiment curve fitting

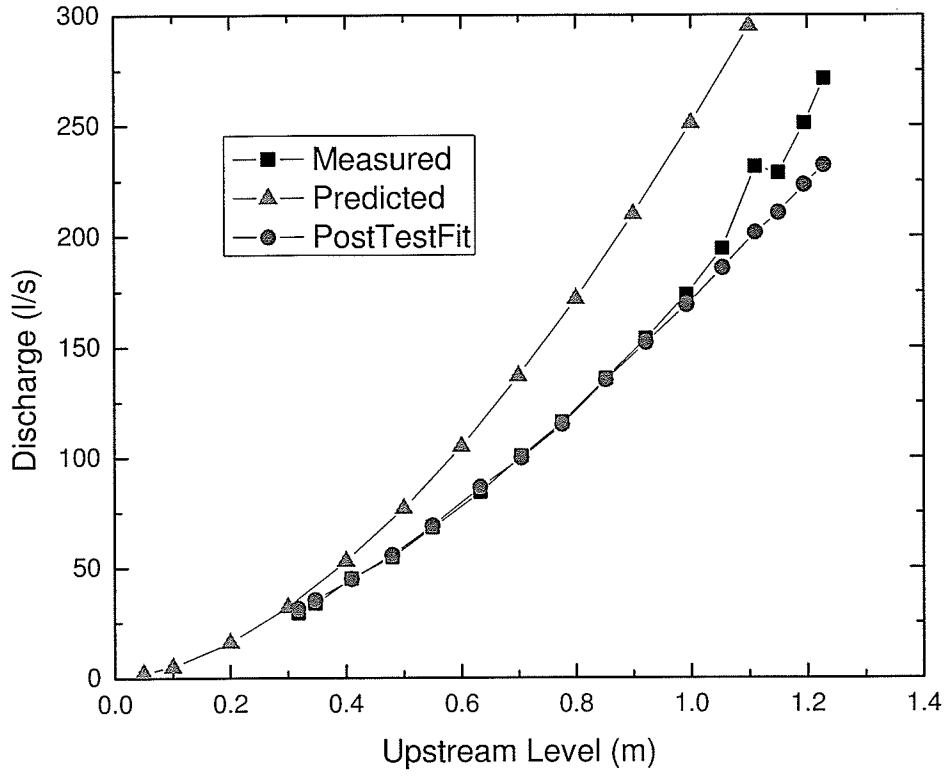

Figure 7.5 – Scale Dam 1V:1.5H, Post experiment curve fitting

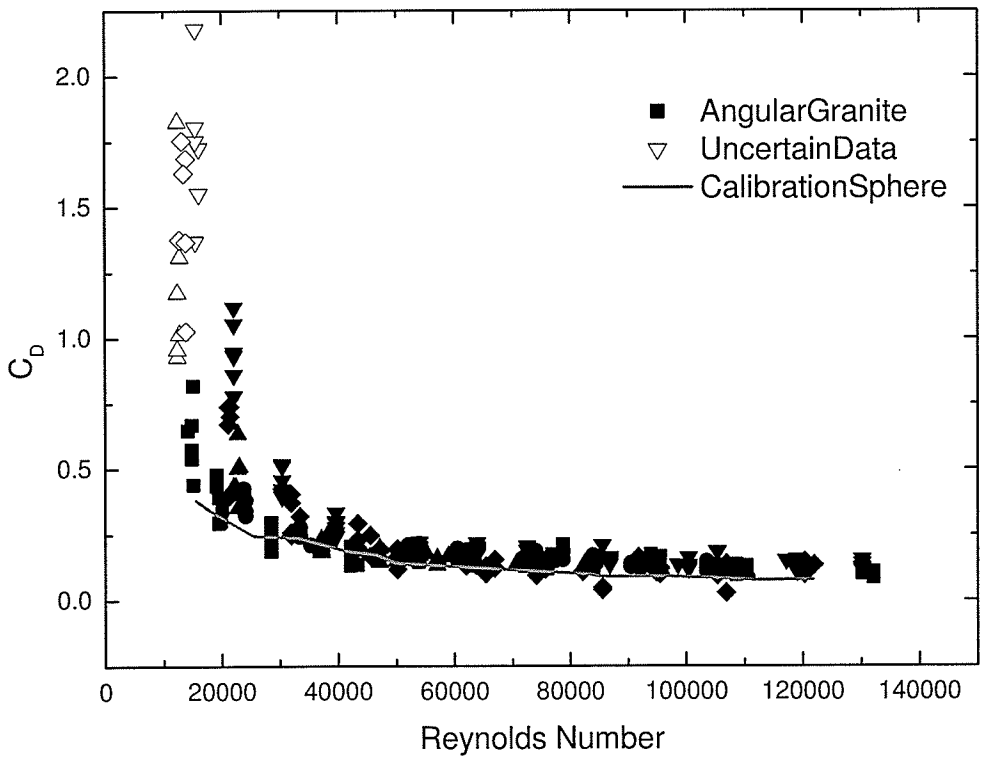

Figure 7.6 – Drag Tank Data, (Figure 3.14 Rescaled)

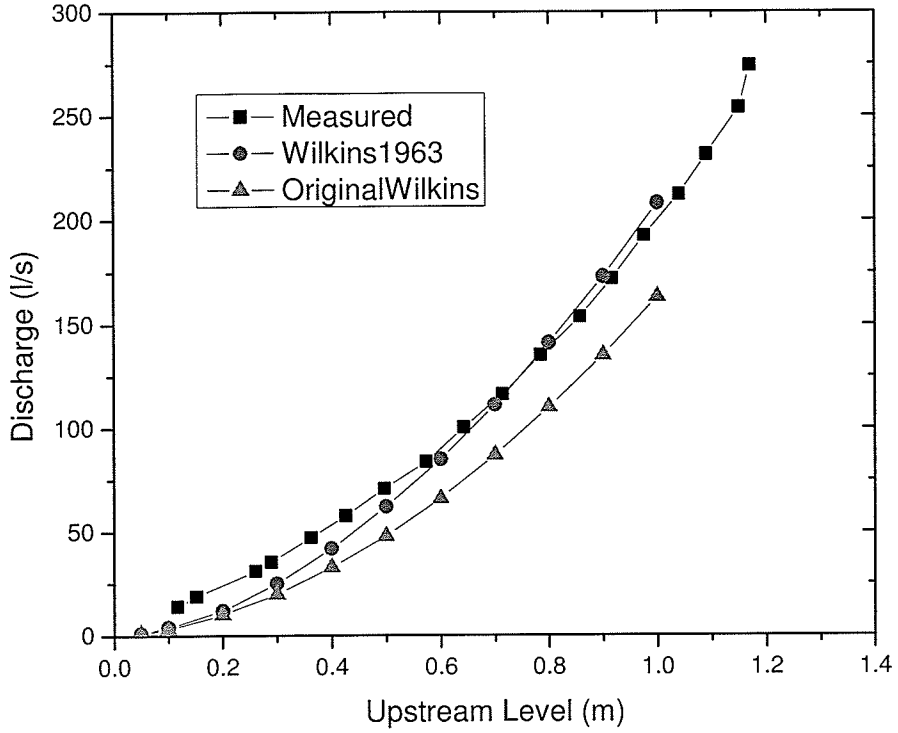

Figure 7.7 – Scale Dam 1V:1H Stage-Discharge, Wilkins 1955 and 1963 Comparison

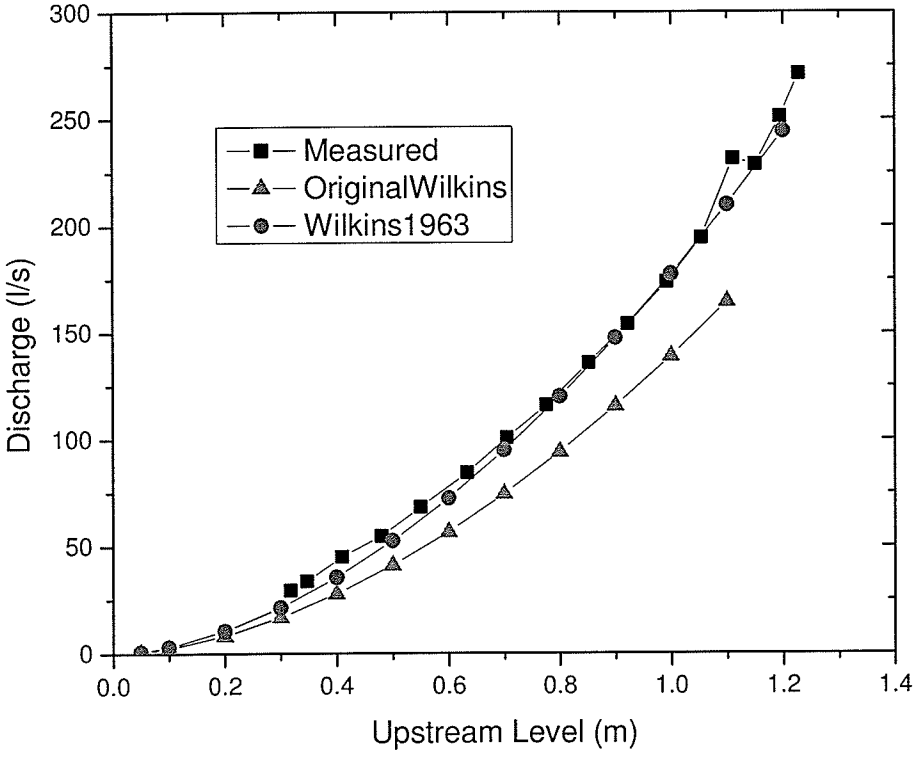

Figure 7.8 – Scale Dam 1V:1.5H Stage-Discharge, Wilkins 1955 and 1963 Comparison

8 CONCLUSION AND RECOMMENDATIONS

8.1 CONCLUSION

In flow-through rockfill dams the quantity of seepage can be substantial. Whether intentionally constructed as a flow-through structure or as a consequence of events, rockfill dams should be designed with consideration to flow through. Flow through rockfill is generally a non-Darcy flow and requires a non-linear relationship. A variety of relationships exist for describing non-Darcy flow through porous media. Wilkins' (1955) equation is used extensively for turbulent flow through rockfill.

This study carried out an experimental program in four areas: particle characterization, large-scale permeameter test, flow-through mini dams, and flow-through scale dams. Data from the experimental program was used to develop a unique set of flow-through parameters, check the validity of non-Darcy flow relationships proposed by others, and validate initiation of particle movement equations proposed by others for local rockfill.

8.1.1 Coefficient of Drag

The drag tank-testing program examined the combined effects of surface roughness and angularity of individual rocks. A series of specimens were selected based on variability in size, shape, angularity, and perceived surface roughness and placed in open channel flow. Measurements of water velocity

and force applied to the suspended specimen were recorded. To calibrate the test method, apparatus, and test results, a smooth sphere was tested.

Results provide understanding of the relationship between rock particles and idealized spherical particles. When selecting a value of the coefficient of drag for use in analysis of initiation of particle movement on the seepage face, the variability of angularity, shape, surface roughness, and local flow velocity requires that a range of C_D be considered to represent the range of particles.

8.1.2 Non-Darcy Flow

The basic equation for flow through rockfill is a formula for turbulent flow, and can be expressed with a power-law relationship. The physical properties of the rockfill, that affects flow, including porosity, particle shape, particle size, roughness, and tortuosity of the voids induce fully turbulent flow at low velocities.

Few studies have used a large-scale permeameter apparatus to determine specific hydraulic properties. Rockfill tests conducted in the HRTF using the large-scale permeameter were shown to reach fully turbulent flow at low hydraulic gradients. Coefficients for the power-law relationship between hydraulic gradient and bulk velocity were determined. As well, equations proposed by others were reviewed and validated with the large-scale permeameter data.

8.1.3 Effects of Dam Parameters on Flow Through

Fifteen laboratory tests of miniature dams was undertaken to vary embankment geometry, void ratio, and gradation. The experimental program was intended to confirm the flow-through properties of the rockfill, and to test the initiation of particle movement.

Several conclusions were drawn from the experiments, and are generally in agreement with other authors.

i. Two gradations, a well-graded and a poorly-graded, may have the same size of dominant particle but the well-graded material will generally have a lower porosity and a lower value of hydraulic mean radius.

ii. The general trend between increasing upstream water level, decreasing exit height and slope is observed, for a given discharge. The exit height of the seepage face will generally be higher on a dam with a shallower downstream slope.

iii. It can be concluded that an increase in void ratio will effectively increase the flow through rockfill. While being placed in thin lifts, compaction can significantly reduce the bulk void ratio of rockfill and would reduce the flow and hydraulic gradient.

iv. Restraint of the toe of a dam from erosion significantly increased the discharge at which initiation of particle movement will occur.

8.1.4 Design of Rockfill Dams

Hansen *et al.* (2005) identify three important design criteria for flow-through rockfill structures: the gross volumetric rate through the structure, the height of the seepage face associated with the flow, and which particle within the seepage face is the most unstable.

The stage-discharge rating curve presented by Hansen *et al.* (1995) is an empirical equation obtained for experimental data. In developing the stage-discharge equation (Equation 2.9), the aspect ratio of each dam and the relative upstream water level were of key importance. Hansen *et al.* (1995) discuss six non-Darcy flow equations and present Wilkins' (1955) equation as favoured by the mining industry. Wilkins' (1955) equation: requires determination of the hydraulic mean radius, which for well-graded material is difficult to determine. If the data is available, a hydraulic gradient versus bulk velocity relationship can be determined and Wilkins' equation would not be required.

Wilkins (1955) used a simplified version of Equation 2.10 to construct turbulent flow nets. From the flow net, pore pressures at any location can be estimated. A finite element modeling computer program, such as GeoStudio can be used to model the flow and piezometric head through a rockfill structure. The finite element program can also be used to model the phreatic surface and exit height within a structure. The above-mentioned software was designed and intended to

use Darcy's Law, and hence valid only in a laminar flow regime, but provided a reasonable approximation.

8.2 Recommendations for Further Research

The following are several suggestions for future testing. These suggestions include further research into the flow through aspects of rockfill and the improvement of future experiments.

a) The application of statistical theory to define the dominant particle in a non-uniform gradation. This is not limited to laboratory samples, but should include field-sized samples.
b) Discrete measurements and or calculations of the force imparted on a particle for a given exit gradient. This is difficult to develop as there are factors such as exit height, buoyancy, and projected surface area that will need to be considered.
c) Further testing of the mini dams to explore rockfill characteristics in detail. These tests were simple to construct and quick to test, and capable of providing quality information for little effort.
d) Testing of the large-scale permeameter for wall effects. Wall effects were assumed to be minimal given the overall size of the apparatus, but quantification of the wall effects may prove beneficial.
e) Testing of a different representative diameter for flow through characteristics to provide a broader range of data.

REFERENCES

Abt, S.R. and Johnson, T.L. 1991. Riprap design for overtopping flow. Journal of Hydraulic Engineering, **117**(8): 959-972.

Bailey, A.B. 1974. Sphere drag coefficient for subsonic speeds in continuum and free-molecule flows. Journal of Fluid Mechanics, **65**(2): 401-410.

Canadian Dam Association (CDA). 1999. Dam Safety Guidelines. January 1999.

Canadian Dam Association (CDA). 2006. Dam Safety Guidelines (Draft for Discussion). CDA Conference, October 2006, Quebec City, Quebec.

Darcy, Henry. 1856. LesFontaines publiques de la ville de Dijon. Victor Dalmont, Paris.

Dudgeon C. R. 1964. Flow of water through coarse granular materials. M.Eng. Thesis, Water Research Laboratory, University of New South Wales, Manly Vale, N.S.W., Australia.

Garga, V.K., Townsend, R., and Hansen, D. 1991. A Method for Determining the Surface Area of Quarried Rocks. Geotechnical Testing Journal, **14**(1): 35-45.

Hansen D., Zhao W.Z., and Han S.Y. 2005. Hydraulic performance and stability of coarse rockfill deposits. PICE (UK) Journal of Water Management, **158**(WM4): 163-174.

Hansen D., Garga V. and Townsend R. 1995. Selection and application of a one-dimensional non-Darcy flow equation for two-dimensional flow through rockfill embankments. Canadian Geotechnical Journal, **32**(2): 223-232.

Hansen, D. 1992. The Behaviour of Flowthrough Rockfill Dams. PhD thesis, University of Ottawa, Canada.

Hoeg, K., Lovoll, A., Vaskinn, K.A. 2004. Stability and breaching of embankment dams: Field tests on 6 m high dams. International Journal on Hydropower and Dams, **11**(1): 88-92.

Hubbert, M.K. 1940. The Theory of Ground-Water Motion. Journal of Geology, **48**(8), Part 1: 785-944.

Jensen, O. J. and Klinting, P. 1983. Evaluation of Scale Effects in Hydraulic Models by Analysis of Laminar and Turbulent Flows. Journal of Coastal Engineering, **7**: 319.

Lawson, J.D. 1987. Protection of Rockfill Dams and Cofferdams Against Overflow and Throughflow - The Australian Experience. Transactions of the Institution of Engineers Australia - Civil Engineering Transactions, **29**.

Leps, T. 1973. Flow Through Rockfill. Embankment-Dam Engineering, Casagrande Volume. Pages 87-107.

Martins, R. 1990. Turbulent seepage flow through rockfill structures. Water Power and Dam Construction, **40**(3): 41-45.

McCorquodale, J.A., Hannoura, A.A., and Nasser, M.S. 1978. Hydraulic conductivity of rockfill. Journal of Hydrualic Research, **16**(2): 123-137.

NASA 2006. Shape Effects on Drag. Glenn Research Center, 15 Mar. 2006. http://www.nasa.gov/

NTNU. 2003. Stability and Failure Mechanisms of Dams. Report from Laboratory Tests at NTNU. Department of Hydraulic and Environmental Engineering. Norwegian University of Science and Technology.

Peck R.B. 1973. INFLUENCE OF NONTECHNICAL FACTORS ON THE QUALITY OF EMBANKMENT DAMS. Embankment-Dam Eng, 201-208.

Robinson, K.M., Kadavy, K.C., Rice, C.E. 1998. Rock chutes on slopes between 2 and 40%. Paper No. 982136, ASAE Annual International Meeting, Orlando Florida.

Sabin, G. and Hansen, D. 1994. The Effects of Particle Shape and Surface Roughness on the Hydraulic Mean Radius of a Porous Medium consisting of Quarried Rock. Geotechnical Testing Journal, **17**(1): 43-49.

Scheidegger, A. E. 1974. The physics of flow through porous media 3rd Edition. University of Toronto Press, Toronto, Canada.

Townsend, R.D., Garga, V.K., and Hansen, D. 1991. Finite difference modeling of the variation in piezometric head within a rockfill embankment. Canadian Journal of Civil Engineering, **18**(2): 254-263.

Unland, G., Szczelina P. 2004. Coarse crushing of brittle rocks by compression. International Journal of Mineral Processing, v. 74, supplement 1, 10 December 2004, pp S209.

Venkataraman, P. and Rama Mohan Rao, P. 1998. *Darcian, Transitional and Turbulent Flow through Porous Media.* Journal of Hydraulic Engineering, **124**(8): 840-846.

Wilkins, J.K. 1955. Flow of water through rockfill and its application to design of dams. New Zealand Engineering, **01**(11): 382-387.

APPENDIX A

SAFETY PROCEDURES

UNIVERSITY OF MANITOBA

Department of Civil Engineering
Geotechnical Group

Large Diameter Permeameter

Standard Operating Procedure

Created: January 23, 2006

SCOPE:
To safely conduct a research experiment with the Large Diameter Permeameter in the Hydraulic Research and Testing Facility at the University of Manitoba.

PERSONAL PROTECTIVE EQUIPMENT:
Required items:
- Safety footwear
- Hard hat
- Safety glasses

Discretionary:
- Leather work gloves

EQUIPMENT:
- Large diameter permeameter (LDP)
- A-frame gantry
- Remote activated electric winch

PROCEDURE:
All activities should be conducted in a manner that promotes safety. Personal protective equipment should be worn at all times throughout the operation of the Large Diameter Permeameter. The operation can be broken into 4 activities:

LOADING THE PERMEAMETER:

1. The permeameter is to be resting on the ground, with uprights bolted in place.
2. The gantry must support some small load from the permeameter to prevent movement while loading with rock.
3. The rock shall be placed in a controlled manner from a set height above the already deposited rock.
4. To avoid damage to either the base screen or vibrating wire piezometers, rock shall be gently loaded into the LDP until a layer of 6 inches (150 mm) is deposited. Placement will then resume as before.

OPERATING THE GANTRY:

1. Ensure the base cross bar is in place.
2. Securely attach the electric winch to the mounting bolts in the concrete floor, and attach the cable to the pulling strap on the gantry.
3. Inspect/clean the area of any objects which may inhibit the movement of the gantry and LDP.
4. Using the gantry, lift the LDP approximately 1 inch (25 mm) off the ground.
5. Slowly move the gantry and LDP with the electric winch in the desired direction.

6. When in position, lower the LDP and remove the cable and winch.
7. While the LDP is completely supported by the gantry, movements below the LDP should be minimized.
8. Do not keep the LDP elevated for long periods, and do not leave the elevated LDP unattended

OPERATING THE LARGE DIAMETER PERMEAMETER:

1. Attach the inlet pipe as per the manufacturer's instructions.
2. Ensure the gantry is supporting approximately half of the weight of the LDP, and then move all chains from the gantry away from the top of the LDP.
3. During the test, regularly check the LDP for movement. Little to no movement should be observed.
4. Do not approach the LDP during operation as rocks may be exiting the top at any point.

UNLOADING THE LDP:

1. The LDP must be lowered for this activity, which should be done from the catwalk above the LDP. Do not keep the LDP in a partially lowered position for long periods unattended.
2. The LDP should be supported by a block on the ground such that no load is applied to the gantry.
3. For safe unloading of the rock, removal of rock from the pipe should be done with a physical device such as a garden hoe.
4. Moving the rock to the loading point requires going up one storey and should be done with a cart and an elevator to minimize lifting.

Please Note:

- Operation of the LDP and gantry requires heavy lifting and significant manual labour. Please follow Manitoba Health and Safety Guidelines for safe lifting procedures.
- Refer to SOP# HWP-03 for additional information regarding working alone.
- Carry out good housekeeping by returning all tools and equipment to their respective storage locations.